

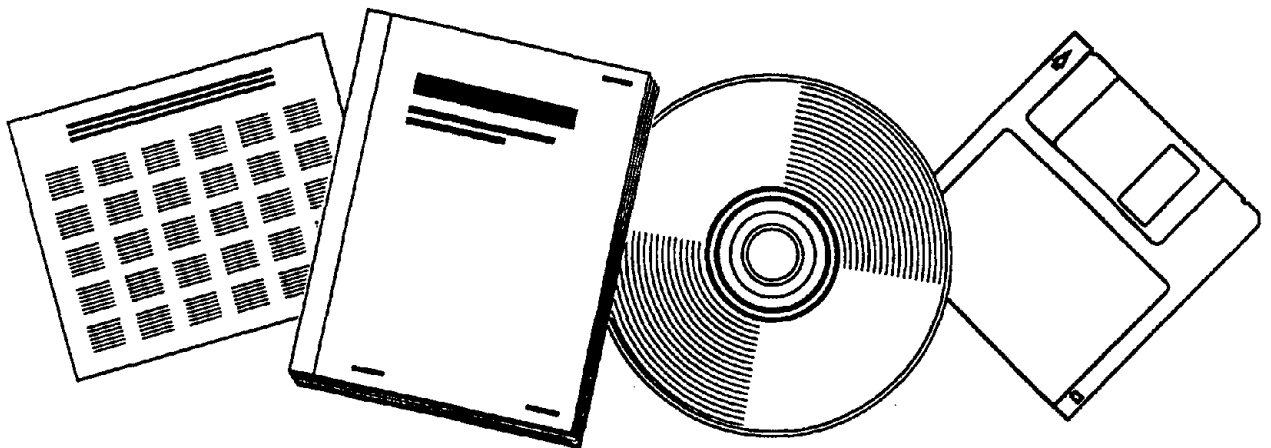


PB98-108988

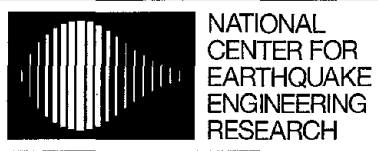
NTIS[®]
Information is our business.

**METHOD FOR EARTHQUAKE MOTION-DRAINAGE
RELATIONSHIP WITH APPLICATION TO REINFORCED
CONCRETE FRAMES**

10 SEP 97



**U.S. DEPARTMENT OF COMMERCE
National Technical Information Service**



NATIONAL
CENTER FOR
EARTHQUAKE
ENGINEERING
RESEARCH

Headquartered at the State University of New York at Buffalo

ISSN 1088-3800



PB98-108988

A Method for Earthquake Motion-Damage Relationships with Application to Reinforced Concrete Frames

by

Ajay Singhal and Anne S. Kiremidjian
The John A. Blume Earthquake Engineering Center
Department of Civil Engineering
Stanford University
Stanford, California 94305

Technical Report NCEER-97-0008

September 10, 1997

This research was conducted at Stanford University and was supported in whole or in part by the National Science Foundation under Grant No. BCS 90-25010 and other sponsors.

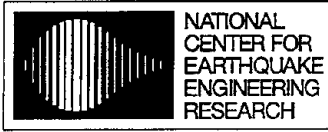
NOTICE

This report was prepared by Stanford University as a result of research sponsored by the National Center for Earthquake Engineering Research (NCEER) through a grant from the National Science Foundation and other sponsors. Neither NCEER, associates of NCEER, its sponsors, Stanford University, nor any person acting on their behalf:

- a. makes any warranty, express or implied, with respect to the use of any information, apparatus, method, or process disclosed in this report or that such use may not infringe upon privately owned rights; or
- b. assumes any liabilities of whatsoever kind with respect to the use of, or the damage resulting from the use of, any information, apparatus, method, or process disclosed in this report.

Any opinions, findings, and conclusions or recommendations expressed in this publication are those of the author(s) and do not necessarily reflect the views of NCEER, the National Science Foundation, or other sponsors.

REPORT DOCUMENTATION PAGE	1. REPORT NO. NCEER-97-0008	2.		
4. Title and Subtitle A Method for Earthquake Motion-Damage Relationships with Application to Reinforced Concrete Frames			5. Report Date September 10, 1997	
7. Author(s) Ajay Singhal and Anne S. Kiremidjian			6.	
9. Performing Organization Name and Address The John A. Blume Earthquake Engineering Center Department of Civil Engineering Stanford University Stanford, California 94305			8. Performing Organization Rept. No.	
12. Sponsoring Organization Name and Address National Center for Earthquake Engineering Research State University of New York at Buffalo Red Jacket Quadrangle Buffalo, New York 14261			10. Project/Task/Work Unit No.	
15. Supplementary Notes This research was conducted at Stanford University and was supported in whole or in part by the National Science Foundation under Grant No. BCS 90-25010 and other sponsors.			11. Contract(C) or Grant(G) No. (C) BCS 90-25010 (G)	
16. Abstract (Limit: 200 words) The research presented in this report provides a general method for developing relationships between earthquake ground motion and damage. The motion-damage relationships were presented as fragility curves and damage probability matrices. The major components of the methodology consist of: (a) characterization of the potential ground motions, (b) characterization of the nonlinear response of the structure when subjected to extreme dynamic loads, (c) application of the methodology to reinforced concrete frames, (d) sensitivity studies for different structural attributes, and (e) development of a Bayesian technique to update the motion-damage relationships.			13. Type of Report & Period Covered Technical report	
17. Document Analysis a. Descriptors b. Identifiers/Open-Ended Terms Damage prediction. Fragility curves. Damage probability matrices. Bayesian statistics. Reinforced concrete frames. Input ground motion. Monte Carlo simulation. Stationary Gaussian processes. Autoregressive moving average (ARMA) models. Earthquake engineering. c. COSATI Field/Group			14.	
18. Availability Statement Release unlimited		19. Security Class (This Report) Unclassified		21. No. of Pages 244
		20. Security Class (This Page) Unclassified		22. Price



NATIONAL
CENTER FOR
EARTHQUAKE
ENGINEERING
RESEARCH

Headquartered at the State University of New York at Buffalo

A Method for Earthquake Motion-Damage Relationships with Application to Reinforced Concrete Frames

by

A. Singhal¹ and A.S. Kiremidjian²

Publication Date: September 10, 1997

Submittal Date: November 26, 1996

Technical Report NCEER-97-0008

NCEER Task Number 93-4101

NSF Master Contract Number BCS 90-25010

- 1 Doctoral Candidate, The John A. Blume Earthquake Engineering Center, Department of Civil Engineering, Stanford University
- 2 Professor and Co-Director, The John A. Blume Earthquake Engineering Center, Department of Civil Engineering, Stanford University

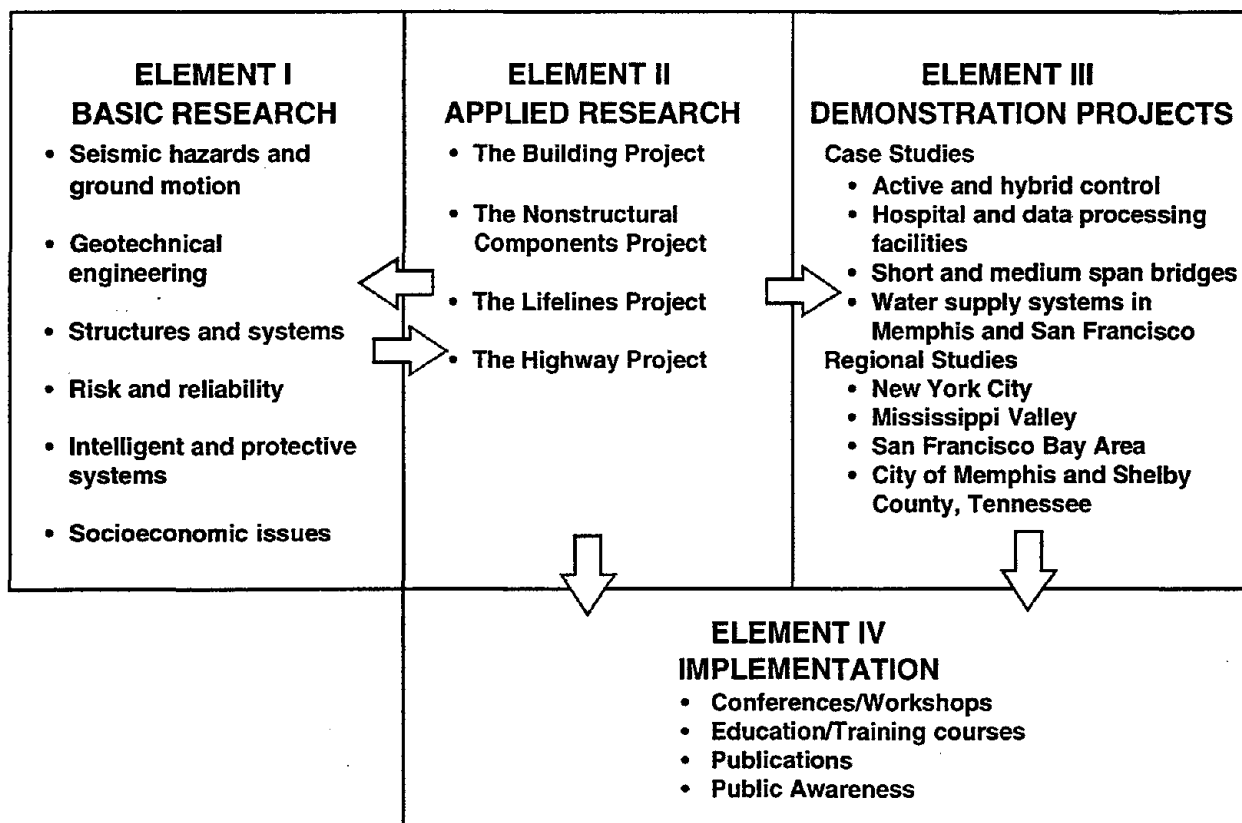
NATIONAL CENTER FOR EARTHQUAKE ENGINEERING RESEARCH
State University of New York at Buffalo
Red Jacket Quadrangle, Buffalo, NY 14261

PREFACE

The National Center for Earthquake Engineering Research (NCEER) was established in 1986 to develop and disseminate new knowledge about earthquakes, earthquake-resistant design and seismic hazard mitigation procedures to minimize loss of life and property. The emphasis of the Center is on eastern and central United States *structures*, and *lifelines* throughout the country that may be exposed to any level of earthquake hazard.

NCEER's research is conducted under one of four Projects: the Building Project, the Nonstructural Components Project, and the Lifelines Project, all three of which are principally supported by the National Science Foundation, and the Highway Project which is primarily sponsored by the Federal Highway Administration.

The research and implementation plan in years six through ten (1991-1996) for the Building, Nonstructural Components, and Lifelines Projects comprises four interdependent elements, as shown in the figure below. Element I, Basic Research, is carried out to support projects in the Applied Research area. Element II, Applied Research, is the major focus of work for years six through ten for these three projects. Demonstration Projects under Element III have been planned to support the Applied Research projects and include individual case studies and regional studies. Element IV, Implementation, will result from activity in the Applied Research projects, and from Demonstration Projects.



Research in the **Building Project** focuses on the evaluation and retrofit of buildings in regions of moderate seismicity. Emphasis is on lightly reinforced concrete buildings, steel semi-rigid frames, and masonry walls or infills. The research involves small- and medium-scale shake table tests and full-scale component tests at several institutions. In a parallel effort, analytical models and computer programs are being developed to aid in the prediction of the response of these buildings to various types of ground motion.

The **risk and reliability program** constitutes one of the important areas of research in the **Building Project**. The program is concerned with reducing the uncertainty in current models which characterize and predict seismically induced ground motion, and resulting structural damage and system unserviceability. The goal of the program is to provide analytical and empirical procedures to bridge the gap between traditional earthquake engineering and socioeconomic considerations for the most cost-effective seismic hazard mitigation. Among others, the following tasks are being carried out:

1. Study seismic damage and develop fragility curves for existing structures.
2. Develop retrofit and strengthening strategies.
3. Develop intelligent structures using high-tech and traditional sensors for on-line and real-time diagnoses of structural integrity under seismic excitation.
4. Improve and promote damage-control design for new structures.
5. Study critical code issues and assist code groups to upgrade seismic design code.
6. Investigate the integrity of nonstructural systems under seismic conditions.

The research presented in this report provides a general method for developing relationships between earthquake ground motion and damage. The motion-damage relationships were presented as fragility curves and damage probability matrices. The major components of the methodology consist of: (a) characterization of the potential ground motions, (b) characterization of the nonlinear response of the structure when subjected to extreme dynamic loads, (c) application of the methodology to reinforced concrete frames, (d) sensitivity studies for different structural attributes, and (e) development of a Bayesian technique to update the motion-damage relationships.

ABSTRACT

Recent earthquakes have shown their devastating effects on structures. Damage to structures has significant socio-economic consequences. Before the occurrence of an earthquake, planners can use estimates of structural damage to predict the likely extent of building damage, economic loss, and number of casualties. Immediately after an earthquake, damage estimates can be used by emergency response planners to assess the vulnerability of a structure to aftershocks and to decide whether the building is safe to enter or not. Post-earthquake rehabilitation decisions require estimates of structural damage to decide whether to repair or to demolish a damaged structure.

Structural damage to buildings can be estimated by using seismic site hazard along with relationships between earthquake ground motion severity and structural damage. This report deals only with the latter relationships. These relationships are most frequently described in the form of conditional probability distributions of damage at specified ground motion intensities. These motion-damage relationships are usually expressed in terms of fragility curves and damage probability matrices. The development of fragility curves and damage probability matrices requires the characterization of the ground motion and the identification of the different degrees of structural damage.

This study presents a systematic approach for developing motion-damage relationships that does not rely either on heuristics or on empirical data. Instead, the probability of damage is estimated by quantifying the response of a structure subjected to a significant ensemble of ground motions with a wide range of parameter variations. The quantification of the structural response also includes the variability in structural parameters. For this purpose, a Monte Carlo simulation approach is used to determine the probabilities of structural damage, and the ensemble of ground motions is generated using an appropriate model for ground motion simulation. The models for ground motion simulation include the stationary Gaussian model with modulating functions and the autoregressive moving average (ARMA) models. The Latin hypercube technique is used to increase the efficiency of the Monte Carlo simulation.

The approach developed in this study is then applied to obtain fragility curves and damage probability matrices for reinforced concrete moment resisting frames. Reinforced concrete frames are divided into three classes based on the number of stories in the frames. These include low rise concrete frames that are 1-3 stories tall, mid rise frames that are 4-7 stories tall, and high rise frames that are 8 stories or taller. The ground motion for these three classes of frames is characterized by the average spectral acceleration over period bands corresponding to the three classes of frames. Sample structures for the three classes of frames are used to develop the motion-damage relationships. Parametric studies are performed to assess the effect of geometric variations in the performance of concrete frame structures.

In order to combine observed earthquake damage data with analytical motion-damage relationships, a Bayesian statistical method is developed in this report. Using damage data from the Northridge earthquake, the fragility curves for low rise frames are updated by implementing the Bayesian method. It is found that the synthetic fragility curves, obtained by the Monte Carlo simulation, provide the best estimates of the updated probabilities of the different damage states for these frames. The uncertainty associated with the motion-damage relationships is presented in terms of confidence bounds on the fragility curves.

ACKNOWLEDGMENT

The authors would like to express their gratitude to Dr. Andrei Reinhorn for providing us with the program IDARC2D. In addition, Dr. J. P. Conte provided input to the ARMA modeling of earthquake ground motions. The Governor's Office of Emergency Services for the State of California provided information on the inventory for RC frame buildings in the city of Los Angeles. Their help is gratefully appreciated.

TABLE OF CONTENTS

SECTION	TITLE	PAGE
1	INTRODUCTION	1
1.1	Background	1
1.2	Objectives	3
1.3	Scope	3
1.4	Organization of the Report	4
2	REVIEW OF PARAMETERS FOR CHARACTERIZATION OF GROUND MOTION AND STRUCTURAL DAMAGE	7
2.1	Ground Motion Characterization	7
2.1.1	Strong Motion Duration	8
2.1.2	Ground Motion Amplitude	9
2.1.3	Housner's Spectral Intensity	10
2.1.4	Arias Intensity	11
2.1.5	Root Mean Square Acceleration	12
2.1.6	Destructiveness Potential Factor	12
2.1.7	Response Spectrum	13
2.1.8	Modified Mercalli Intensity	16
2.2	Measures of Structural Damage	16
2.2.1	Local Damage Indices	18
2.2.2	Global Damage Indices	25
2.3	Summary	31
3	METHODOLOGY FOR DEVELOPING MOTION-DAMAGE RELATIONSHIPS	33
3.1	General Framework for Motion-Damage Relationships	33
3.2	Fragility and DPM Simulation	37

TABLE OF CONTENTS (Cont'd)

SECTION	TITLE	PAGE
3.3	Characterization of Structural Damage.....	41
3.4	Characterization of Ground Motion.....	44
3.4.1	Models for Simulation of Ground Motion	45
3.4.1.1	Geophysical Models	45
3.4.1.2	Stationary Gaussian Models with Modulating Functions	46
3.4.1.3	ARMA Models	47
3.4.2	Modeling of Uncertainty in Ground Motion	51
3.4.2.1	Uncertainties in Kanai-Tajimi Spectrum	51
3.4.2.2	Uncertainties in Dynamic Amplification Factors	52
3.4.2.3	Moving Window Technique for Estimating ARMA Parameters	55
3.4.2.4	Relationship Between RMS Acceleration and Strong Motion Duration	55
3.4.2.5	Relationship Between Spectral Acceleration and Strong Motion Duration	61
3.4.3	Simulation of Ground Motion	66
3.4.3.1	Simulation of Time Histories with Specified RMS Acceleration and Duration	66
3.4.3.2	Simulation of Time Histories with Specified Spectral Acceleration	73
3.5	Bayesian Technique for Updating Fragility Curves	76
3.6	Summary	78
4	MODELING OF REINFORCED CONCRETE FRAMES FOR FRAGILITY ANALYSIS.....	81
4.1	Ground Motion Characterization for RC Frames	81
4.2	Computation of Section Properties for Damage Evaluation	86
4.2.1	Computation of Ultimate Rotation Capacity of a Section	86
4.2.2	Computation of Yield Moment for a Section.....	89

TABLE OF CONTENTS (Cont'd)

SECTION	TITLE	PAGE
4.3	Evaluation of Structural Damage for Buildings on Firm Sites	90
4.3.1	Description of the Sample Structures	90
4.3.2	Modeling of Uncertainties in Structural Capacities and Demands	92
4.3.3	Structural Modeling in DRAIN-2DX	92
4.3.4	Comparison of DRAIN-2DX with Other Computer Programs.....	97
4.3.4.1	Comparison Between DRAIN-2DX and IDARC.....	97
4.3.4.2	Comparison Between DRAIN-2DX and CU-DYNAMIX	101
4.4	Summary	105
5	FRAGILITY CURVES AND DPMS FOR RC FRAMES.....	107
5.1	Sample Fragility Curves.....	107
5.2	Sample Damage Probability Matrices	111
5.2.1	Relationship Between MMI and Spectral Acceleration.....	113
5.2.2	Comparison of DPMS with those in ATC-13.....	119
5.3	Sensitivity Analysis	121
5.3.1	Sensitivity to Number of Bays	122
5.3.2	Sensitivity to Second Order Effects.....	125
5.3.3	Sensitivity to Site Conditions.....	130
5.4	Relationship Between Damage Caused by Deformation and that by Dissipated Hysteretic Energy	143
5.5	Relationship Between Drift Ratios and Park-Ang Damage Index	145
5.6	Summary	147
6	BAYESIAN UPDATING OF MOTION-DAMAGE RELATIONSHIPS	149
6.1	Randomness and Uncertainty	149

TABLE OF CONTENTS (Cont'd)

SECTION	TITLE	PAGE
6.2	Randomness and Uncertainty in the Response of RC Frames	150
6.2.1	Stiffness and Strength	150
6.2.2	Damping	151
6.2.3	Mass	151
6.2.4	Uncertainty in the Park-Ang Damage Index	152
6.3	Bayesian Updating	152
6.3.1	Estimation of the Likelihood Functions.....	154
6.3.2	Posterior Distribution of the Mean	155
6.4	Bayesian Analysis with Damage Data from Northridge.....	157
6.4.1	Building Inventory	157
6.4.2	Posterior Distribution of the Park-Ang Damage Index	160
6.5	Confidence Bounds on the Fragility Curves	170
6.6	Summary	175
7	CONCLUSIONS AND FUTURE WORK	177
7.1	Conclusions	177
7.2	Future Work	183
8	REFERENCES	187
APPENDIX A COMPUTATION OF MOMENT AND CURVATURE FOR AN EXAMPLE RC SECTION		A-1

LIST OF ILLUSTRATIONS

FIGURE	TITLE	PAGE
2-1	Definition of δ_m in the Park and Ang (1984) index	21
2-2	Damage index definitions by Chung et al. (1987)	24
3-1	Steps in the development of fragility curves and damage probability matrices ..	36
3-2	Steps in the Monte Carlo simulation technique	38
3-3	General probability density function with N intervals used in the Latin hypercube sampling scheme	40
3-4	Parameters of the dynamic amplification factors for firm sites	53
3-5	Comparison of the empirical and fitted probability distributions of DAF at T = 0.5 seconds	53
3-6	Comparison of the empirical and fitted probability distributions of DAF at T = 1.0 seconds	54
3-7	Comparison of the empirical and fitted probability distributions of DAF at T = 1.5 seconds	54
3-8	Comparison of the empirical and fitted probability distributions of DAF at T = 2.0 seconds	55
3-9	Correlation between Trifunac and Brady's (1975) strong motion duration and the RMS acceleration for firm sites with distances to rupture zones less than 50 km	60
3-10	Correlation between Trifunac and Brady's (1975) strong motion duration and the RMS acceleration for firm sites with distances to rupture zones greater than 50 km	61
3-11	Correlation between Trifunac and Brady's (1975) strong motion duration and the average S_a in the period range 0.1-0.5 sec for firm sites	62
3-12	Correlation between Trifunac and Brady's (1975) strong motion duration and the average S_a in the period range 0.5-0.9 sec for firm sites	62

LIST OF ILLUSTRATIONS (Cont'd)

FIGURE	TITLE	PAGE
3-13	Correlation between Trifunac and Brady's (1975) strong motion duration and the average S_a in the period range 0.9-2.5 sec for firm sites	63
3-14	Comparison of the observed and the estimated log normal distribution ($\lambda_{T_s} = 2.391$ and $\xi_{T_s} = 0.331$) of strong motion duration for firm sites	63
3-15	Steps in the simulation of time histories	67
3-16	Representation of the moving-window technique	75
3-17	Comparison of the recorded and simulated spectral shapes	76
4-1	Dynamic amplification factors for firm sites	83
4-2	Normalized spectral velocity curves for firm sites	84
4-3	Relationship between spectral acceleration and velocity for $0.5 \leq T \leq 0.9$ seconds.....	84
4-4	Relationship between spectral acceleration and velocity for $0.9 \leq T \leq 2.5$ seconds.....	85
4-5	Kent and Park's stress-strain relationship for concrete (from Park and Paulay, 1975).....	88
4-6	Plan of the three frames	90
4-7	Elevation of the frames used in the analyses	91
4-8	Two cases used to study the effect of distributed plasticity	93
4-9	Comparison of the interstory drift ratios for the first story of the five story frame.....	95
4-10	Comparison of the overall drift ratios for the five story frame	96
4-11	Comparison of the hysteretic energy dissipation in the first story of the five story frame	96
4-12	Comparison of the overall Park-Ang damage index for the five story frame	97
4-13	Hysteretic parameters in IDARC2D	99

LIST OF ILLUSTRATIONS (Cont'd)

FIGURE	TITLE	PAGE
4-14	Comparison of the Park-Ang damage index for the twelve story frame with no deterioration in the hysteretic behavior	100
4-15	Comparison of the Park-Ang damage index for the twelve story frame with nominal deterioration in the hysteretic behavior	100
4-16	Ground motion time history recorded at Gavilan College in Gilroy during the Loma Prieta earthquake	102
4-17	Lateral displacement at the roof of the five story frame subjected to the ground motion time history recorded at Gavilan College in Gilroy	103
4-18	Lateral displacement at the third floor of the five story frame subjected to the ground motion time history recorded at Gavilan College in Gilroy	103
4-19	Ground motion time history recorded at the UCSC Lab in Santa Cruz during the Loma Prieta earthquake	104
4-20	Lateral displacement at the roof of the five story frame subjected to the ground motion time history recorded at the UCSC Lab in Santa Cruz	104
4-21	Lateral displacement at the third floor of the five story frame subjected to the ground motion time history recorded at the UCSC Lab in Santa Cruz	105
5-1	Comparison of the probability distribution functions for the low rise frame	108
5-2	Comparison of the probability distribution functions for the mid rise frame	109
5-3	Comparison of the probability distribution functions for the high rise frame	109
5-4	Fragility curves for low rise frames	110
5-5	Fragility curves for mid rise frames	110
5-6	Fragility curves for high rise frames	111
5-7	Map showing the MMI contours and the California Strong Motion Instrumentation Program (CSMIP) station numbers (Shakal et al. 1985) for the Morgan Hill earthquake of April 24, 1984 (M_L of 6.2)	114

LIST OF ILLUSTRATIONS (Cont'd)

FIGURE	TITLE	PAGE
5-8	Map showing the MMI contours and the CSMIP station numbers (Shakal et al., 1987) for the Whittier Narrows earthquake of October 1, 1987 (M_L of 6.1)	115
5-9	Map showing the MMI contours and the CSMIP station numbers (Shakal et al., 1989) for the Loma Prieta earthquake of October 18, 1989 (M_L of 7.0 and M_S of 7.1)	116
5-10	Map showing the MMI contours and the United States Geological Survey (USGS) station numbers (Maley et al., 1989) for the Loma Prieta earthquake of October 18, 1989, (M_L of 7.0 and M_S of 7.1)	117
5-11	Relationships for the mean, median, standard deviation, and conditional probability distribution functions of S_a at given MMI, for $0.1 \leq T \leq 0.5$ seconds.....	118
5-12	Relationships for the mean, median, standard deviation, and conditional probability distribution functions of S_a at given MMI, for $0.5 \leq T \leq 0.9$ seconds.....	118
5-13	Relationships for the mean, median, standard deviation, and conditional probability distribution functions of S_a at given MMI, for $0.9 \leq T \leq 2.5$ seconds.....	119
5-14	Plan of the three bay, five story frames.....	123
5-15	Comparison of the overall drift ratios for the two five story frames	124
5-16	Comparison of the total dissipated hysteretic energies for the two five story frames	124
5-17	Comparison of the Park and Ang damage indices for the two five story frames	125
5-18	Comparison of the overall drift ratio for the one bay, five story frame.....	127
5-19	Comparison of the total dissipated hysteretic energies for the one bay, five story frame	128

LIST OF ILLUSTRATIONS (Cont'd)

FIGURE	TITLE	PAGE
5-20	Comparison of the Park-Ang damage index for the one bay, five story frame...	128
5-21	Comparison of the overall drift ratio for the one bay, twelve story frame	129
5-22	Comparison of the total dissipated hysteretic energies for the one bay, twelve story frame.....	129
5-23	Comparison of the Park-Ang damage index for the one bay, twelve story frame.....	130
5-24	Dynamic amplification factors for soil sites.....	131
5-25	Comparison of the mean dynamic amplification factors for firm and soil sites .	135
5-26	Comparison of the overall drift ratio for the one bay, two story frame subjected to ground motions recorded on firm and soil sites	135
5-27	Comparison of the total dissipated hysteretic energies for the one bay, two story frame subjected to ground motions recorded on firm and soil sites	136
5-28	Comparison of the Park-Ang damage index for the one bay, two story frame subjected to ground motions recorded on firm and soil sites	136
5-29	Dynamic amplification factors for rock sites	138
5-30	Comparison of the mean dynamic amplification factors for different sites	138
5-31	Comparison of the overall drift ratio for the one bay, two story frame subjected to ground motions recorded on firm and rock sites	139
5-32	Comparison of the total dissipated energy for the one bay, two story frame subjected to ground motions recorded on firm and rock sites	139
5-33	Comparison of the overall Park-Ang damage index for the one bay, two story frame subjected to ground motions recorded on firm and rock sites	140
5-34	Comparison of the overall drift ratio for the one bay, five story frame subjected to ground motions recorded on firm and rock sites	140
5-35	Comparison of the total dissipated energy for the one bay, five story frame subjected to ground motions recorded on firm and rock sites	141

LIST OF ILLUSTRATIONS (Cont'd)

FIGURE	TITLE	PAGE
5-36	Comparison of the overall Park-Ang damage index for the one bay, five story frame subjected to ground motions recorded on firm and rock sites	141
5-37	Comparison of the overall drift ratio for the one bay, twelve story frame subjected to ground motions recorded on firm and rock sites	142
5-38	Comparison of the total dissipated energy for the one bay, twelve story frame subjected to ground motions recorded on firm and rock sites	142
5-39	Comparison of the overall Park-Ang damage index for the one bay, twelve story frame subjected to ground motions recorded on firm and rock sites	143
5-40	Relative contributions of the two terms in the Park-Ang damage index for the low rise frame	144
5-41	Relative contributions of the two terms in the Park-Ang damage index for the mid rise frame	144
5-42	Relative contributions of the two terms in the Park-Ang damage index for the high rise frame	145
5-43	Relationship between the overall drift ratio and the overall Park-Ang damage index for the low rise frame.....	146
5-44	Relationship between the overall drift ratio and the overall Park-Ang damage index for the mid rise frame	146
5-45	Relationship between the overall drift ratio and the overall Park-Ang damage index for the high rise frame.....	147
6-1	Variability of the coefficient of variation of the Park-Ang damage index for the low rise frame at different levels of ground motion	153
6-2	Variability of the coefficient of variation of the Park-Ang damage index for the mid rise frame at different levels of ground motion	153

LIST OF ILLUSTRATIONS (Cont'd)

FIGURE	TITLE	PAGE
6-3	Variability of the coefficient of variation of the Park-Ang damage index for the high rise frame at different levels of ground motion.....	154
6-4	Geographical location of about 1240 RC frame buildings in the city of Los Angeles.....	158
6-5	Geographical location of all 35 yellow-tagged RC frame buildings in the city of Los Angeles.....	159
6-6	Geographical location of all 22 red-tagged RC frame buildings in the city of Los Angeles.....	159
6-7	Spectral acceleration contours from the Northridge earthquake for the east-west component at $T = 0.3$ seconds; the contours are spaced at an interval of $0.05g$ and the value of the innermost contour is $1.4g$	161
6-8	Spectral acceleration contours from the Northridge earthquake for the north-south component at $T = 0.3$ seconds; the contours are spaced at an interval of $0.05g$ and the value of the innermost contour is $1.4g$	161
6-9	184 low rise, ductile RC frame buildings and the average spectral acceleration contours from the Northridge earthquake at $T = 0.3$ seconds; the contours are spaced at an interval of $0.05g$ and the value of the innermost contour is $1.4g$...	162
6-10	Seventeen low rise, ductile RC frame buildings for which damage was observed and the average spectral acceleration contours from the Northridge earthquake at $T = 0.3$ seconds; the contours are spaced at an interval of $0.05g$ and the value of the innermost contour is $1.4g$	162
6-11	Mapping of damage factor to the Park-Ang damage index.....	165
6-12	Updated fragility curves for low rise frames.....	169
6-13	90% confidence bounds and the median fragility curves for <i>Minor</i> and <i>Severe</i> damage states for low rise frames.....	172

LIST OF ILLUSTRATIONS (Cont'd)

FIGURE	TITLE	PAGE
6-14	90% confidence bounds and the median fragility curves for <i>Moderate</i> and <i>Collapse</i> damage states for low rise frames	172
6-15	90% confidence bounds and the median fragility curves for <i>Minor</i> and <i>Severe</i> damage states for mid rise frames	173
6-16	90% confidence bounds and the median fragility curves for <i>Moderate</i> and <i>Collapse</i> damage states for mid rise frames	173
6-17	90% confidence bounds and the median fragility curves for <i>Minor</i> and <i>Severe</i> damage states for high rise frames	174
6-18	90% confidence bounds and the median fragility curves for <i>Moderate</i> and <i>Collapse</i> damage states for high rise frames	174
A-1	Details of the example section	A-1
A-2	Stress-strain relationship for reinforcing steel	A-2

LIST OF TABLES

TABLE	TITLE	PAGE
3-I	Park and Ang's damage index for different damage states	42
3-II	Chung, Meyer and Shinozuka's (1987) damage index for different damage states as defined by Hatamoto et al. (1990)	42
3-III	Trifunac and Brady's (1975) strong motion duration and the RMS acceleration values for the Loma Prieta, Whittier Narrows, and Morgan Hill earthquakes for sites with distances to rupture zones less than 50 km	58
3-IV	Trifunac and Brady's (1975) strong motion duration and the RMS acceleration values for the Loma Prieta and Whittier Narrows earthquakes for sites with distances to rupture zones greater than 50 km	59
3-V	Parameters for the estimation of the mean and the variance of the conditional strong motion duration given the RMS acceleration	60
3-VI	Average spectral acceleration and MMI values for the Loma Prieta, Whittier Narrows, and Morgan Hill earthquakes	64
4-I	Average spectral acceleration values for the Landers, Petrolia, and Northridge earthquakes	82
5-I	Damage probability matrix for the sample low rise building	112
5-II	Damage probability matrix for the sample mid rise building	112
5-III	Damage probability matrix for the sample high rise building	112
5-IV	Mapping of ATC-13 damage states to those used in this study	120
5-V	ATC-13 DPM for low rise, ductile moment resisting frames	120
5-VI	ATC-13 DPM for mid rise, ductile moment resisting frames	121
5-VII	ATC-13 DPM for high rise, ductile moment resisting frames	121
5-VIII	Average spectral acceleration values for ground motions recorded on soil sites ..	132

LIST OF TABLES (Cont'd)

TABLE	TITLE	PAGE
6-I	Estimated distributions for geometrical properties of beams (from Mirza and Macgregor, 1979).....	151
6-II	Estimated distributions for column dimensions (from Mirza and Macgregor, 1979).....	151
6-III	Whitman et al.'s relationship between damage factors and damage states	163
6-IV	Total number of low rise RC frame buildings at different levels of ground motion.....	166
6-V	Geographical locations, spectral accelerations, and the estimated Park-Ang damage indices for the low rise frames for which damage was observed	167
6-VI	Logarithmic standard deviation (assumed deterministic) of the Park-Ang damage index for the low rise frames when subjected to different levels of ground motion.....	167
6-VII	Parameters of the prior distribution of the mean of the logarithm of the Park-Ang damage index for the low rise frames when subjected to different levels of ground motion.....	168
6-VIII	Parameters of the posterior distribution of the mean of the logarithm of the Park-Ang damage index for the low rise frames at different levels of ground motion.....	169
6-IX	Median and logarithmic standard deviations of the median and the bounding fragility curves for low rise frames	171
6-X	Median and logarithmic standard deviations of the median and the bounding fragility curves for mid rise frames	171
6-XI	Median and logarithmic standard deviations of the median and the bounding fragility curves for high rise frames	171

LIST OF SYMBOLS

$a(t)$	ground acceleration at time t
A_n	amplitude of n^{th} sinusoid
b''	width of concrete core measured to outside of hoops
d	diameter of reinforcing bar
D_T	Park and Ang global damage index
D_g	Chung, Meyer and Shinozuka's global damage index
E_n	normalized dissipated energy
e_k	stationary discrete white-noise process
f_c	stress in concrete
f_{yh}	yield strength of confining steel
g	acceleration due to gravity
I_H	Housner's spectral intensity
I	Arias intensity
$I(t)$	envelope function
P_{ik}	probability of reaching damage state d_i at ground motion level y_k
P_{ik}	probability of reaching or exceeding damage state d_i at ground motion level y_k
Q_y	yield strength of an element
S_0	intensity of white noise excitation at bedrock
s_b	spacing of hoops
T_d	total duration of the earthquake
T_s	strong motion duration
T	natural period of a structure
T_0	initial natural period of a structure
T_{\max}	maximum natural period of an equivalent linear system
w_{\max}	maximum crack width

LIST OF SYMBOLS (Cont'd)

ε_c	strain in concrete
ε_s	strain in tensile reinforcement
ε_{sm}	strain in reinforcement at maximum tensile stress
ρ	correlation coefficient
ρ_s	volumetric ratio of transverse reinforcement
ϕ_{max}	maximum curvature
ϕ_y	yield curvature
ϕ_n	Phase angle of n^{th} sinusoid
μ_θ	Rotation ductility
μ_ϕ	Curvature ductility
$\Psi(t)$	Envelope function
σ_0	Root mean square acceleration
θ_{max}	Maximum rotation
θ_y	Yield rotation
ϕ_1, ϕ_2, θ_1	ARMA parameters
δ_m	Maximum response under earthquake
δ_u	Ultimate deformation capacity under monotonic loading
δ_M	Dipasquale and Cakmak's maximum softening index
ω_g	Predominant ground natural frequency
ω_n	Frequency of n^{th} sinusoid
ξ_g	Effective damping coefficient of the ground
λ_{RMS}	Expected value of $\text{Ln}(\text{RMS})$

SECTION 1

INTRODUCTION

Earthquakes can have a seriously negative impact on society by causing human suffering and economic losses due to building damage. Earthquakes affect structures in various ways which include damage to structural elements as well as nonstructural components and contents. The main structural components affected are those of the lateral load resisting system. Nonstructural components include exterior curtain walls, interior partition walls, and mechanical and electrical equipment. Nonstructural damage can occur even at low levels of ground shaking when there is little or no structural damage. While nonstructural components are important, this study is confined to evaluating structural damage as a result of earthquakes.

1.1 Background

Disaster planning and post-earthquake rehabilitation decisions require estimation of structural damage. Information on structural damage is of critical importance for reliable economic loss evaluation for a structure or a region that has been or that might be affected by an earthquake. The extent of structural damage is also important in determining expected casualties from collapsed buildings or from falling debris. Relationships between earthquake ground motion severity and structural damage along with seismic site hazard analysis can be used to assess structural damage, casualties, and subsequent long term economic losses due to earthquakes. Planners can use estimates of structural damage before the occurrence of an earthquake to predict the likely extent of building damage, economic loss, and number of casualties. Damage estimates immediately after an earthquake can be used by emergency response planners to assess vulnerability of a structure to aftershocks and to decide whether the building is safe to enter or not. Post-earthquake rehabilitation decisions require estimates of structural damage to decide whether to repair or to demolish a damaged structure. Estimates of structural damage are used by governmental agencies and large corporations in the prioritization process for retrofit of a large stock of structures. This prioritization of structures is needed as in reality there may be a limited stream of funds over a long time period.

Designers can use motion-damage relationships to evaluate the performance levels of structures. The different performance levels of a structure include serviceability, prevention of casualties, and prevention of collapse of the structure. The serviceability performance level may include immediate occupancy of the building or limited damage. Immediate occupancy of a building is required for emergency response centers and hospitals. Knowing the expected ground motion and the motion-damage relationships for different structural classes, a designer can choose a structural system that fulfills the specified performance requirements.

Relationships between earthquake ground motion severity and structural damage are most frequently used to characterize the damage distribution over a region. These motion-damage relationships are in the form of probability distributions of damage at specified ground motion intensities and are usually expressed in terms of fragility curves or damage probability matrices (DPMs). Currently there are only two studies that provide DPMs (ATC-13, 1985) and fragility curves (NIBS, 1995) for a wide variety of structural classes. The DPMs in ATC-13 are based on expert opinion since actual damage data are very limited. The fragility curves in the standardized earthquake loss estimation methodology (NIBS, 1995) are based on interpretation of test data and engineering judgment.

Fragility curves and DPMs describe the conditional probabilities of sustaining different degrees of damage at given levels of ground motion. Thus, the development of fragility curves and DPMs requires the characterization of the ground motion and the identification of the different degrees of structural damage. Earthquake ground motion amplitude, frequency content, and strong motion duration are some important characteristics that affect structural response and damage. Thus, they need to be taken into consideration in the development of fragility curves and DPMs. Reliable damage estimation requires sufficient information on the degree of structural damage. Structural damage is caused by the maximum inelastic deformation as well as by the cumulative inelastic deformation under repeated stress reversals.

1.2 Objectives

The objective of this study is to develop a methodology for obtaining relationships between ground motion and structural damage for different types of structures. This methodology is then applied to develop motion-damage relationships for reinforced concrete structures. The formulation of motion-damage relationships is based on analytical models, in contrast to the currently available motion-damage relationships which are subjective in nature. This objective is achieved through the following steps:

- Identification of suitable ground motion parameters,
- Identification of different damage states based on suitable structural response parameters,
- Evaluation of the probability of a concrete structure being in different damage states,
- Parametric study of the motion-damage relationships for different structural attributes, and
- Application of the Bayesian technique to update the analytical motion-damage relationships by incorporating information on buildings damaged during past earthquakes.

1.3 Scope

This study presents a systematic approach for developing motion-damage relationships that does not rely either on heuristics or on empirical data. Instead, the probability of damage is estimated by quantifying the response of a structure subjected to a significant ensemble of ground motions with a wide range of parameter variations. For this purpose, a Monte Carlo simulation approach is used to determine the probabilities of structural damage, and the ensemble of ground motions is generated using an appropriate model for ground motion simulation. The models for ground motion simulation include the stationary Gaussian model with modulating function and the autoregressive moving average (ARMA) models. This methodology is then applied to obtain fragility curves and DPMS for reinforced concrete moment resisting frames located on firm soils. Damage due to landslides and liquefaction is not considered in the development of the motion-damage relationships for reinforced concrete frames. Only damage due to ground motion is included.

Reinforced concrete frames are divided into three classes based on the number of stories in the frames. These include low rise concrete frames that are 1-3 stories tall, mid rise frames that are 4-7 stories tall, and high rise frames that are 8 stories or taller. This classification is the same as that defined in ATC-13 (1985) and similar to that used in the standardized earthquake loss estimation methodology (NIBS, 1995). The ground motion for these three classes of frames is characterized by spectral acceleration over period bands corresponding to the three classes of frames. Fragility curves and DPMs are developed for these three classes of structures. Parametric studies are performed to assess the effect of geometric variations in the performance of concrete frame structures.

1.4 Organization of the Report

The first part of Section 2 reviews the various parameters used to characterize ground motion levels. In this study, the ground motion is characterized by spectral acceleration and modified Mercalli intensity (MMI). Spectral acceleration is chosen to characterize the ground motion as it is a simple parameter and can easily be used in regional damage evaluation. Furthermore, spectral acceleration provides an approximate estimate of the input seismic energy. MMI is used for developing the DPMs. The second part of this section describes the various damage measures. Cumulative damage measures are preferred as structural damage is believed to be caused by high stress excursions as well as repeated stress reversals. Most of the damage indices have been formulated by assuming that the failure in the structural components is governed by flexural behavior. Since it is beyond the scope of this study to develop a new damage index or to modify an existing damage index, shear behavior is assumed not to influence significantly the damage in building structures considered for the development of motion-damage relationships in this study.

Section 3 presents a method for the development of fragility curves. In contrast to previous approaches for developing fragility curves and DPMs, the method presented in this section does not rely on heuristics or on empirical data. The methodology can be applied to a wide range of structural classes. The methodology is presented for two ground motion parameters: spectral

acceleration and root mean square acceleration. However, it is possible to use other ground motion parameters presented in Section 2. The Monte Carlo simulation approach is adopted to determine the probabilities of structural damage. The Latin hypercube sampling technique is employed to reduce the number of simulation cycles.

Section 3 also presents the estimation of the different damage states for reinforced concrete frames, based on the different damage measures. This study adopts an equivalent form of the Park and Ang damage index to represent structural damage (Bertero and Bertero, 1992). The Park and Ang index is used because it is simple in its computation and because it has been calibrated using experimental data. Estimating structural repair cost due to an earthquake is an important aim of damage evaluation. Such an estimation for reinforced concrete frames can be achieved if information on crack sizes and extent, degree of crushing and spalling, and accumulated strain in reinforcing steel is available. In Section 3 a new method is proposed for defining the damage states in terms of crack width.

Furthermore, earthquake ground motion time histories are needed for the analysis. Although there are a large number of recordings obtained from recent earthquakes, a consistent ensemble of time histories that cover all the different parameter ranges that can be discriminated according to distance to the fault, local soil parameters, and spectral characteristics is currently not available. Thus, it is proposed that ensembles of time histories be simulated at each specified ground motion parameter level. A summary of the different simulation techniques is presented in Section 3.

Section 4 presents the modeling of reinforced concrete frames for the development of motion-damage relationships. The ground motion is characterized by spectral values in the period bands corresponding to the three classes of reinforced concrete frames. The period bands for the three classes of frames are identified, and the relationship between the average spectral acceleration and the average spectral velocity is investigated for the mid rise and the high rise frames. This section also describes the modeling of uncertainties in system parameters. The randomness in structural demand and capacities are presented.

Sample structures for the three classes of frames are used to develop the motion-damage relationships. The structural modeling in the computer programs for evaluating the nonlinear response is discussed. This study uses DRAIN-2DX (Prakash and Powell, 1992) for performing the nonlinear dynamic analysis. The results from DRAIN-2DX are compared with those from IDARC2D (Kunnath and Reinhorn, 1994) and CU-DYNAMIX (El-Tawil, 1996).

Section 5 presents the motion-damage relationships in terms of fragility curves and DPMs for special moment resisting reinforced concrete frames located on firm sites. The relationships between spectral acceleration in the three period bands and MMI are developed in this section. These relationships are used to obtain the DPMs from the fragility curves.

In addition, Section 5 also summarizes the results of the sensitivity analyses carried out to study the influence of the different structural attributes on the nonlinear dynamic behavior of structures. These sensitivity analyses are carried out to study how structural damage is affected by the different structural attributes. The structural attributes included in the sensitivity studies are the number of bays in a structure, the second-order effects, and the site conditions.

Section 6 presents the Bayesian technique that enables the incorporation of observed damage data with fragility curves. The uncertainties associated with the motion-damage relationships are also discussed in this section. Such uncertainties can be reduced by incorporating observed damage data in the development of fragility curves. Using damage data from the Northridge earthquake, Section 6 presents the updated fragility curves for low rise frames presented in Section 5. In addition, the uncertainties in the motion-damage relationships are presented as confidence bounds on the fragility curves.

Section 7 enumerates the conclusions of this study and the recommendations for future work.

SECTION 2
REVIEW OF PARAMETERS FOR CHARACTERIZATION OF GROUND MOTION
AND STRUCTURAL DAMAGE

Reliable damage estimation and rehabilitation decisions require information on the degree of structural damage. The motion-damage relationships are usually expressed in terms of fragility curves and damage probability matrices (DPMs). Fragility curves and DPMs describe the conditional probability of a structure reaching a particular damage state at a given level of ground motion. One must characterize ground motion and identify damage states in order to evaluate these conditional probabilities.

This section first reviews the various earthquake ground motion parameters that can be correlated to structural damage. Then, the different indices available to describe structural damage are discussed. Structural damage indices are used to identify the different damage states of a structure.

2.1 Ground Motion Characterization

It is difficult to determine a single parameter that best characterizes earthquake ground motion. Recorded time histories, even at the same site, show variations in details. Earthquake ground motion amplitude, frequency content, duration, and the number of peaks in the time history above a certain amplitude are some of the characteristics important for determining structural response and damage. Ground motion amplitude is measured in terms of acceleration, velocity and displacement. The frequency content of an earthquake time history is important in identifying the amount of energy imparted at different frequencies. The strong motion duration of an earthquake time history is the time interval during which most of the energy of that time history is contained. Various measures of strong motion duration are presented in Section 2.1.1.

Numerous parameters have been used to relate ground motion to the degree of damage sustained by a structure. Peak ground acceleration (PGA) has frequently been used as a parameter to

characterize ground motion. Other parameters include Housner's spectral intensity, Arias intensity, root mean square (RMS) acceleration, response spectrum, and modified Mercalli intensity (MMI).

This study uses response spectrum and MMI as the parameters to characterize earthquake ground motion. Although only these two parameters are used in this study, the methodology for developing motion-damage relationships, which is presented in Section 3, can be generalized to any ground motion parameter discussed in this section.

2.1.1 Strong Motion Duration

Several measures of strong motion duration have been discussed in the literature. The different definitions of strong motion duration include those by Bolt (1973), Trifunac and Brady (1975), McCann and Shah (1979), and Vanmarcke and Lai (1980). The Trifunac and Brady (1975) definition of strong motion duration is used in this study as it is based on the concept of cumulative energy. The Trifunac and Brady strong motion duration is the time interval required to accumulate 90 percent of the total energy.

The following two equations represent the time at which the Trifunac and Brady strong motion starts, T_1 , and the time at which the strong motion ends, T_2 :

$$\int_0^{T_1} a^2(t) dt = 0.05 \int_0^{T_d} a^2(t) dt \quad (2.1)$$

and

$$\int_0^{T_2} a^2(t) dt = 0.95 \int_0^{T_d} a^2(t) dt \quad (2.2)$$

where:

T_d = total duration of the earthquake and

$a(t)$ = ground acceleration at time t .

Trifunac and Brady's strong motion duration is thus given as:

$$T_s = T_2 - T_1 \quad (2.3)$$

The strong motion duration is needed for evaluating the root mean square acceleration (discussed in Section 2.1.5).

2.1.2 Ground Motion Amplitude

The parameters used to describe ground motion amplitude include PGA, peak ground velocity (PGV), and peak ground displacement (PGD). As the inertia forces depend directly on acceleration, peak ground acceleration is one of the parameters widely used to describe the intensity and damage potential of an earthquake at a given site. However, PGA is a poor indicator of damage, as time histories with the same PGA could be very different in frequency content, strong motion duration, and energy level, thus causing varying amounts of damage. A large recorded PGA associated with a short duration impulse will cause less damage than a more moderate PGA associated with a long-duration impulse. Therefore, PGA represents only a single amplitude and does not incorporate any of the other characteristics considered to be important for damage evaluation.

A better representation of the ground motion can be achieved by using the relationships between the peak ground motion parameters. Mohraz (1976) used two ratios: the ratio of PGV to PGA, v/a , and the ratio of the product of PGA and PGD to the square of PGV, ad/v^2 . Mohraz concluded that the v/a ratios for rock are substantially lower than those for alluvium.

Zhu et al. (1988) suggest that the ratio of PGA to PGV (a/v) provides information on the frequency content and the strong motion duration of the ground motion. They show that ground

motions with a high frequency content correspond to high a/v ratios, whereas those with long-duration acceleration pulses are associated with low a/v ratios. The a/v ratios are high for sites close to the earthquake source and low for sites far from the source. Ground motions at moderate distances from the source have intermediate a/v ratios. The variation of the a/v ratio with distance is due to the attenuation of the ground motion velocity being slower than the attenuation of ground motion acceleration.

Zhu et al. (1988) further investigated the effect of the a/v ratio on structural damage. They found that the effect of the a/v ratio on damage sustained by different systems depends on the period and the yield strength level of the structure. Flexible systems with low yield strength show significantly different behavior for different a/v ratios. They found that for systems with low yield strength, the decrease in ductility demands, with increase in period, is more significant for records with high a/v ratio than for records with low a/v ratio. They also found that since ground motions with low a/v ratio tend to have longer strong motion durations, they impose larger hysteretic energy demands on the system compared to ground motions with high a/v ratios.

2.1.3 Housner's Spectral Intensity

Housner (1952) defined a measure for expressing the relative severity of earthquakes in terms of the area under the pseudo-velocity spectrum between 0.1 and 2.5 seconds. Housner's spectral intensity can be defined by the following equation:

$$I_H = \int_{0.1}^{2.5} S_v(T, \xi) dT = \frac{1}{2\pi} \int_{0.1}^{2.5} S_a(T, \xi) T dT \quad (2.4)$$

where:

$S_v(T, \xi)$ = pseudo-velocity at undamped natural period T and damping ratio ξ and

$S_a(T, \xi)$ = pseudo-acceleration at undamped natural period T and damping ratio ξ .

Thus, Housner's spectral intensity is the first moment of the area of S_a ($0.1 \leq T \leq 2.5$ sec) about the S_a axis, implying that the Housner spectral intensity is larger for ground motions with a significant amount of low frequency content. Therefore, ground motions with larger Housner's spectral intensity could cause more damage to tall structures. Housner's spectral intensity, however, does not provide information on the strong motion duration.

2.1.4 Arias Intensity

Arias (1970) defined the intensity, I , of an earthquake as the sum of the energy input (per unit weight) into all linear single degree of freedom oscillators having different periods. Thus

$$I = \int_0^{\infty} E \, d\omega \quad (2.5)$$

where:

E = energy input by the earthquake ground motion into a unit-weight, linear single degree of freedom oscillator and

ω = frequency of the oscillator.

Using Parsevaal's theorem, equation 2.5 can be written as:

$$I = \frac{\pi}{2g} \int_0^{T_d} a^2(t) \, dt \quad (2.6)$$

where:

I = intensity at zero damping,

$a(t)$ = ground acceleration at time t ,

T_d = total duration of earthquake motion, and

g = acceleration due to gravity.

As can be seen from the definition, Arias intensity provides an estimate of the total energy of an earthquake. However, Arias intensity does not incorporate any information on the frequency content and strong motion duration of the earthquake.

2.1.5 Root Mean Square Acceleration

RMS acceleration is a parameter incorporating the total intensity and the strong motion duration. RMS acceleration is defined as

$$\sigma_0 = \left[\frac{1}{T_s} \int_{T_s} a^2(t) dt \right]^{\frac{1}{2}} \quad (2.7)$$

where:

σ_0 = RMS acceleration of the strong ground motion,

T_s = strong motion duration, and

$a(t)$ = ground motion acceleration at time t .

RMS acceleration is a measure of the average rate of energy input to the structure. However, it does not provide any information about the frequency content as it is the sum of input power at all frequencies.

2.1.6 Destructiveness Potential Factor

Araya and Saragoni (1984) proposed the destructiveness potential factor, P_D , that considers both the Arias intensity and the rate of zero crossings, ν_0 . The destructiveness potential factor is defined by the following equation:

$$P_D = \frac{I_A}{v_0^2} \quad (2.8)$$

where:

P_D = destructiveness potential factor,

I_A = Arias intensity, and

v_0 = rate of zero crossings.

The destructiveness potential factor simultaneously considers the effect of the ground motion amplitude, strong motion duration, and frequency content on the relative destructiveness of different ground motion records. The amplitude of ground motion acceleration and strong motion duration are incorporated in the Arias intensity. The frequency content is considered in the rate of zero crossings. Araya and Saragoni (1984) demonstrated that the destructiveness potential correlates very well with the MMI values. However, it is possible that two different time histories could have similar destructiveness potential factors but very different values of the zero crossing rate and Arias intensity. For example, a time history with a small zero-crossing rate would cause less damage to short period structures than a time history with a larger zero crossing rate close to the fundamental period of the structures, although both time histories have the same destructiveness potential factor. Structural damage is determined by seismic energy input into the structure. Thus, the second time history with a larger zero-crossing rate causes more damage as it results in more seismic energy being input into the structures. The concept of input seismic energy is presented in Section 2.1.7.

2.1.7 Response Spectrum

The linear elastic response spectrum represents the maximum acceleration, maximum relative velocity, or maximum relative displacement of a single-degree-of-freedom (SDOF) system subjected to a particular ground motion. Seismic ground motions result in energy being transmitted from the ground into the structure. During an earthquake, the maximum input

energy that is stored in a linear, elastic SDOF system (without including the damping energy) can be estimated as:

$$E = \frac{1}{2}kS_d^2(T, \xi) = \frac{1}{2}mS_{pv}^2(T, \xi) \quad (2.9)$$

where:

E = maximum input energy,

m = mass of the SDOF system,

k = stiffness of the SDOF system,

ξ = damping ratio of the SDOF system,

S_d = spectral displacement ordinate at the natural period of the SDOF system, and

S_{pv} = pseudo-spectral velocity ordinate at the natural period of the SDOF system.

For a nonlinear SDOF system, the seismic energy input into the system by the ground motion can be estimated by integrating the following equation of motion of the system:

$$m\ddot{x}_t + c\dot{x} + f_s = 0 \quad (2.10)$$

where:

m = mass of the SDOF system,

c = viscous damping coefficient of the SDOF system during its excitation,

f_s = restoring force for the SDOF system,

x_t = $x + x_g$ = absolute displacement of the mass,

x = relative displacement of the mass with respect to the ground, and

x_g = earthquake ground displacement.

The restoring force, f_s , for an elastic system may be expressed as kx , where k is the stiffness of the SDOF system. By using the relationship $\ddot{x}_t = \ddot{x} + \ddot{x}_g$, equation 2.10 may be written as:

$$m\ddot{x} + c\dot{x} + f_s = -m\ddot{x}_g \quad (2.11)$$

Uang and Bertero (1990) show that equations 2.10 and 2.11 lead to different values of the input seismic energy. Integrating equation 2.10 with respect to the relative displacement, x , leads to the following equation:

$$\frac{m\dot{x}_t^2}{2} + \int c\dot{x} dx + \int f_s dx = \int m\ddot{x}_t dx_g \quad (2.12)$$

The first term in equation 2.12 represents the absolute kinetic energy, the second term represents the damping energy, and the third represents the recoverable strain energy and the irrecoverable hysteretic energy. The right-hand-side term of equation 2.12 is defined as the absolute input energy.

Integrating equation 2.11 with respect to the relative displacement, x , the following equation is obtained:

$$\frac{m\dot{x}^2}{2} + \int c\dot{x} dx + \int f_s dx = - \int m\ddot{x}_g dx \quad (2.13)$$

The first term in equation 2.13 represents the relative kinetic energy and is different from the first term in equation 2.12 which represents the absolute kinetic energy. The second and third terms of equations 2.12 and 2.13 are the same. The right-hand-side term of equation 2.13 is the relative input energy due to the ground motion. Whereas the absolute input energy represents the physical energy input, the relative input energy ignores the effect of the rigid body translation of the structure. Akiyama (1985) showed that the relative input energy of a SDOF system can provide a good estimate of the input energy for multistory buildings. Uang and Bertero (1990) concluded that the absolute input energy of a SDOF system can be used to estimate the absolute input energy for multistory buildings.

Housner (1956) assumed that the input seismic energy given by equation 2.9 can be used as the energy demand for an inelastic system in his proposed limit design method. Uang and Bertero (1990) compared the energy demand estimated from equation 2.9 and that from equation 2.12 for 5% damping and a ductility ratio of 5 when the structure was subjected to ground motions from the El Centro, Mexico City, and San Salvador earthquakes. Their results indicate that equation 2.9 can significantly underestimate the input seismic energy. Although it would be preferable to use the absolute input seismic energy as the ground motion parameter, the computation of the absolute energy involves the assumption of the ductility capacities of the structures. For regional damage evaluation, the ductility capacities of the structures could vary greatly. Thus, in this study, the linear response spectral values are used to characterize the ground motion. These spectral values provide a lower bound to the energy input due to seismic ground motion.

2.1.8 Modified Mercalli Intensity

The earthquake intensity at a location is a qualitative measure of the size of the earthquake in terms of observed damage and human reactions at that location. The Rossi-Forel scale is one of the earliest measures of intensity (Richter, 1958). The Rossi-Forel scale has mostly been replaced by the MMI scale. The MMI scale was obtained in 1931 by modifications to the original scale proposed by Mercalli (Richter, 1958). MMI is based on the performance of unreinforced masonry buildings, chimneys and some other older construction. The MMI scale is often used to specify the severity of ground shaking in a given geographic region. It is also used to describe the distribution of damage over a region. The main advantage of the MMI scale is that it has been in use for a long time and that some motion-damage relationships exist in terms of the MMI scale (ATC-13, 1985). However, its use is subjective, and differences in interpretation are substantial.

2.2 Measures of Structural Damage

Structural damage occurs when the deformations of structures under environmental loads are large and permanent. The severity and nature of seismic damage depends on the building

material, and the structural configuration. Yao et al. (1986) presented a review of structural damage for different types of buildings. They suggest that structural damage may be defined as a ratio of the demand to the ultimate structural capacity. Extensive studies have been carried to determine the imposed demand, but only limited studies have been carried out to estimate the structural capacity. Structural damage in relatively ductile systems, such as steel frames, depends on the cumulative inelastic deformation. For relatively brittle systems, such as masonry buildings, shear behavior is dominant, and the damage can be expressed in terms of the maximum deformation. The damage in reinforced concrete structures depends on both the maximum inelastic deformation and the cumulative deformation under repeated stress reversals.

Since damage to reinforced concrete structures is caused by stress reversals as well as high stress excursions, more realistic measures of damage include not only the peak inelastic response but also the effect of reversals of inelastic deformations. The earlier ductility-based measures of damage did not account for cumulative damage under repeated cycles of deformation. The more recent measures of damage include the dissipated hysteretic energy to account for cumulative damage.

There are many damage models which characterize the state of structures after earthquakes in terms of a damage index. A damage model is realistic if the numerical value of the damage index shows correlation with observed seismic damage in structures. This correlation can be used to assess damage to structures by first estimating the damage index under a given ground motion. Structural damage is frequently represented by various local and global damage indices which aim to quantify numerically the damage sustained under earthquake loading. The local indices quantify the damage in individual members, and the global indices describe the state of all or a large part of a structure. Most of the damage models first consider the damage to individual structural elements. Global damage is then defined as a combination of the damage to individual elements. Williams and Sexsmith (1995) provide a comprehensive review of the damage measures for reinforced concrete structures.

2.2.1 Local Damage Indices

Local indices are used to express the damage sustained by individual elements, and usually employ the concepts of ductility and dissipated energy. Ductility and interstory drift are the two earliest forms of damage index which are based only on maximum deformation and fail to account for the effects of repeated cycling under seismic loading. However, they are still widely used because of their simplicity and ease of interpretation. The ductility ratio can be expressed in terms of rotation, curvature or displacement. The rotation ductility, μ_θ , is the ratio of the maximum rotation, θ_{max} , to the rotation at yielding, θ_y . The rotation ductility is expressed as follows:

$$\mu_\theta = \frac{\theta_{max}}{\theta_y} \quad (2.14)$$

Banon et al. (1981) suggested that the member can be assumed to yield in antisymmetric bending in order to compute the yield rotation, θ_y . The computation of curvature ductility does not need any assumption on the bending mode of the member as it applies only to a section of the member, usually the section with the maximum stresses. The curvature ductility, μ_ϕ , can be expressed as follows:

$$\mu_\phi = \frac{\phi_{max}}{\phi_y} \quad (2.15)$$

Banon et al. (1981) proposed the flexural damage ratio in an attempt to overcome the shortcomings of the ductility ratios. The flexural damage ratio is defined as the ratio of the initial tangent stiffness to a reduced secant stiffness at maximum deformation. Banon et al. also defined two more measures of damage in order to incorporate damage accumulation due to cyclic loading. These are the normalized cumulative rotation and the normalized dissipated energy. The normalized cumulative rotation is defined as the ratio of the sum of all plastic rotations to yield rotation. The normalized dissipated energy, E_n , is the ratio of the energy

dissipated by inelastic rotation at one end of the member to half of the maximum elastic energy stored in the member in anti-symmetric bending. The normalized dissipated energy is thus given by the following equation:

$$E_n(t) = \frac{\int_0^t M(\tau)\theta d(\tau)}{\frac{1}{2}M_y\theta_y} \quad (2.16)$$

where:

t = time elapsed since the beginning of loading and

$\theta(d\tau)$ = the rotation increment of the inelastic spring at one end of the member during the time interval between τ and $\tau + d\tau$.

For steel components, the damage model proposed by Krawinkler and Zohrei (1983) is often used. There are several models for definitions of local damage in reinforced concrete components. These measures for reinforced concrete include the measures proposed by Park and Ang (1984), by Chung, Meyer and Shinozuka (1987), and by Bracci et al. (1989). These damage indices are discussed in the following paragraphs.

Krawinkler and Zohrei's Damage Index

Krawinkler and Zohrei (1983) proposed a damage model for steel components. Their damage model is given by the following equation:

$$D = C \sum_{i=1}^N (\Delta\delta p_i)^q \quad (2.17)$$

where:

D = damage measure,

C, q = structural performance parameters,

N = number of inelastic excursions caused by the earthquake, and

$\Delta\delta p_i$ = plastic deformation range of excursion i .

The plastic deformation ranges, $\Delta\delta p_i$, in equation 2.17 are estimated by means of the rainflow cycle counting method. In the rainflow cycle counting method, the ranges are usually reordered so that small excursions constitute only interruptions of the larger cycles. Nassar and Krawinkler (1991) show that for bilinear systems, the hysteretic energy, HE, and the sum of the plastic deformation ranges can be related as follows:

$$HE \approx F_y \sum_{i=1}^N \Delta\delta p_i \quad (2.18)$$

Park and Ang's Local Damage Index

Park et al. (1984) proposed a damage index which is a linear combination of the damage caused by excessive deformation and that contributed by repeated cyclic loading effect. The Park and Ang damage index is expressed as follows:

$$D = \frac{\delta_m}{\delta_u} + \frac{\beta}{P_y \delta_u} \int dE \quad (2.19)$$

or

$$D = \frac{\delta_m}{\delta_u} + \beta \int \left(\frac{\delta}{\delta_u} \right)^\alpha \frac{dE}{E_c(\delta)} \quad (2.20)$$

where:

δ_m = maximum response deformation under an earthquake shown in figure 2-1,

- δ_u = ultimate deformation capacity under monotonic loading,
- P_y = calculated yield strength,
- $E_c(\delta)$ = hysteretic energy per cycle at deformation δ ,
- α, β = non-negative parameters,
- δ = amplitude of deformation in each cycle of oscillation, and
- dE = incremental dissipated hysteretic energy.

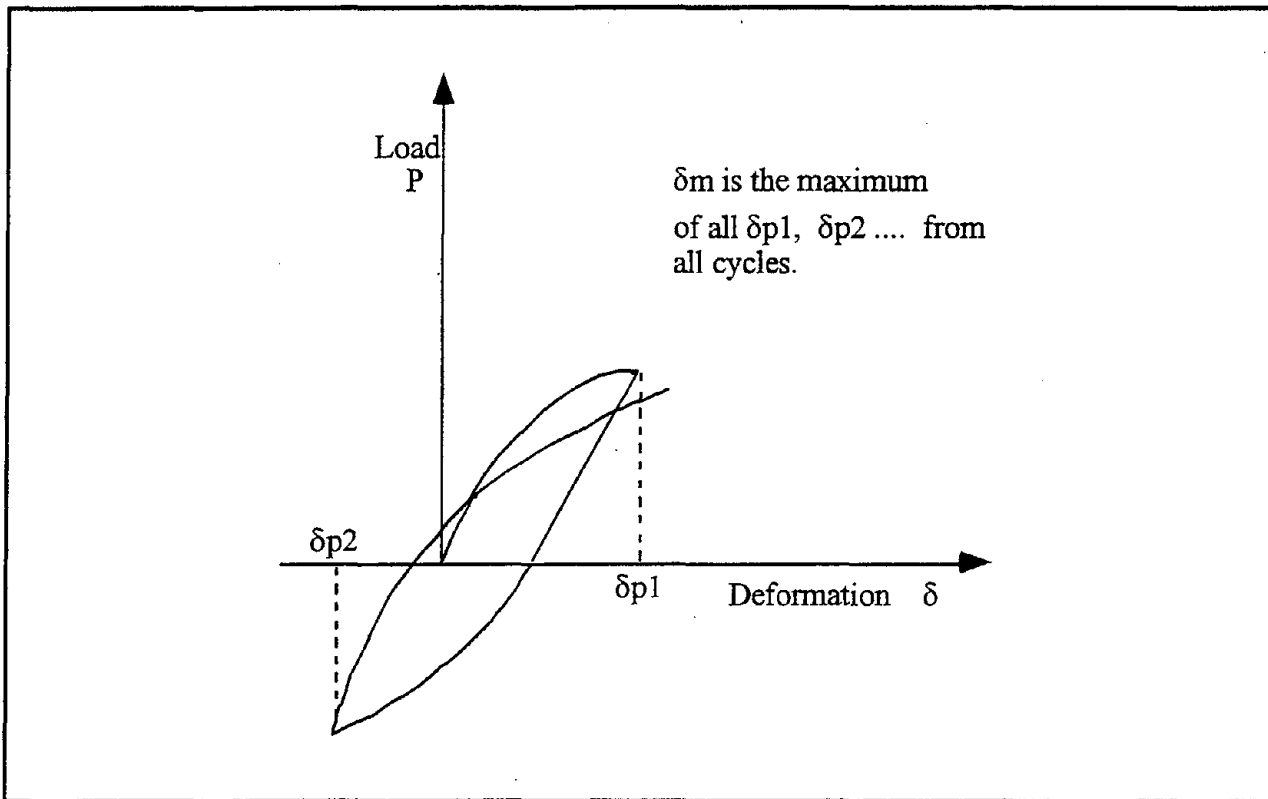


FIGURE 2-1 Definition of δ_m in the Park and Ang (1984) index

The first term in the expression for the damage index (equations 2.19 and 2.20) represents the damage due to maximum deformation experienced during seismic loading, and the second term represents the damage due to cumulative hysteretic energy dissipation. The load deformation terms are shown in figure 2-1, where $\delta_{p1}, \delta_{p2}, \dots, \delta_{pn}$ represent the deformation in each cycle. The parameter δ_m is the maximum of $\delta_{p1}, \delta_{p2}, \dots, \delta_{pn}$ for all the cycles. The deformation at

yield under monotonic loading is represented by δ_y . The damage index, D , is 0 when there is no damage and is 1 for collapse.

The ultimate deformation capacity of a member under monotonic loading, δ_u , is an indicator of the ductility capacity of a member. Reinforced concrete members with about the same level of yield deformation and about the same axial load can have different ultimate deformation values depending on the confinement ratios. The ultimate deformation appears to be more important than the yield deformation in predicting damage. Cosenza et al. (1990) found that the value of $\beta = 0.15$ correlates closely with results based on other damage models. This study uses this value of β .

For reinforced concrete structures, the Park and Ang model has been used widely in recent years because it is simple and because it has been calibrated using data from various structures damaged during past earthquakes. An equivalent form of the Park and Ang index is used in this study (Bertero and Bertero, 1992). The damage index for the plastic hinge locations at the ends of a member is defined as follows:

$$D = \frac{\theta_m}{\theta_u} + \frac{\beta}{M_y \theta_u} \int dE \quad (2.21)$$

where:

- θ_m = maximum positive or negative plastic hinge rotation,
- θ_u = plastic hinge rotation capacity under monotonic loading,
- β = model parameter (0.15 in this study),
- M_y = calculated yield strength, and
- dE = incremental dissipated hysteretic energy.

The damage index for the member is computed as the weighted average of the damage indices at

the ends. The weighted average is computed using equation 2.24 where the weighting factor λ_i is the ratio of the energy dissipated at end i to the sum of the energies dissipated at the two ends.

Chung, Meyer and Shinozuka's Local Damage Index

Chung et al. (1987) proposed a damage index which combines a modified version of Miner's Hypothesis with damage modifiers that reflect the effect of the loading history. This index considers the difference in response of members to positive and negative moments and is evaluated by the following expression. The terms in this index are shown in figure 2-2.

$$D_e = \sum_i \left(\alpha_i^+ \frac{n_i^+}{N_i^+} + \alpha_i^- \frac{n_i^-}{N_i^-} \right) \quad (2.22)$$

where:

i = indicator of displacement or curvature level,

N_i = $\frac{M_i - M_{fi}}{\Delta M_i}$ = number of cycles to cause failure at curvature level i,

n_i = number of cycles actually applied at curvature level i,

α_i = damage modifier,

M_i = initial strength at curvature level i,

M_{fi} = final strength at curvature level i,

ΔM_i = strength drop at curvature level i, in a single load cycle, and

+, - = loading and unloading, respectively.

The effect of loading history is taken into account by damage modifier, α_i , which for positive moment loading is defined as:

$$\alpha_i^+ = \frac{\sum k_{ij}^+}{n_i^+ \bar{k}_i^+} \cdot \frac{\phi_i^+ + \phi_{i-1}^+}{2\phi_i^+} \quad (2.23)$$

where:

$$k_{ij}^+ = \frac{M_{ij}^+}{\phi_i^+} = \text{stiffness during the } j^{\text{th}} \text{ cycle up to load level } i,$$

$$\bar{k}_i^+ = \frac{1}{N_i^+} \sum_{j=1}^{N_i^+} k_{ij}^+ = \text{average stiffness during } N_i^+ \text{ cycles up to load level } i, \text{ and}$$

$$M_{ij}^+ = M_{i1}^+ - (j-1)\Delta M_i^+ = \text{moment reached after } j \text{ cycles up to load level } i.$$

For negative loading, the damage modifier is defined similarly. The damage index definition by Chung et al. does not explicitly account for the damage caused by the maximum deformation experienced by the element.

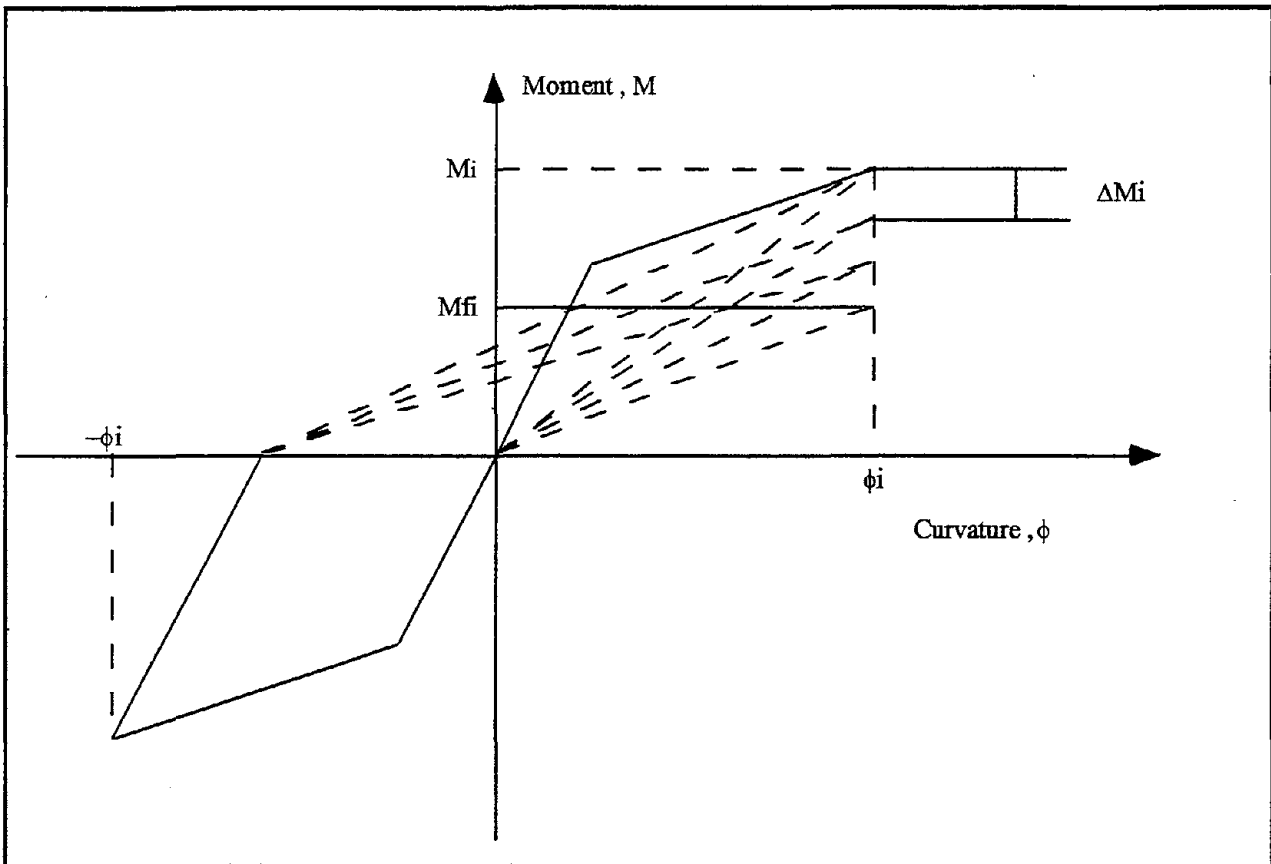


FIGURE 2-2 Damage index definitions by Chung et al. (1987)

Bracci et al.'s Local Damage Index

Bracci et al. (1989) defined a damage index in terms of the ratio of the damage consumption to the damage potential of a component. The damage potential is defined as the total area between the monotonic load-deformation curve and the fatigue failure envelope. The damage consumption occurs due to strength damage and deformation damage. Strength damage is caused by strength deterioration and dissipated hysteretic energy. Strength damage results in the lowering of the upper-bound load-deformation curve. Strength damage is determined as the area between the upper-bound curve and the monotonic load-deformation curve. Deformation damage occurs due to irrecoverable permanent deformations.

2.2.2 Global Damage Indices

Global damage indices provide information about the damage to the overall structure. When a structure is statically determinate, local damage at the most damaged member is enough to determine the damage state of the entire structure. However, a global damage index which accounts for the extent and distribution of localized damage is required for redundant structures. A global damage index can be obtained either by computing a weighted average of the local damage indices for all the members of a structure or by considering some overall structural characteristic like the modal periods. The different types of global damage indices are described below.

Park and Ang's Global Damage Index

Park and Ang's (1984) global damage index is defined as a weighted average of the local damage indices of each element. The weighting function for each element is proportional to the energy dissipated in the element. The global damage index is thus given by the following equation:

$$D_T = \sum_{i=1}^N \lambda_i D_i \quad (2.24)$$

where:

$$\lambda_i = \frac{E_i}{\sum_{i=1}^N E_i},$$

N = number of elements, and

E_i = energy dissipated in element i .

In addition to the overall damage index, story-level damage indices can also be obtained by using equation 2.24 except that the summation in that equation is carried out over all the members of that story. The story-level damage indices can be used to identify the story with the highest damage.

The global damage index, as defined by equation 2.24, does not properly account for the local concentration of damage. It is possible for a few structural members of the building to have undergone severe damage without the global index reflecting it. However, in general, the locations having high damage indices will also be the ones that dissipate large amounts of hysteretic energy. Therefore, equation 2.24 assigns higher weighting to the more heavily damaged members of the structure. Thus, the structure damage index reflects the state of the most heavily damaged members in the structure.

Chung, Meyer and Shinozuka's Global Damage Index

Chung et al. (1987) used the damage index from each story to define the global damage index. The story damage index is obtained as a weighted average of the local damage indices of all elements in the story, with the energy dissipated in the member as the weighting function. The story damage index is obtained by the following equation:

$$D_{sk} = \frac{\sum_{i=1}^n D_i^k E_i^k}{\sum_{i=1}^n E_i^k} \quad (2.25)$$

where:

D_i^k = local damage at location i on story k ,

E_i^k = energy dissipated at location i on story k , and

n = number of locations at which the local damage is computed for story k .

This definition of the story damage index is similar to the definition of the Park and Ang global damage index provided by equation 2.24. However, the local damage indices D_i and D_i^k in equations 2.24 and 2.25 are the respective local damage indices.

The global damage index is obtained as a weighted average of the story damage indices using a triangular weighting function with the maximum at the base. Thus, the global damage index is given by the following equation:

$$D_g = \sum_{k=1}^N D_{sk} I_k \quad (2.26)$$

where:

$I_k = \frac{N+1-k}{N}$ = weighting factor for story k and

N = number of stories

Bracci et al.'s Global Damage Index

Bracci et al. (1989) presented a global damage index in terms of the local damage index by means of the following equation:

$$D_g = \frac{\sum w_i D_i^{(m+1)}}{\sum w_i D_i^m} \quad (2.27)$$

where:

D_g = global damage index,

D_i = local damage index,

w_i = importance factor for component i , and

m = control weighting factor for component i .

A high value of the exponent, m , results in more emphasis on the most severely damaged elements. Bracci et al. (1989) defined the weight w_i as the gravity load supported by element i divided by the total weight of the structure. Thus, damage to the columns is assigned larger weights than those to the beams, and the damage at the base of the structure is assigned a much larger weighting factor than damage to the upper stories.

Softening Damage Indices

Softening damage indices relate the changes in the first few natural periods of a structure to the level of damage sustained by the structure. Roufaiel and Meyer (1987) proposed a relationship between a global damage parameter, expressed in terms of deflections at the roof level of a structure, and the change in fundamental frequency of the structure given by the following equation:

$$D = \frac{\delta_r - \delta_y}{\delta_f - \delta_y} = \frac{14.2\delta_y(\sqrt{\omega_e / \omega} - 1)}{\delta_f - \delta_y} \quad (2.28)$$

where:

δ_r = maximum roof deflection under earthquake excitation,

δ_y = roof displacement at which the first member of the structure reaches yield strength, assuming the frame displaces in its first mode only,

δ_f = roof deflection at which the structure is assumed to fail,

ω_e = fundamental frequency of the undamaged or elastic structure, and

ω = fundamental frequency of the structure after being damaged.

DiPasquale and Cakmak (1990) proposed two softening damage indices, the maximum softening index and the final softening index. These two indices are given by the following two equations:

$$\delta_m = 1 - \frac{T_0}{T_{\max}} \quad (2.29)$$

and

$$\delta_f = 1 - \frac{T_0^2}{T_f^2} \quad (2.30)$$

where:

δ_m = maximum softening index,

δ_f = final softening index,

T_0 = initial natural period,

T_{\max} = maximum natural period of an equivalent linear system, and

T_f = final natural period of an equivalent linear system.

DiPasquale and Cakmak (1990) showed that the final softening index, δ_f , is approximately equal to the average reduction in stiffness across the structure. The maximum softening index, δ_m , depends on the combined effect of stiffness degradation and plastic deformations. The response of the structure to input ground motion must be known in order to compute the softening indices. Thus, it is necessary to specify the ground acceleration time history and the structural response at various locations of the structure. The final softening can be assessed on the basis of information on the state of the structure before and after the earthquake, with no need for information on the structural response during the earthquake.

The softening indices provide very little information about the distribution of damage sustained by different members within the structure. Mork (1992) tried to improve this aspect by extending the maximum softening index to include the second mode as shown in the following two equations:

$$\delta_1 = 1 - \sqrt{\frac{k_{1,\max}}{k_{1,0}}} \quad (2.31)$$

and

$$\delta_2 = 1 - \sqrt{\frac{k_{2,\max}}{k_{2,0}}} \quad (2.32)$$

where:

δ_1 = maximum softening index corresponding to the first mode,

δ_2 = maximum softening index corresponding to the second mode,

$k_{1,0}$ = initial stiffness of an equivalent linear system for the first mode,

$k_{2,0}$ = initial stiffness of an equivalent linear system for the second mode,

$k_{1,\max}$ = maximum stiffness of an equivalent linear system for the first mode, and

$k_{2,\max}$ = maximum stiffness of an equivalent linear system for the second mode.

The damage measures δ_1 and δ_2 can be taken to represent damage in the lower and the upper parts of the structure, respectively.

Nielsen et al. (1992) showed that contours for the overall softening index, δ_m , can be obtained in the δ_1 - δ_2 plane by using the following relationship:

$$\delta_2 = 1 - \sqrt{\frac{1}{4\lambda} \sqrt{\frac{\delta^2 - 2\delta(1 - \delta_1)^2}{\delta - (1 - \delta_1)^2}}} \quad (2.33)$$

where:

$$\lambda = \frac{k_{2,0}}{k_{1,0}} \text{ and}$$

$$\delta = (1 - \delta_m)^2 \left(1 + 2\lambda - \sqrt{1 + 4\lambda^2} \right).$$

However, the softening indices do not explicitly account for the dissipated hysteretic energy. Therefore, the softening indices are not strict measures of cumulative damage, though they do approximately account for degradation in strength and stiffness as reflected in the first few modal periods.

2.3 Summary

The first part of this section reviewed the various parameters used to characterize ground motion levels. In this study, the ground motion is chosen to be characterized by spectral acceleration and MMI. The spectral acceleration in three period bands corresponding to three classes of reinforced concrete frames is used in the development of fragility curves in Sections 4 and 5. Spectral acceleration is chosen to characterize the ground motion as it is a simple parameter and can be easily used in regional damage evaluation. Furthermore, spectral acceleration provides a lower bound to the input seismic energy. MMI is used for developing the DPMs in Section 5.

The second part of this section described the various damage measures. Cumulative damage measures are preferred as structural damage is believed to be caused by high stress excursions as well as repeated stress reversals. Most of the damage indices have been formulated by assuming that the failure in the structural components is governed by flexural behavior. Since it is beyond the scope of this study to develop a new damage index or to modify an existing damage index, shear behavior is assumed not to influence significantly the damage in building structures considered for the development of motion-damage relationships in Sections 4 and 5.

However, shear and combined shear-flexure behavior may lead to significant number of failures in structures. The significant difference between shear and flexural behaviors is the usual brittle mode of collapse when shear behavior dominates the structural response. Shear behavior is likely to dominate in short, stocky components. In building structures where slender beams and columns are used, shear behavior is not expected to be significant. Still, shear behavior may dominate in some cases where the effective length of the columns may be reduced due to nonstructural walls adjoining the columns.

The estimation of the different damage states for reinforced concrete frames, based on the different damage measures, is presented in Section 3. This study adopts an equivalent form of the Park and Ang damage index to represent structural damage. The Park and Ang index is used because it lends itself to numerical computation and because it has been calibrated using experimental data.

SECTION 3

METHODOLOGY FOR DEVELOPING MOTION-DAMAGE RELATIONSHIPS

Ground-motion-versus-damage relationships characterize the level of damage to a particular class of structures as a function of a ground motion parameter. In order to represent the variability in earthquake ground motion and the uncertainties in structural behavior, these relationships are most frequently described in the form of probabilities of damage conditional on the ground motion parameter. The two most widely used forms of motion-damage relationships are fragility curves and damage probability matrices (DPMs).

3.1 General Framework for Motion-Damage Relationships

A fragility curve describes the probability of reaching a damage state at a specified ground motion level. Thus, a fragility curve for a particular damage state is obtained by computing the conditional probabilities of being in that damage state at various levels of ground motion. A plot of the computed conditional probabilities versus the ground motion parameter describes the fragility curve for that damage state. The conditional probabilities are defined as follows:

$$p_{ik} = P[D = d_i | Y = y_k] \quad (3.1)$$

where:

p_{ik} = probability of being in damage state d_i given the ground motion is y_k ,

D = damage random variable defined on the damage state vector $\mathbf{D} = \{d_0, d_1, \dots, d_n\}$,

Y = ground motion random variable.

An alternate representation of fragilities is given by the probabilities of reaching or exceeding a specified damage state given a ground motion level. This definition is used to obtain the fragility curves for reinforced concrete frames in Section 5. The conditional probabilities can be evaluated from equation 3.1 as follows:

$$P_{ik} = P[D \geq d_i | Y = y_k] = \sum_{j=i}^n P_{jk} \quad (3.2)$$

Damage states can be defined to characterize the physical state of the structure. A numerical damage scale in terms of the ratio of repair cost to replacement value of the structure can also be specified. Section 2 discussed the different damage measures. The segregation of some of the damage measures into damage states is discussed later in this section. Several different parameters used to describe ground motion have been discussed in Section 2. The methodology can be used with any ground motion parameter. However, root mean square (RMS) acceleration and spectral acceleration, S_a , for a specified structural period range are used to develop the methodology in this section.

Another commonly used representation of structural damage as a function of the earthquake ground motion is the DPM. A DPM specifies the discrete probabilities of reaching a damage state at different ground motion levels. In this study, modified Mercalli intensity (MMI) is used as the ground motion parameter for the DPMs. Relationships between spectral acceleration, in the relevant period band, and MMI are developed and used to obtain DPMs from fragility curves. The formulation for obtaining DPMs is shown as follows:

$$P_{D|MMI}[d|MMI] = \int_{S_a} P_{D|MMI, S_a}[d|MMI, S_a] \cdot f_{S_a|MMI}[s_a|MMI] ds_a \quad (3.3)$$

where:

$P_{D|MMI}[d|MMI]$ = probability of being in or exceeding a given damage state at a specified MMI,

$P_{D|MMI, S_a}[d|MMI, S_a]$ = probability of being in or exceeding a given damage state at specified MMI and spectral acceleration, and

$f_{S_a|MMI}[s_a|MMI]$ = conditional probability density of spectral acceleration at specified MMI, obtained by assuming this density function to be lognormal with parameters determined later in Section 5 for concrete frames.

The above formulation can be simplified by assuming that the probability of reaching or exceeding a given damage state at specified MMI and spectral acceleration is the same as the probability of reaching or exceeding a given damage state at specified spectral acceleration. Both spectral acceleration and MMI are used as ground motion parameters. Thus, representing the probability of damage as a function only of spectral acceleration should not have significant effect on the conditional probabilities for the DPMs. This assumption can be verified as additional data become available. Equation 3.3 can then be simplified as follows:

$$P_{D|MMI}[d|MMI] = \int_{S_a} P_{D|S_a}[d|S_a] \cdot f_{S_a|MMI}[s_a|MMI] ds_a \quad (3.4)$$

While simple fragility formulations have been developed and used extensively for components and mechanical assemblies in nuclear power plant safety analyses (Kennedy et al., 1980, Kennedy and Ravindra, 1984), no systematic approach for developing such fragility curves has been presented for complex structural systems. This section presents such an approach.

The major components of the proposed methodology consist of (a) characterization of the structure when subjected to extreme dynamic loads, (b) characterization of the potential ground motions, and (c) quantification of the structural response that includes the variability in ground motion and the uncertainty in structural parameters. It is difficult to develop analytical closed-form solutions for motion-damage relationships because neither the ground motion nor the nonlinear behavior of the structure can be described in an analytical form. Thus, a Monte Carlo simulation approach is used to estimate the probabilities of damage conditional on different ground motion levels. Figure 3-1 describes the general framework of this methodology.

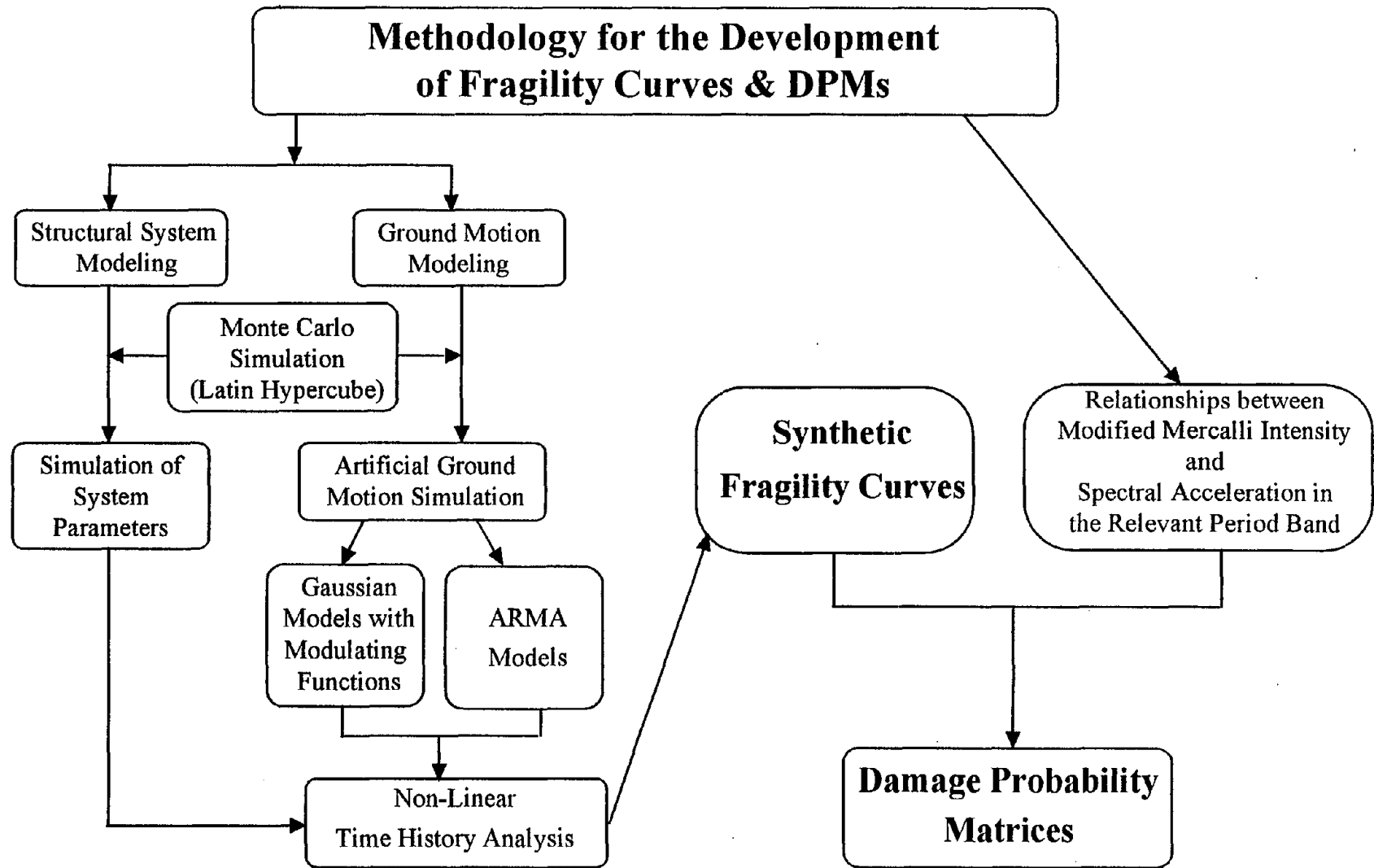


Figure 3-1 Steps in the development of fragility curves and damage probability matrices

Damage to structures subjected to severe earthquake ground shaking depends on their dynamic characteristics and their nonlinear behavior. This evaluation of damage requires that nonlinear dynamic analyses be performed for a wide range of earthquake ground motion time histories. For the nonlinear dynamic analysis, the hysteretic behavior of structural components must be specified. When fragility curves are needed for many different classes of structures, the structural properties need to be representative of a wide range of structures that might fall within that specified structural category. For this purpose, a generic structure should be designed for a specified structural system reflecting a particular design code specification. The behavior of individual structures is likely to differ from the behavior of the generic structure used in the development of fragility curves. However, the damage estimated from the generic structure is expected to be representative on the average over the range of different structures within this structural class.

3.2 Fragility and DPM Simulation

The Monte Carlo simulation technique is used for the computation of the fragility curves defined by equations 3.1 and 3.2. DPMs are obtained from the fragility curves by using equation 3.4. Simulation is a numerical technique for conducting experiments on a digital computer. Rubinstein (1981) defines simulation as a technique that performs sampling experiments on the model of the system. Stochastic simulation, also known as Monte Carlo simulation, includes the sampling of variables from probability distributions. Historically, the Monte Carlo technique has been considered a method for the solution of a model using random numbers.

In damage analysis, the uncertainties associated with structural capacities and demands need to be modeled. Structural capacities and demands can be characterized by a number of parameters which have an important effect on the response statistics and overall reliability of the system. Structural capacities are defined in terms of the capacities of members as part of the structure. Much greater uncertainty is associated with seismic demands than with other demands on the structure. Artificial ground motion simulation is carried out to incorporate this uncertainty. Gaussian models with modulating functions and autoregressive moving average (ARMA)

models are used for this purpose. This study treats the uncertainties associated with structural capacities and demands independently.

The Monte Carlo technique as applied for the development of fragility curves and DPMs involves the selection of values of the input capacity random variables required for non-linear dynamic analyses, the generation of artificial ground motion, and the simulation of damage to a structure. An overview of the Monte Carlo simulation technique is presented in figure 3-2. Examples of input random variables to model capacities for reinforced concrete structures include the strengths of steel and concrete. The procedure for the generation of artificial time histories is discussed later in the section. The means, variances, and distribution functions of the output random variable, the quantitative measures of damage in this study, are estimated from the simulations for an ensemble of time histories corresponding to a given level of ground motion. The probabilities of different damage states are evaluated from the probability distributions of the damage measure.

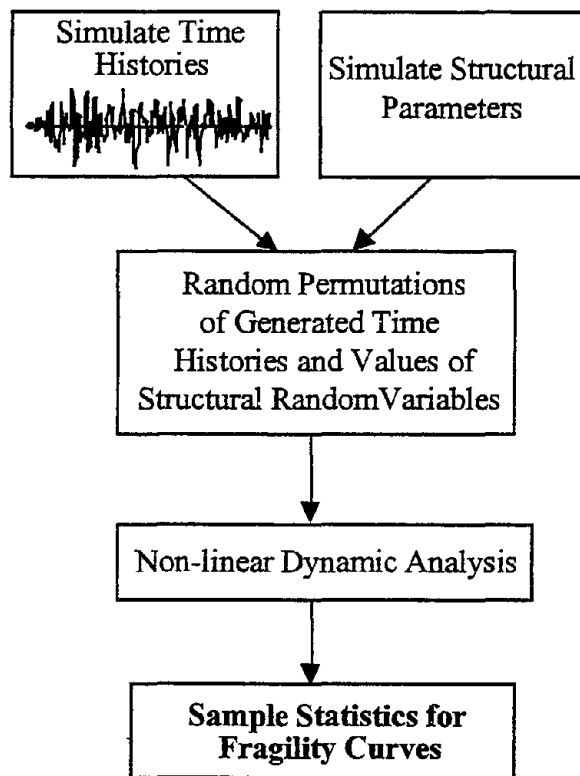


FIGURE 3-2 Steps in the Monte Carlo simulation technique

The direct Monte Carlo technique requires a large number of simulation cycles to achieve an acceptable level of confidence in the estimated probabilities. In this study, the Latin hypercube technique is used to reduce the number of simulation cycles. Iman and Conover (1980) provide a good description of the Latin hypercube sampling technique. Using the Latin hypercube technique for selecting values of the input variables, the estimators from the simulation are close to the real values of the quantities being estimated. The Latin hypercube technique uses stratified sampling of the input variables which usually results in a significant decrease in the variance of estimators. This decrease in variance is accomplished because stratified sampling forces the entire range of the input variables to be represented in the set of values for the input variables. Furthermore, through random permutations, the Latin hypercube technique assures that every stratum of one variable has some possibility of being coupled with each stratum of all other variables. If there are only two input variables, this method of sampling is known as the Latin square technique.

The Latin hypercube sampling scheme involves the partitioning of the range of each variable into N non-overlapping intervals, corresponding to N simulation cycles, such that all intervals have the same probability of occurrence. The intervals for a general probability density function are shown in figure 3-3. N different values for each random variable in each of the N non-overlapping intervals are then randomly selected. The generation of the values of the random variable is accomplished by generating N uniform random numbers between 0 and 1 which are transformed to the random numbers in the non-overlapping intervals by using the following equation:

$$U_m = \frac{U}{N} + \frac{m-1}{N} \quad (3.5)$$

where:

m = interval number,

U = uniform random number in the range (0,1), and

U_m = random number in the m^{th} interval.

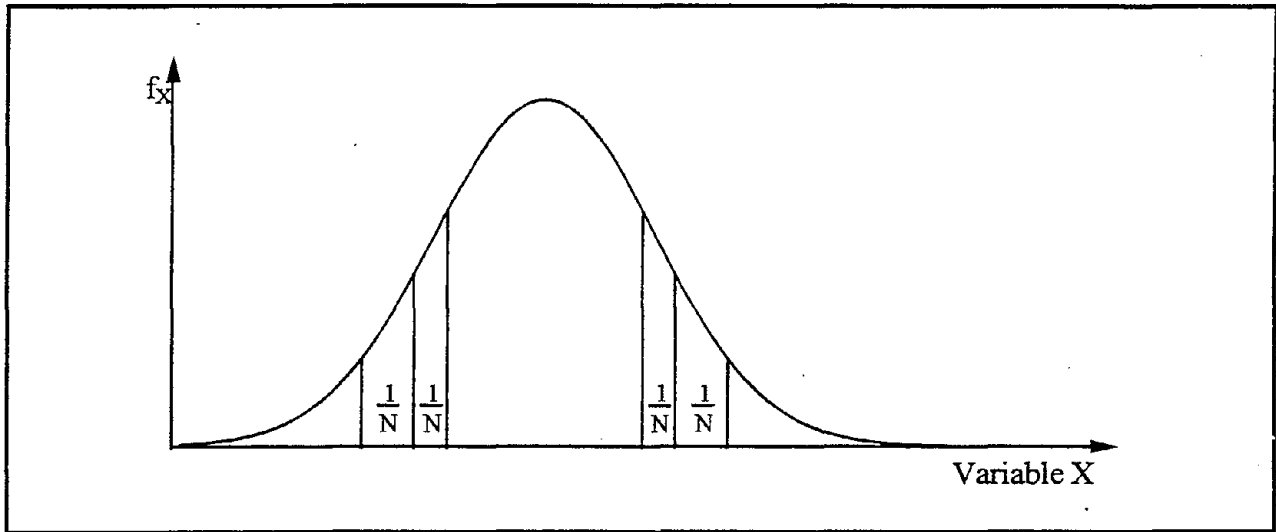


FIGURE 3-3 General probability density function with N intervals used in the Latin hypercube sampling scheme

Only one generated value falls within each interval because $\frac{m-1}{N} < U_m < \frac{m}{N}$. The values of the random variables are generated by evaluating the inverse of the cumulative distribution functions at the generated values (given by equation 3.5). This inverse transformation can be expressed as follows:

$$x_m = F_X^{-1}(U_m) \quad (3.6)$$

where:

x_m = m^{th} generated value for variable X and

F_X^{-1} = inverse of the cumulative distribution function for variable X .

The Latin hypercube samples are obtained by random permutation of the generated values of all the random variables. A procedure for obtaining a random sequence of the generated values of a random variable is illustrated by the following shuffling algorithm.

Let $\{x_1, x_2, \dots, x_N\}$ be the initial order of the values generated for random variable X . The random sequence r_1, r_2, \dots, r_N is produced by the following steps:

1. Set $r_1 = x_1, r_2 = x_2, \dots, r_N = x_N$ and $m = N$.
2. Generate an integer I uniformly distributed between 1 and m . Interchange r_I and r_m .
3. Set $m = m-1$. If $m = 1$, return r_1, r_2, \dots, r_N and exit. Otherwise go to 2.

The generated values of all the variables are placed in a random sequence. The n^{th} sample is now obtained by selecting the n^{th} value of all the random variables.

3.3 Characterization of Damage

Various damage measures were discussed in Section 2. The Krawinkler index (1987) is a measure frequently used to quantify damage in steel components. For reinforced concrete structures, the Park and Ang model has been used widely in recent years because it lends itself to simple numerical computation and because it has been calibrated using data from various structures damaged during past earthquakes.

In order to estimate economic loss or casualties as a result of structural damage, the structural damage must be expressed in terms of discrete damage states. Discrete damage states allow the damage sustained by a structure to be expressed in terms of the nature and extent of the damage suffered by its components. Thus, structural damage, which is a continuous function of building response, is quantified by discrete damage states. The five discrete damage states used in this study are: *none, minor, moderate, severe, and collapse*. To obtain these discrete damage states, ranges for the damage measures discussed earlier need to be specified.

In this study, the different damage states of a concrete building are identified based on the Park-Ang global damage indices of the overall structure. Park et al. (1984) calibrated the damage index with the observed damage to nine reinforced concrete buildings caused by different earthquakes. The report by Park et al. (1987) gave the semantic definitions for the ranges of damage corresponding to different values of the Park and Ang damage index. Gunturi (1992) further investigated these damage states and simplified them according to his findings. Further

calibration of the Park-Ang damage index was performed by De Leon and Ang (1993) using data from eight reinforced concrete buildings that sustained different levels of damage during the 1985 Mexico City earthquake. Stone and Taylor (1994) also calibrated the Park-Ang damage index based on an extensive study of reinforced concrete columns. The ranges of the Park and Ang index for different damage states have been established to reflect damage to concrete frames more realistically and are presented in table 3-I. Table 3-I also presents the physical description of the different damage states as proposed by Park et al. (1984).

TABLE 3-I Park and Ang's damage index for different damage states

Damage State	Range of the Park and Ang index	Physical Description of the Damage State
Minor	0.1 - 0.2	Minor cracks throughout building, partial crushing of concrete in columns
Moderate	0.2 - 0.5	Extensive large cracks, spalling of concrete in weaker elements
Severe	0.5 - 1.0	Extensive crushing of concrete, disclosure of buckled reinforcement
Collapse	> 1.0	Partial or total collapse of building

Hatamoto et al. (1990) defined four damage states based on the Chung, Meyer and Shinozuka (1987) damage index. The four damage states that they considered are: *Minor*, *Repairable*, *Irrepairable* and *Unsafe*. The ranges of the damage index for these four damage states are presented in table 3-II.

TABLE 3-II Chung, Meyer and Shinozuka's (1987) damage index for different damage states as defined by Hatamoto et al. (1990)

Damage State	Range of the damage index
Minor	0.0 - 0.2
Repairable	0.2 - 0.5
Irrepairable	0.5 - 1.0
Structure Unsafe	≥ 1.0

Another method for the identification of the *Minor* and *Moderate* damage states investigated in this study is based on crack width in the elements. The advantage of using crack width as a damage measure is that it can be directly related to the dollar-loss ratio. Various techniques for estimating crack width in concrete members are available. Some are based on empirical relationships (e.g., Gergely and Lutz, 1968) while others (e.g., Bazant and Oh, 1983a and 1983b) are based on analytical formulations using the concept of fracture energy. The prediction of crack width based on the formulation presented by Oh and Kang (1987) is presented below.

The formulas for the prediction of crack width proposed by Oh and Kang are based on the cracking theory developed by Bazant and Oh (1983a and 1983b). Tests on reinforced concrete beams were also carried out by Oh and Kang to check the validity of the proposed formulas. Their equation that gives the best prediction of the maximum crack width in a member is given as:

$$\frac{w_{\max}}{d} = a_0(\varepsilon_s - 0.0002) R \quad (3.7)$$

where:

w_{\max} = maximum crack width,

d = diameter of reinforcing bar,

ε_s = strain in tensile reinforcement,

R = h_2/h_3 ,

$$a_0 = 159 \left(\frac{t_b}{h_2} \right)^{4.5} + 2.83 \left(\frac{A_1}{A_{s1}} \right)^{1/3}$$

A_1 = effective area of concrete surrounding one reinforcing bar,

A_{s1} = average area of one tensile reinforcing bar,

t_b = concrete cover for tensile reinforcement,

h_2 = distance from extreme tension fiber to the neutral axis, and

h_3 = distance from the centroid of steel to the neutral axis.

It may be pointed out that the above formulation is applicable for cracking under static loads. The effect of dynamic loading on the crack widths should be investigated. Beshara (1993) provided a relationship between the dynamic cracking strain and the static cracking strain as a function of effective strain rate. In general, the crack widths can be computed based on the residual strain in the member after dynamic analysis.

The *Manual for Repair Methods of Civil Engineering Structures Damaged by Earthquakes* (1987) suggested that cracks with widths in the range of 0.5 mm - 0.8 mm can be repaired with epoxy injection. That manual also suggested that cracks with widths greater than 0.8 mm require V-cut before repair. Thus, if the maximum crack width in an element is in the range 0.5 mm - 0.8 mm, it is in *Minor* damage state. This definition of *Minor* damage implies that the damage can be repaired by epoxy injection. A crack width larger than 0.8 mm can be defined to be the lower bound of the *Moderate* damage state. A more detailed study is needed in order to arrive at crack widths under dynamic loading and to correlate crack widths with *Minor* and *Moderate* damage states. The damage states for the structure can be estimated based on the proportion of the elements in different damage states, and the importance of those elements. Since elements in the lower part of the structure are vital for the functionality of the entire structure, these elements should be assigned a larger importance factor.

3.4 Characterization of Ground Motion

In order to characterize earthquake ground motion for the purposes of evaluating structural performance, the amplitude, frequency content, and duration of ground motion must be described. Thus, it is difficult to specify a single parameter that captures the above important characteristics of ground motion. Various parameters used to characterize ground motion were discussed in Section 2. Although the methodology can be used with any ground motion parameter, spectral acceleration and RMS acceleration are used to characterize the ground motion in the development of the methodology. MMI is used to identify the different levels of ground motion for the DPMS. The relationship between MMI and these parameters needs to be investigated in order to obtain DPMS from fragility curves. The relationship between spectral

acceleration and MMI is presented in Section 5. DPMs for concrete frame structures are then developed using the relationship between spectral acceleration and MMI.

Furthermore, earthquake ground motion time histories are needed for the analysis. If a large sample of earthquake ground motion time histories that cover all the different parameter ranges is available, these time histories can be discriminated according to distance to the fault, local soil parameters and spectral characteristics, and then can be used for the dynamic analysis of the structure and the evaluation of the fragility curves. Such a consistent ensemble of time histories is not currently available, even though there are a large number of recordings obtained from recent earthquakes. Thus, it is proposed that ensembles of time histories be simulated at each specified ground motion parameter level.

3.4.1 Models for Simulation of Ground Motion

Several procedures are available for the generation of artificial time histories. These include the geophysical models, the stationary Gaussian models with modulating functions, and the ARMA models. Deodatis and Shinozuka (1989) developed a stochastic wave model with evolutionary power to simulate ground motion. This model is useful for simulating ground motions for large scale structures where the spatial variation of ground motion is important.

3.4.1.1 Geophysical Models

Several techniques using geophysical models are available for the simulation of earthquake ground motions. These include ray tracing techniques, Green's function techniques, and the normal mode method (Suzuki and Kiremidjian, 1989). It is difficult to simulate long duration and wide-band frequency waves with ray tracing methods. Green's function methods become difficult to apply when a multilayered earth structure is considered. When the normal mode method is used, it is difficult to generate high frequency waves at intermediate and far distances unless a large number of modes are used. The major difficulty with the normal mode method is the enormous computational effort involved in obtaining the normal modes for the earth. The

geophysical models are too complex, computationally involved, and regionally dependent, thus making it difficult to implement them in this study.

3.4.1.2 Stationary Gaussian Models with Modulating Functions

Stationary Gaussian models with modulating functions have been proposed by Shinozuka and Sato (1967), Liu and Jhaveri (1969), and Vanmarcke (1976) among many others. In stationary Gaussian models with modulating functions, the ground motion is expressed as follows:

$$X(t) = I(t) \sum_n A_n \sin(\omega_n t + \phi_n) \quad (3.8)$$

where:

A_n = amplitude of the n^{th} sinusoid,

ω_n = frequency of the n^{th} sinusoid,

ϕ_n = phase angle of the n^{th} sinusoid, assumed to be uniformly distributed between 0 and 2π ,
and

$I(t)$ = envelope function.

The amplitudes are determined from the power spectral density as follows:

$$\frac{A_n^2}{2} = G(\omega_n) \Delta\omega \quad (3.9)$$

where:

$G(\omega)$ = one sided power spectral density.

The product, $G(\omega_n) \Delta\omega$, can be thought of as the contribution of the sinusoid with frequency ω_n to the total power. The nonstationarity is introduced by using an envelope function $I(t)$. SIMQKE (1976) is one of the programs which uses this procedure.

SIMQKE can be used to generate time histories corresponding to a given response spectrum. The probability distributions of the dynamic amplification factors discussed later in this section can be used to obtain an ensemble of response spectra corresponding to a given spectral ordinate. The parameters of the envelope function should be chosen to satisfy the strong motion duration. The relationship between spectral acceleration and strong motion duration is discussed in Section 3.4.2.5.

3.4.1.3 ARMA Models

ARMA models are often applied to generate artificial time histories (e.g., Polhemus and Cakmak, 1981 and Conte et al., 1992). ARMA models consist of a discrete stationary linear transfer function applied to a white noise process. A white noise process is a random process in which all frequencies contribute equally to the mean square value of the process. A white noise process has an infinite variance due to the contribution of all frequencies and therefore is not physically realizable. The autocorrelation and power spectral density functions of white noise process $W(t)$ are expressed mathematically by means of the following two equations:

$$R_{WW}(\tau) = 2\pi\phi_0\delta(\tau) \quad (3.10)$$

and

$$\phi_{WW}(\omega) = \phi_0 \quad (3.11)$$

where:

$\delta(t)$ = Dirac delta function and

ϕ_0 = constant power spectral density of the white noise process.

A shot noise process with homogeneous Poisson arrival times tends to a Gaussian white noise as the mean occurrence rate λ tends to infinity and σ^2 tends to zero in such a way that $\lambda\sigma^2$ remains a constant (Housner & Jennings, 1964).

The stationary ARMA model of order (p,q) is represented by the following equation:

$$a_k - \phi_1 a_{k-1} - \dots - \phi_p a_{k-p} = e_k - \theta_1 e_{k-1} - \dots - \theta_q e_{k-q} \quad (3.12)$$

where:

$a_k = a(k\Delta t)$, $k = 0, 1, 2, \dots$ = a discrete stationary correlated process,

$e_k = e(k\Delta t)$ = a zero-mean Gaussian white-noise process with variance σ_e^2 ,

Δt = sampling time interval,

ϕ_i , $i = 1, \dots, p$ = autoregressive parameters, and

θ_i , $i = 1, \dots, q$ = moving average parameters.

A special case of ARMA models is the stationary ARMA(2,1) model defined by the following difference equation:

$$a_k - \phi_1 a_{k-1} - \phi_2 a_{k-2} = e_k - \theta_1 e_{k-1} \quad (3.13)$$

This model is completely defined by the two autoregressive parameters, the moving average parameter, and the variance of the white noise process.

The process a in equation 3.13 should be stationary and invertible in order to be physically realizable. The stationarity conditions ensure that the process a has a finite variance. The stationarity is controlled by the autoregressive part only and is achieved when the following conditions are satisfied:

$$\begin{aligned}
\phi_1 + \phi_2 &< 1 \\
\phi_1 - \phi_2 &< 1 \\
|\phi_2| &< 1
\end{aligned}
\tag{3.14}$$

The idea of invertibility is illustrated by means of a first order moving average process represented by the following equation .

$$a_k = e_k - \theta_1 e_{k-1} \tag{3.15}$$

Equation 3.15 can be written in terms of the previous values of e_k as shown in the following equation:

$$a_k = e_k - \theta_1 a_{k-1} - \theta_1^2 a_{k-2} - \dots - \theta_1^n a_{k-n} - \theta_1^{n+1} e_{k-n-1} \tag{3.16}$$

If a_k is not to depend on some point in the remote past, θ_1 must be less than one in absolute value. If n is allowed to go to infinity, the last term in equation 3.16 vanishes and a_k can be written as an infinite autoregressive process with declining weights as shown in the following equation:

$$a_k = \sum_{n=1}^{\infty} -\theta_1^n a_{k-n} + e_k \tag{3.17}$$

The reason for excluding the non-invertible processes is that they are not physically realizable. In a non-invertible process a small perturbation in the distant past can have a tremendous effect on the present process a_k .

Conte et al. (1992) show that a linear, viscously damped single-degree-of-freedom (SDOF) system is the underlying physical system for the ARMA(2,1) model. For example, the natural

frequency, ω_g , and the damping, ξ_g , of the underdamped SDOF system can be represented by the following equations when $\phi_1^2 + 4\phi_2 < 0$, and $\phi_2 < 0$:

$$\omega_g = \frac{1}{2\Delta t} \sqrt{[\ln(-\phi_2)]^2 + 4\lambda_d^2} \quad (3.18)$$

and

$$\xi_g = \frac{-\ln(-\phi_2)}{\sqrt{[\ln(-\phi_2)]^2 + 4\lambda_d^2}} \quad (3.19)$$

where:

$$\lambda_d = \arccos\left(\frac{\phi_1}{2\sqrt{-\phi_2}}\right), \quad 0 \leq \lambda_d \leq \pi$$

Recorded earthquake time histories exhibit nonstationarities in amplitude and frequency content. In order to incorporate these two nonstationarities, a dynamic version of the ARMA model is used. This model is represented by the following equation:

$$a_k - \phi_1 a_{k-1} - \dots - \phi_p a_{k-p} = e_k - \theta_1 e_{k-1} - \dots - \theta_q e_{k-q} \quad (3.20)$$

The nonstationarity in amplitude is represented by the variance envelope of the underlying white-noise process, $\sigma_{e,k}^2$, and the nonstationarity in frequency content is modeled by the time varying ARMA parameters, $\phi_{i,k}$ and $\theta_{i,k}$. The uncoupling of these two nonstationarities is possible if the standard deviation envelope, $\sigma_{e,k}$, is slowly varying in time compared to the periods of the earthquake motion.

3.4.2 Modeling of Uncertainty in Ground Motion

The uncertainty associated with seismic demands on a structure is much larger than the uncertainties associated with demands imposed by dead and live loads. Ground motion can be simulated from power spectral density functions, or from normalized spectral shapes, or from recorded time histories. The procedure for incorporating the uncertainties when simulating earthquake ground motion is discussed in the following sections. In addition, the relationships between RMS acceleration and strong motion duration and those between spectral acceleration and strong motion duration are also examined. These relationships are necessary when simulating ground motions corresponding to a specified level of RMS acceleration or spectral acceleration.

3.4.2.1 Uncertainties in Kanai-Tajimi Parameters

The Kanai-Tajimi (Tajimi, 1960) power spectral density is one of the most commonly used functions to characterize the power of the ground motion at different frequencies. This function is defined by the following equation:

$$S(\omega) = \frac{1 + 4\xi_g^2 \left(\frac{\omega}{\omega_g}\right)^2}{\left[1 - \left(\frac{\omega}{\omega_g}\right)^2\right]^2 + 4\xi_g^2 \left(\frac{\omega}{\omega_g}\right)^2} \cdot S_0 \quad (3.21)$$

where:

S_0 = intensity of the ideal white noise excitation at the bedrock level,

ω_g = predominant ground natural frequency, and

ξ_g = effective damping coefficient of the ground.

The Kanai-Tajimi power spectral density is defined by two random variables ω_g and ξ_g . Lai (1982) proposed a gamma probability density function for ω_g and a lognormal probability

density function for ξ_g . He used 22 rock site records to arrive at the means and standard deviations of ω_g and ξ_g . The mean and standard deviation of ω_g are estimated as 26.7 rad/sec and 10.6 rad/sec, respectively. The mean and standard deviation of ξ_g are found to be 0.35 and 0.14, respectively. These distributions can be used to arrive at different power spectral density functions for each simulation. A time history can then be simulated for each power spectral density function.

3.4.2.2 Uncertainties in Dynamic Amplification Factors

The spectral values at different periods are frequently represented by means of dynamic amplification factors. The dynamic amplification factors represent the normalized spectral values at specified damping, obtained as a ratio of the spectral acceleration to the peak ground acceleration. Figure 3-4 shows the dynamic amplification factors obtained at a damping ratio of 5% of the critical damping from the firm site records of the Loma Prieta, Whittier Narrows, and Morgan Hill earthquakes. Although the average spectral shapes shown in figure 3-4 appear to be smooth in each period band, the individual time histories may have sharp peaks in their spectra. Our interest, however, is in the average response of the structures over all the time histories. Since a structure is likely to be subjected to many different ground motions during its economic life, it is important to consider an ensemble of ground motions that have a wide range of characteristics.

Kiremidjian and Shah (1980) demonstrated the applicability of lognormal distribution to dynamic amplification factors. The firm site records from the Loma Prieta, Whittier Narrows, and Morgan Hill earthquakes are used for obtaining the parameters of the lognormal distributions of the dynamic amplification factors at different periods. The computed mean and standard deviations of the dynamic amplification factors are shown in figure 3-4. As a part of this study, Kolmogorov-Smirnov analysis was performed on the dynamic amplification data at four periods: 0.5, 1.0, 1.5 and 2.0 seconds. The sample cumulative frequencies and the theoretical distribution functions are shown in figures 3.5 through 3.8. The lognormal model was verified at the 5% significance level.

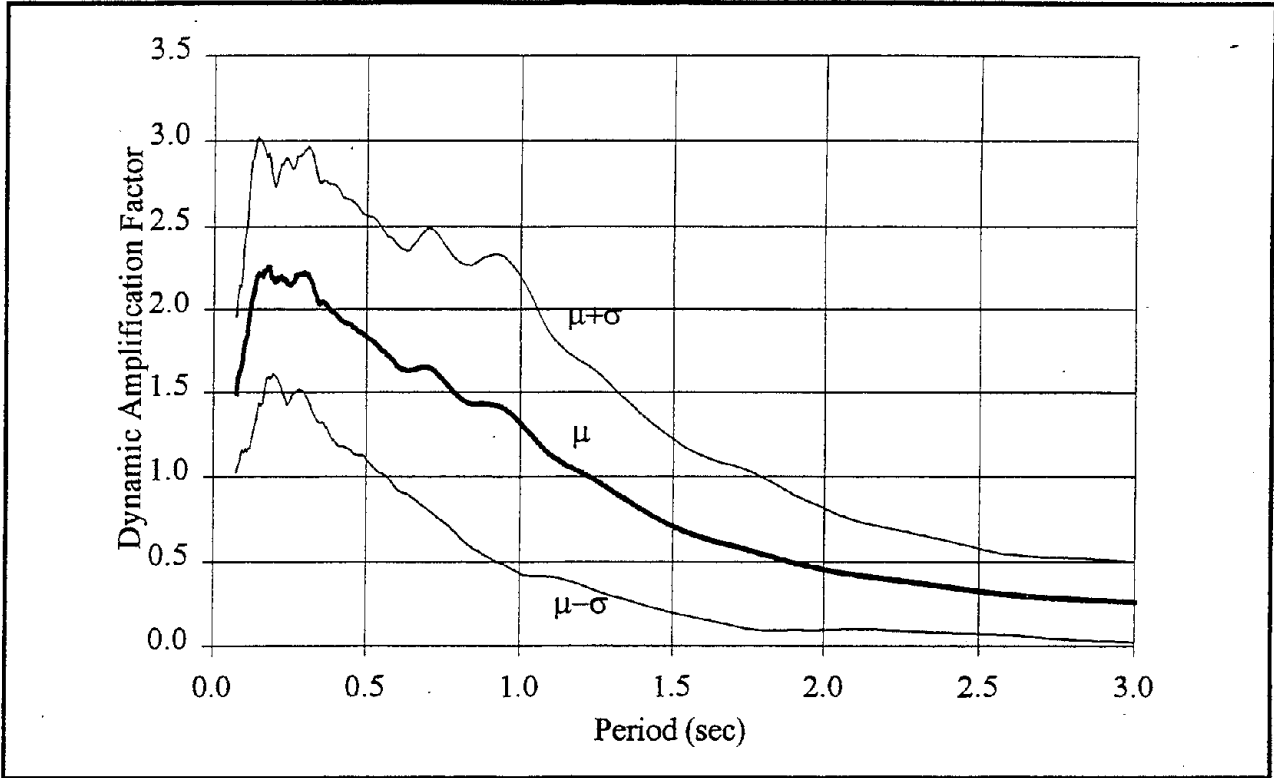


FIGURE 3-4 Parameters of the dynamic amplification factors for firm sites

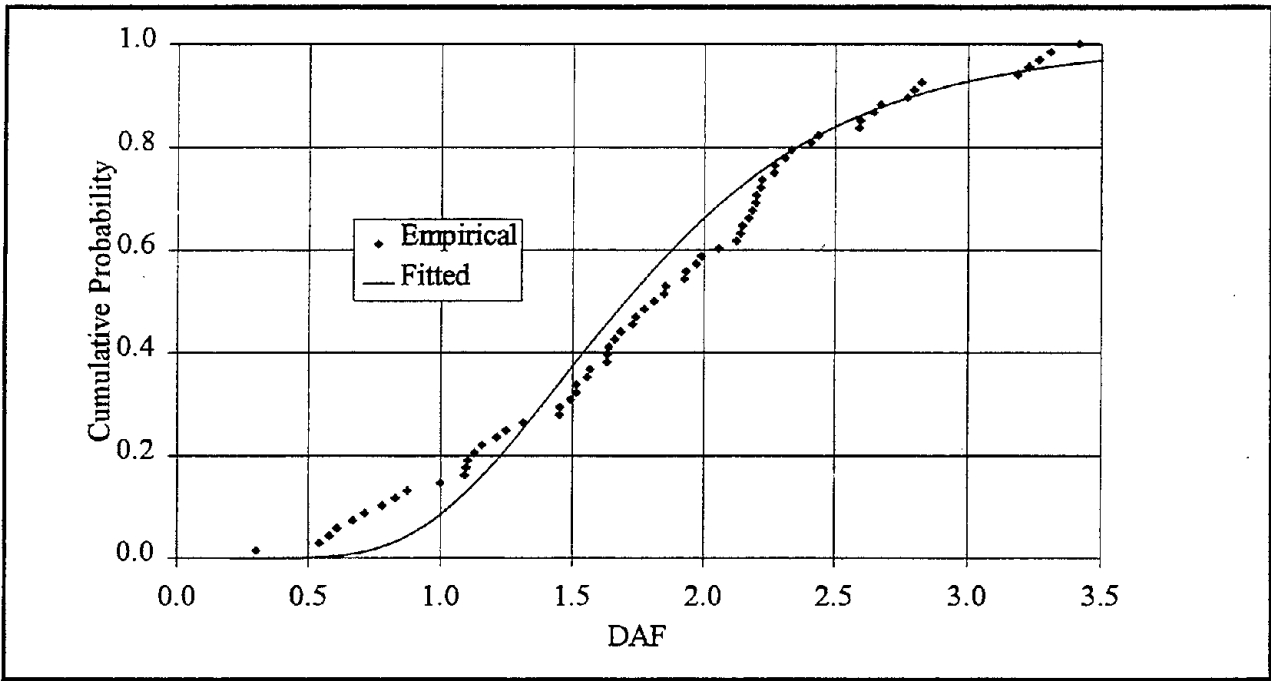


FIGURE 3-5 Comparison of the empirical and fitted probability distributions of DAF at T = 0.5 seconds

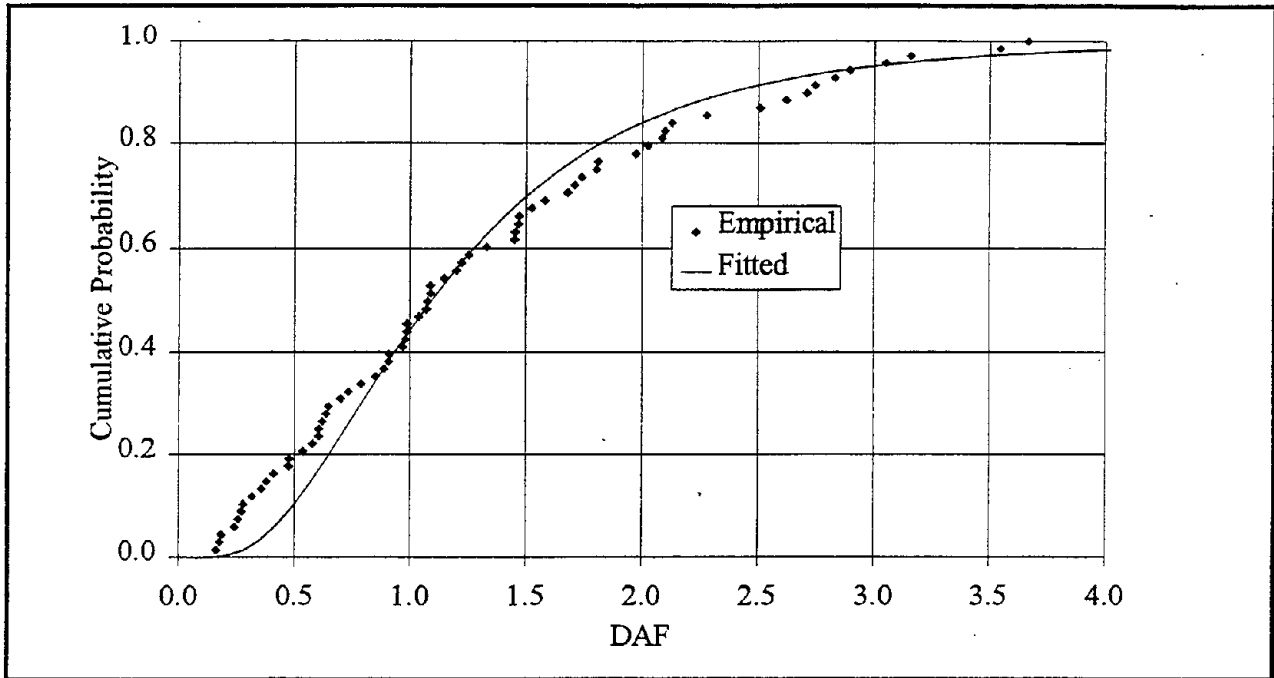


FIGURE 3-6 Comparison of the empirical and fitted probability distributions of DAF at T = 1.0 seconds

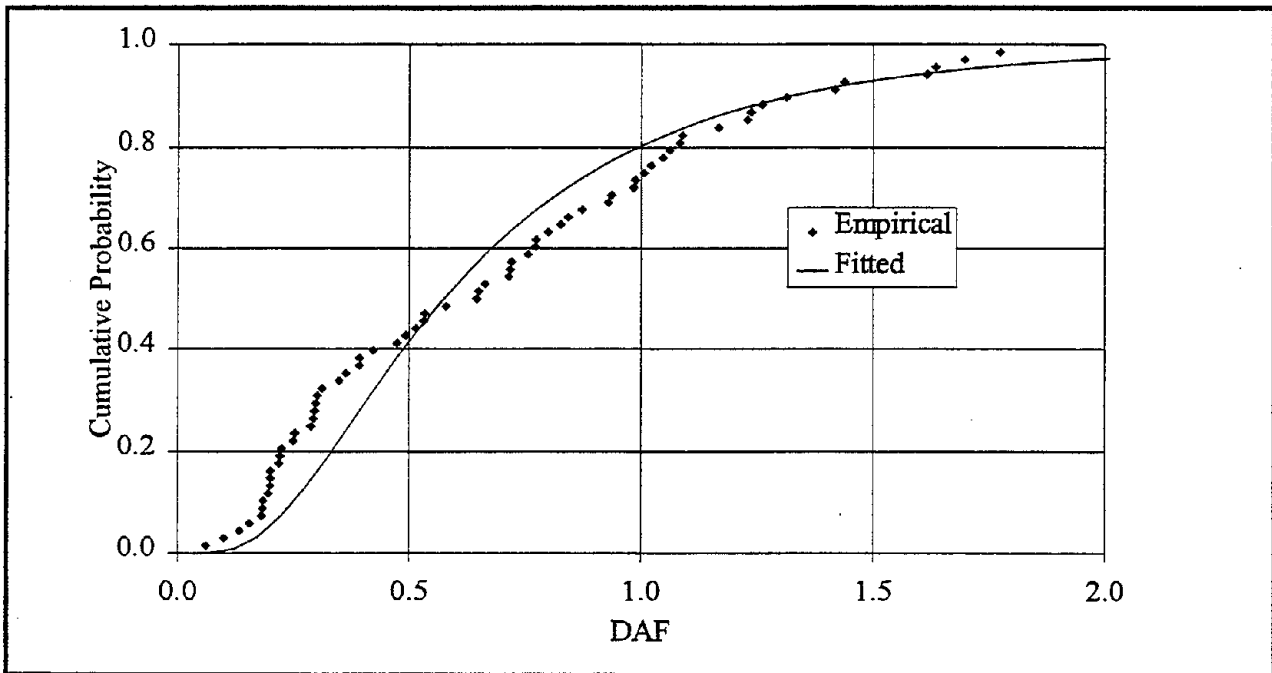


FIGURE 3-7 Comparison of the empirical and fitted probability distributions of DAF at T = 1.5 seconds

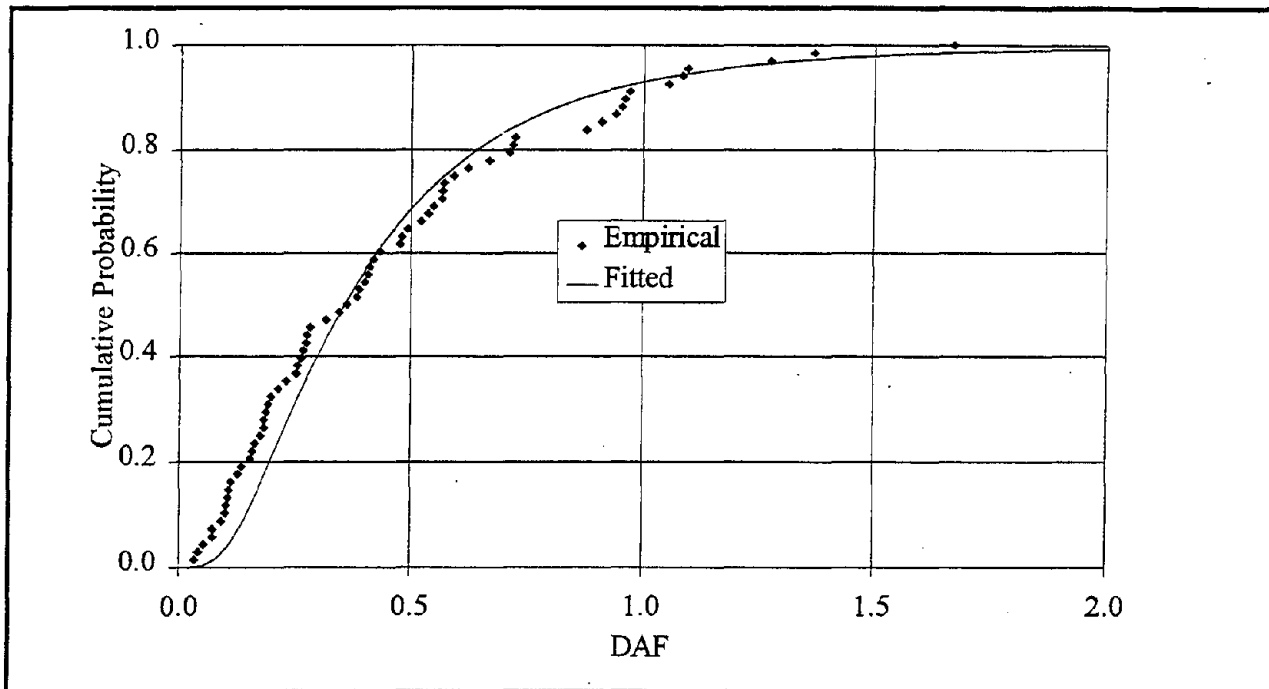


FIGURE 3-8 Comparison of the empirical and fitted probability distributions of DAF at $T = 2.0$ seconds

3.4.2.3 Moving Window Technique for Estimating ARMA Parameters

Another approach for incorporating the uncertainties in earthquake ground motion is to estimate ARMA parameters from an ensemble of recorded time histories. The estimated ARMA parameters then can be used to simulate ground motion. The moving-window technique is frequently used to estimate ARMA parameters. This technique assumes that the time history is stationary within a time window. In this study, the moving-window technique is used to estimate the ARMA parameters of recorded ground motion from the Loma Prieta, Whittier Narrows, and Morgan Hill earthquakes. Details on ground motion simulation using the moving-window technique are presented later in this section.

3.4.2.4 Relationship Between RMS Acceleration and Strong Motion Duration

Trifunac and Brady's (1975) definition of strong motion duration, given by equations 2.1 through 2.3, is used in this study. The probability distributions of the strong motion duration T_s

for firm sites given the RMS acceleration, $f_{T_s|RMS}(t_s|RMS)$, are derived using the firm site data from the Loma Prieta, Whittier Narrows, and Morgan Hill earthquakes. Only the free-field records are considered in this study to avoid possible soil-structure interaction effects. The conditional probability distributions of strong motion duration at a given RMS acceleration are obtained by assuming the RMS acceleration and strong motion duration to be jointly lognormally distributed. The distributions of the strong motion duration given the RMS acceleration are therefore lognormal with parameters λ'_{T_s} and ξ'_{T_s} defined by the following two expressions:

$$\lambda'_{T_s} = E[\ln(T_s)|RMS = r] = \lambda_{T_s} + \rho \frac{\xi_{T_s}}{\xi_{RMS}} (\ln(r) - \lambda_{RMS}) \quad (3.22)$$

$$\xi'^2_{T_s} = (1 - \rho^2) \xi^2_{T_s} \quad (3.23)$$

where:

T_s = strong motion duration,

λ_{RMS} = expected value of \ln RMS acceleration,

T_s = strong motion duration,

λ_{T_s} = expected value of \ln strong motion duration,

ξ^2_{RMS} = variance of \ln RMS acceleration,

$\xi^2_{T_s}$ = variance of \ln strong motion duration, and

ρ = correlation coefficient of \ln RMS acceleration and \ln strong motion duration.

The expected value of the strong motion duration given the RMS acceleration can thus be written as:

$$\begin{aligned}
E[T_s | \text{RMS} = r] &= \exp\left(\lambda'_{T_s} + \frac{1}{2} \xi'^2_{T_s}\right) \\
&= r^{\rho \frac{\xi_{T_s}}{\xi_{\text{RMS}}}} \exp\left[\frac{1}{2}(1-\rho^2)\xi^2_{T_s} + \lambda_{T_s} - \rho\lambda_{\text{RMS}} \frac{\xi_{T_s}}{\xi_{\text{RMS}}}\right]
\end{aligned} \tag{3.24}$$

and the variance of T_s given the RMS acceleration, can be written as:

$$\text{var}(T_s | \text{RMS} = r) = \omega(\omega - 1) r^{2\rho \frac{\xi_{T_s}}{\xi_{\text{RMS}}}} \exp\left[2\left(\lambda_{\text{RMS}} - \rho\lambda_{\text{RMS}} \frac{\xi_{T_s}}{\xi_{\text{RMS}}}\right)\right] \tag{3.25}$$

where:

$$\omega = \exp\left[(1-\rho^2)\xi^2_{T_s}\right] \tag{3.26}$$

The dependence of the parameters of the distributions on the distance from the rupture zone is taken into account by dividing the recording stations into two groups: one with distance to the rupture zone less than 50 km and the other with distance greater than 50 km. Due to the limited amount of data available for each group, further subdivision into more groups based on the distance from the rupture zone will result in a very small data set and consequently the parameters determined from each group will be quite unreliable. Moreover, further subdivision would require more simulations which would be economically prohibitive. The data considered for computing the parameters for the distributions are presented in tables 3-III and 3-IV. These tables show the different recording stations located on firm sites for the Loma Prieta, Whittier Narrows and Morgan Hill earthquakes. These tables also show the Trifunac and Brady strong motion duration and the corresponding RMS acceleration values for the two directions of recorded ground motion at each recording station.

TABLE 3-III Trifunac and Brady's (1975) strong motion duration and the RMS acceleration values for the Loma Prieta, Whittier Narrows, and Morgan Hill earthquakes for sites with distances to rupture zones less than 50 km

SITE NAME AND NUMBER	EARTHQUAKE	AZIMUTH	DURATION (sec)	RMS (cm/sec²)
Corralitos - Eureka Canyon 57007	Loma Prieta	360	6.86	163.240
		90	7.98	134.521
Crystal Springs - Pulgas 58378	Loma Prieta	0	15.12	32.871
		90	16.10	24.841
Crystal Springs - Skyline 58373	Loma Prieta	0	16.76	26.600
		90	15.98	30.071
Gilroy #1 - G.C. Water Tank 47379	Loma Prieta	360	3.70	159.600
		90	6.64	94.680
Gilroy #6 - San Ysidro 57383	Loma Prieta	90	12.66	44.473
		360	12.98	31.244
Monterey City Hall 47377	Loma Prieta	0	13.28	18.542
		90	11.96	16.448
SAGO South 47189	Loma Prieta	261	14.80	18.065
		351	18.84	16.979
Santa Cruz - UCSC 58135	Loma Prieta	360	9.50	125.522
		90	9.70	108.757
Saratoga - Aloha Ave. 58065	Loma Prieta	360	9.40	93.345
		90	8.26	86.349
Stanford Linear Accelerator 1601	Loma Prieta	360	11.62	66.926
		270	12.56	50.524
Woodside - Fire Station 58127	Loma Prieta	90	15.92	21.274
		0	18.06	18.468
Mt. Wilson 24399	Whittier Narrows	90	8.40	41.208
		0	10.08	27.014
Inglewood 14196	Whittier Narrows	90	11.24	41.040
		0	7.84	59.742
LA-116th St. School 14403	Whittier Narrows	360	6.58	86.373
		270	9.52	52.197
LA - Baldwin Hills 24157	Whittier Narrows	90	14.42	32.247
		0	13.62	30.604
Long Beach Park (14241)	Whittier Narrows	90	23.18	10.467
Pacoima (24088)	Whittier Narrows	90	9.90	32.824
Ranchoff (23497)	Whittier Narrows	90	14.96	12.045
Corralitos - Eureka Canyon 57007	Morgan Hill	310	10.30	22.842
		220	11.52	17.988
Gilroy #1 - G.C. Water Tank 47379	Morgan Hill	320	9.10	19.161
		230	9.80	17.442
Gilroy #6 - San Ysidro 57383	Morgan Hill	90	6.50	86.931
		0	7.30	54.609
Gilroy Gavilan College 47006	Morgan Hill	67	8.60	19.364
		337	8.54	18.971

TABLE 3-IV Trifunac and Brady's (1975) strong motion duration and the RMS acceleration values for the Loma Prieta and Whittier Narrows earthquakes for sites with distances to rupture zones greater than 50 km

SITE NAME AND NUMBER	EARTHQUAKE	AZIMUTH	DURATION (sec)	RMS (cm/sec ²)
Berkeley - LB Lab 58471	Loma Prieta	90	8.16	32.149
		0	18.22	14.115
Hayward - CSUH Stadium 58219	Loma Prieta	90	19.30	17.421
		0	19.06	15.371
Piedmont Jr. High School 58338	Loma Prieta	45	11.98	15.043
		315	11.72	15.667
Point Bonita 58043	Loma Prieta	297	8.34	24.743
		207	10.08	18.947
S.F. - Cliff House 58132	Loma Prieta	90	7.26	32.441
		360	10.28	22.420
S.F. - Diamond Heights 58130	Loma Prieta	90	9.42	25.080
		360	8.78	29.915
S.F. - Pacific Heights 58131	Loma Prieta	270	11.10	16.557
		360	12.40	13.467
S.F. - Presidio 58222	Loma Prieta	90	8.56	41.682
		360	10.54	28.719
S.F. - Rincon Hill 58181	Loma Prieta	90	11.52	18.173
		360	13.88	14.943
S.F. - Telegraph Hill 58133	Loma Prieta	90	9.48	16.586
		360	11.46	11.312
S.S.F. Siera Point 58539	Loma Prieta	205	9.48	21.470
		115	11.68	15.039
Yerba Buena Island 58163	Loma Prieta	90	8.32	16.986
		360	21.66	6.509
Vasqpark (24047)	Whittier Narrows	0	9.22	12.877

The parameters of the distributions are determined using the method of maximum likelihood. For RMS acceleration, the parameters are determined using the following two equations:

$$\lambda_{\text{RMS}} = \frac{\sum_{i=1}^n \ln(\text{RMS}_i)}{n} \quad (3.27)$$

and

$$\xi_{\text{RMS}}^2 = \frac{1}{n} \sum_{i=1}^n (\ln(\text{RMS}_i) - \lambda_{\text{RMS}})^2 \quad (3.28)$$

where RMS_i is the RMS acceleration value of the i^{th} ground motion and n is the number of samples in the data.

The parameters λ_{T_s} and ξ_{T_s} are computed in a similar manner. Figures 3-9 and 3-10 show the plot of the data. As can be seen from these figures, there is a strong negative correlation between natural log of RMS acceleration and natural log of strong motion duration, T_s . Table 3-V presents the values of the parameters of the distributions.

TABLE 3-V Parameters for the estimation of the mean and the variance of the conditional strong motion duration given the RMS acceleration

Parameters	Distance less than 50 km.	Distance greater than 50 km.
λ_{RMS}	3.633	2.916
ξ_{RMS}	0.751	0.398
λ_{T_s}	2.378	2.413
ξ_{T_s}	0.361	0.293
Correl. coeff. $\rho_{\ln T_s, \ln RMS}$	-0.705	-0.686

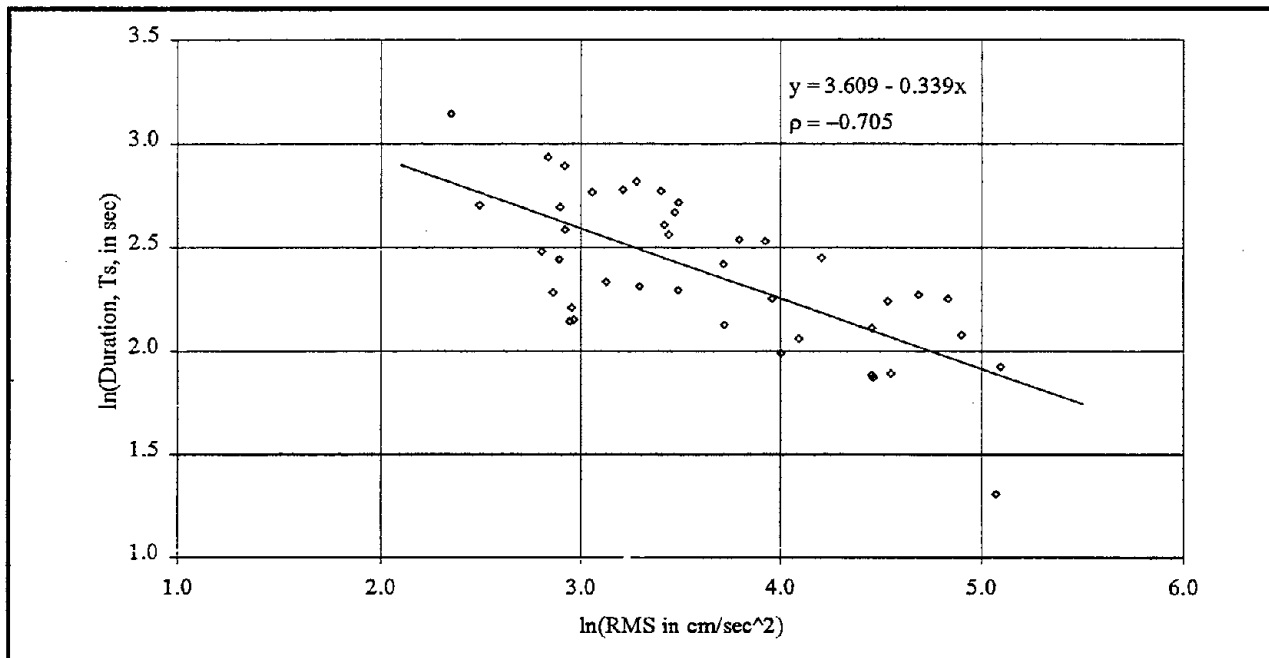


FIGURE 3-9 Correlation between Trifunac and Brady's (1975) strong motion duration and the RMS acceleration for firm sites with distances to rupture zones less than 50 km

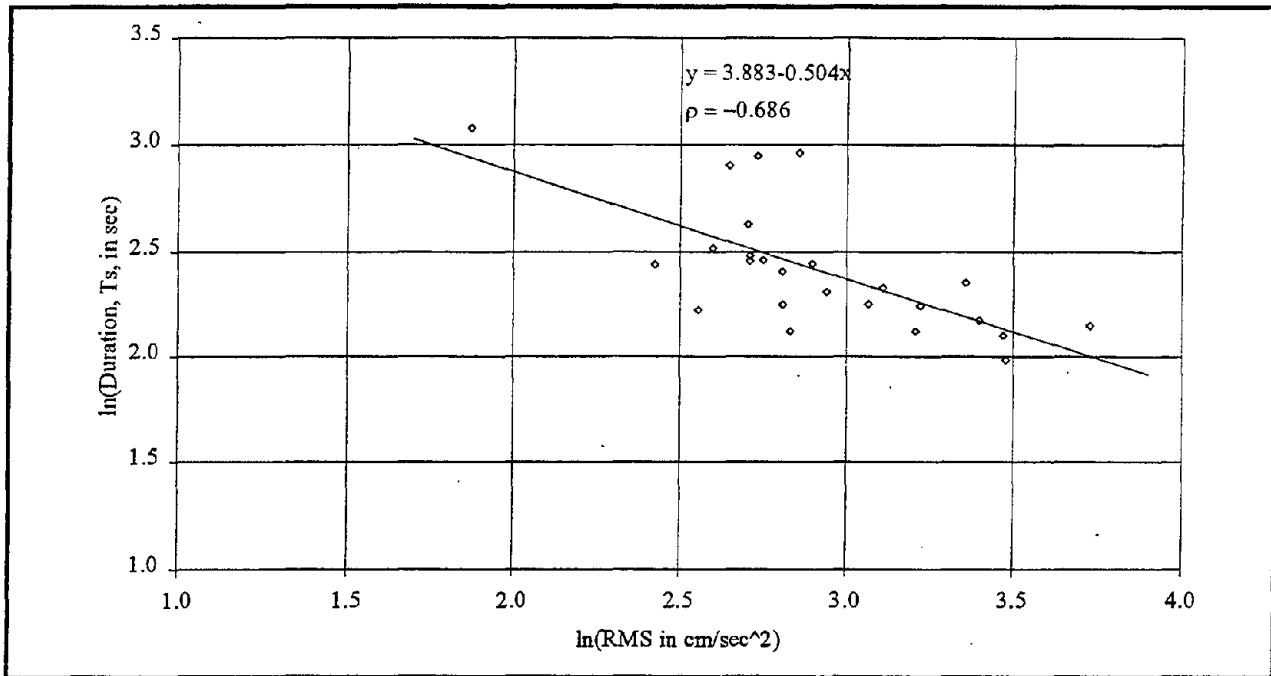


FIGURE 3-10 Correlation between Trifunac and Brady's (1975) strong motion duration and the RMS acceleration for firm sites with distances to rupture zones greater than 50 km

3.4.2.5 Relationship Between Spectral Acceleration and Strong Motion Duration

The spectral acceleration in three period bands is used in order to investigate its relationship with strong motion duration. The three period ranges used are representative of three classes of reinforced concrete frames and are based on the study reported in FEMA 223 (1992). Details on arriving at the three ranges are provided in Section 4. The spectral acceleration appears to be poorly related to strong motion duration. Table 3-VI shows the average spectral acceleration in the three ranges along with the MMI values at the recording stations. The strong motion duration for the horizontal components of ground motion listed in table 3-VI can be obtained from tables 3-III and 3-IV. At a recording station, the two components of ground motion in table 3-VI are listed in the same order as in tables 3-III and 3-IV. Figures 3-11 through 3-13 show the plot of the data and the correlation between the strong motion duration and the spectral acceleration in the three period bands. A lognormal probability density independent of the spectral acceleration is assumed for the strong motion duration when generating time histories for a given spectral acceleration. The parameters of the distribution are $\lambda_{T_s} = 2.391$ and $\xi_{T_s} =$

0.331. Figure 3-14 presents the comparison of the lognormal distribution with these parameters and the observed distribution.

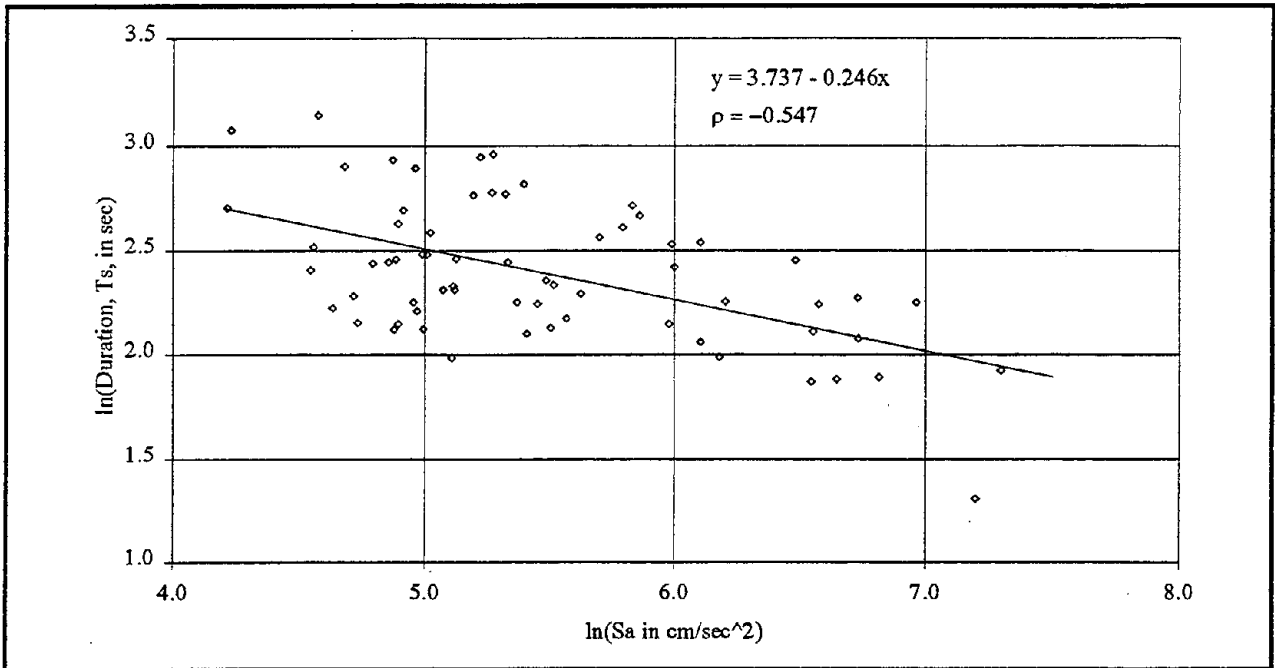


FIGURE 3-11 Correlation between Trifunac and Brady's (1975) strong motion duration and the average S_a in the period range 0.1-0.5 sec for firm sites

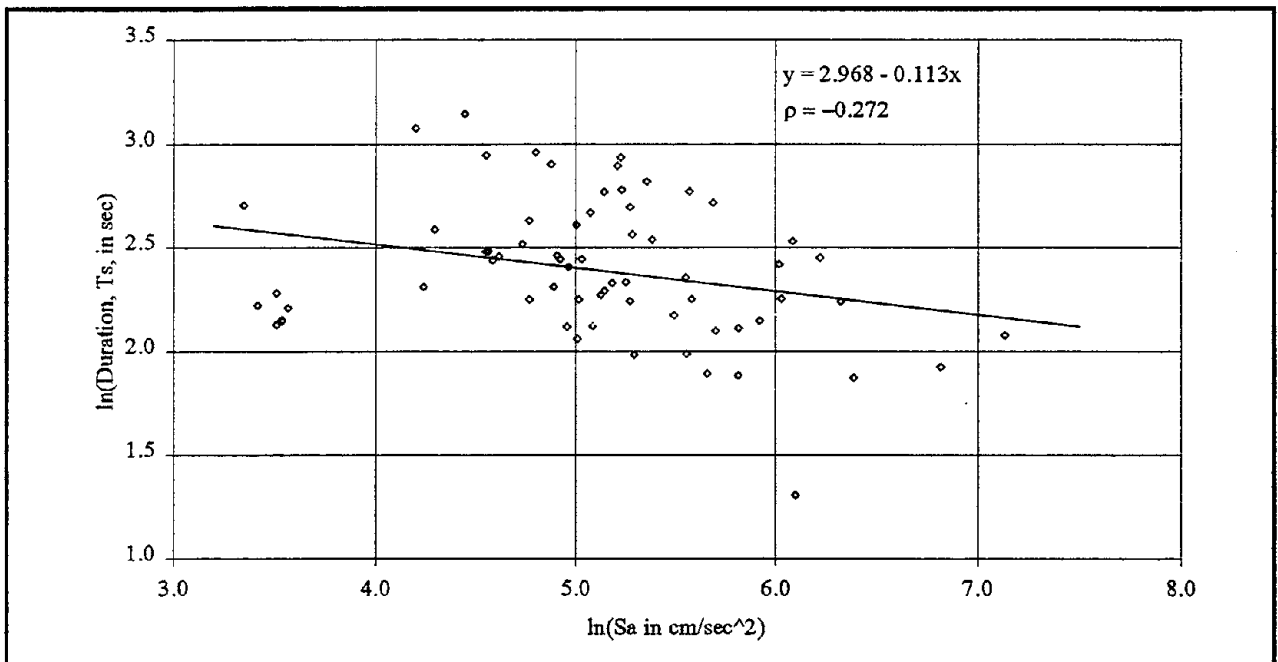


FIGURE 3-12 Correlation between Trifunac and Brady's (1975) strong motion duration and the average S_a in the period range 0.5-0.9 sec for firm sites

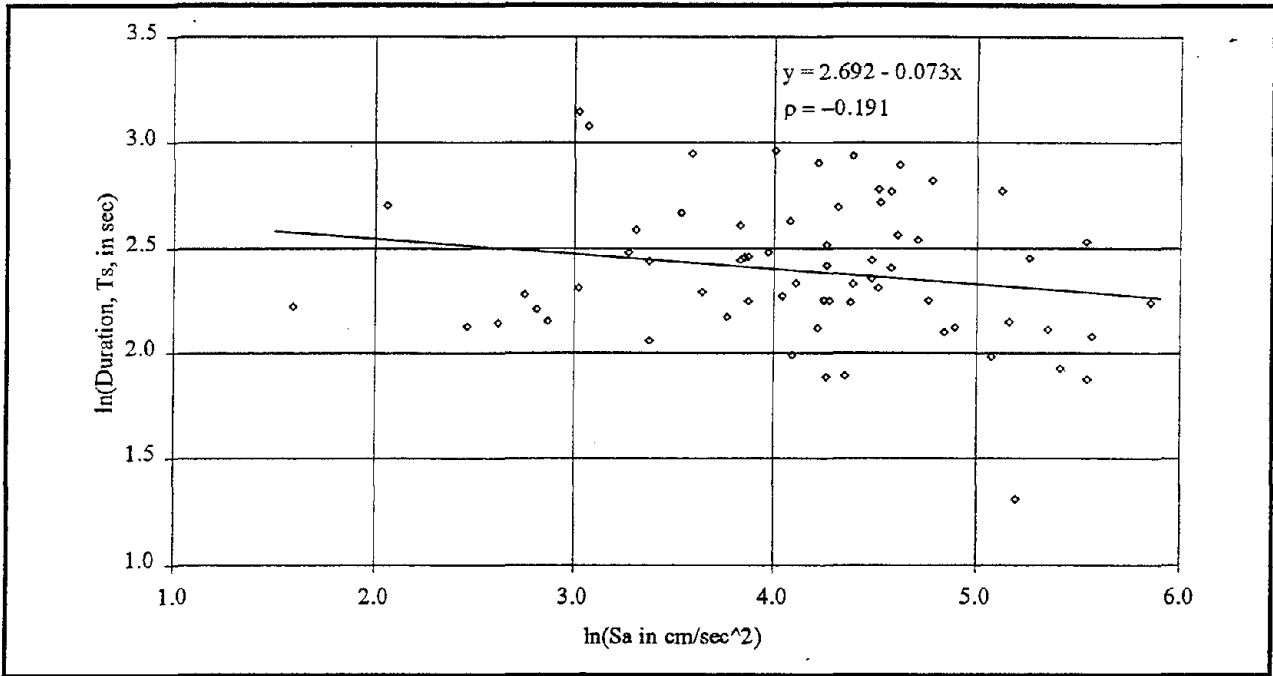


FIGURE 3-13 Correlation between Trifunac and Brady's (1975) strong motion duration and the average S_a in the period range 0.9-2.5 sec for firm sites

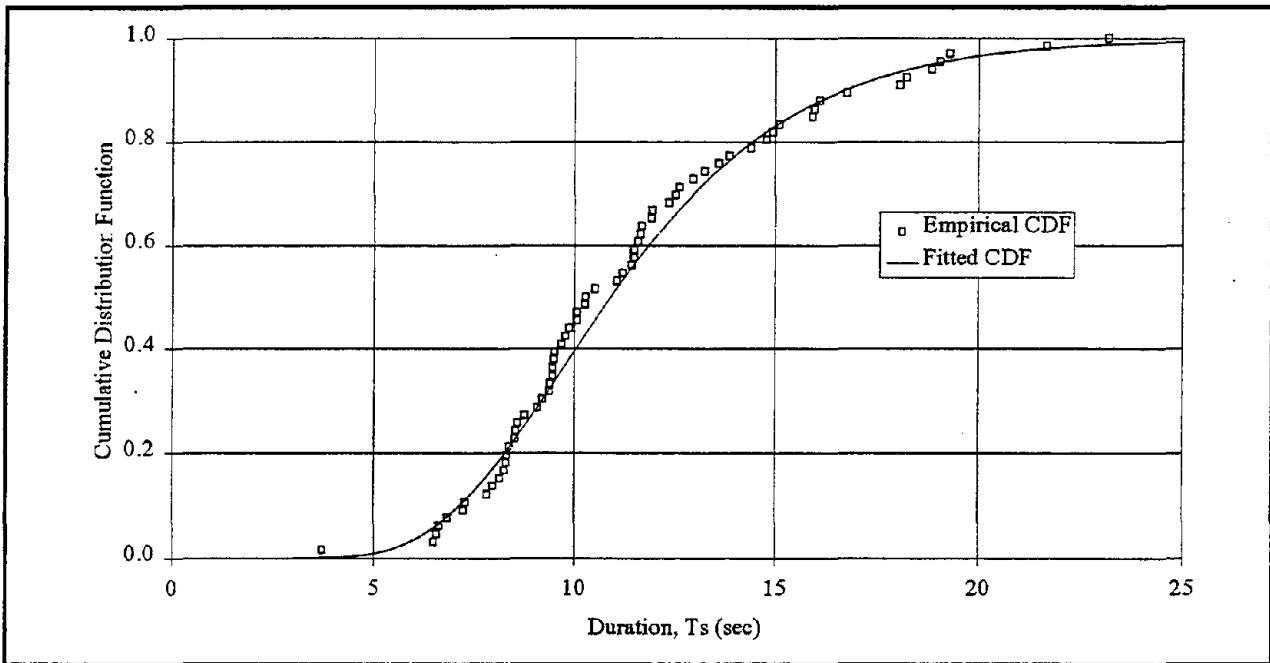


FIGURE 3-14 Comparison of the observed and the estimated log normal distribution ($\lambda_{T_s} = 2.391$ and $\xi_{T_s} = 0.331$) of strong motion duration for firm sites

TABLE 3-VI Average spectral acceleration and MMI values for the Loma Prieta, Whittier Narrows, and Morgan Hill earthquakes

SITE NAME AND NUMBER	EARTHQUAKE	MMI	Average S_a ($0.1 \leq T \leq 0.5$) (g)	Average S_a ($0.5 < T \leq 0.9$) (g)	Average S_a ($0.9 < T \leq 2.5$) (g)
Berkeley - LB Lab 58471	Loma Prieta	7	0.228	0.306	0.129
			0.110	0.134	0.069
Corralitos - Eureka Canyon 57007	Loma Prieta	8	1.506	0.934	0.228
			0.856	1.277	0.267
Crystal Springs - Pulgas 58378	Loma Prieta	7	0.348	0.302	0.094
			0.198	0.191	0.093
Crystal Springs - Skyline 58373	Loma Prieta	7	0.225	0.216	0.121
			0.209	0.268	0.171
Gilroy #1 - G.C. Water Tank 47379	Loma Prieta	7	1.363	0.454	0.184
			0.932	0.293	0.079
Gilroy #6 - San Ysidro 57383	Loma Prieta	6	0.457	0.222	0.113
			0.305	0.201	0.102
Hayward - CSUH Stadium 58219	Loma Prieta	6	0.199	0.124	0.056
			0.189	0.097	0.037
Monterey City Hall 47377	Loma Prieta	6	0.155	0.075	0.028
			0.153	0.097	0.027
Piedmont Jr. High School 58338	Loma Prieta	7	0.150	0.098	0.054
			0.172	0.138	0.049
Point Bonita 58043	Loma Prieta	6	0.151	0.165	0.136
			0.163	0.136	0.093
SAGO South 47189	Loma Prieta	7	0.139	0.199	0.076
			0.133	0.190	0.082
Santa Cruz - UCSC 58135	Loma Prieta	8	1.080	0.271	0.119
			0.853	0.172	0.058
Saratoga - Aloha Ave. 58065	Loma Prieta	8	0.731	0.567	0.356
			0.714	0.343	0.215
S.F. - Cliff House 58132	Loma Prieta	7	0.169	0.203	0.163
			0.170	0.182	0.082
S.F. - Diamond Heights 58130	Loma Prieta	6	0.238	0.199	0.081
			0.267	0.248	0.044
S.F. - Pacific Heights 58131	Loma Prieta	7	0.096	0.146	0.099
			0.097	0.116	0.072
S.F. - Presidio 58222	Loma Prieta	7	0.403	0.380	0.178
			0.246	0.263	0.090

TABLE 3-VI (cont' d) Average spectral acceleration and MMI values for the Loma Prieta, Whittier Narrows, and Morgan Hill earthquakes

SITE NAME AND NUMBER	EARTHQUAKE	MMI	Average S_a ($0.1 \leq T \leq 0.5$) (g)	Average S_a ($0.5 < T \leq 0.9$) (g)	Average S_a ($0.9 < T \leq 2.5$) (g)
S.F. - Rincon Hill 58181	Loma Prieta	7	0.131	0.156	0.090
			0.136	0.120	0.060
S.F. - Telegraph Hill 58133	Loma Prieta	7	0.145	0.120	0.073
			0.123	0.100	0.030
S.S.F. Siera Point 58539	Loma Prieta	7	0.219	0.154	0.049
			0.135	0.103	0.048
Stanford Linear Accelerator 1601	Loma Prieta	7	0.666	0.512	0.196
			0.407	0.447	0.259
Woodside - Fire Station 58127	Loma Prieta	7	0.184	0.175	0.099
			0.146	0.187	0.103
Yerba Buena Island 58163	Loma Prieta	7	0.134	0.145	0.069
			0.070	0.068	0.022
Mt. Wilson 24399	Whittier Narrows	6	0.251	0.034	0.012
			0.171	0.071	0.021
Inglewood 14196	Whittier Narrows	6	0.412	0.418	0.072
			0.458	0.153	0.030
LA-116th St. School	Whittier Narrows	6	0.786	0.343	0.072
			0.506	0.423	0.071
LA - Baldwin Hills 24157	Whittier Narrows	6	0.358	0.163	0.035
			0.335	0.152	0.047
Long Beach Park (14241)	Whittier Narrows	6	0.099	0.087	0.021
Pacoima (24088)	Whittier Narrows	5	0.283	0.175	0.039
Ranchoff (23497)	Whittier Narrows	5	0.069	0.029	0.008
Vasqpark (24047)	Whittier Narrows	5	0.105	0.031	0.005
Corralitos - Eureka Canyon 57007	Morgan Hill	6	0.254	0.195	0.062
			0.211	0.140	0.047
Gilroy #1 - G.C. Water Tank 47379	Morgan Hill	6	0.147	0.036	0.017
			0.114	0.034	0.016
Gilroy #6 - San Ysidro 57383	Morgan Hill	6	0.710	0.605	0.261
			0.494	0.264	0.061
Gilroy Gavilan College 47006	Morgan Hill	6	0.116	0.035	0.018
			0.136	0.035	0.014

3.4.3 Simulation of Ground Motion

Artificial time histories are required for the Monte Carlo simulation technique of obtaining motion-damage relationships. This section describes the simulation of ground motion time histories for two ground motion parameters: RMS acceleration and spectral acceleration. Figure 3-15 provides the overview of the procedure for ground motion simulation. For simulating time histories for a specified level of RMS acceleration, the ARMA parameters are computed for a Kanai-Tajimi power spectrum. There are two ways of simulating ground motion when spectral acceleration is used to characterize the ground motion. These include the stationary Gaussian models with modulating functions and the ARMA models.

3.4.3.1 Simulation of Time Histories with Specified RMS Acceleration and Duration

Artificial time histories corresponding to a specified RMS acceleration are generated using the ARMA model. The ARMA parameters are computed for the Kanai-Tajimi power spectral density function. The parameters of the ARMA(2,1) model corresponding to the Kanai-Tajimi stochastic earthquake model (equation 3.21) can be computed from the following equations when the system is assumed to be underdamped (Conte et al., 1992):

$$\phi_1 = 2 e^{-\xi_g \omega_g \Delta t} \cos\left(\omega_g \sqrt{1 - \xi_g^2} \Delta t\right) \quad (3.29)$$

$$\phi_2 = - e^{-2\xi_g \omega_g \Delta t} \quad (3.30)$$

θ_1 is the solution of:

$$\theta_1^2 + \frac{2\rho_1\phi_1 - \phi_1^2 + \phi_2^2 - 1}{\phi_1 - \rho_1(1-\phi_2)} \theta_1 + 1 = 0, \quad |\theta_1| < 1 \quad (3.31)$$

where:

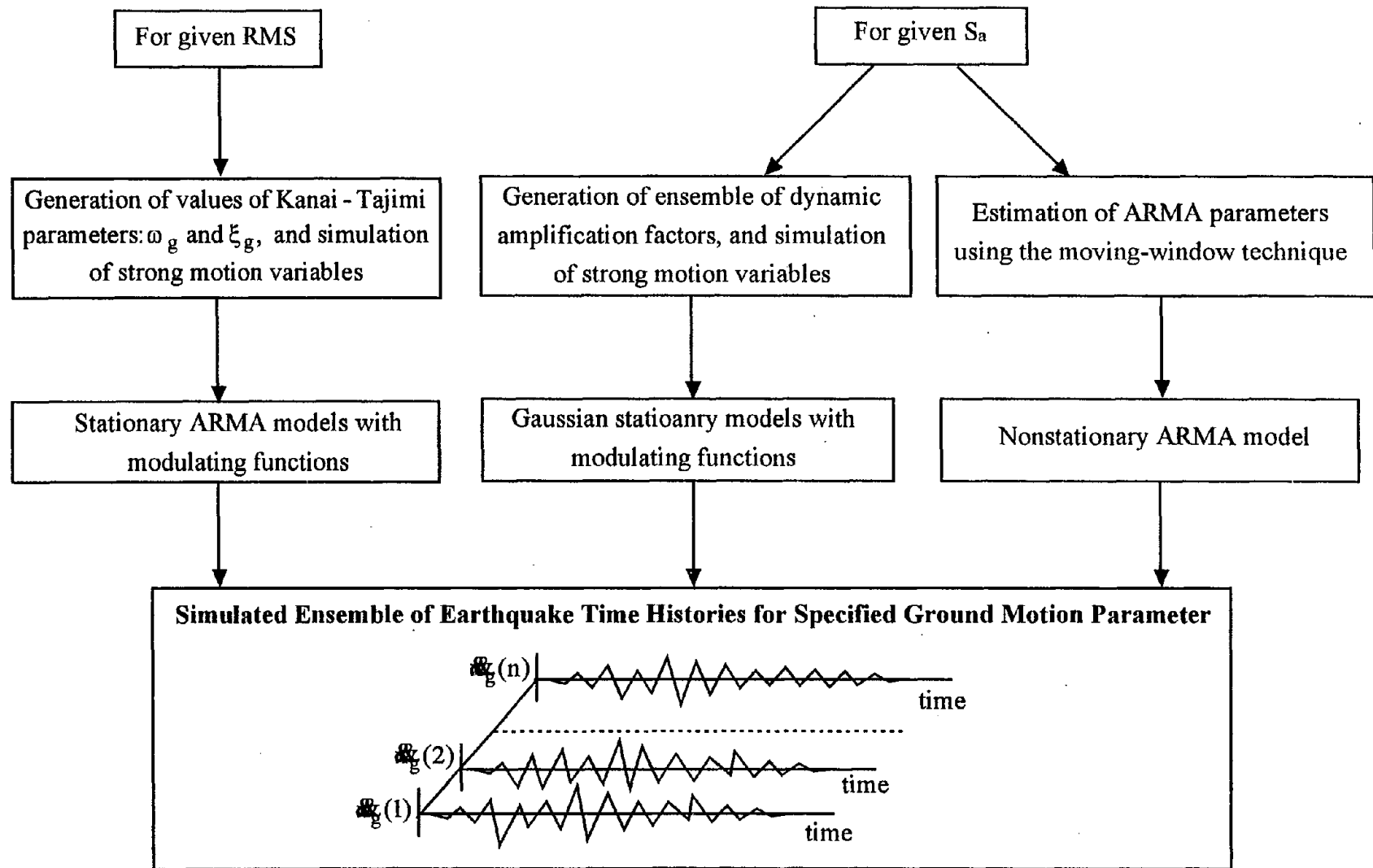


FIGURE 3-15 Steps in the simulation of time histories

$$\rho_1 = \rho(\Delta t) = \frac{1}{2} \frac{1 - 4\xi_g^2}{1 + 4\xi_g^2} \frac{\xi_g}{\sqrt{1 - \xi_g^2}} \sqrt{-(\phi_1^2 + 4\phi_2)} + \frac{1}{2}\phi_1 \quad (3.32)$$

The ARMA(2,1) spectrum is defined for all frequencies smaller or equal to the Nyquist frequency. Therefore the following condition should be satisfied:

$$0 < \omega_g \sqrt{1 - \xi_g^2} \leq \frac{\pi}{\Delta t} \quad (3.33)$$

The parameters ω_g and ξ_g are the parameters used to define the Kanai-Tajimi power spectral density.

Thus, the following steps are involved in the generation of artificial time histories using ARMA models:

1. Generation of a stationary discrete white-noise $\{e_k, k = 1, \dots, N\}$ where e_k is the shot noise impulse at time t_k .
2. Time modulation of the stationary white-noise by means of the following equation:

$$w_k = \psi(t_k) e_k \quad k = 1, \dots, N \quad (3.34)$$

where $\psi(t_k)$ is the envelope function.

3. ARMA filtering of the non-stationary white-noise. The ARMA (2,1) model given by equation 3.14 is used in the simulation process.

The time enveloping function suggested by Shinozuka and Sato (1967) may be used in step 2. This envelope function is given by:

$$\psi(t) = e^{-\alpha t} - e^{-\beta t} \quad \beta > \alpha > 0 \quad (3.35)$$

The parameters α and β in the above function need to be determined to correspond to the known strong motion duration.

Duration Calibration

The parameters α and β of the envelope function can be determined by means of the following two equations based on the Trifunac and Brady definition of strong motion duration:

$$0.05 \int_0^{T_d} |\psi(t)|^2 dt = \int_0^{T_1} |\psi(t)|^2 dt \quad (3.36)$$

and

$$0.95 \int_0^{T_d} |\psi(t)|^2 dt = \int_0^{T_2} |\psi(t)|^2 dt \quad (3.37)$$

where:

T_1 = start of the strong motion duration,

T_2 = end of the strong motion duration,

T_s = strong motion duration, and

T_d = total duration of the motion.

Using equation 3.35, equations 3.36 and 3.37 can be expressed as follows:

$$\frac{\alpha^2 - 2\alpha\beta + \beta^2 + 4\alpha\beta e^{-(\alpha+\beta)T_d} - \alpha\beta e^{-2\alpha T_d} - \alpha\beta e^{-2\beta T_d} - \alpha^2 e^{-2\beta T_d} - \beta^2 e^{-2\alpha T_d}}{20 \alpha\beta(\alpha + \beta)} = \frac{\alpha^2 - 2\alpha\beta + \beta^2 + 4\alpha\beta e^{-(\alpha+\beta)T_1} - \alpha\beta e^{-2\alpha T_1} - \alpha\beta e^{-2\beta T_1} - \alpha^2 e^{-2\beta T_1} - \beta^2 e^{-2\alpha T_1}}{\alpha\beta(\alpha + \beta)} \quad (3.38)$$

and

$$\frac{\alpha^2 - 2\alpha\beta + \beta^2 + 4\alpha\beta e^{-(\alpha+\beta)T_d} - \alpha\beta e^{-2\alpha T_d} - \alpha\beta e^{-2\beta T_d} - \alpha^2 e^{-2\beta T_d} - \beta^2 e^{-2\alpha T_d}}{20 \alpha\beta(\alpha + \beta)} =$$

$$\frac{\alpha^2 - 2\alpha\beta + \beta^2 + 4\alpha\beta e^{-(\alpha+\beta)T_2} - \alpha\beta e^{-2\alpha T_2} - \alpha\beta e^{-2\beta T_2} - \alpha^2 e^{-2\beta T_2} - \beta^2 e^{-2\alpha T_2}}{19\alpha\beta(\alpha + \beta)} \quad (3.39)$$

Applying the conditions that $T_2 - T_1$ is a known strong motion duration and $\alpha > \beta > 0$, equations 3.38 and 3.39 are solved by a predictor-corrector method for the parameters α and β .

The values of α and β obtained by solving equations 3.38 and 3.39 would satisfy the given strong motion duration if the time history is ergodic. However, in reality, the time history is not ergodic. Therefore, iterations need to be performed in the neighborhood of the values of α and β until the duration of the generated ground motion is close to the desired duration.

RMS Acceleration Calibration

The ARMA parameters are computed for the Kanai-Tajimi power spectral density function using equations 3.29 through 3.31. The procedure to determine the variance of the shot noise process, e_k in equation 3.13, is presented in this section.

Let $X(t)$ represent the stationary filtered process obtained after ARMA filtering and $Y(t)$ be the process obtained after $X(t)$ is modulated by the enveloping function. Thus

$$Y(t) = \psi(t) X(t) \quad (3.40)$$

The Arias intensity, I , of the final process $Y(t)$ is given by:

$$I = \int_0^{T_d} Y^2(t) dt \quad (3.41)$$

where:

T_d = total duration of the simulated process.

The expected value of the Arias intensity can be written as follows:

$$E[I] = \int_0^{T_d} E[Y^2(t)] dt = \int_0^{T_d} \sigma_Y^2 dt \quad (3.42)$$

Since $Y(t)$ is a process with zero mean, $E[Y^2] = \sigma_Y^2$.

Nigam (1983) shows that

$$\sigma_Y^2 = \sigma_X^2 |\psi(t)|^2 \quad (3.43)$$

where:

$$\sigma_X^2 = E[X^2(t)]$$

Equations 3.42 and 3.43 can be combined to yield:

$$E[I] = \int_0^{T_d} E[\psi(t)X(t)]^2 dt = \sigma_X^2 \int_0^{T_d} |\psi(t)|^2 dt \quad (3.44)$$

The variance σ_X can be related to the expected value of RMS acceleration based on equations 2.7 and 3.44. To a first order approximation for the expected values, the relationship between the two parameters is expressed as follows:

$$E[\text{RMS}] = \sqrt{\frac{0.9 E[I]}{T_s}} = \frac{\sigma_X}{\sqrt{T_s}} \sqrt{0.9 \int_0^{T_d} |\psi(t)|^2 dt} \quad (3.45)$$

or

$$\sigma_X = E[\text{RMS}] \sqrt{\frac{T_s}{0.9 \int_0^{T_d} |\psi(t)|^2 dt}} \quad (3.46)$$

where:

T_d = total duration of the simulated process and

T_s = Trifunac-Brady strong motion duration.

A factor of 0.9 is used in equation 3.46 as the Trifunac-Brady definition of strong motion is the time interval to accumulate 90 % of the total energy.

The variance of the stationary, filtered process $X(t)$ can be related to the variance of the input shot noise process by means of the following equation (Conte et al., 1992):

$$\sigma_X^2 = \frac{(1-\phi_2)(1+\theta_1^2) - 2\phi_1\theta_1}{(1+\phi_2)((1-\phi_2)^2 - \phi_1^2)} \sigma_e^2 \quad (3.47)$$

where:

σ_e^2 = variance of the shot noise process,

ϕ_1, ϕ_2, θ_1 = ARMA parameters, and

σ_X^2 = variance of the stationary filtered process $X(t)$.

The value of the variance of the shot noise process, σ_e^2 , has to match the expected value of RMS acceleration. This value is determined by solving equations 3.46 and 3.47 simultaneously. It is obvious that using this value of the variance of the shot noise process will lead to the RMS acceleration being satisfied only in the ensemble mean.

In order to match the desired RMS acceleration, the process generated by using the calculated value of σ_e^2 needs to be modified. Let the generated process be denoted by $Y_1(t)$ and its RMS acceleration by RMS_1 . The ratio of the desired RMS acceleration to RMS_1 is then used to scale the amplitudes of the time history $Y_1(t)$ to yield $Y(t)$. The resulting time history $Y(t)$ has the desired strong motion duration and RMS acceleration.

3.4.3.2 Simulation of Time Histories with Specified Spectral Acceleration

There are different ways of simulating the ground motion for a specified level of spectral acceleration. These include the stationary Gaussian models with modulating functions and the ARMA models. The input required to obtain time histories using the stationary Gaussian models with modulating functions is relatively simple, the target response spectrum and the envelope function are required. However, these models produce time histories which are nonstationary in amplitude but stationary in frequency content. Yeh and Wen (1990) show that the nonstationarity in frequency content has significant effect on the response of non-linear systems. To capture the nonstationarity in the frequency content of the ground motion, nonstationary ARMA models may be used to simulate time histories. However, in comparison to the Gaussian models with modulating functions, the nonstationary ARMA models require more input in terms of the time-varying ARMA parameters at different instants of time.

The response spectra for simulating time histories using the stationary Gaussian models with modulating functions are obtained from the dynamic amplification factors. The parameters of the lognormal distributions of the dynamic amplification factors at different periods are obtained from the mean and standard deviations shown in figure 3-4. These lognormal distribution

functions are used to generate values of the dynamic amplification factors at different periods. These dynamic amplification factors are then scaled to obtain an ensemble of response spectra corresponding to a given average ordinate of spectral acceleration in the period range corresponding to each structure class (for example, $0.1 \leq T \leq 0.5$ sec for low rise reinforced concrete frames). Earthquake time histories are then generated corresponding to these response spectra.

The moving-window technique or the Kalman filtering technique may be used to estimate the parameters of the nonstationary ARMA model. In this study, the moving time-window technique is used to estimate the parameters of the nonstationary ARMA model from ground motions recorded during the Loma Prieta, Whittier Narrows, and Morgan Hill earthquakes. The program MATLAB (1994) is used to estimate the ARMA parameters within each window. The ARMA parameters estimated for each window are assumed to be representative of the center point of the window. The parameter estimation is repeated for successive equidistant window positions. Based on a parametric study conducted to estimate the size of the ARMA model and the window size, it was found that the ARMA(2,1) model with a window size of 3 seconds gives reasonable results in terms of the spectral acceleration of the simulated time histories. The window is moved by 0.2 seconds between successive window positions. The moving-window technique for an acceleration time history is shown in figure 3-16. When generating time histories for a particular level of spectral acceleration, each simulated time history is scaled to match the desired spectral acceleration.

In addition, baseline correction is also performed using a high-pass, bi-lateral Butterworth filter to remove the low frequency components. The bi-lateral Butterworth filter is a pure amplitude filter and does not cause any phase shift in the resulting time history. Hamming (1987) provides a good description of different filters. The velocity and displacement time histories obtained by integrating the acceleration time history are also corrected. Using the least squares method, a straight line is fit to the displacement time history to obtain the corrected displacement. The slope of this straight line is added to the velocity, obtained by integration of the acceleration, to get the corrected velocity time history.

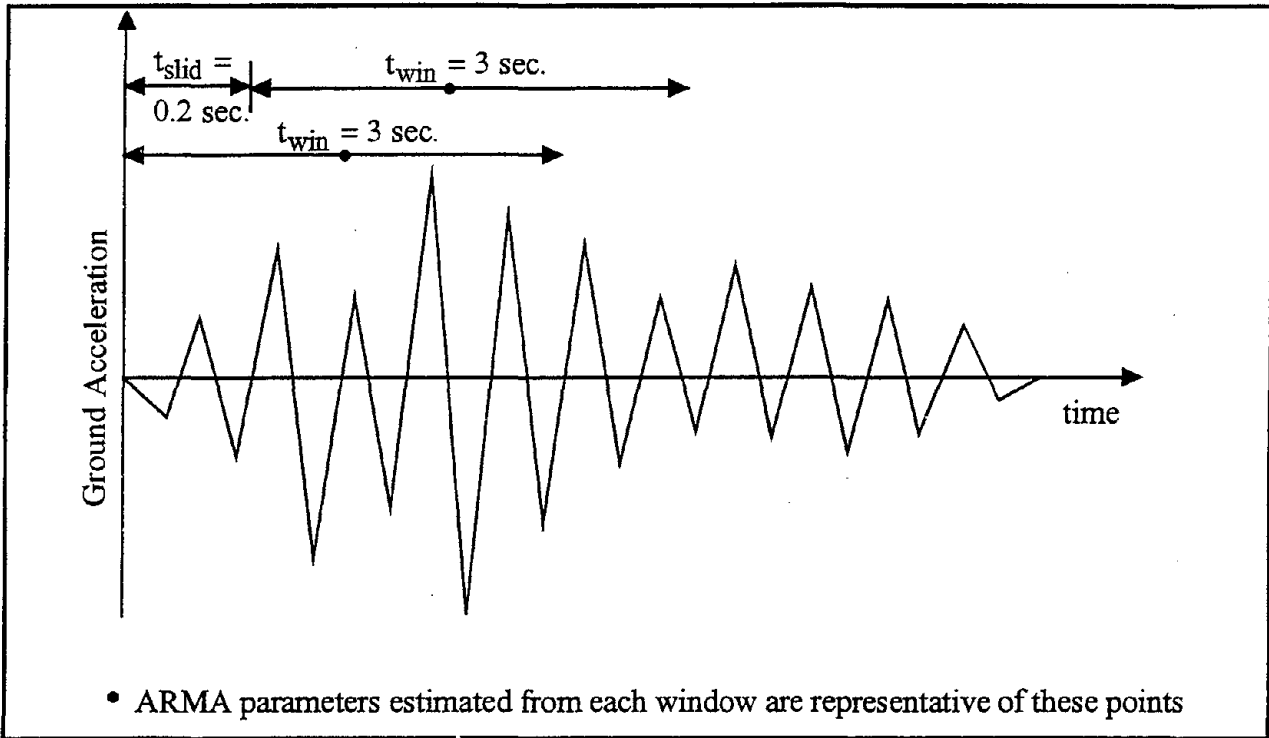


FIGURE 3-16 Representation of the moving-window technique

RMS acceleration is used to normalize the spectral shapes because it is insensitive to isolated peaks in the ground motion and is an average statistic for the entire time history. A comparison of the mean normalized spectral shapes computed from recorded time histories, obtained from the Loma Prieta, Whittier Narrows, and Morgan Hill earthquakes, and an ensemble of simulated time histories is presented in figure 3-17.

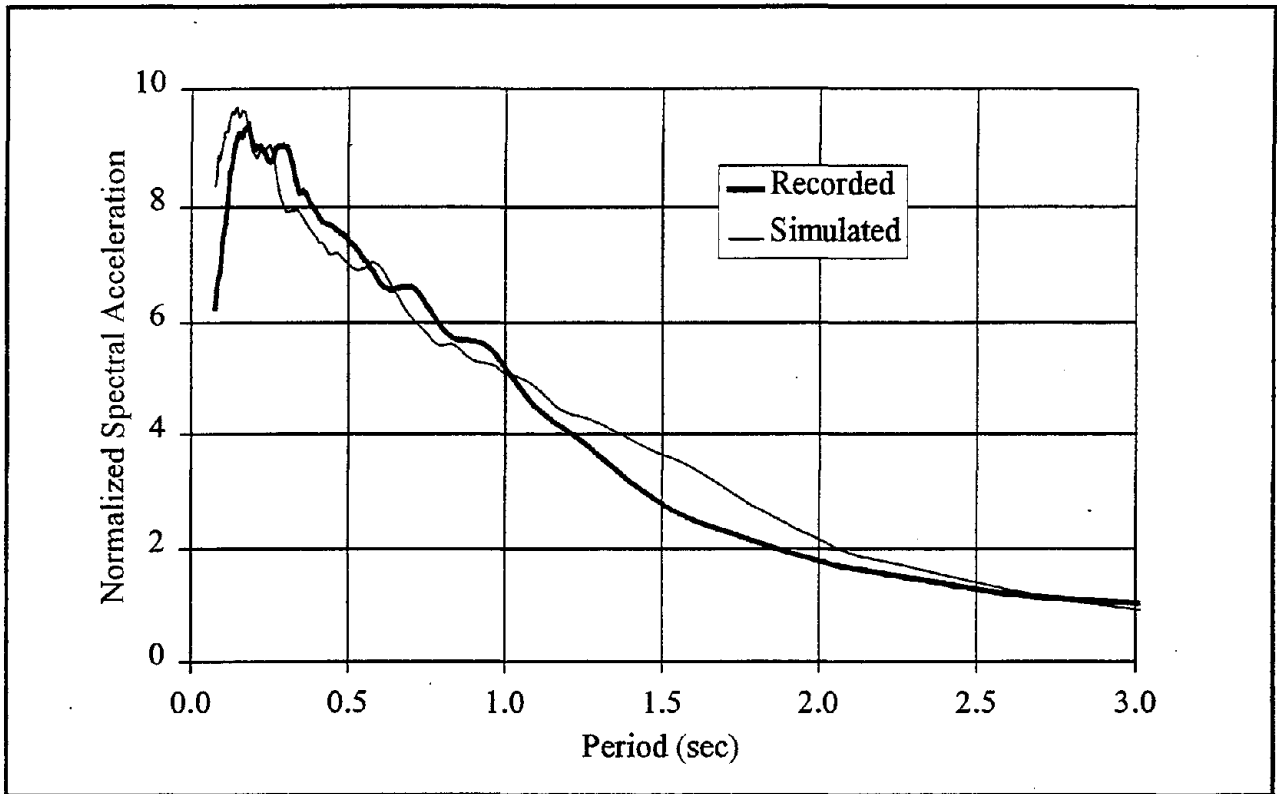


FIGURE 3-17 Comparison of the recorded and simulated spectral shapes

3.5 Bayesian Technique for Updating Fragility Curves

Fragility curves and DPMs, ideally, should be developed from observed data on seismic damage. Since such data are very limited at the present time, they can at best be used to revise or update the analytical fragility curves developed using the methodology presented earlier in this section. Bayesian analysis is used to combine the analytical estimates with observed data on damage. The remaining portion of this section provides a general description of the Bayesian analysis method. The application of the Bayesian analysis to update fragility curves is presented in Section 6. Section 6 also presents the probability distributions relevant to the fragility curves for reinforced concrete frames.

Bayes' theorem provides an approach for updating subjective knowledge with experimental results. If the experimental outcome is a set of observed values x_1, x_2, \dots, x_n , from a population X with underlying probability density function $f_{X|\theta}(x|\theta)$, the parameters of the

distribution, represented by the vector Θ , are revised in light of the experimental results by the following expression:

$$f''_{\Theta}(\Theta) = \frac{\left[\prod_{i=1}^n f_{X| \Theta}(x_i | \Theta) \right] f'_{\Theta}(\Theta)}{\int_{\Theta} \left[\prod_{i=1}^n f_{X| \Theta}(x_i | \Theta) \right] f'_{\Theta}(\Theta) d\Theta} \quad (3.48)$$

where:

$f'_{\Theta}(\theta)$ = prior density function of the parameters Θ ,

$f''_{\Theta}(\theta)$ = posterior density function of Θ , and

$f_{X| \Theta}(x|\theta)$ = probability distribution function of the basic random variable X.

The density $f'_{\Theta}(\theta)$ incorporates all prior knowledge about the unknown parameters. The prior knowledge can be in the form of subjective information. Equation 3.48 can be written as:

$$f''_{\Theta}(\Theta) = kL(X|\Theta)f'_{\Theta}(\Theta) \quad (3.49)$$

where:

$$k = \text{normalizing constant} = \left[\int_{\Theta} \left(\prod_{i=1}^n f_{X| \Theta}(x_i | \theta) \right) f'_{\Theta}(\theta) d\theta \right]^{-1} \text{ and}$$

$$L(X | \Theta) = \text{likelihood function} = \prod_{i=1}^n f_{X| \Theta}(x_i | \theta)$$

The likelihood function is proportional to the probability of making specific observations, $X = x_i$, given the values θ of the parameters. The initial belief about the stochastic behavior of the parameters of the distributions is thus updated using the observations.

Considerable mathematical simplification can be achieved if the distributions of the parameters are appropriately chosen with respect to the underlying random variable X . Such pairs of distributions are known as conjugate distributions. By choosing prior distributions that are conjugate of the distribution of the underlying random variable, one thereby obtains convenient posterior distributions, which are usually of the same mathematical form as the prior.

The uncertainty associated with parameters Θ is combined with the inherent variability of the underlying random variable, X , to obtain the total uncertainty associated with X . Using the total probability theorem, the posterior probability density function of X is expressed as follows:

$$f''_X(x) = \int_{\Theta} k L(X|\Theta) f_X(x | \Theta) f'(\Theta) d\Theta \quad (3.50)$$

3.6 Summary

This section presented a method for the development of fragility curves. In contrast to previous approaches for developing fragility curves and DPMs, the method presented in this section does not rely on heuristics or on empirical data. The methodology can be applied to a wide range of structural classes. The methodology is presented for two ground motion parameters: spectral acceleration and RMS acceleration. However, it is possible to use one of the other ground motion parameters presented in Section 2. The methodology is used to obtain fragility curves and DPMs for reinforced concrete frames in Sections 4 and 5. Section 6 presents the application of Bayesian analysis to update the fragility curves using actual data on building damage.

This section also reviewed the various techniques for simulating ground motion. Although there are a large number of recordings obtained from recent earthquakes, a consistent ensemble of time histories that cover all the different parameter ranges that can be discriminated according to distance to the fault, local soil parameters and spectral characteristics is currently not available. Thus, it is proposed that ensembles of time histories be simulated at each specified ground motion parameter level. The different models for ground motion simulation include the geophysical model, the stationary Gaussian models with modulating functions, and the ARMA models. Whereas the stationary Gaussian models with modulating functions incorporate nonstationarity of the amplitudes of the time histories, the nonstationary ARMA models are capable of accounting for nonstationarities in both the amplitude and the frequency content of the time histories. As these two nonstationarities significantly influence the response of non-linear systems, the non-stationary ARMA(2,1) model is used to simulate time histories in this study.



SECTION 4

MODELING OF REINFORCED CONCRETE FRAMES FOR FRAGILITY ANALYSIS

This section presents the application of the methodology presented in Section 3 to develop motion-damage relationships for reinforced concrete (RC) frames. Three classes of RC frames are considered. These include low rise frames that are 1-3 stories tall, mid rise frames that are 4-7 stories tall, and high rise frames that are 8 stories or taller. This classification is consistent with that defined in ATC-13 (1985) and is similar to that used in the standardized earthquake loss estimation methodology (NIBS, 1995). The motion-damage relationships for RC frames are obtained by using a representative building in each building class. The fragility curves are developed by using the Monte Carlo simulation technique. The nonstationary ARMA(2,1) model is used to generate artificial time histories corresponding to a specified value of average spectral acceleration.

4.1 Ground Motion Characterization for RC Frames

The average spectral acceleration ordinate in the period range corresponding to the three classes of reinforced concrete frames is used to characterize the ground motion for fragility curves. The three period bands used in this study are 0.1-0.5 seconds, 0.5-0.9 seconds, and 0.9-2.5 seconds. These period bands are based on the study reported in FEMA 223 (1992) and are estimated to reflect the natural periods of buildings belonging to the three classes of reinforced concrete frames. FEMA 223 suggests the following equation for estimating the periods of RC frames:

$$T = 0.035 h_n^{0.75} \quad (4.1)$$

where h_n is the height of the building in feet. Equation 4.1 is based on periods computed from accelerograph records obtained from RC frames during the 1971 San Fernando earthquake. The design codes (e.g., SEAOC, 1990) estimate the periods of reinforced concrete buildings conservatively using a coefficient of 0.03 in contrast to the value of 0.035 used in this study. FEMA 223 also estimates the average story height in reinforced concrete frames to be 9.65 feet. However, an integer value of 10 feet is used for the story height in this study.

Although the acceleration spectrum is likely to vary considerably over the long-period bands, the pseudo-velocity spectrum is expected to show much less variation as shown in figures 4-1 and 4.2. The normalized spectral curves are computed from the firm site records of six earthquakes. In comparison to Section 3 where ground motions recorded during the Loma Prieta, Whittier Narrows, and Morgan Hill earthquakes were used, recorded motions from three more earthquakes, Landers, Petrolia, and Northridge, are used here to arrive at the normalized spectral shapes. The average spectral acceleration in the three period bands for these ground motions are shown in table 4-I. The additional ground motions are considered here so as to have a larger number of ground motion records which are used in the sensitivity analysis later in this section. However, the number of recorded ground motions is still not large enough to be used in the development of fragility curves. Therefore, ground motion simulation is carried out to develop the fragility curves.

TABLE 4-I Average spectral acceleration values for the Landers, Petrolia, and Northridge earthquakes

SITE NAME AND NUMBER	EARTHQUAKE	Average S_a ($0.1 \leq T \leq 0.5$) (g)	Average S_a ($0.5 < T \leq 0.9$) (g)	Average S_a ($0.9 < T \leq 2.5$) (g)
Amboy 21081	Landers	0.356	0.236	0.163
		0.293	0.212	0.132
Joshua Tree 22170	Landers	0.533	0.700	0.335
		0.567	0.626	0.246
Puerta La Cruz 12168	Landers	0.084	0.023	0.014
		0.073	0.025	0.013
Silent Valley - Poppet Fl. 12206	Landers	0.086	0.033	0.020
		0.084	0.063	0.020
Twenty Nine Palms 22161	Landers	0.128	0.043	0.017
		0.120	0.032	0.020
Cape Mendocino 89005	Petrolia	2.320	1.111	0.395
		1.124	0.366	0.257
Shelter Cove Airport 89530	Petrolia	0.390	0.042	0.013
		0.321	0.049	0.017
LA - 116th St. School 14403	Northridge	0.396	0.215	0.083
		0.373	0.250	0.060
LA - Baldwin Hills 24157	Northridge	0.499	0.262	0.130
		0.453	0.263	0.137
LA - Hollywood Storage 24303	Northridge	0.837	0.615	0.164
		0.517	0.431	0.160

The dynamic amplification factors shown in figure 4-1 show very minor variations from those in figure 3-4. The ratio of the largest to the smallest mean dynamic amplification factors in the period band corresponding to high rise frames is about 4. The same ratio for normalized spectral velocity is only about 1.25. For mid rise frames, the differences between the normalized spectral acceleration and spectral velocity are less significant. The largest to the smallest dynamic amplification factors have a ratio of almost 1.35 compared to a ratio of 1.25 for the normalized spectral velocity in the mid rise period band.

The spectral acceleration used for the fragility curves can easily be converted into equivalent pseudo-spectral velocity at the centroidal periods in each period band. The relationship between the average spectral acceleration and the average spectral velocity for mid rise and high rise frames is shown in figures 4-3 and 4-4. As expected, the correlation coefficient between the spectral acceleration and velocity is more than 99%. The slope of the regression line is equal to $\bar{T}/2\pi$, where \bar{T} is the centroidal period used to convert spectral velocity into spectral acceleration in each period band. From the slopes of the regression lines shown in figures 4-3 and 4-4, the centroidal periods for the mid rise and high rise frames are estimated as 0.70 and 1.7 seconds, respectively. These centroidal periods correspond to the midpoint in the respective period bands.

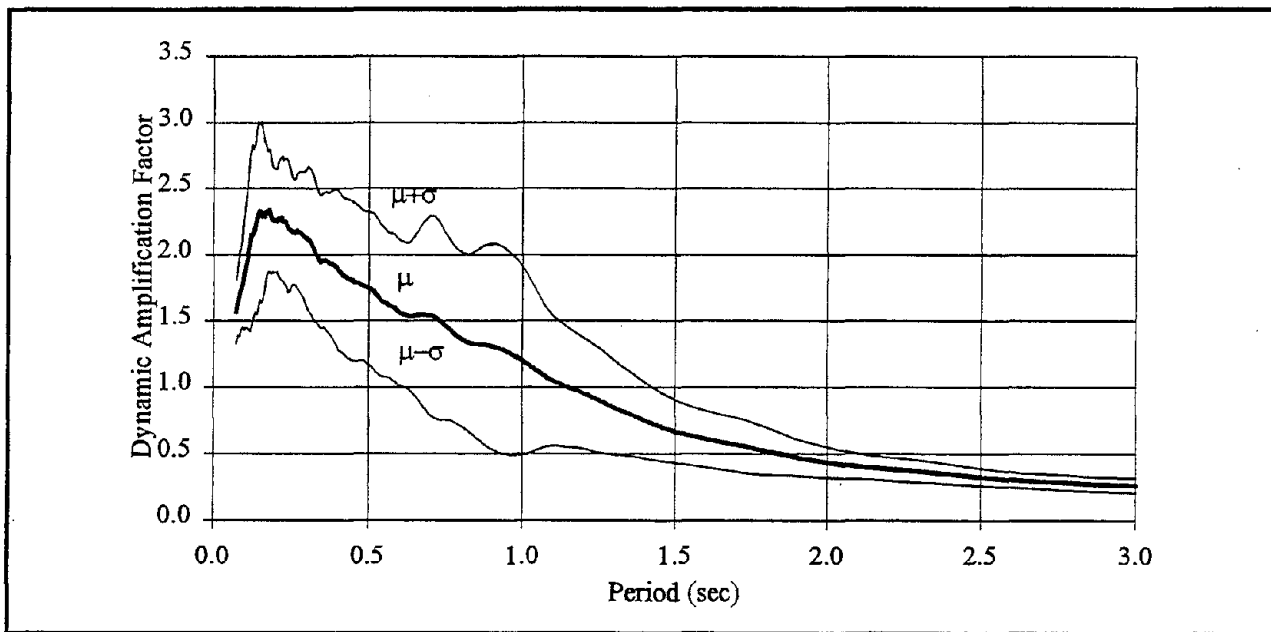


FIGURE 4-1 Dynamic amplification factors for firm sites

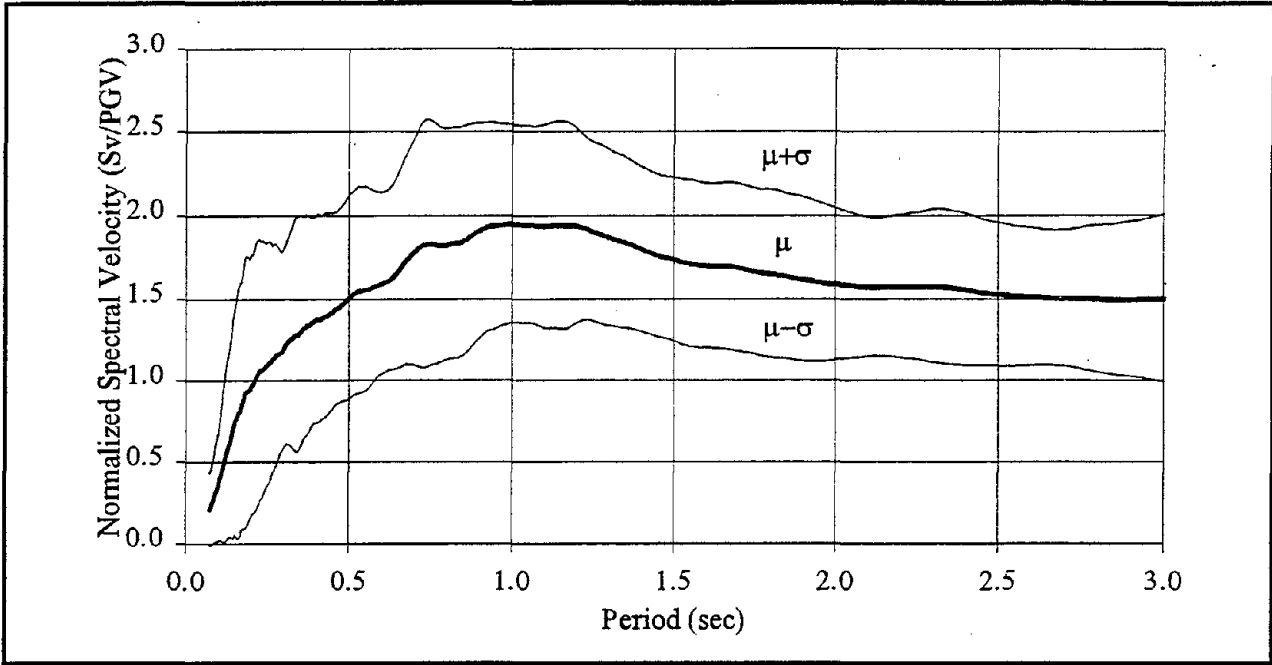


FIGURE 4-2 Normalized spectral velocity curves for firm sites

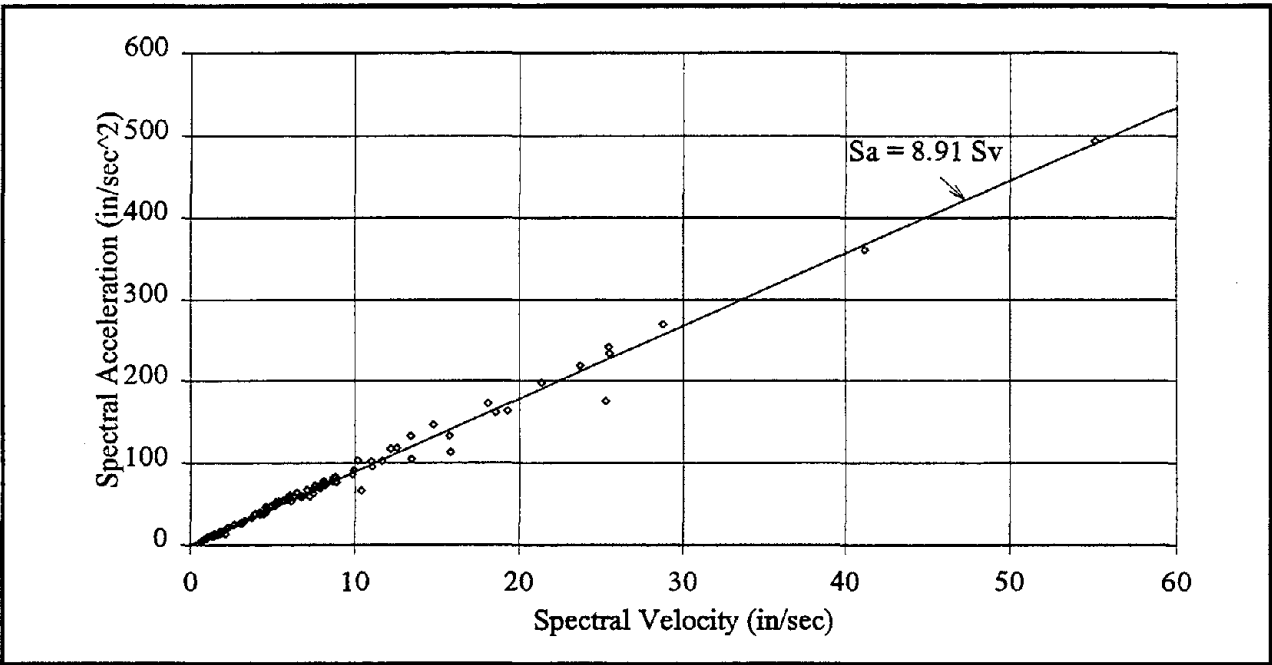


FIGURE 4-3 Relationship between spectral acceleration and velocity for $0.5 \leq T \leq 0.9$ seconds

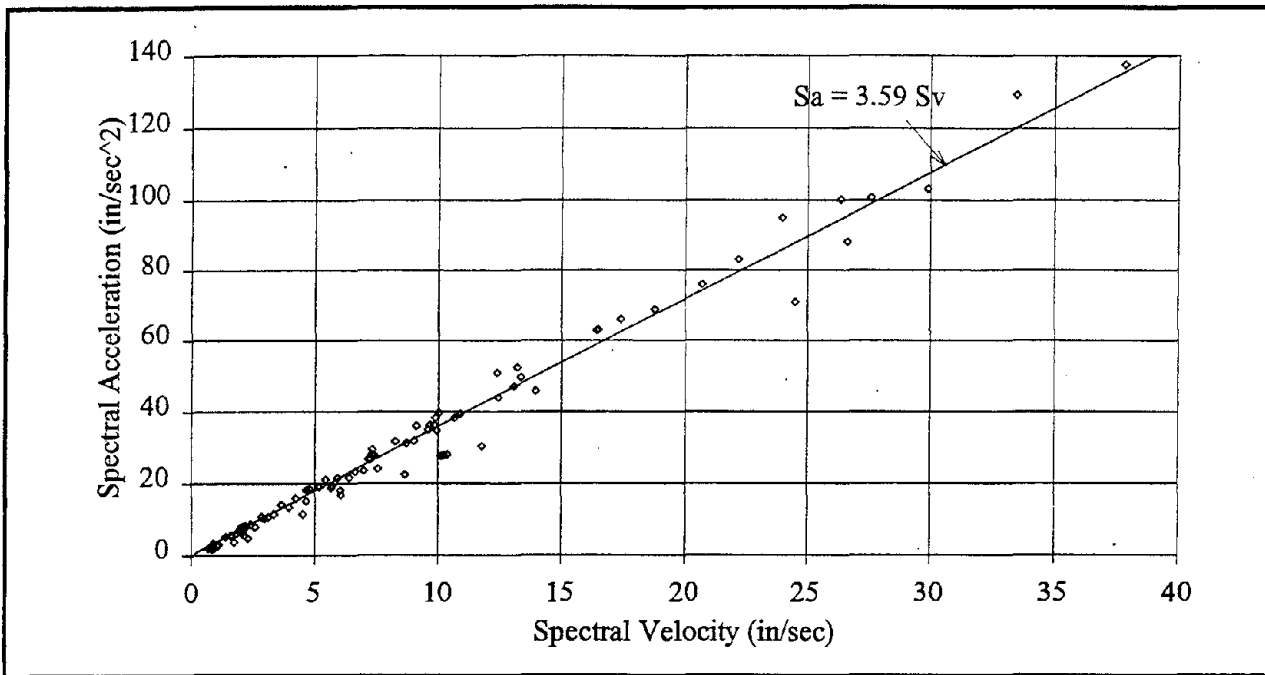


FIGURE 4-4 Relationship between spectral acceleration and velocity for $0.9 \leq T \leq 2.5$ seconds

Another way of determining the relationship between the average spectral acceleration and average spectral velocity is by assuming that spectral acceleration is equal to the pseudo-spectral acceleration and that the spectral velocity is constant in the respective period band. Thus, the average spectral acceleration can be expressed by means of the following two equations for mid rise and high rise frames, respectively.

$$S_a = \frac{1}{0.4} \int_{0.5}^{0.9} \frac{2\pi}{T} S_v dT = 9.233 S_v \quad 0.5 \leq T \leq 0.9 \quad (4.2)$$

$$S_a = \frac{1}{1.6} \int_{0.9}^{2.5} \frac{2\pi}{T} S_v dT = 4.012 S_v \quad 0.9 \leq T \leq 2.5 \quad (4.3)$$

The average values of spectral acceleration as functions of spectral velocity computed by using the regression analysis, presented above, are about 97% and 90% of the values given in equations 4.2 and 4.3 for the mid rise and the high rise frames, respectively.

4.2 Computation of Section Properties Needed for Damage Evaluation

The two section properties needed for evaluating the Park-Ang member damage are the ultimate rotation capacity, θ_u , and the yield moment, M_y . In this study, these properties are computed in the program IDARC2D (Kunnath et al., 1994). A brief description of the procedure adopted to compute these properties is presented in the following sub-sections. The computation of the properties for an example section is presented in Appendix A.

4.2.1 Computation of Ultimate Rotation Capacity of a Section

The following assumptions are made in IDARC2D (Kunnath and Reinhorn, 1994) when arriving at the ultimate rotation capacity. The ultimate curvature capacity of a member is assumed to be reached when a specified ultimate compressive strain in the extreme concrete fiber is reached or when the specified ultimate strength of one of the reinforcement bars is reached. The ultimate compressive strain in concrete is specified as the level of strain when the stress has dropped to 20% of the compressive strength of concrete. The details on arriving at this level of strain are presented below. The ultimate curvature is converted into ultimate rotation by assuming the plastic hinge length at each member end to be equal to 9% of the member length.

The behavior of the reinforcing steel is specified in terms of a trilinear stress-strain relationship with an initial elastic portion, a horizontal yield plateau, and a linear strain hardening portion. The stress-strain relationship for concrete as defined by the Kent and Park (1971) relationship and summarized by Park and Paulay (1975) is used in IDARC2D. This relationship is presented in figure 4-5. The expressions for stress at different levels of strain are given below.

For concrete strain, $\epsilon_c \leq 0.002$, the stress, f_c , is given by:

$$f_c = f'_c \left[\frac{2\epsilon_c}{0.002} - \left(\frac{\epsilon_c}{0.002} \right)^2 \right] \quad (4.4)$$

where:

f'_c = concrete cylinder strength.

Equation 4.4 is the expression for the ascending portion of the stress-strain curve in figure 4-5. The Kent and Park model assumes that the confining steel has no effect on the shape of this portion of the curve.

When the concrete strain exceeds 0.002, the stress, f_c , is given by:

$$f_c = f'_c [1 - Z(\epsilon_c - 0.002)] \quad (4.5)$$

where:

$$Z = \frac{0.5}{\epsilon_{50c} - 0.002}$$

Equation 4.5 describes the descending portion of the stress-strain curve when the concrete strain is greater than 0.002 and the concrete stress has not dropped to 20% of the concrete compressive strength. The parameter Z specifies the slope of this linear portion. The parameter ϵ_{50c} in the expression for Z specifies the strain in confined concrete when the stress has dropped to 50% of the compressive strength of concrete. ϵ_{50c} is defined by the following expression:

$$\epsilon_{50c} = \frac{3 + 0.002f'_c}{f'_c - 1000} + \frac{3}{4} \rho_s \sqrt{\frac{b''}{s_h}} \quad (4.6)$$

where:

ρ_s = ratio of volume of transverse reinforcement to volume of concrete core measured to outside of hoops,

b'' = width of confined core measured to outside of hoops, and

s_h = spacing of hoops.

The first term in equation 4.4 is the strain in unconfined concrete when the stress has dropped to 50% of the concrete strength. This term is represented as ϵ_{50u} in figure 4-5. The second term in equation 4.6 provides the additional ductility capacity due to confinement provided by the hoop reinforcement. However, the maximum stress reached by both the confined and the unconfined concrete is the cylinder strength f'_c .

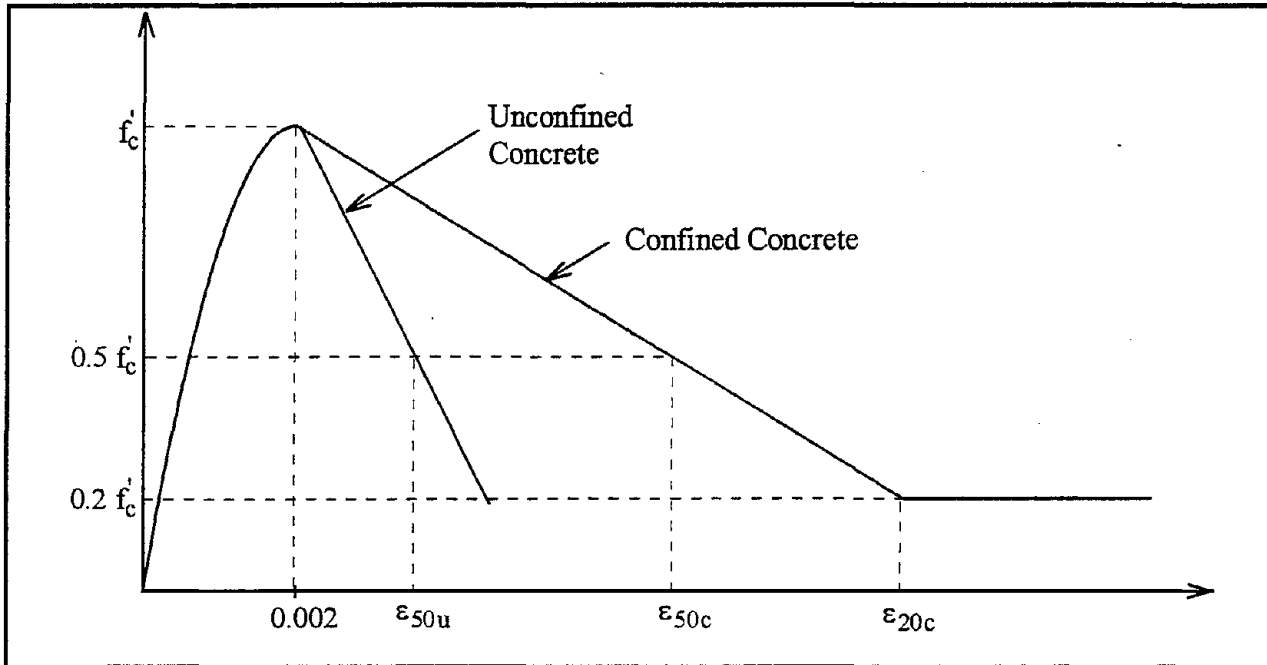


FIGURE 4-5 Kent and Park's stress-strain relationship for concrete (from Park and Paulay, 1975)

Paulay and Priestley (1992) suggest an increase in the compressive strength of concrete due to confinement. They also suggest that the ultimate compressive strain in confined concrete may be obtained by equating the strain energy capacity of the transverse steel at fracture to the increase in energy absorbed by the concrete. According to them, the ultimate compressive strain is given by the following expression:

$$\epsilon_{cu} = 0.004 + 1.4 \rho_s f_{yh} \epsilon_{sm} / f'_{cc} \quad (4.7)$$

where:

ρ_s = volumetric ratio of confining steel,

- f_{yh} = yield strength of confining steel,
- ε_{sm} = steel strain at maximum tensile stress, and
- f'_{cc} = compressive strength of confined concrete.

According to Paulay and Priestley, typical values of the ultimate compression strain in confined concrete range from 0.012 to 0.05, an increase of 4 to 16 times the values assumed for unconfined concrete.

When computing the ultimate curvature for a section, Bertero and Bertero (1992) also check that the buckling of compression steel has not occurred when the ultimate strain is reached in concrete or the ultimate strength of tensile steel is reached. They use the following expression to compute the critical buckling stress:

$$f_{cr} = 2E_t(\varepsilon_s)\pi^2 \frac{(0.25\phi_L)^2}{s^2} \tag{4.8}$$

where:

- $E_t(\varepsilon_s)$ = tangent modulus of steel stress-strain relation,
- ϕ_L = diameter of longitudinal bar, and
- s = spacing of stirrups.

4.2.2 Computation of Yield Moment for a Section

In this study, the yield moment capacity of a section is defined as the moment required to produce yielding of the tensile steel. If a section has a very high reinforcement ratio, or is subjected to a high axial load, yielding of the tensile steel may not occur till a high compressive strain has been developed in concrete. For these cases, Paulay and Priestley (1992) suggest that that the yield moment may be defined as the applied moment required to produce a compressive strain in concrete equal to 0.0015.

4.3 Evaluation of Structural Damage for Buildings on Firm Sites

The fragility curves and damage probability matrices (DPMs) are first developed for buildings located on firm sites. The dynamic amplification factors for these sites were presented in Section 3. However, the influence of soil sites is presented in the later part of this section.

4.3.1 Description of the Sample Structures

For the purposes of this study, a typical structure was considered to have five bays in the longitudinal direction and one bay in the transverse direction. The sample building for each class of concrete frames was designed according to the 1990 SEAOC Recommendations for special moment resisting frames. The thickness of the floor slab in these buildings was assumed to be 7 in. A uniformly distributed dead load of 30 psf was superimposed on the self weight of the structure and used in the design of the members. In addition, reduced live loads for member design were represented by a uniformly distributed load of 25 psf. The plans of the three structures are the same, and the plan of a typical structure is shown in figure 4-6. A typical interior frame for each of the three structures was used in the nonlinear time history analysis to estimate damage at different levels of ground shaking. As explained in Section 4.1, a story height of 10 feet is used for these buildings. figure 4-7 shows the elevations for the three frames used in the analysis.

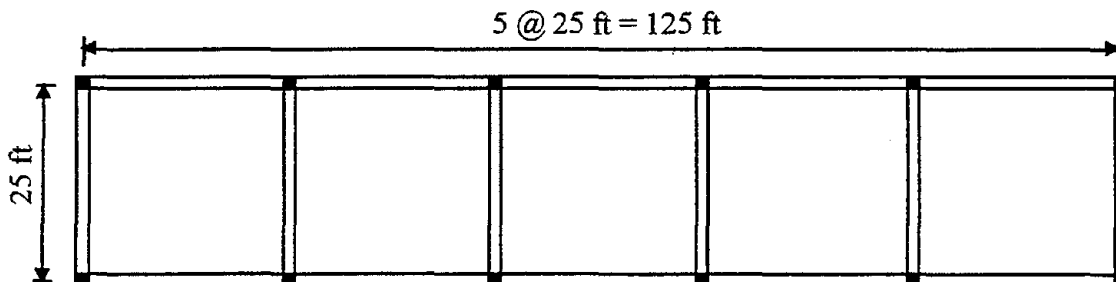


FIGURE 4-6 Plan of the three frames

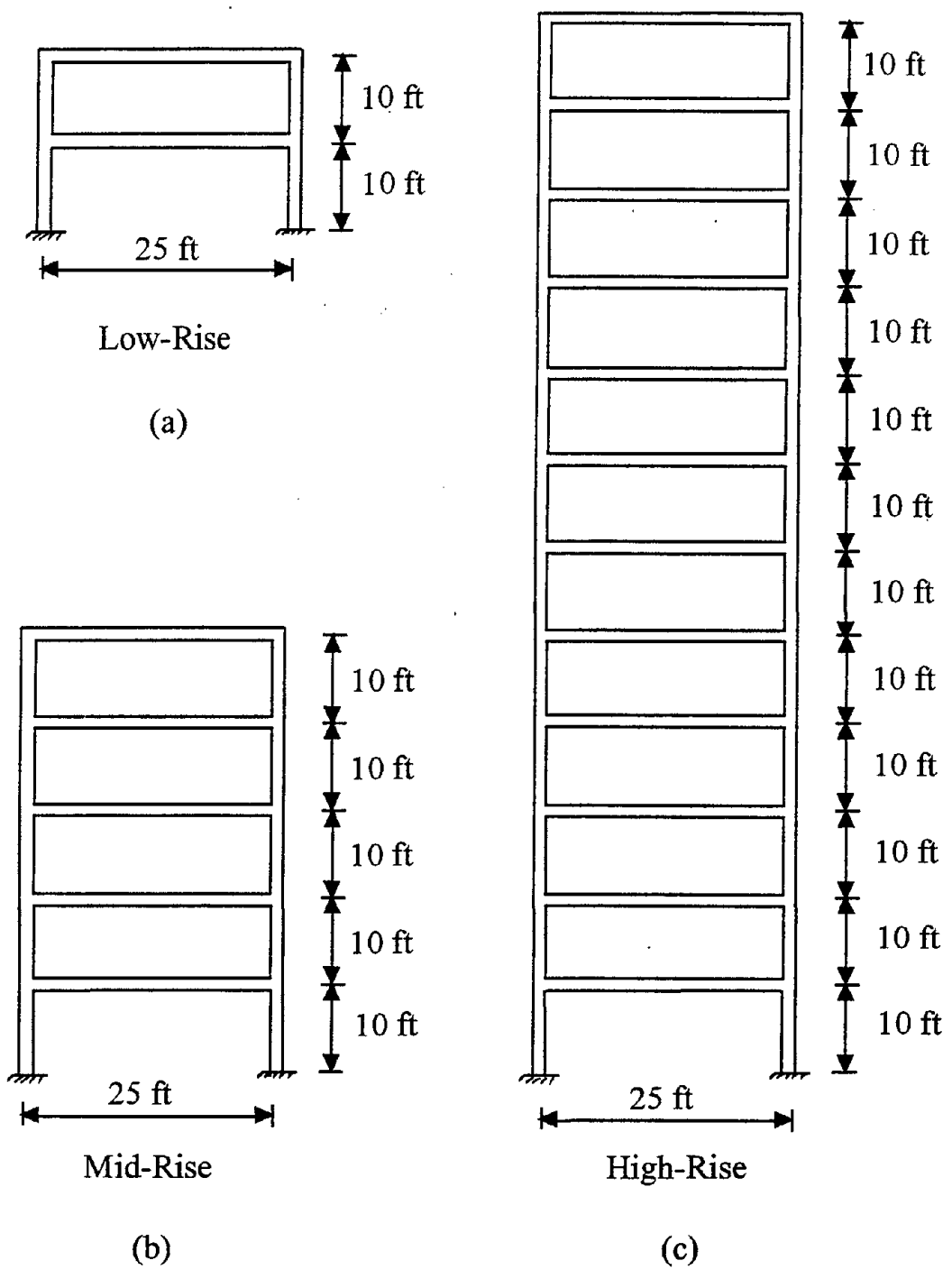


FIGURE 4-7 Elevation of the frames used in the analyses

4.3.2 Modeling of Uncertainties in Structural Capacities and Demands

The structural capacities and demands need to be specified stochastically before the Monte Carlo simulation can be performed. The following two paragraphs discuss the uncertainties associated with the capacity and demand parameters for reinforced concrete frames.

Capacity parameters: The different parameters which affect the resistance of the structure include the compressive strength of concrete, the yield strength of reinforcing steel, hysteretic behavior, damping ratio, physical dimensions of the different components, and the amount of reinforcing steel. The compressive strength of concrete and the yield strength of steel are the only parameters treated as the strength random variables in this study. Following Galambos et al. (1982), a normal probability distribution for concrete strength and a lognormal probability distribution for steel strength are used in this study. Concrete strength has a mean of 1.14 times the nominal concrete strength and a coefficient of variation of 0.14. Steel strength has a mean of 1.05 times the nominal strength and a coefficient of variation of 0.11.

Demand parameters: The uncertainty associated with dead and live loads is considerably smaller compared to the uncertainty in seismic load. In this study, only the earthquake load is modeled as a nonstationary stochastic process. The different models for simulating ground motion were discussed in Section 3.

4.3.3 Structural Modeling in DRAIN-2DX

The beam-column element (Type 02) available in DRAIN-2DX is used to model the beams and columns in a reinforced concrete frame. This element as modeled in DRAIN-2DX consists of two fibers. One of the fibers has an elastoplastic moment-curvature relationship, and the other always remains elastic to model the strain hardening in the moment-curvature relationship of the member. Thus, this element is able to capture “lumped” plasticity at the ends of the member. In reality, the member has distributed plasticity, i.e., the member can have nonlinearities along the

length as well as across the depth of the member. The effect of distributed plasticity on nonlinear dynamic response is evaluated by considering the sample five story frame discussed earlier. Throughout this research, a bilinear hysteretic model is used for the nonlinear dynamic analysis performed by DRAIN-2DX.

Distributed plasticity is considered by subdividing each member into three elements before performing nonlinear analysis using DRAIN-2DX. Each member consists of two short elements at the ends and one long element in the middle. The length of the short elements is 15% of the member length. This approach captures the spread of plasticity along the length of a member. The spread of plasticity across the depth of a member can be considered by using more fibers to represent the cross section of the member. The present approach uses two fibers, one of which remains elastic and the other is elastoplastic.

The effect of subdividing the member into shorter elements on the nonlinear dynamic response of the structure was studied. The two cases used in the study are shown graphically in figure 4-8. Nonlinear time history analyses were carried out for each of the two cases. Ensembles of ground motion corresponding to different values of spectral acceleration in the period range 0.5-0.9 seconds were used in the analyses.

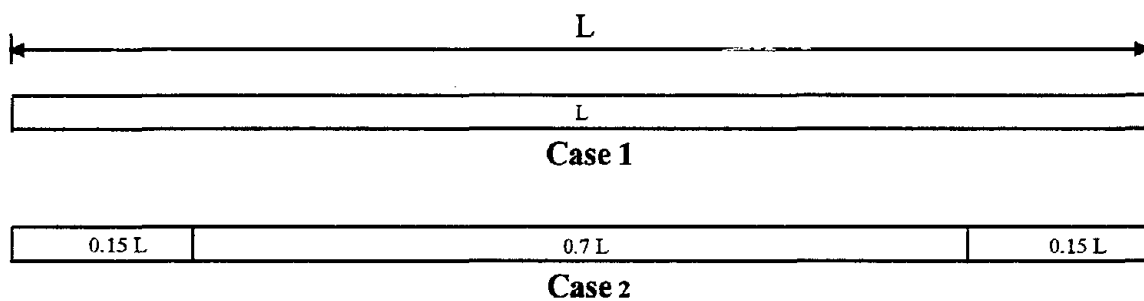


FIGURE 4-8 Two cases used to study the effect of distributed plasticity

The Monte Carlo method, with random sampling, would make independent runs at different levels of discretization and compare the results obtained. The aim is to determine the differences among the different cases. Therefore, correlated sampling, one of the most powerful variance

reduction techniques, was used in the Monte Carlo technique. If the simulations use the same random numbers, their results can have a high positive correlation, and a reduction in variance of the differences between two simulation results can be achieved. The aim of correlated sampling is to produce a high positive correlation between two similar processes so that the variance of the difference is much smaller than the case where the processes are statistically independent. Therefore, the recorded ground motions from the six earthquakes, discussed earlier in Section 4.1, are scaled to different levels of spectral acceleration and used for the purpose of the comparison between the two cases. Using three elements to model each member, DRAIN-2DX produced results similar to those from IDARC2D (Kunnath and Reinhorn, 1994) and CUDYNAMIX (EL-Tawil, 1996). The details on the comparison of the results are presented in Section 4.3.4.

Drift Ratios

The interstory drift ratios for the two cases are shown in figures 4-9 for the first story where the largest difference was observed. The overall drift ratios, obtained as the ratio of the roof displacement to the structure height, for the two cases are shown in figure 4-10. The interstory drift ratios for all stories decrease from Case 1, where only one element is used, to Case 2 where 3 elements are used. The effect of accounting for the spread of plasticity along the length of members decreases from bottom to top of the structure. Thus, for the top story there are no significant differences between the two cases because of the decrease in seismic demand from bottom to top of the structure.

Park-Ang Damage Index

This section examines how damage, in terms of the Park-Ang index, is affected by subdividing the member into three elements. The Park-Ang damage index is computed at the member end irrespective of the number of elements. The hysteretic energies dissipated and the plastic rotations at the element ends are accumulated at the member end closest to the element end for the computation of the damage index. Figure 4-11 shows the hysteretic energies dissipated by

the frame elements of the first story where the maximum dissipation of hysteretic energy occurs. The total dissipated energies are similar for all cases and thus independent of the level of discretization.

Figures 4-12 shows the overall Park-Ang story damage indices for the two cases. The overall Park-Ang damage index for Case 1 is significantly larger than that Case 2. When the member is discretized, plastic deformations can occur inside the member. The damage indices computed using three elements are found to be consistent with those from IDARC2D. The comparison between DRAIN-2DX and IDARC2D is presented in Section 4.3.4.1.

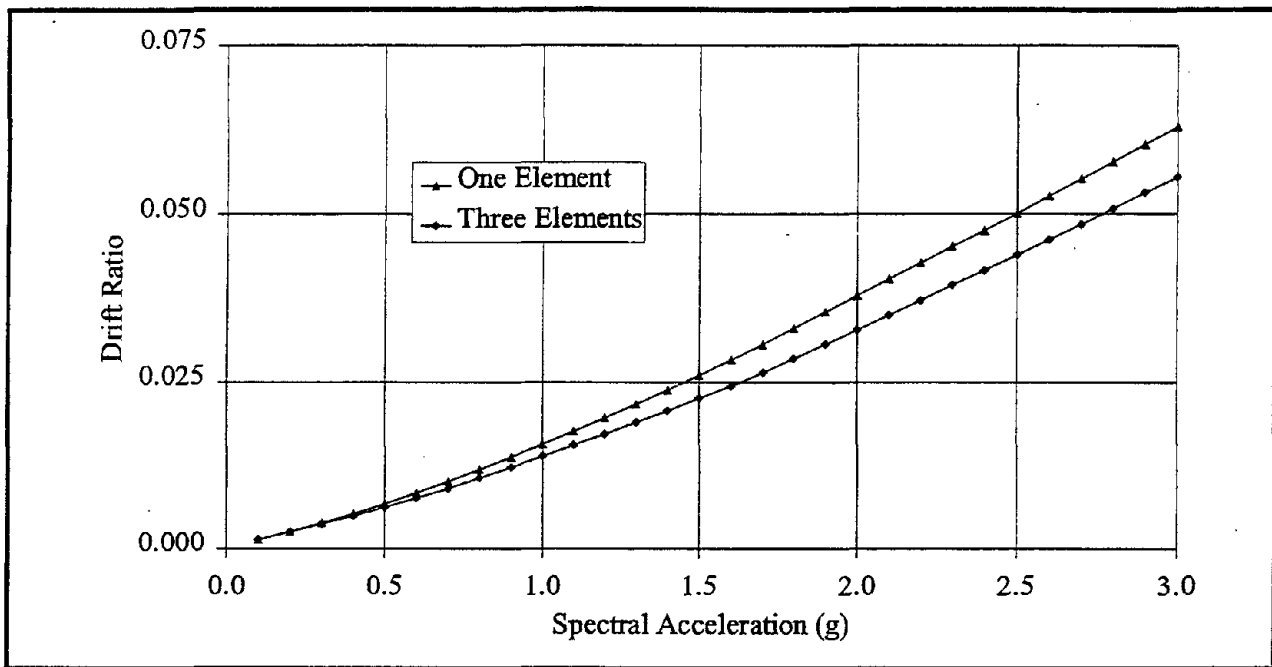


FIGURE 4-9 Comparison of the interstory drift ratios for the first story of the five story frame

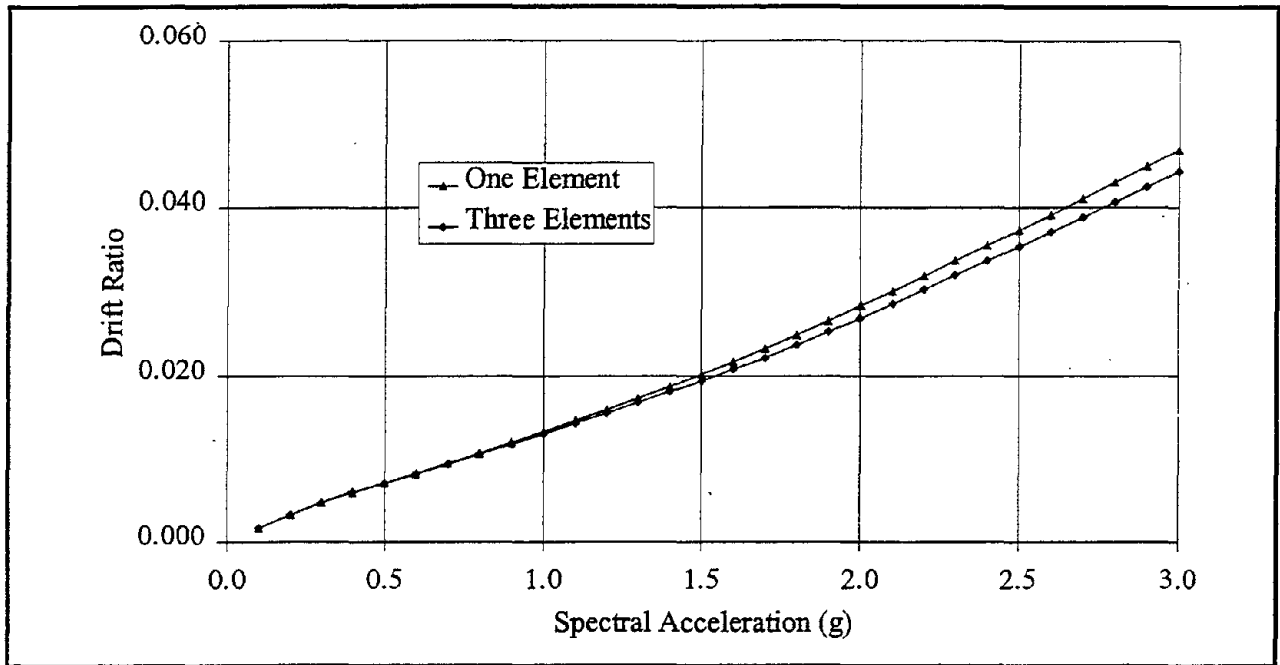


FIGURE 4-10 Comparison of the overall drift ratios for the five story frame

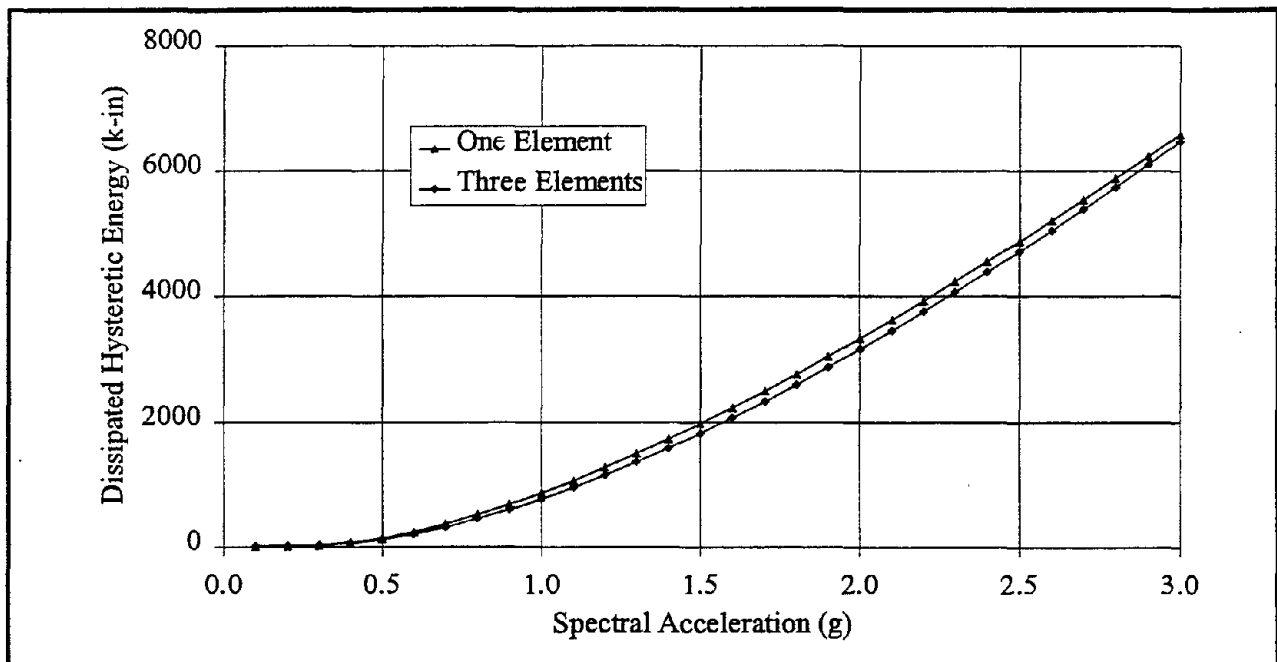


FIGURE 4-11 Comparison of the hysteretic energy dissipation in the first story of the five story frame

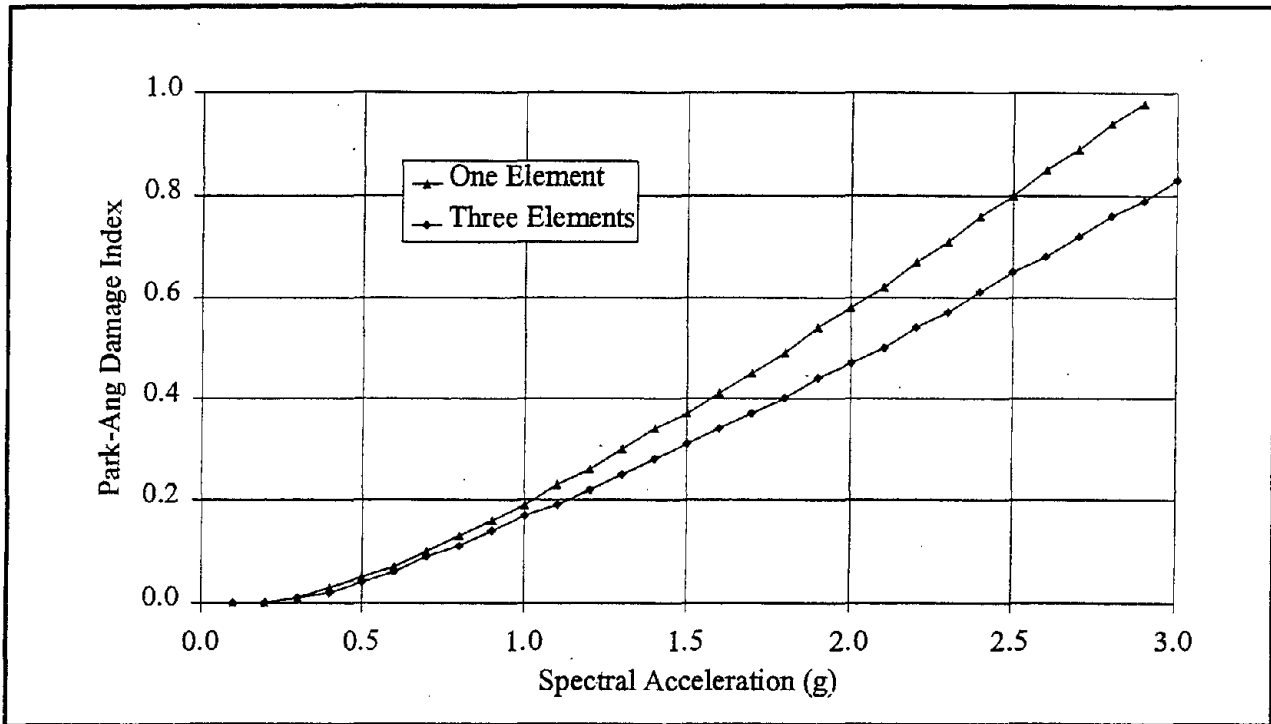


FIGURE 4-12 Comparison of the overall Park-Ang damage index for the five story frame

4.3.4 Comparison of DRAIN-2DX with Other Computer Programs

Several computer programs are available for evaluating the nonlinear dynamic response of a structure, including DRAIN-2DX (Prakash and Powell, 1993), IDARC2D (Kunnath and Reinhorn, 1994), and CU-DYNAMIX (El-Tawil, 1996). In this study, the program DRAIN-2DX is used for performing the nonlinear dynamic analysis, the results of which are then used to evaluate the Park-Ang damage index. However, it is useful to compare the results obtained from DRAIN-2DX to the those obtained from the other two programs in order to examine the bounds within which the response of the structures may lie. The comparisons of the results are presented in the next two sections.

4.3.4.1 Comparison Between DRAIN-2DX and IDARC

The program IDARC2D uses a trilinear moment-curvature relationship in contrast to the bilinear relationship used in DRAIN-2DX. The trilinear relationships in IDARC2D are shown in figure

4-13. Furthermore, IDARC2D uses a general distributed flexibility model to model distributed plasticity, whereas DRAIN-2DX uses a lumped plasticity model. However, the effect of the spread of plasticity along the length of a member is captured in DRAIN-2DX by discretizing a member into smaller elements as discussed in the previous section. Also, the hysteretic model in IDARC2D is able to incorporate stiffness degradation, strength deterioration, and pinching. The parameters used to describe these characteristics of the hysteretic model are shown in figure 4-13.

The results of the nonlinear dynamic analyses performed using IDARC2D and DRAIN-2DX are compared in terms of the Park-Ang damage index for the twelve story, one bay frame shown in figures 4-6 and 4-7. Correlated sampling is again used to compare the results from these two programs. Whereas IDARC2D computes the Park-Ang damage index, the member outputs from DRAIN-2DX are used to compute the damage index. Thus, the plastic rotations and the dissipated hysteretic energies of each member obtained from DRAIN-2DX are used to compute the damage index. As only mass-proportional damping is implemented in IDARC2D, the mass-proportional damping coefficient is computed so as to provide 5% damping in the first vibrational mode. Furthermore, IDARC2D does not use an event-to-event strategy used in DRAIN-2DX. Therefore, an integration step of 0.0001 seconds is used when performing the nonlinear dynamic analysis in IDARC2D.

Figure 4-14 shows the comparison of the damage indices computed from the two programs when no deterioration in the hysteretic behavior is considered. Figure 4-15 shows the comparison when nominal degradation is considered in IDARC2D. Kunnath et al. (1992) suggest that for nominal degradation in stiffness, a value of 2 be used for the stiffness degradation parameter, α . They also suggest that a value of 0.1 be used for the strength degradation parameter, β , to obtain nominal degradation in strength. In the present study, the parameter β used for strength degradation is different from the parameter β in the expression for the Park-Ang damage index. As mentioned in Section 2, a value of 0.15 is used for the parameter β to compute the Park-Ang damage index.

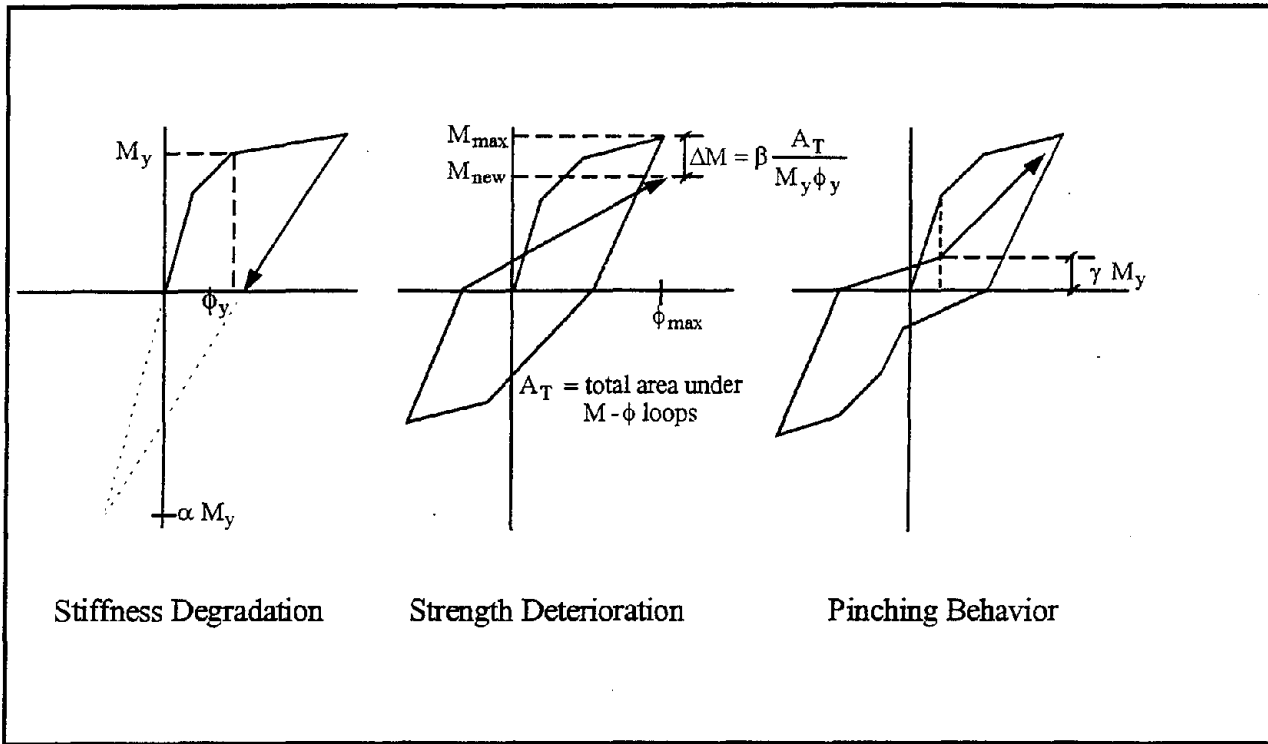


FIGURE 4-13 Hysteretic parameters in IDARC2D

From figures 4-14 and 4-15, it is observed that the damage index computed using the analysis results from DRAIN-2DX are very similar to those obtained from IDARC2D. At present there is some numerical instability in IDARC2D when performing nonlinear dynamic analysis in certain cases. These instabilities are expected to be due to errors in modeling of some segments of the hysteretic behavior. During the simulations, it was observed that if one of these segments was traversed, the response of the structure would “blow up”. Therefore, the program is not used to generate fragility curves in this study.

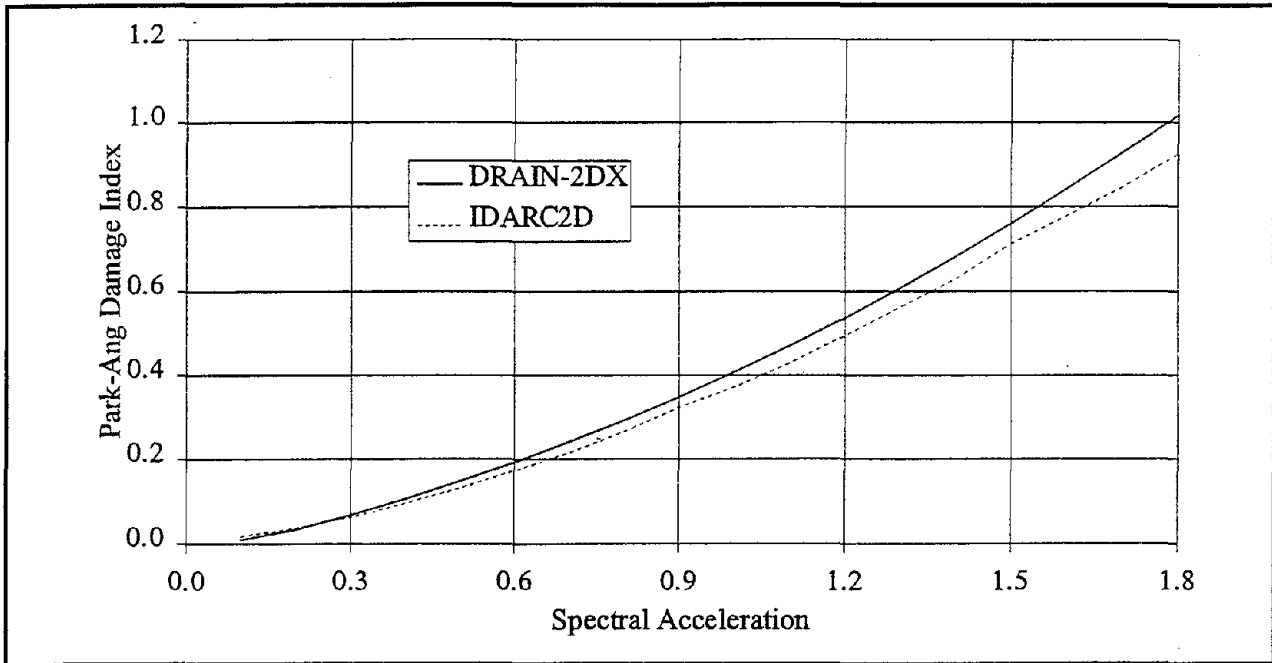


FIGURE 4-14 Comparison of the Park-Ang damage index for the twelve story frame with no deterioration in the hysteretic behavior

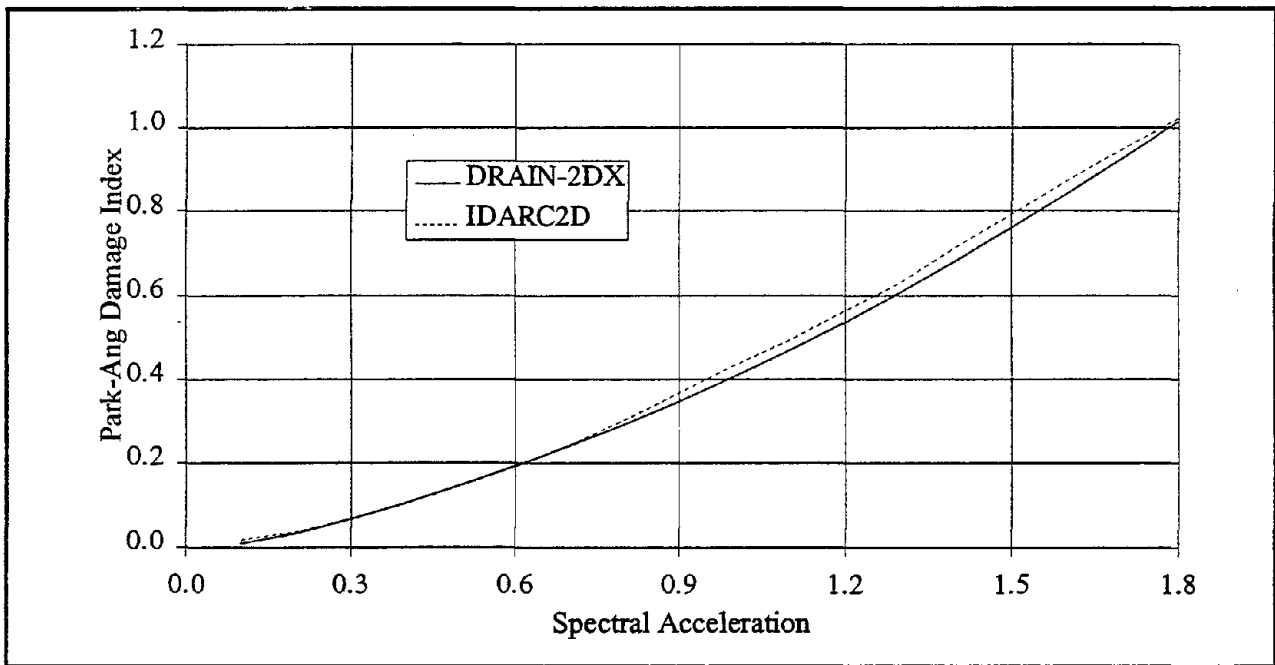


FIGURE 4-15 Comparison of the Park-Ang damage index for the twelve story frame with nominal deterioration in the hysteretic behavior

4.3.4.2 Comparison Between DRAIN-2DX and CU-DYNAMIX

The computer program CU-DYNAMIX (El-Tawil, 1996) is capable of performing two- and three-dimensional analyses on building systems. The stiffness of the elements are based on a flexibility approach, i.e., the flexibility matrix is used to obtain the stiffness matrix of each member. The element flexibility matrix is calculated from the sectional flexibility matrix which relates sectional forces and strains. A bounding strength surface defined for bisymmetric sections is used to determine the stiffnesses in the principal bending and axial directions of a section. The bounding surface is estimated based on the interaction among the axial force and the bending moments in the two principal directions. The stiffness in a principal direction is defined as a function of the distance between the current location inside the bounding surface and the bounding surface in that direction. Stiffness degradation is defined as a function of the accumulated plastic strain energy per unit length of the member.

Currently, the program CU-DYNAMIX can only be used in an interactive mode, which makes the implementation of the program for the development of fragility curves difficult. Also, the program requires that the sections be bisymmetric. In reinforced concrete frames, the beams are almost never bisymmetric. However, it is still worth comparing the responses from CU-DYNAMIX with DRAIN-2DX. For this purpose, a five story frame with bisymmetric beams is subjected to two ground motions recorded during the Loma Prieta earthquake. The ground motion time histories used were recorded at Gavilan College in Gilroy and the UCSC Lab in Santa Cruz. The time histories along with the comparisons of the displacement time histories at the roof and the third floor are presented in figures 4-16 through 4-21. In the nonlinear dynamic analyses in both the programs, the interaction between the moment and the axial force in the members was not considered. Furthermore, three elements were used to model each member in CU-DYNAMIX.

Figures 4-17 and 4-18 show that DRAIN-2DX predicts a permanent deformation, whereas CU-DYNAMIX does not. Otherwise, the peak displacements and the number of cycles that the structure goes through are similar for the two programs. The permanent deformation shown in

figure 4-17 is due to cumulative permanent deformations experienced at the lower stories as the permanent deformation shown in figure 4-18 is smaller than in figure 4-17. The permanent deformation for the first story is much smaller than in figures 4-17 and 4-18.

Figures 4-20 and 4-21 show that the responses from DRAIN-2DX and CU-DYNAMIX are very similar in terms of the peak displacements and number of cycles. However, the responses from the two programs are slightly out of phase. The differences in the response predicted by the two programs are likely due to the modeling of strain-hardening and the formulation of the basic inelastic model in the two programs. Whereas CU-DYNAMIX uses a flexibility approach to model the stiffness of a member by monitoring the flexibility of the member at the Gauss-points, DRAIN-2DX uses a direct stiffness approach to arrive at the stiffness of an element. The Park-Ang damage index computed from the results of the two programs should be similar as the damage index is based on the maximum deformation and dissipated hysteretic energy which are similar for the two programs.

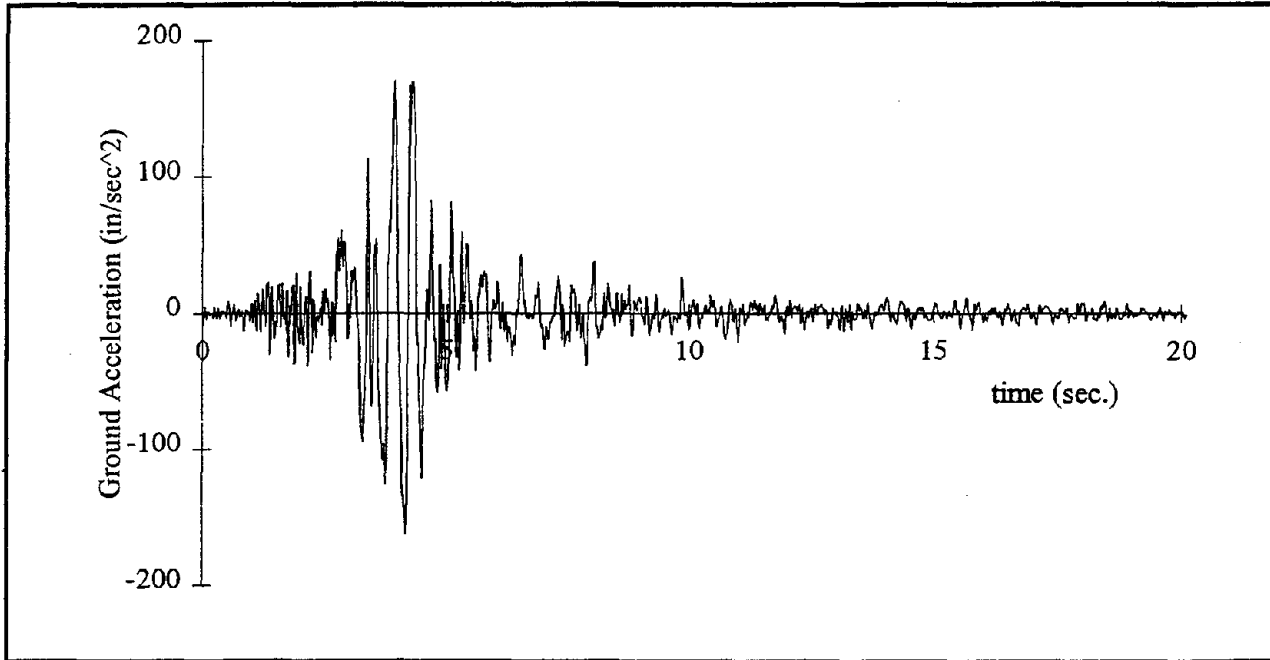


FIGURE 4-16 Ground motion time history recorded at Gavilan College in Gilroy during the Loma Prieta earthquake

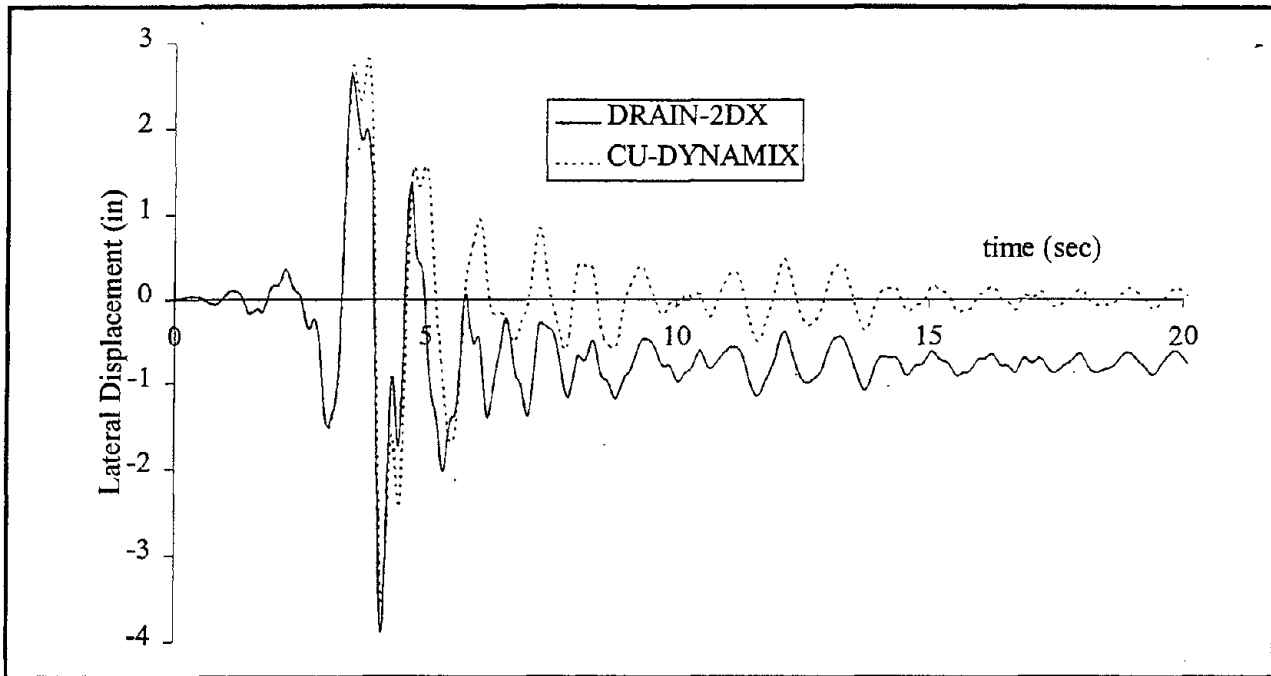


FIGURE 4-17 Lateral displacement at the roof of the five story frame subjected to the ground motion time history recorded at Gavilan College in Gilroy

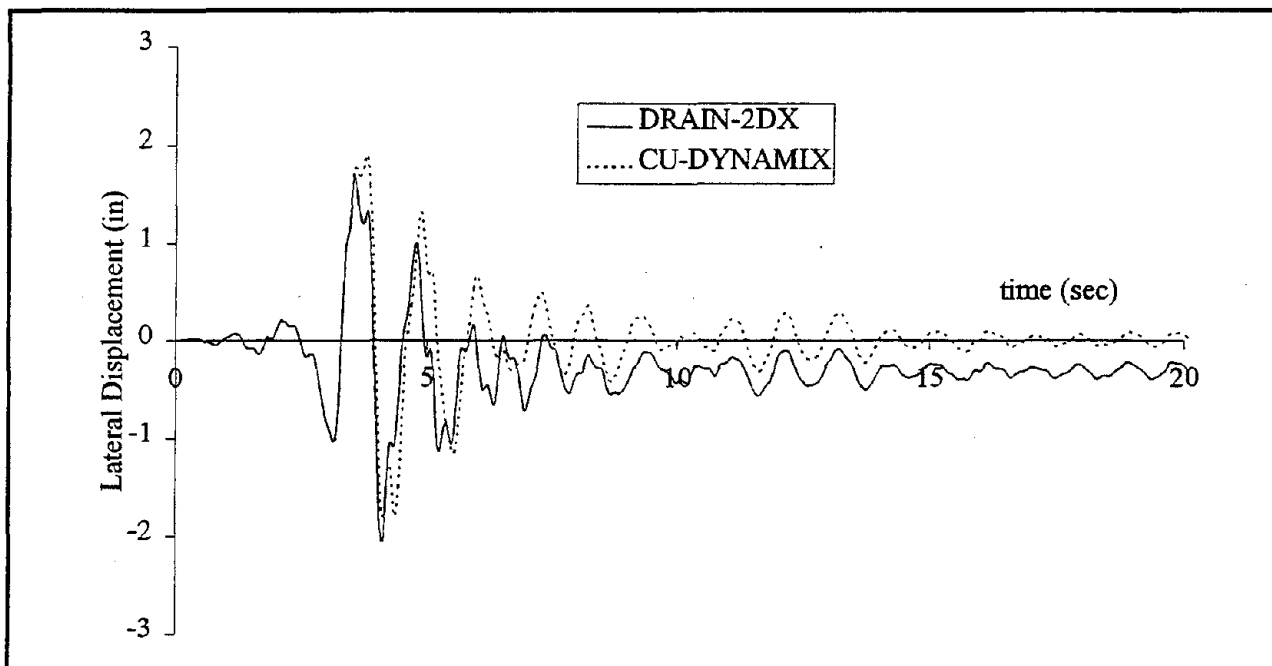


FIGURE 4-18 Lateral displacement at the third floor of the five story frame subjected to the ground motion time history recorded at Gavilan College in Gilroy

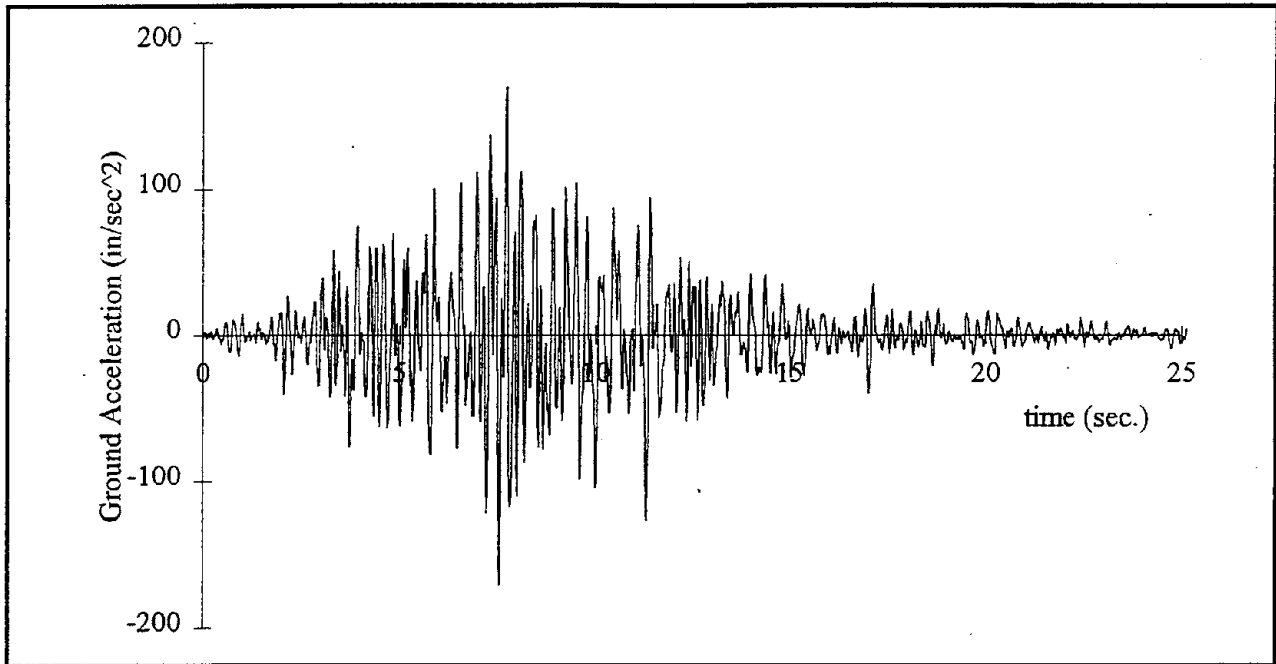


FIGURE 4-19 Ground motion time history recorded at the UCSC Lab in Santa Cruz during the Loma Prieta earthquake

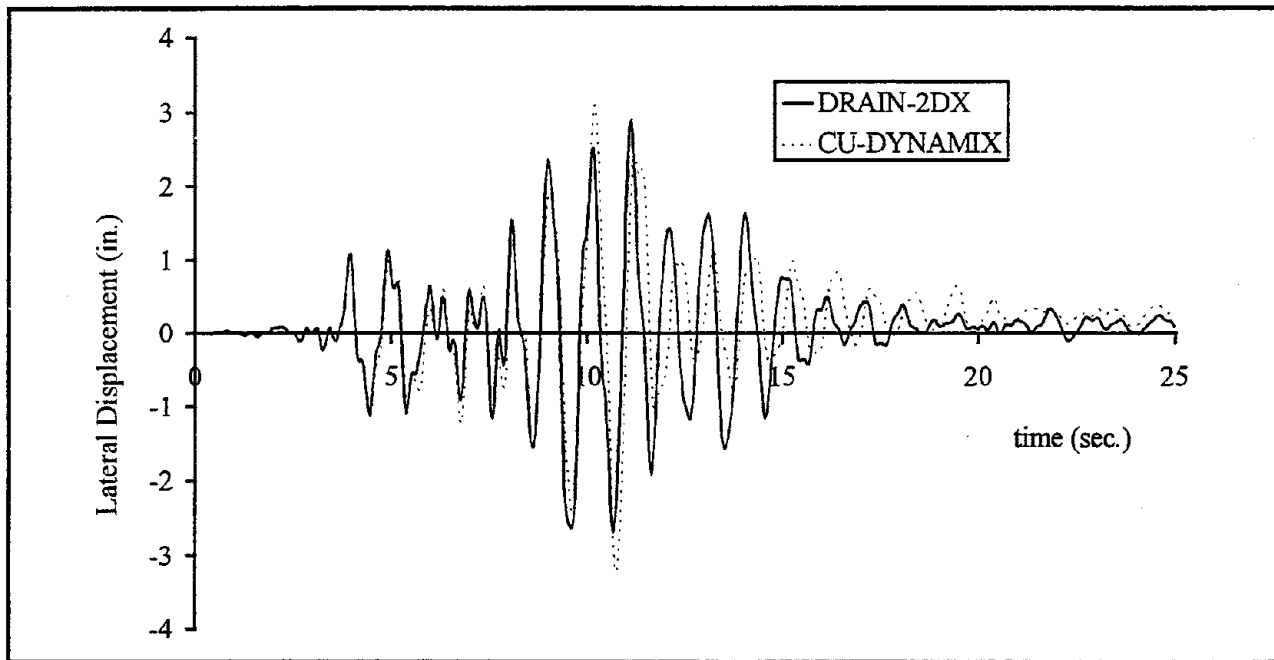


FIGURE 4-20 Lateral displacement at the roof of the five story frame subjected to the ground motion time history recorded at the UCSC Lab in Santa Cruz

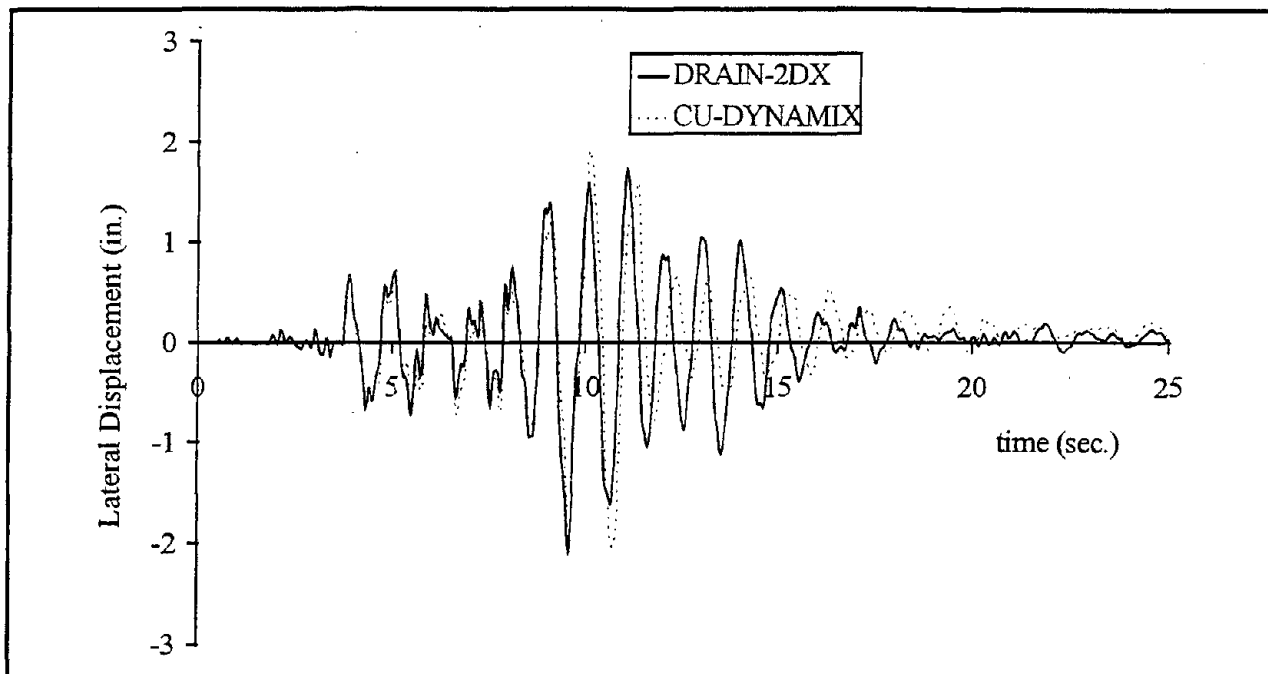


FIGURE 4-21 Lateral displacement at the third floor of the five story frame subjected to the ground motion time history recorded at the UCSC Lab in Santa Cruz

4.4 Summary

This section presented application of the methodology for the development of motion-damage relationships for RC frames. The general methodology for the development of these relationships was presented in Section 3. In contrast to previous approaches for developing fragility curves and DPMs, the method used in this study does not rely on heuristics or on empirical data. The ground motion is characterized by spectral values in the period bands corresponding to the three classes of RC frames. The period bands for the three classes of frames are identified, and the relationship between average spectral acceleration and the average spectral velocity is investigated for the mid rise and the high rise frames.

Sample structures for the three classes of frames were described. The structural modeling in the computer programs for evaluating the nonlinear response was discussed. In this study, DRAIN-2DX was used for performing the nonlinear dynamic analysis. The results from DRAIN-2DX

were compared with those from IDARC and CU-DYNAMIX. The motion-damage relationships for RC frames are presented as fragility curves and DPMs in Section 5.

SECTION 5

FRAGILITY CURVES AND DPMs FOR RC FRAMES

This section presents the fragility curves and damage probability matrices (DPMs) for special moment resisting frames located on firm soils. The general methodology for developing the motion-damage relationships was presented in Section 3, and the application of that methodology for concrete frames was presented in Section 4. In addition, sensitivity analyses are carried out to study the influence of different structural attributes which include the plan layout of the buildings, the second-order effects, and the effect of site conditions on the response of buildings.

5.1 Sample Fragility Curves

The computer programs IDARC2D (Kunnath and Reinhorn, 1994) and DRAIN-2DX (Prakash and Powell, 1992) are used for damage analysis. The member properties in terms of moment-rotation relationships are evaluated in IDARC2D. These properties are then used for the nonlinear dynamic analyses performed in DRAIN-2DX. The spread of plasticity along the length of each member is captured by a discretization of the members into smaller elements. Each member is divided into three elements with one small element of length equal to 15% of the member length at each end along with a larger middle element.

Nonlinear dynamic analysis is performed for 100 simulated ground motions generated at each value of spectral acceleration. An integration time step of 0.002 seconds is used in the analysis. The damping matrix was obtained as a linear combination of the mass and stiffness matrices. The coefficients for the mass and stiffness matrices were selected to give 5% of critical damping in the first two vibrational modes. The Park-Ang damage index given by equations 2.21 and 2.24 is computed from the results of the time history analysis performed in DRAIN-2DX. Only the length of a time history corresponding to its strong motion portion was used in the dynamic analysis.

The statistics of the Park and Ang damage index, obtained at each spectral acceleration value, are used to obtain the parameters of a lognormal probability distribution function at that ground motion level. Figures 5-1 through 5-3 show the comparison between the empirical probability distributions obtained from simulation results and the fitted lognormal distributions at spectral acceleration value of 2g. These lognormal distributions are verified at a 5% significance level based on the Kolmogorov-Smirnov significance test.

The lognormal probability functions at each level of ground motion are then used to obtain the probabilities of the different damage states by computing the probabilities of the damage index being in the ranges given in table 3-I. Smooth fragility curves are obtained by arbitrarily fitting lognormal distribution functions to the simulation results. Smooth fragility curves facilitate their use in regional loss-estimation and vulnerability assessment studies. The simulation results and the fitted curves are shown as discrete points and smooth curves respectively, in figures 5-4 through 5-6. The confidence bounds on the fragility curves shown in figures 5-4 through 5-6 are established in Section 6. The fragility curves of figures 5-4 through 5-6 represent the maximum likelihood curves. These curves are referred to as the median fragility curves in Section 6. The parameters of these fragility curves are given in tables 6-IX through 6-XI.

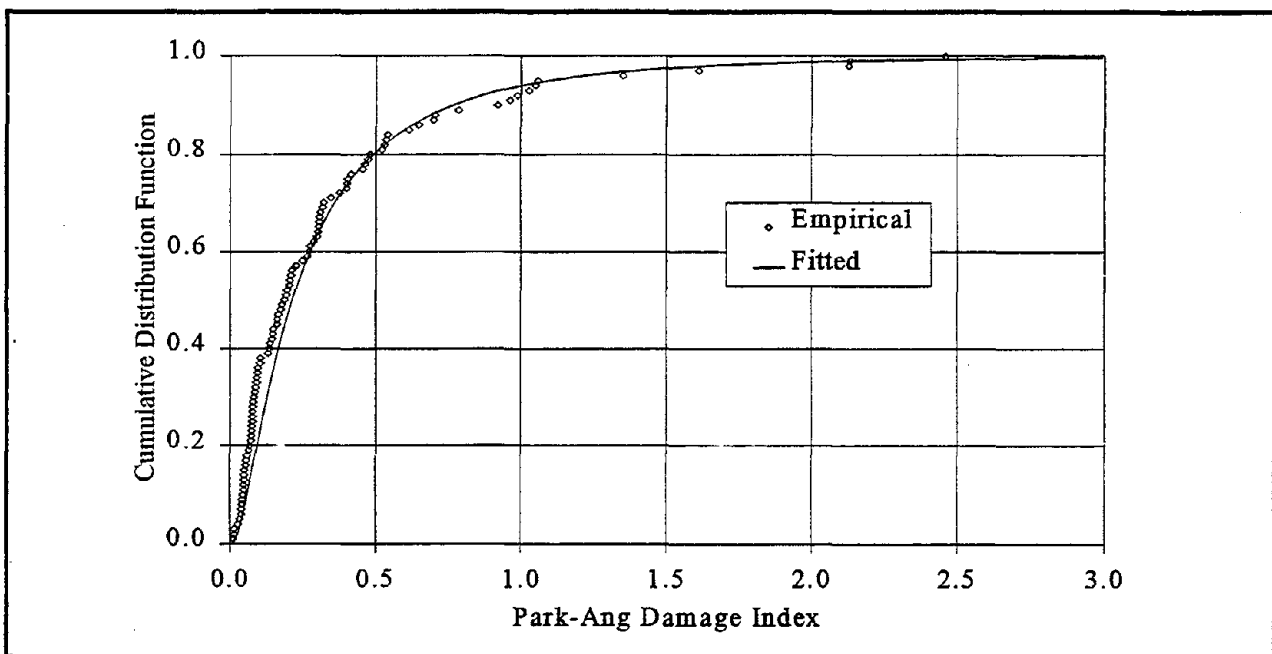


FIGURE 5-1 Comparison of the probability distribution functions for the low rise frame

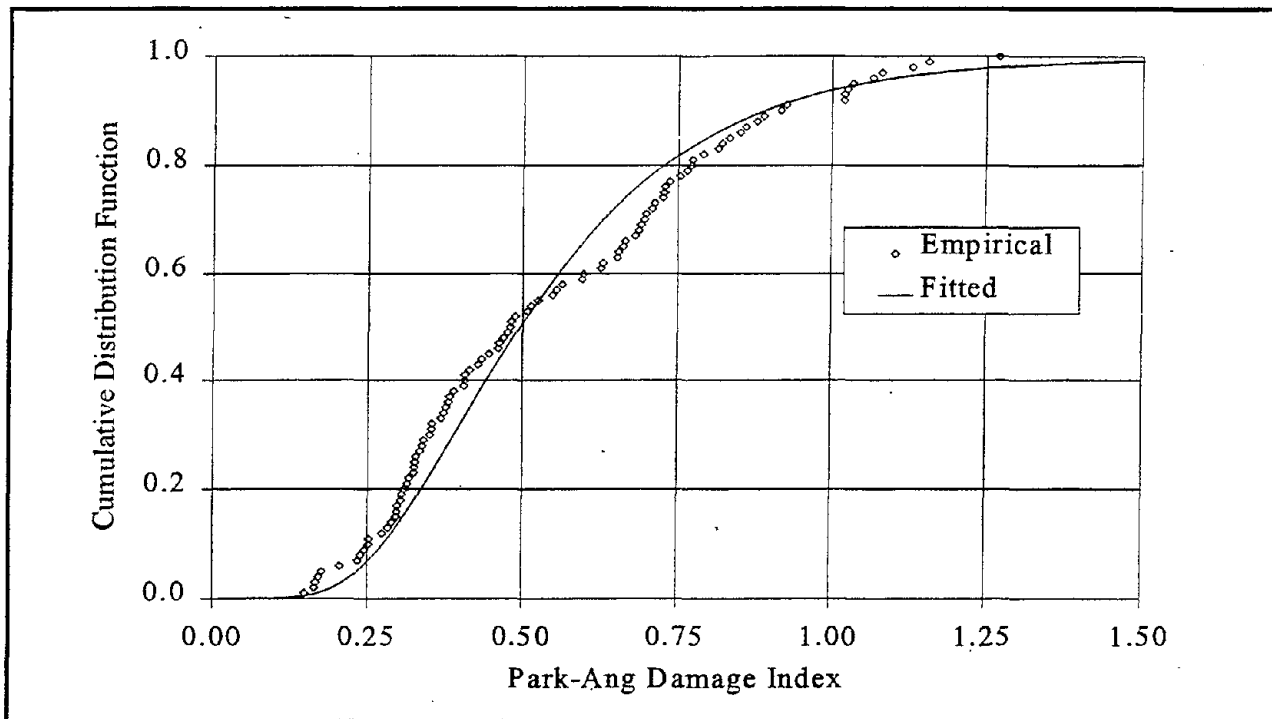


FIGURE 5-2 Comparison of the probability distribution functions for the mid rise frame

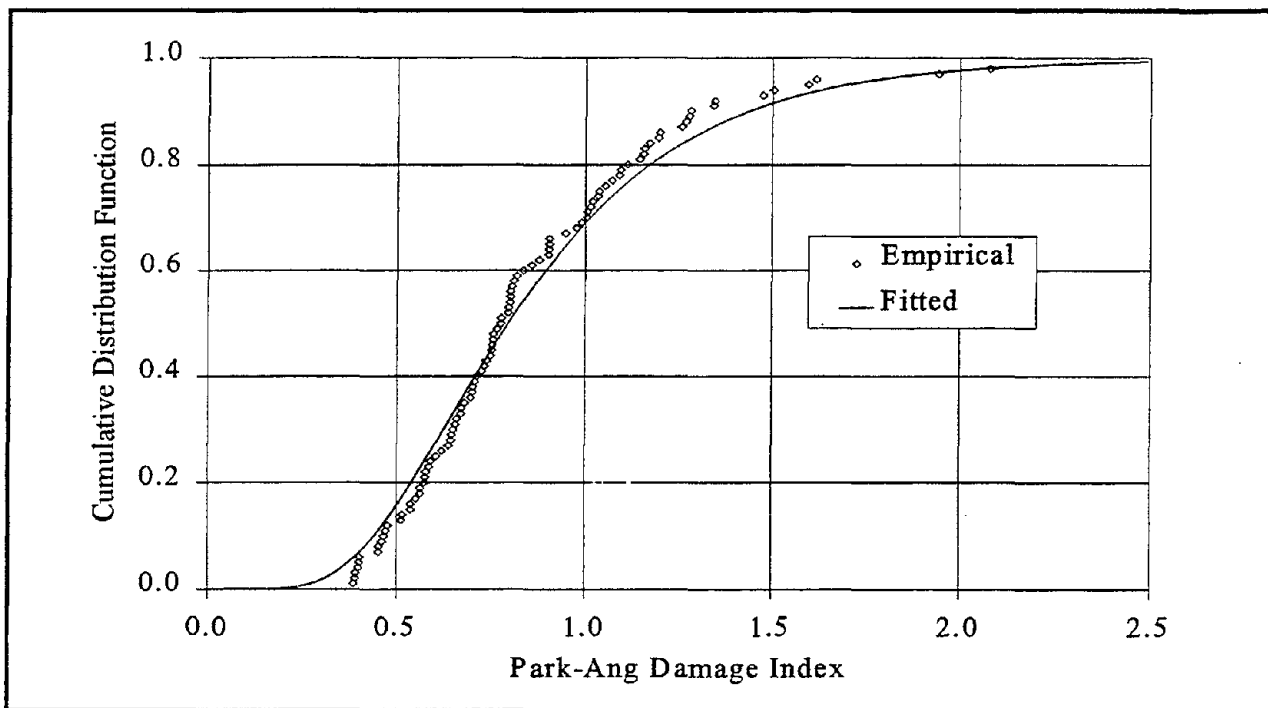


FIGURE 5-3 Comparison of the probability distribution functions for the high rise frame

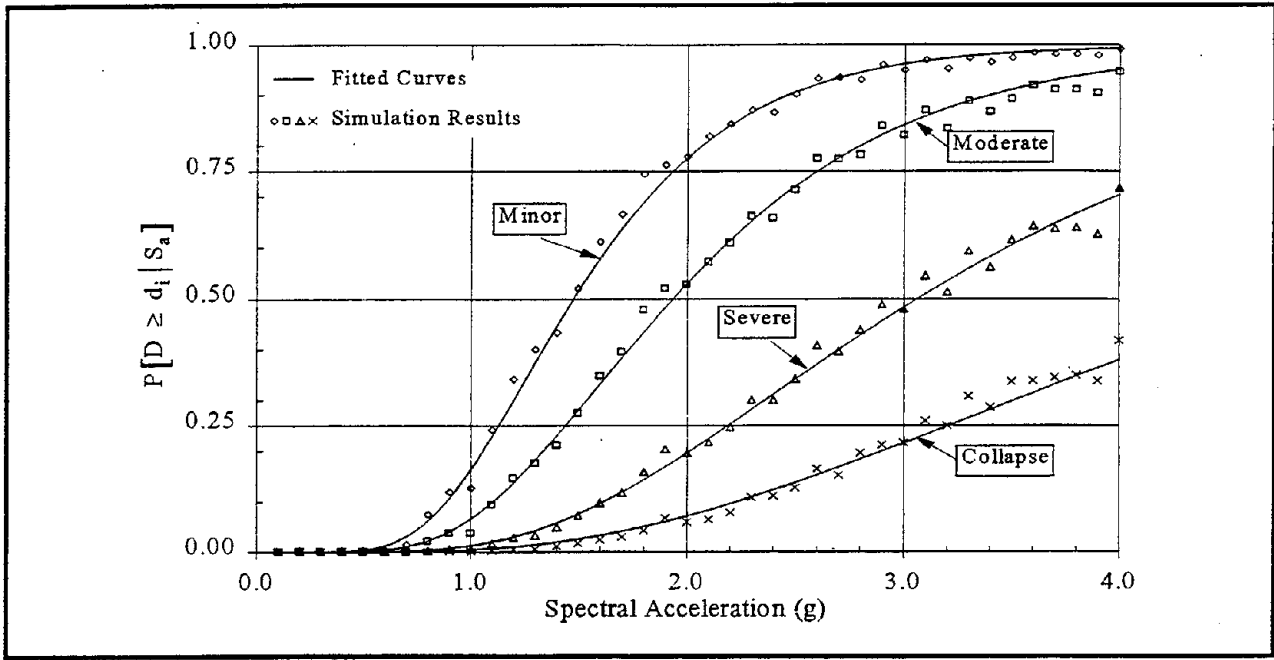


FIGURE 5-4 Fragility curves for low rise frames

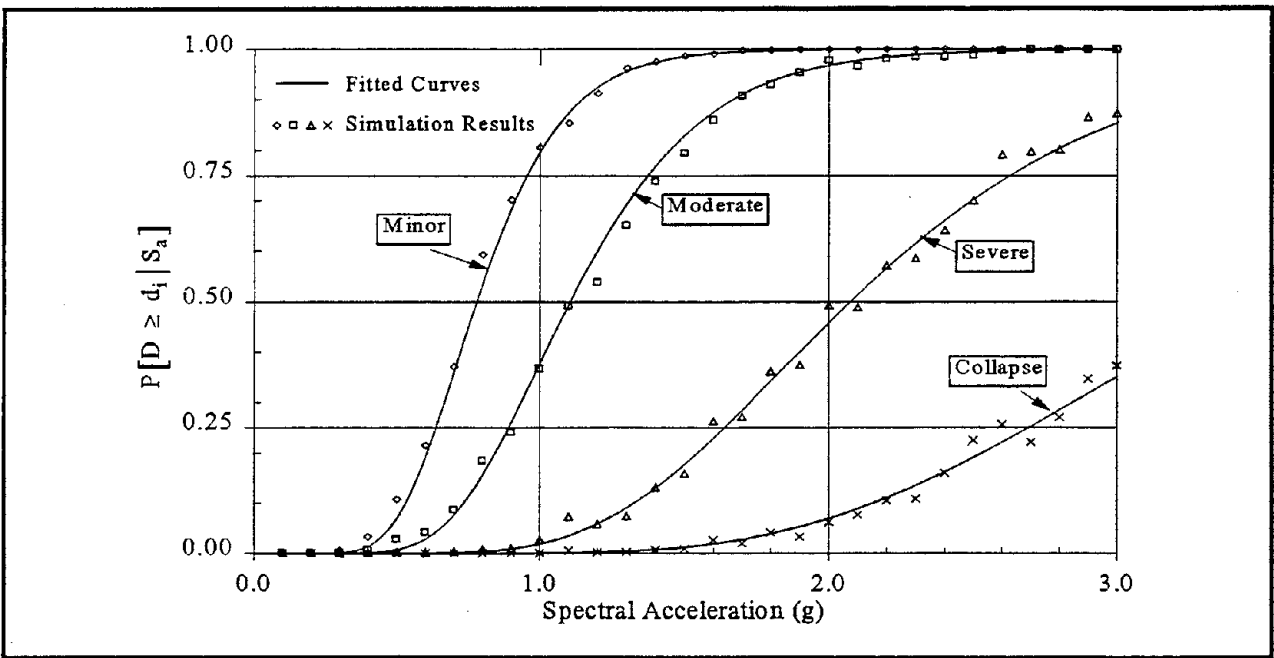


FIGURE 5-5 Fragility curves for mid rise frames

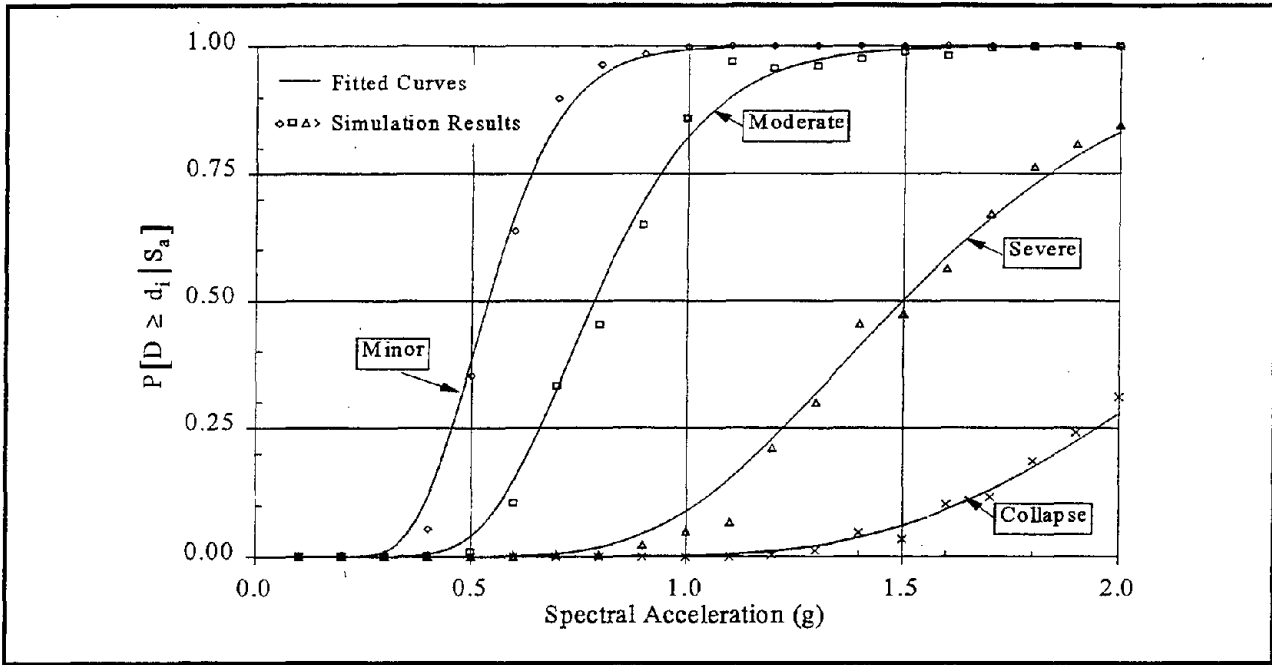


FIGURE 5-6 Fragility curves for high rise frames

5.2 Sample Damage Probability Matrices

The DPMs for the sample buildings are developed from the fragility curves presented in the previous section along with the relationship between modified Mercalli intensity (MMI) and spectral acceleration. The relationship between MMI and spectral acceleration is presented in the next section. The integral in equation 3.4 is evaluated numerically by using the subroutine QDAGI in IMSL (1991). This subroutine uses a 21-point Gauss-Kronrod rule to estimate the integral. The probability of the structure being in a particular damage state at a specified MMI is estimated by taking the difference in probabilities of two adjacent damage states evaluated by means of equation 3.4. For example, the probability of the structure being in the moderate damage state is given by the probability of the structure reaching or exceeding the severe damage state minus the probability of the structure reaching or exceeding the moderate damage state. These probabilities are computed at the ground motion level of interest.

Tables 5-I through 5-III show the DPMs evaluated for the representative buildings. Even though not appreciably different, these matrices show an increase in the probability of the collapse

damage state at higher MMI values as the building height is increased. The collapse damage state as defined by Park et al. (1987) includes total or partial collapse of the building. Thus, as the building height is increased, it is reasonable to expect the probability of partial collapse anywhere in the building to increase.

TABLE 5-I Damage probability matrix for the sample low rise building

Damage state	Modified Mercalli Intensity						
	VI	VII	VIII	IX	X	XI	XII
None	99.5	97.0	85.4	52.9	14.1	0.9	
Minor	0.3	1.6	6.9	16.9	15.5	3.4	0.1
Moderate	0.2	1.1	5.4	18.5	30.5	17.6	2.8
Severe		0.2	1.4	7.0	20.7	28.0	14.6
Collapse		0.1	0.9	4.7	19.2	50.1	82.5

TABLE 5-II Damage probability matrix for the sample mid rise building

Damage state	Modified Mercalli Intensity						
	VI	VII	VIII	IX	X	XI	XII
None	99.0	93.5	70.0	24.5	1.6		
Minor	0.7	4.2	15.8	23.0	6.1	0.1	
Moderate	0.3	2.1	12.0	36.6	33.7	4.9	0.2
Severe		0.2	1.9	12.5	34.6	22.3	1.8
Collapse			0.3	3.4	24.0	72.7	98.0

TABLE 5-III Damage probability matrix for the sample high rise building

Damage state	Modified Mercalli Intensity						
	VI	VII	VIII	IX	X	XI	XII
None	100.0	99.7	93.0	35.3	0.2		
Minor		0.3	5.7	35.3	3.3		
Moderate			1.3	26.9	45.9	0.7	
Severe				2.4	38.9	11.8	
Collapse				0.1	11.7	87.5	100.0

5.2.1 Relationship Between MMI and Spectral Acceleration

The firm site records of the Loma Prieta, Whittier Narrows, and Morgan Hill earthquakes are used for estimating the relationship between the average spectral acceleration and MMI. The average spectral acceleration of the larger of the two horizontal components of the ground motions recorded on firm sites and the MMI values from these earthquakes at the respective recording stations are used to develop these relationships. Figures 5-7 through 5-10 show the MMI contours along with the station numbers of the sites where ground motion was recorded. The data used to develop these relationships were also presented in table 3-VI.

The average spectral acceleration in each period range is assumed to have a conditional lognormal probability density function at given values of MMI. Regression analysis is performed between the natural logarithm of the mean of the average spectral acceleration and MMI. Similar regression analysis is performed between the standard deviation of the average spectral acceleration and MMI. The resulting regression curves are used to estimate the means and standard deviations of the average spectral acceleration at higher MMI values for which observed data are not available. The regression equations for the mean and standard deviation of the average spectral acceleration, expressed in cm/sec² in each period band, are shown below:

$$\mu_{S_a|MMI} = 7.49 e^{0.59 MMI} \quad \text{for } 0.1 \leq T \leq 0.5 \quad (5.1)$$

$$\sigma_{S_a|MMI} = 16.35 e^{0.41 MMI} \quad \text{for } 0.1 \leq T \leq 0.5 \quad (5.2)$$

$$\mu_{S_a|MMI} = 2.78 e^{0.68 MMI} \quad \text{for } 0.5 \leq T \leq 0.9 \quad (5.3)$$

$$\sigma_{S_a|MMI} = 5.95 e^{0.52 MMI} \quad \text{for } 0.5 \leq T \leq 0.9 \quad (5.4)$$

$$\mu_{S_a|MMI} = 0.31 e^{0.85 MMI} \quad \text{for } 0.9 \leq T \leq 2.5 \quad (5.5)$$

$$\sigma_{S_a|MMI} = 1.54 e^{0.55 MMI} \quad \text{for } 0.9 \leq T \leq 2.5 \quad (5.6)$$

The curves representing the mean values, mean plus and minus one standard deviation values, and the median values of the average spectral acceleration are shown in figures 5-11 through 5-13. These figures also show the conditional distributions for the average spectral acceleration, with MMI in the V to VIII range.

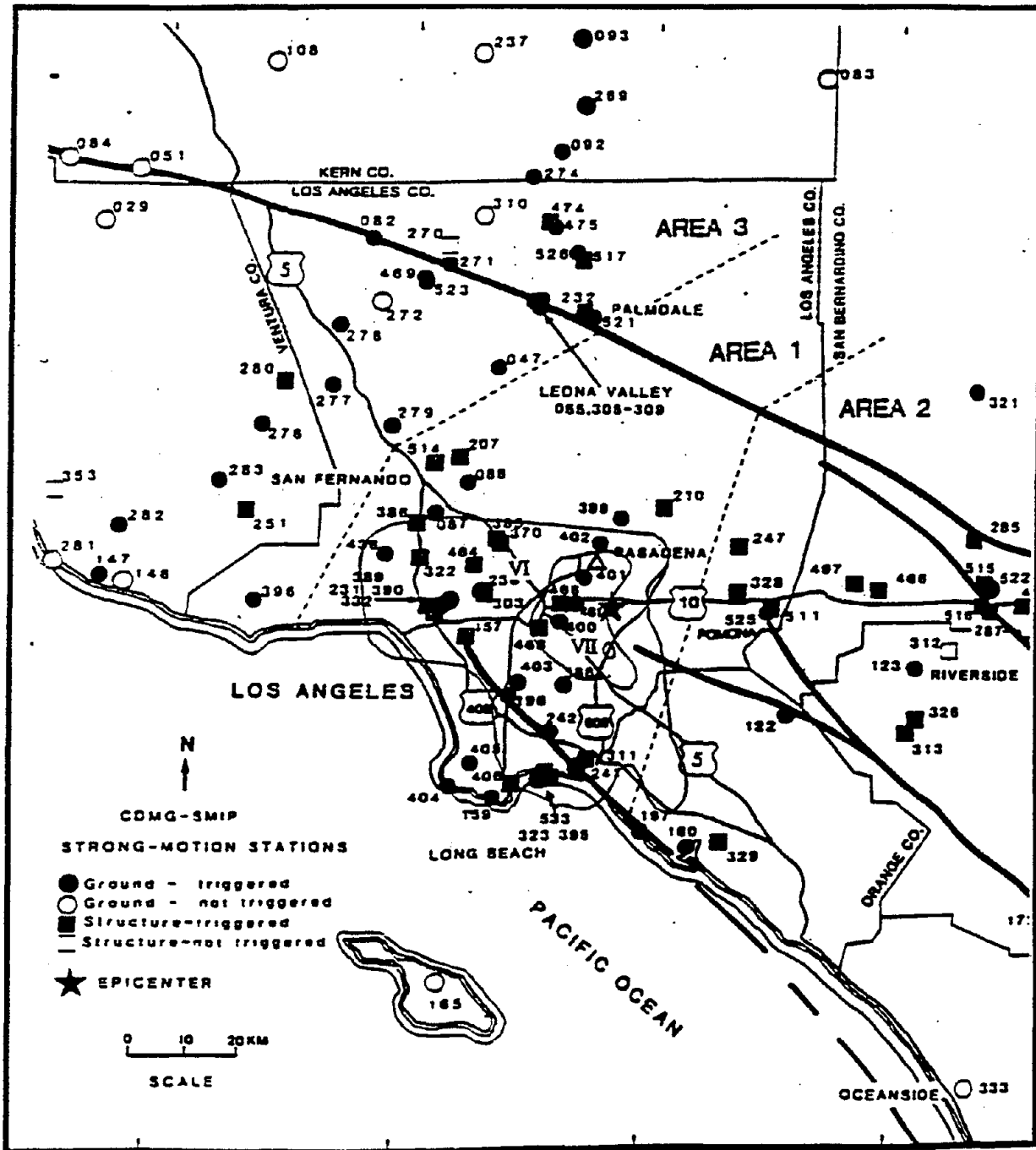


FIGURE 5-8 Map showing the MMI contours and the CSMIP station numbers (Shakal et al., 1987) for the Whittier Narrows earthquake of October 1, 1987 (M_L of 6.1)

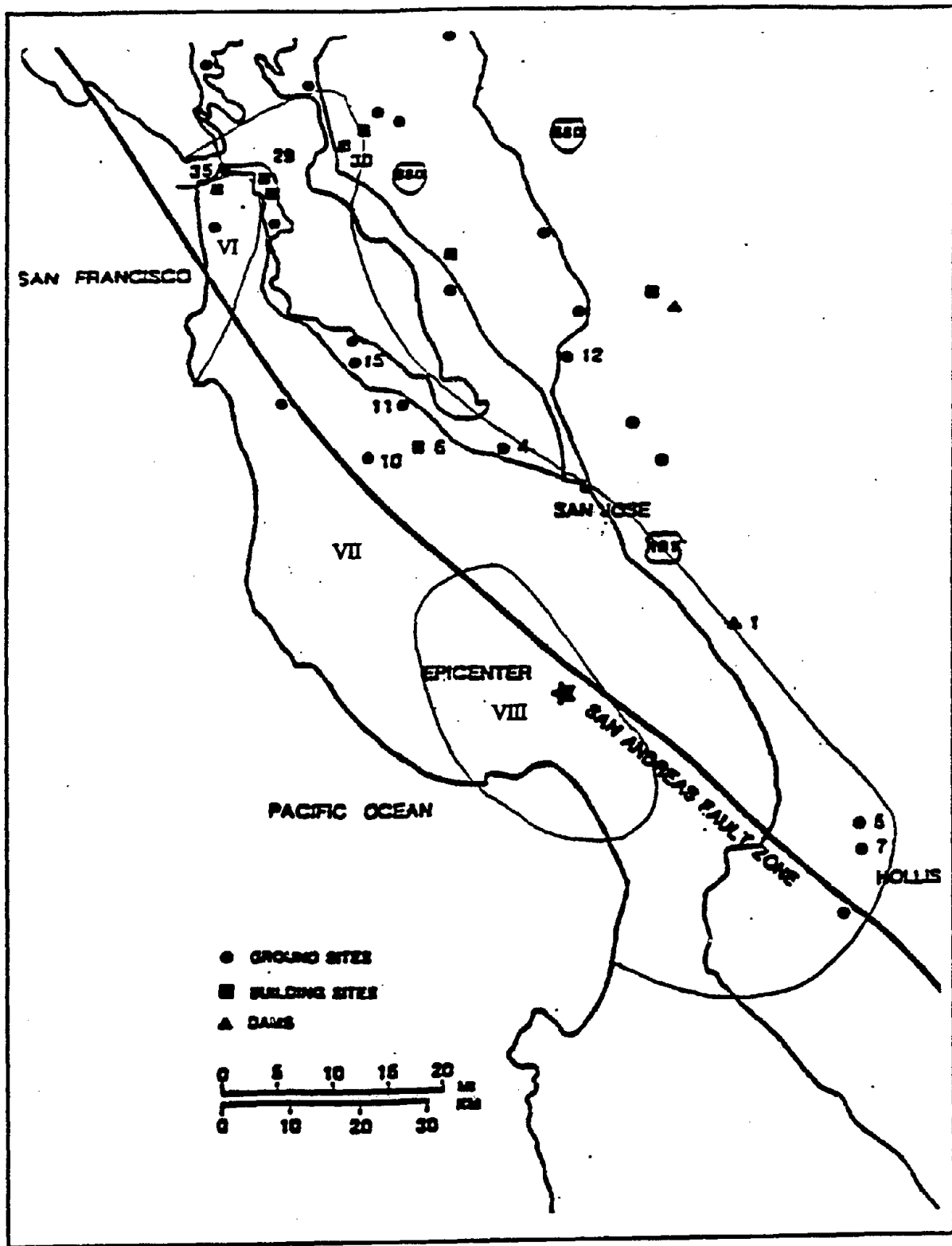


FIGURE 5-10 Map showing the MMI contours and the United States Geological Survey (USGS) station numbers (Maley et al., 1989) for the Loma Prieta earthquake of October 18, 1989, (M_L of 7.0 and M_S of 7.1)

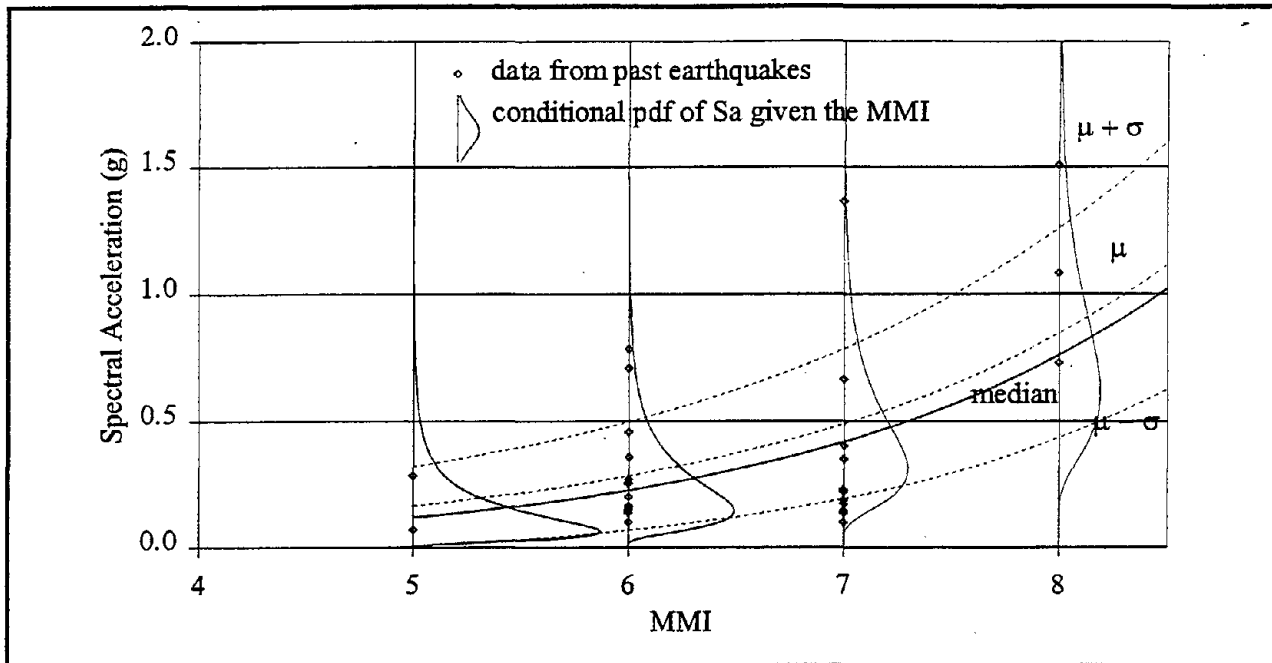


FIGURE 5-11 Relationships for the mean, median, standard deviation, and conditional probability distribution functions of S_a at given MMI, for $0.1 \leq T \leq 0.5$ seconds

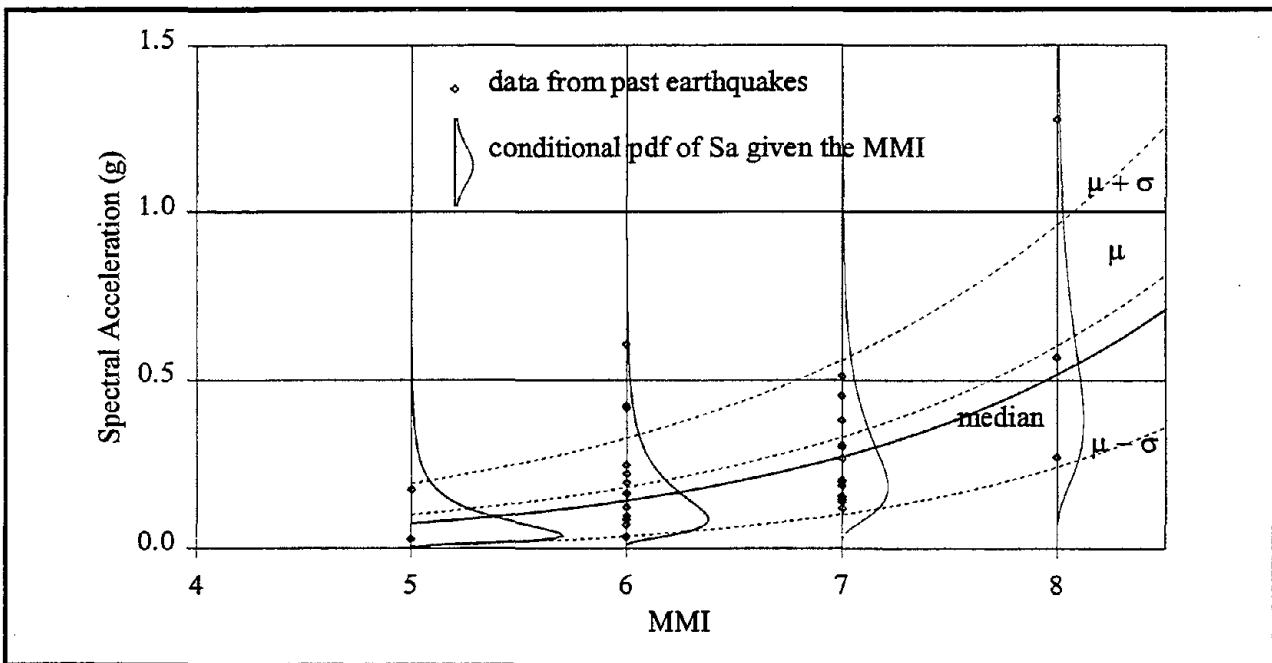


FIGURE 5-12 Relationships for the mean, median, standard deviation, and conditional probability distribution functions of S_a at given MMI, for $0.5 \leq T \leq 0.9$ seconds

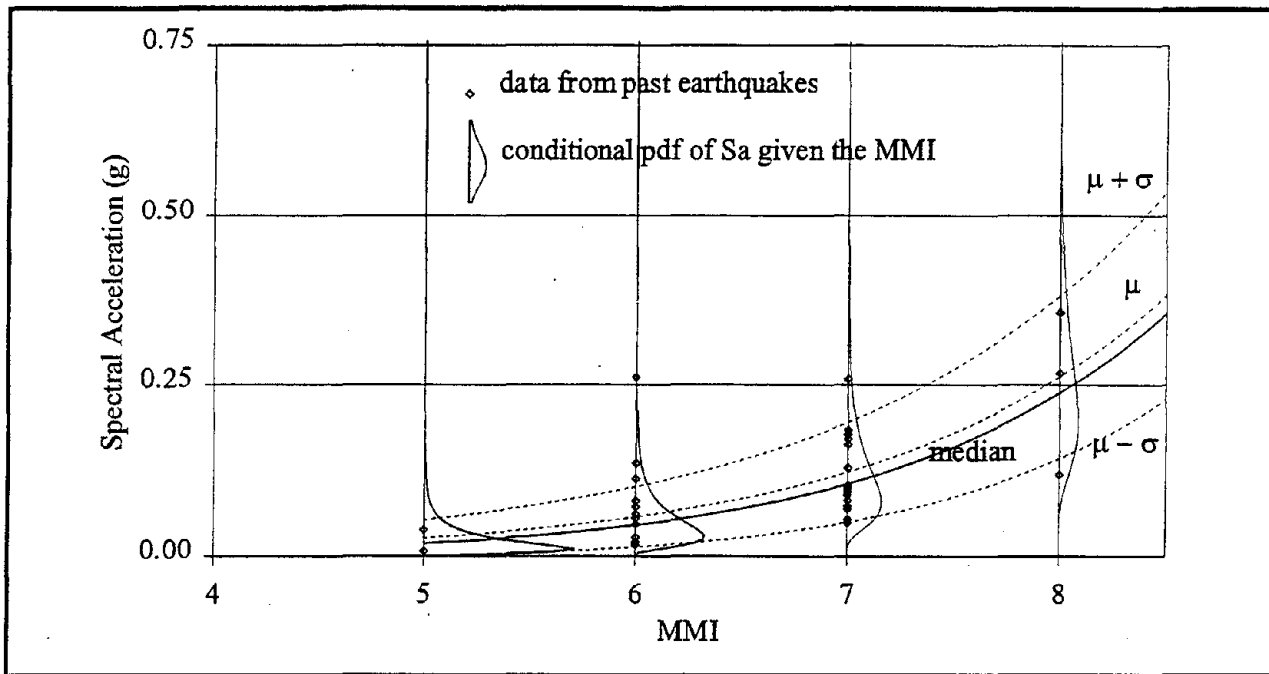


FIGURE 5-13 Relationships for the mean, median, standard deviation, and conditional probability distribution functions of Sa at given MMI, for $0.9 \leq T \leq 2.5$ seconds

5.2.2 Comparison of DPMs with those in ATC-13

The DPMs of ATC-13 (1985) were transformed to correspond to the damage states used in this study. The mapping of the ATC-13 damage states to the damage states used in this study is presented in table 5-IV. Tables 5-V through 5-VII present the transformed DPMs for ductile reinforced concrete frames. The DPMs of ATC-13 show significant probabilities only for a few damage states, whereas those from this study show significant non-zero probabilities for more damage states at a given level of MMI. Moreover, the DPMs of ATC-13 show much less damage at higher levels of MMI. This result may be due to some differences in the definitions of damage states used in ATC-13 and in the current study. The negligible probability of collapse of the frames at MMI values of XI and XII given in ATC-13 appear rather unrealistic, particularly in view of the performance of concrete frame structures in recent large earthquakes. It is also possible that the spectral accelerations predicted at higher MMI using the MMI-spectral acceleration relationships developed above may be exaggerated due to the fact that the

relationships are derived using observations at lower MMI values. Ground motion recordings at larger MMI values are needed in order to accurately predict the spectral acceleration values at higher MMI levels.

TABLE 5-IV Mapping of ATC-13 damage states to those used in this study

ATC-13		Present Study
Damage State	Damage Factor Range (%)	Damage State
None	0	None
Slight	0 - 1	Minor
Light	1 - 10	
Moderate	10 - 30	Moderate
Heavy	30 - 60	
Major	60-100	Severe
Destroyed	100	Complete

TABLE 5-V ATC-13 DPM for low rise, ductile moment resisting frames

Damage state	Modified Mercalli Intensity						
	VI	VII	VIII	IX	X	XI	XII
None	2.5						
Minor	97.5	100.0	99.6	63.2	7.3	0.1	
Moderate			0.4	36.8	92.7	99.9	99.5
Severe							0.5
Collapse							

TABLE 5-VI ATC-13 DPM for mid rise, ductile moment resisting frames

Damage state	Modified Mercalli Intensity						
	VI	VII	VIII	IX	X	XI	XII
None	0.3						
Minor	99.7	99.8	91.8	46.7	9.0		
Moderate		0.2	8.2	53.3	91.0	100.0	99.6
Severe							0.4
Collapse							

TABLE 5-VII ATC-13 DPM for high rise, ductile moment resisting frames

Damage state	Modified Mercalli Intensity						
	VI	VII	VIII	IX	X	XI	XII
None							
Minor	100.0	100.0	83.6	27.6	3.1	0.4	0.1
Moderate			16.4	72.4	96.9	99.2	96.4
Severe						0.4	3.5
Collapse							

5.3 Sensitivity Analysis

The fragility curves and DPMs for reinforced concrete frames developed earlier in the section were obtained by designing a representative building in each of the three classes. However, a class of frames is likely to consist of many frames having different characteristics. This section attempts to address some of the issues associated with the different structural characteristics of frames composing a particular class. Sensitivity studies are conducted for the following properties:

- plan layout of the buildings,
- second-order effects, and
- site condition.

These properties are studied with respect to the buildings used earlier in this section for the development of motion-damage relationships. Structural damage is primarily caused by high stress excursion as well as repeated stress reversals. Most damage measures, including those discussed in Section 2, depend on one or both of these response variables. Therefore in this sensitivity study, the interstory drift ratio and the dissipated hysteretic energies are used to characterize the damage variables: stress excursions and repeated stress reversals. The comparisons presented in the following sub-sections are in terms of the mean values of the drift ratios, the dissipated hysteretic energy, and the Park-Ang damage index obtained for ensembles of time histories.

The aim in this sensitivity study is to determine the influence of the different parameters. Correlated sampling is again used for these sensitivity analyses. As mentioned in Section 4.3.3, the aim of correlated sampling is to produce a high positive correlation between two similar processes so that the variance of the difference is much smaller than the case where the processes are statistically independent. Therefore, the recorded ground motions from the six earthquakes, discussed earlier in Section 4.1, are scaled to different levels of spectral acceleration and used for the purpose of these sensitivity studies. The time histories recorded on firm sites are used to study the sensitivity to number of bays and to second-order effects. To study the sensitivity to site conditions, a subset is selected from these time histories to correspond to rock sites. A different set of time histories is used for soil sites. Only the lengths of the time histories corresponding to their strong motion portions were used for the nonlinear dynamic analyses.

5.3.1 Sensitivity to Number of Bays

The sample buildings selected in each of the three classes of concrete frames are one bay frames. In reality, the buildings in each class could have a different number of bays. Therefore, it is worthwhile to examine the effect of the number of bays on structural damage. To study this effect, a three bay, five story building is designed using the recommendations of SEAOC (1990).

The plan of this building is shown in figure 5-14. The story height in this building is also 10 feet.

The responses of the three bay and the one bay frames are compared in terms of the overall drift ratio defined as the ratio of the maximum drift at the roof level to the height of the building, the total dissipated hysteretic energy, and the Park-Ang structure damage index. The comparisons of the responses of the two frames presented in figures 5-15 through 5-17 show that the responses of the two frames are very similar. In this study, we assumed that the different members in the structure have the same strengths of steel and concrete. In reality, the strengths of steel and concrete in the different elements may not be the same but a high correlation coefficient is expected between the strengths of steel and concrete for members of the same structure. If the strengths of steel and concrete in the members are not the same, some redistribution of the internal forces is expected as members progressively yield.

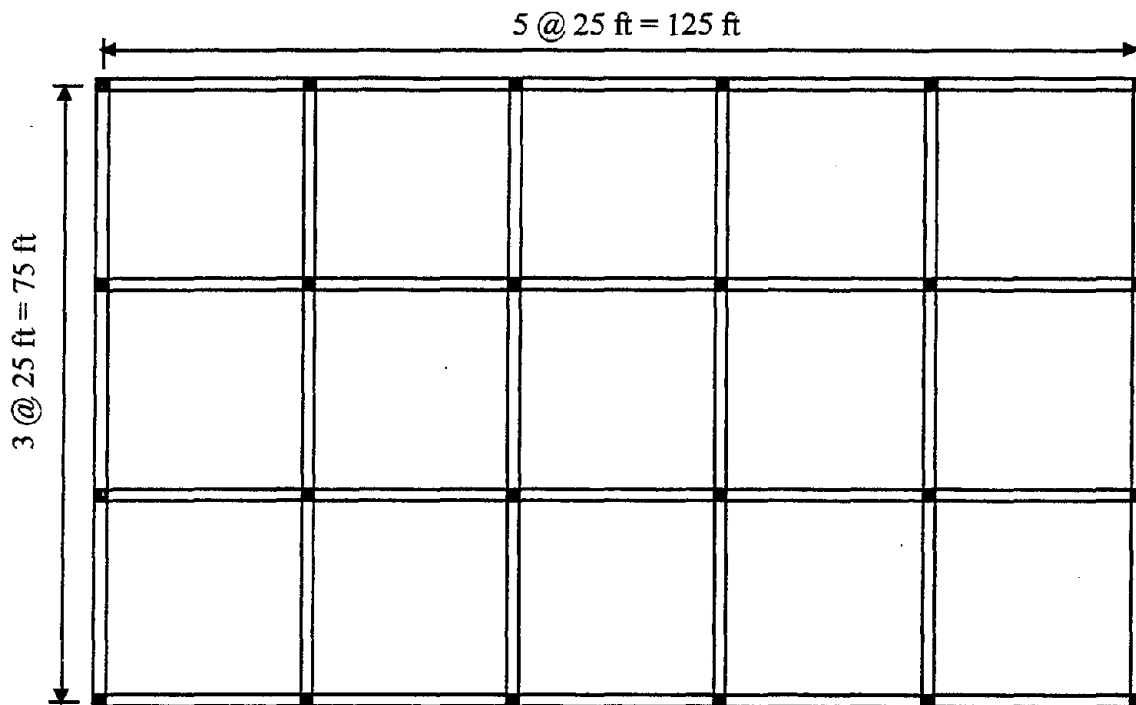


FIGURE 5-14 Plan of the three bay, five story frames

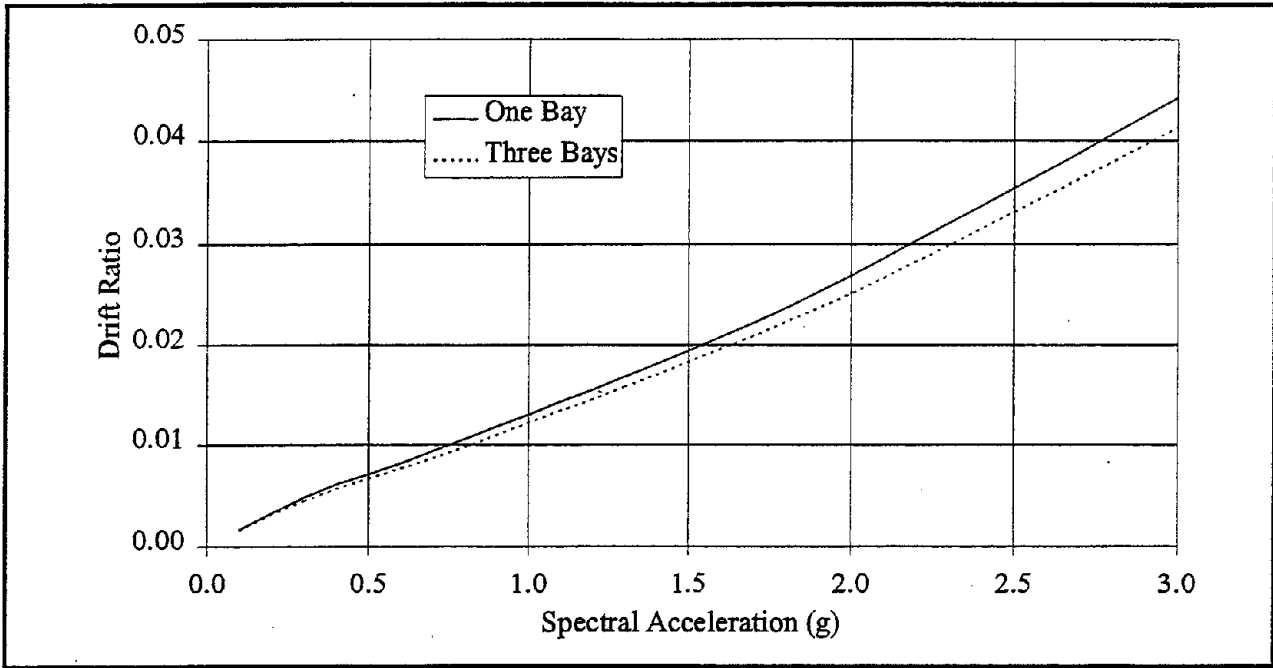


FIGURE 5-15 Comparison of the overall drift ratios for the two five story frames

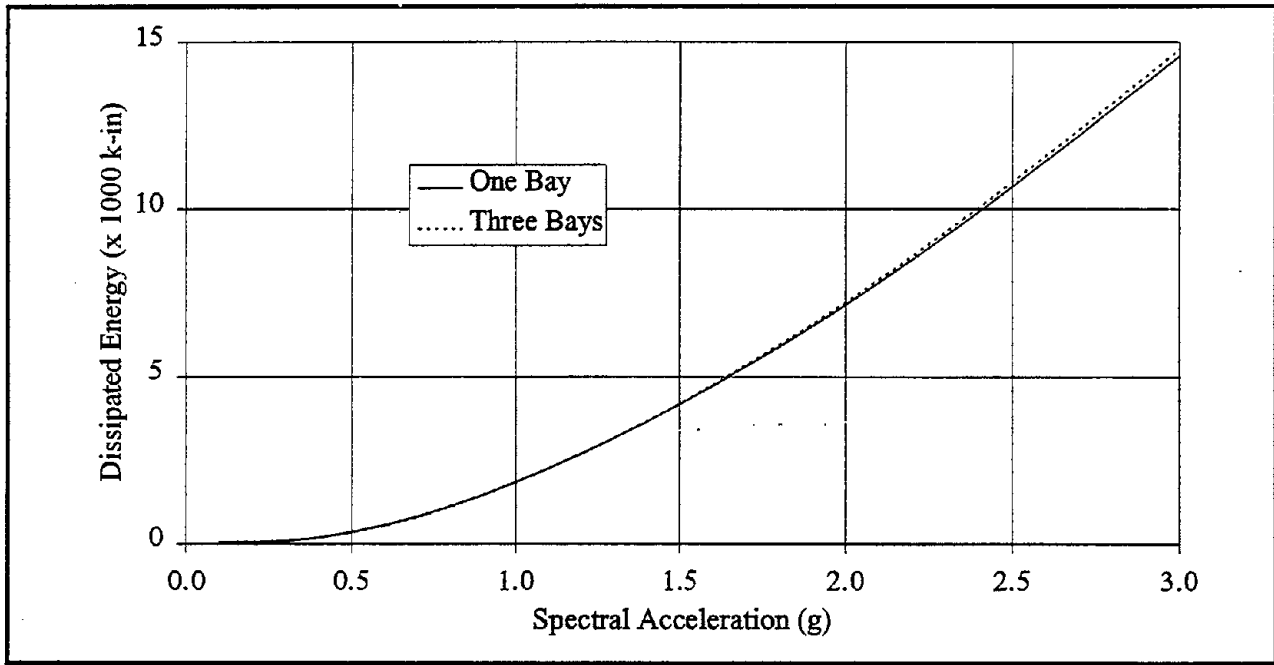


FIGURE 5-16 Comparison of the total dissipated hysteretic energies for the two five story frames

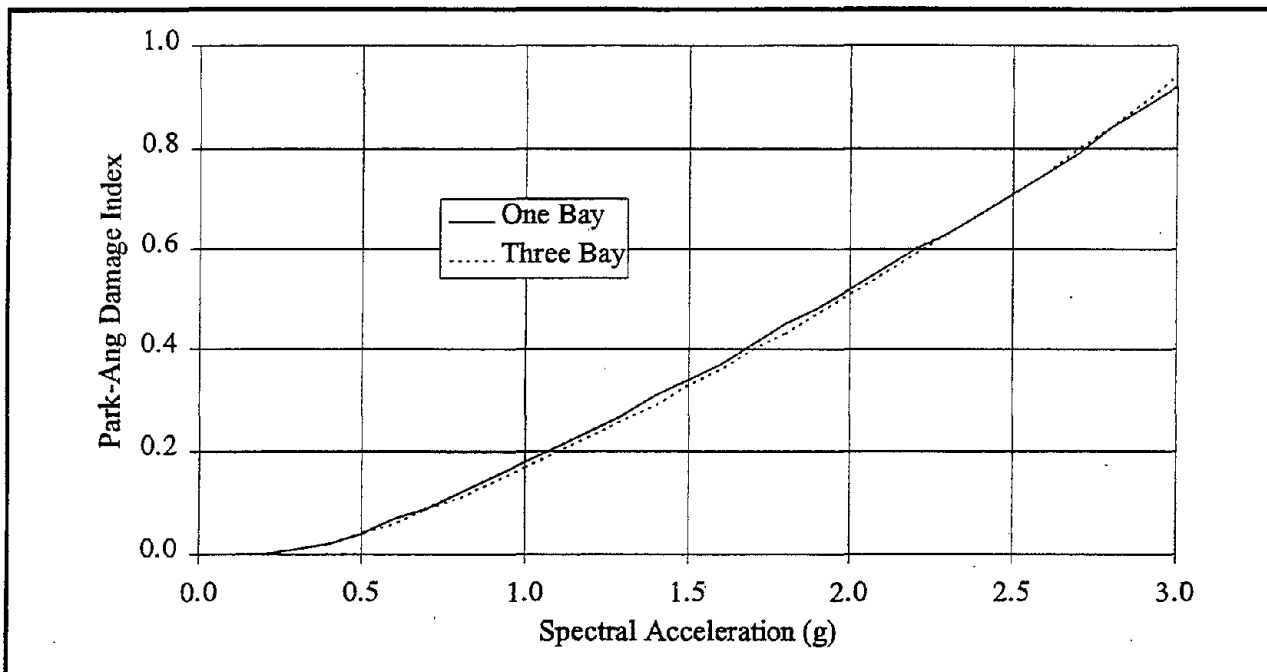


FIGURE 5-17 Comparison of the Park and Ang damage indices for the two five story frames

5.3.2 Sensitivity to Second-Order Effects

The dynamic analyses considered in developing the fragility curves, shown in figures 5-4 through 5-6, are first-order dynamic analyses as the distribution of internal forces in the structures ignored the effect of sway deformation on the equilibrium equations and the influence of axial forces on the stiffnesses of members. Second-order effects in building systems are associated with the movement of the structural mass to a deformed position which give rise to second-order overturning moments due to the lateral displacement. Thus, second-order effects refer to the effect of geometric nonlinearity on the behavior of a structure. In geometric nonlinear analysis of a structure, the equilibrium equations are formulated in the deformed configuration of the structure. Geometric nonlinear analyses may be carried out at the structure level only or may also include member curvature effects. When carried out at the structure level only, the geometric nonlinear analyses, also referred to as P- Δ analyses, only include the effect of member chord rotation. P- δ analyses on the other hand include nonlinearity arising out of

member curvature. While the P- Δ effect reduces the element flexural stiffness against sidesway, the P- δ effect reduces the member stiffness in both sidesway and non-sidesway modes of deformation.

Strictly speaking, the solution of second-order effects is iterative, as the second-order moments depend on the lateral displacements which in turn depend on the total applied moments. For building structures, Wilson and Habibullah (1987) suggest that the P- Δ problem can be linearized and the solution to the problem obtained directly and exactly without iteration as the weight of the structure is constant during lateral motions and the structural displacements can be assumed to be small compared to the building dimensions. They assume that the total axial force at a story level is equal to the weight of the building above that level, a weight which does not change during the application of the lateral loads. Therefore, the sum of the column geometric stiffness terms associated with the lateral loads cancel, and only the axial forces due to the weight of the structure need to be included in the evaluation of the negative stiffness terms for the entire building.

In this study, the P- Δ effects are investigated for the five story and the twelve story frames using the program DRAIN-2DX. The geometric stiffnesses used for dynamic analyses are based on the axial forces resulting from gravity loads. The program's manual suggests that considering only the gravity axial loads will often be accurate for building frames as the translational geometric stiffness for a story depends only on the sum of the axial forces in all columns of a story. The sum of the axial forces in all columns of a story is a constant equal to the gravity load if there are no vertical inertial forces.

The responses of the one bay, five story frame are compared in terms of the overall drift ratio, total dissipated hysteretic energy, and the Park-Ang structure damage index. The comparisons of the responses with and without P- Δ effect are presented in figures 5-18 through 5-20. Furthermore, the P- Δ effect was also investigated for the sample high rise building. The results for the twelve story frame are presented in figures 5-21 through 5-23. Figures 5-18 through 5-23 suggest that the P- Δ effect is negligible for lower levels of ground motion. Furthermore, the

P- Δ effect is more significant for the high rise frame compared to the mid rise frame. Wilson and Habibullah (1987) suggest that if the lateral displacements obtained from analyses with and without P- Δ effects at the design level differ by more than 10 or 15%, the basic design is too flexible. As the ground motion level is increased, the P- Δ effect becomes significant. The structures become unstable at still larger levels of ground motion as the geometric stiffness begins to dominate and reduces the effective stiffness of the system. The P- Δ effect for the low rise frame was not expected to be significant and therefore was not investigated.

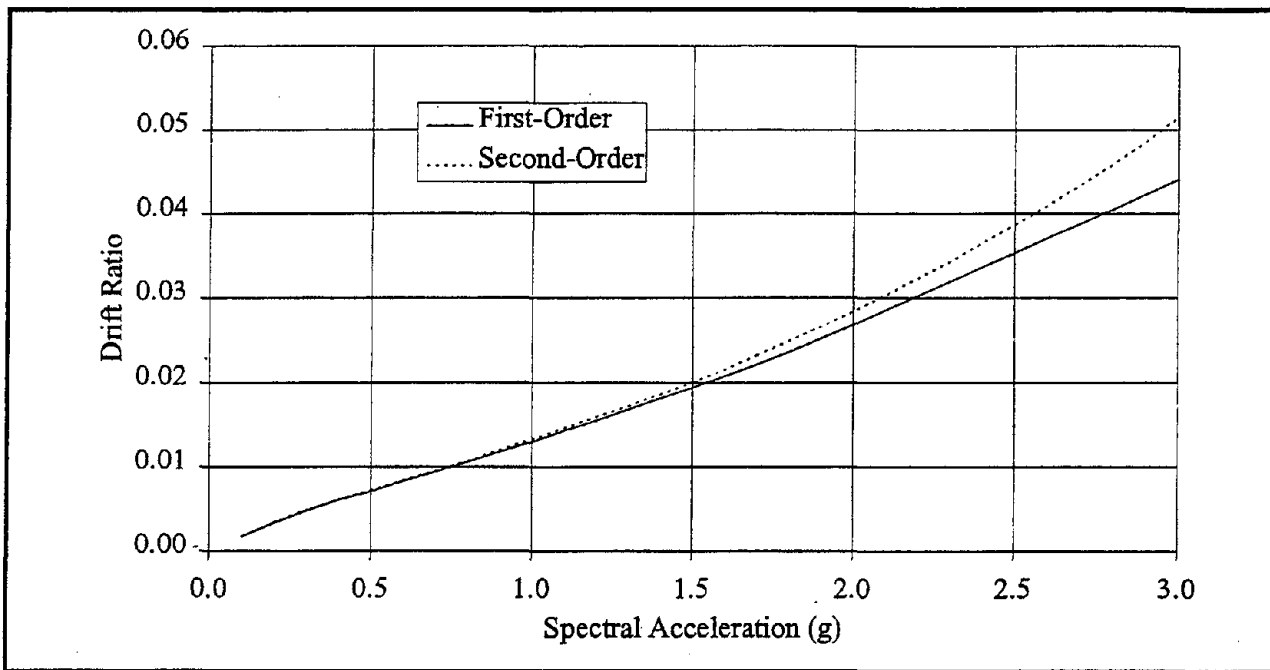


FIGURE 5-18 Comparison of the overall drift ratio for the one bay, five story frame

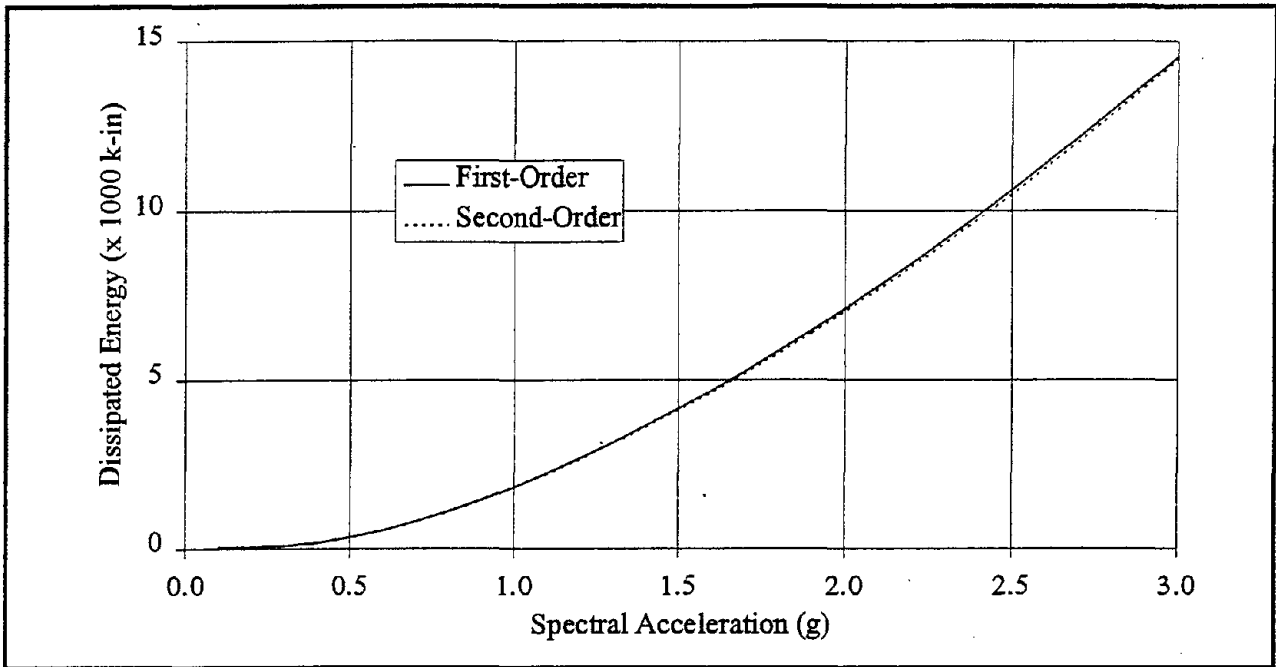


FIGURE 5-19 Comparison of the total dissipated hysteretic energies for the one bay, five story frame

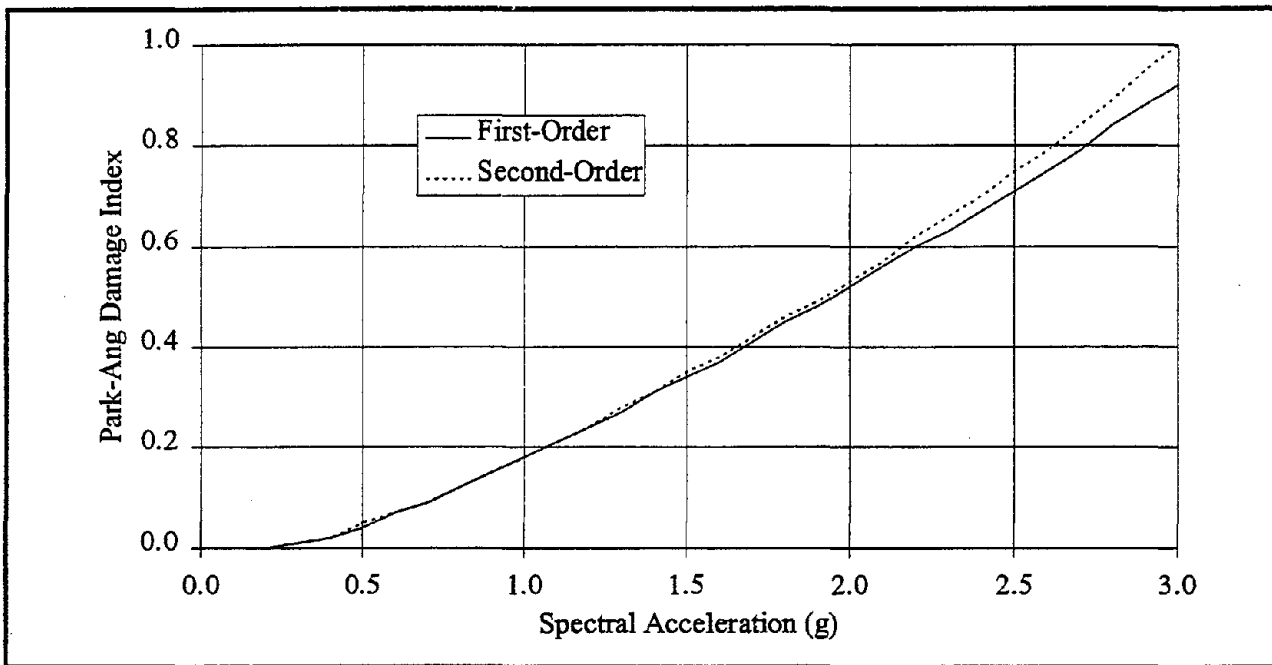


FIGURE 5-20 Comparison of the Park-Ang damage index for the one bay, five story frame

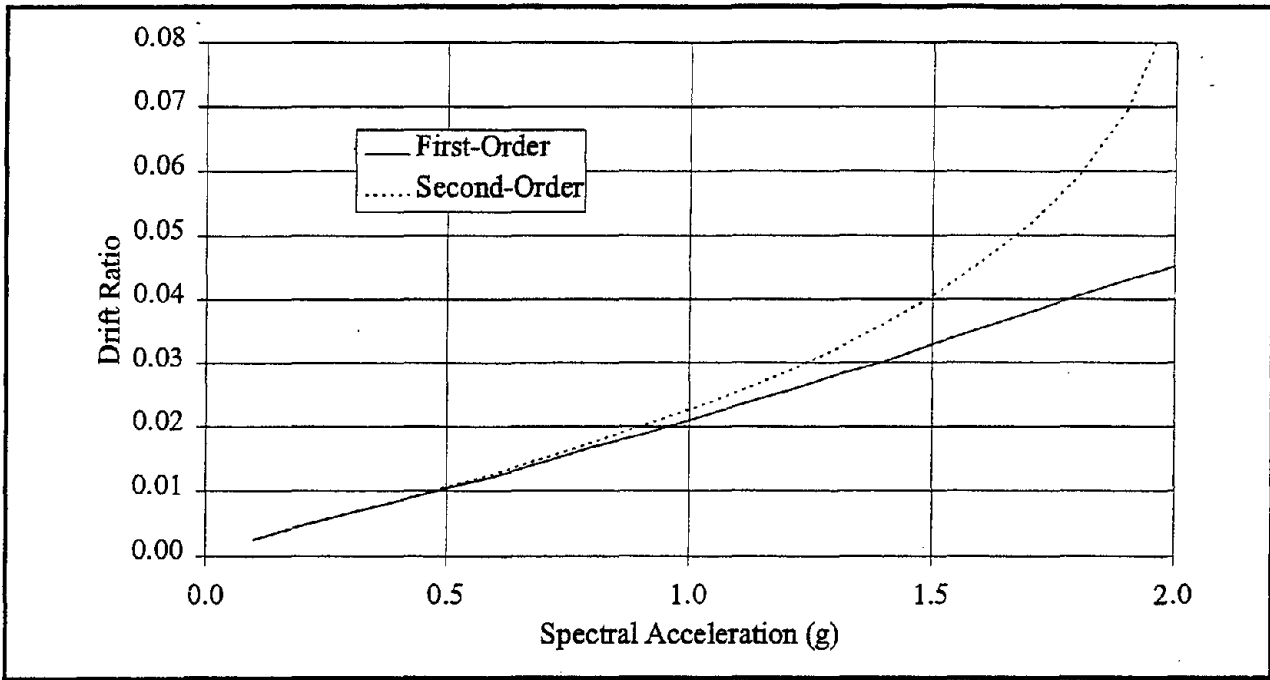


FIGURE 5-21 Comparison of the overall drift ratio for the one bay, twelve story frame

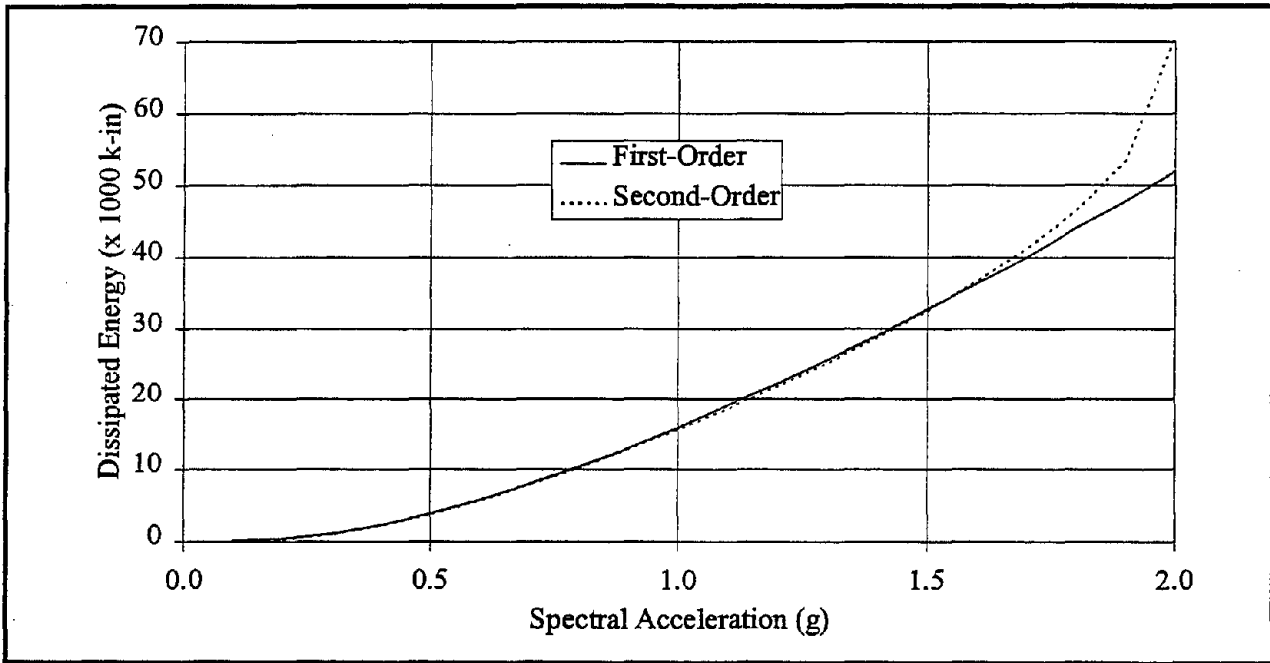


FIGURE 5-22 Comparison of the total dissipated hysteretic energies for the one bay, twelve story frame

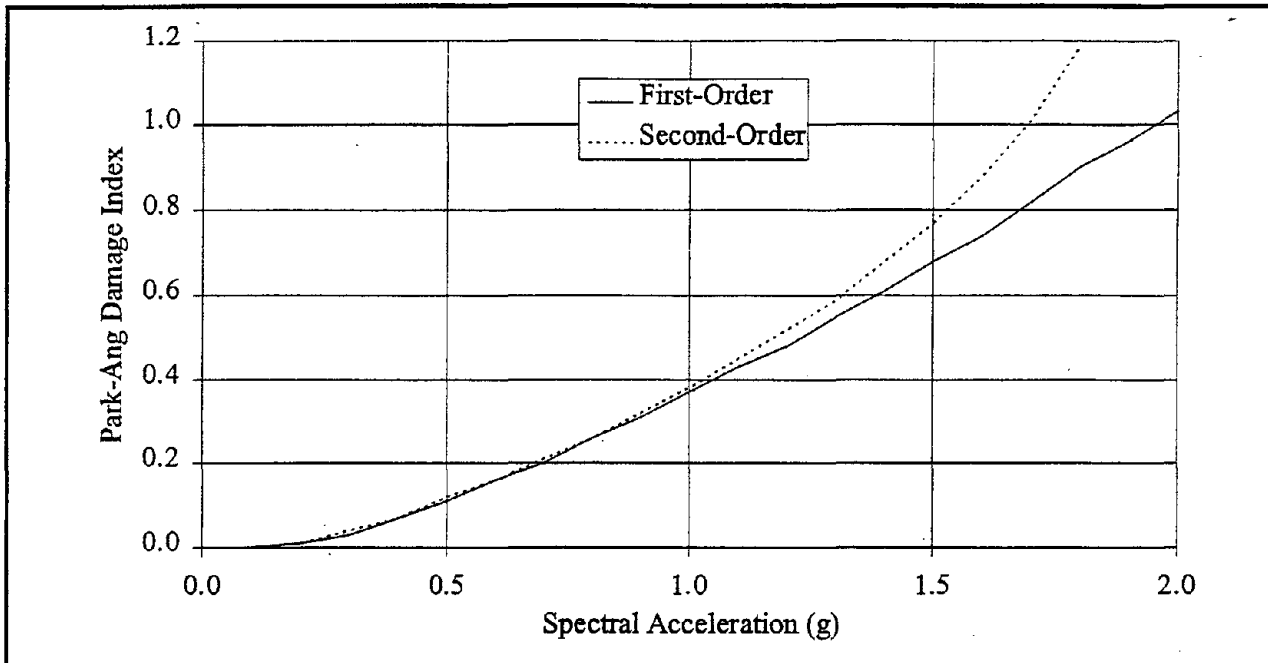


FIGURE 5-23 Comparison of the Park-Ang damage index for the one bay, twelve story frame

5.3.3 Sensitivity to Site Conditions

The response of buildings can be influenced by the soil on which the building is founded. The response spectra of ground motion recorded on firm sites is different from those recorded on softer sites. Furthermore, the ground motion recorded close to a building would be different from that which would have been recorded if the building had not been present. This modification of the ground motion is referred to as soil-structure interaction. Jennings and Bielak (1973) suggest that the soil-structure interaction effects depend on the relative stiffness of the building and its foundation. Soil-structure interaction has been considered by various researchers, including Veletsos and Prasad (1989), Luco and Mita (1987), and Veletsos and Meek (1974). In most instances, soil-structure interaction has been shown to reduce the fundamental frequency of the structure and increase its damping from the case where the structure is assumed to be located on a firm base.

Although the consideration of the soil-structure interaction effect is beyond the scope of the current study, it is still useful to consider the effect of different mean spectral shapes on the

dynamic response of structures. Thus, ground motions recorded on soil sites during the Landers, Loma Prieta, Morgan Hill, Northridge, and Whittier Narrows earthquakes are used. These ground motions are selected on the basis of the average shear wave velocities at the recording stations. These ground motions correspond to site class SC-III in the classification proposed by Borchardt (1994). The time histories used, and the average spectral acceleration in the three period bands are shown in table 5-VIII. The statistics on the dynamic amplification factors are presented in figure 5-24. Figure 5-25 shows the comparison of the mean dynamic amplification factors corresponding to firm and soil sites. As expected, the dynamic amplification for soil sites has a large plateau in the short-period range. However, in the long-period range, the dynamic amplification factors are similar for firm and soil sites. In this study, the two story frame described in Section 4 is used. The two story frame is selected as it is likely to be effected most by the change in the spectral shapes. The mid rise and the high rise frames lie in the descending portions of the dynamic amplification factors, where the dynamic amplification factors for firm and soil sites are similar. The comparison of the results in terms of the overall drift ratios, dissipated hysteretic energies, and the Park-Ang damage index are presented in figures 5-26 through 5-28, respectively.

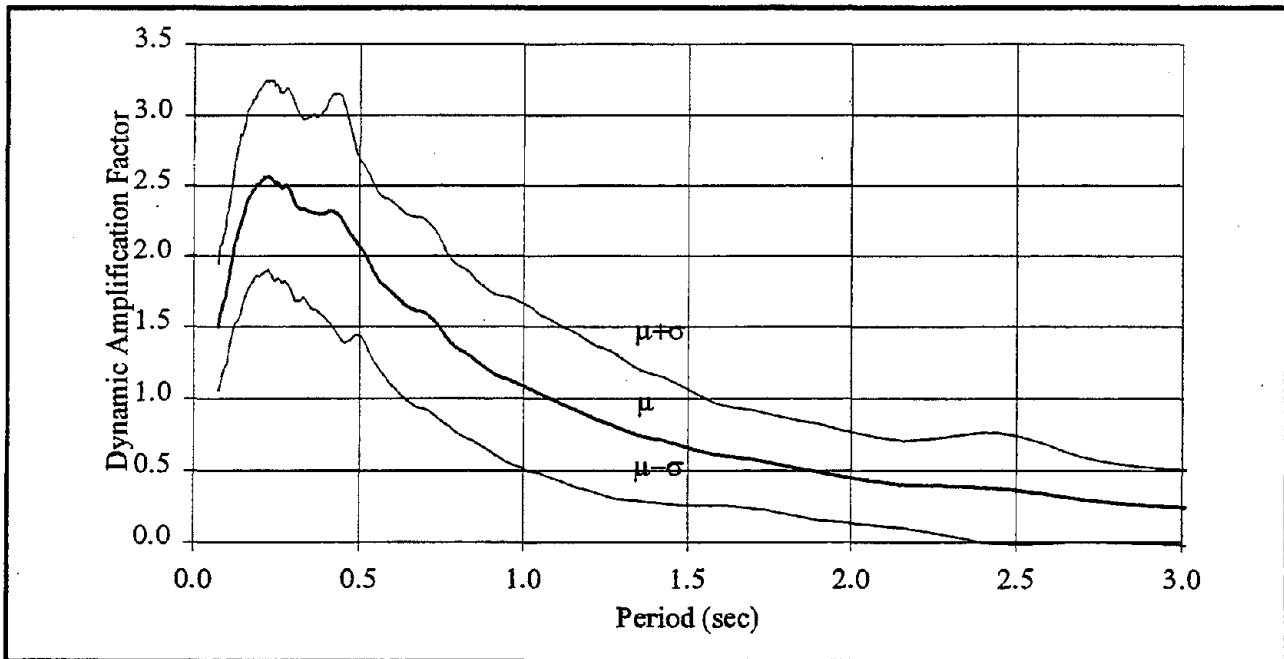


FIGURE 5-24 Dynamic amplification factors for soil sites

TABLE 5-VIII Average spectral acceleration values for ground motions recorded on soil sites

SITE NAME AND NUMBER	EARTHQUAKE	Average S_a ($0.1 \leq T \leq 0.5$) (g)	Average S_a ($0.5 < T \leq 0.9$) (g)	Average S_a ($0.9 < T \leq 2.5$) (g)
Hemet - Fire Station CSMIP 12331	Landers	0.171	0.115	0.055
		0.141	0.112	0.049
Indio - Coachella Canal CSMIP 12026	Landers	0.232	0.230	0.130
		0.254	0.208	0.094
Palm Springs Airport CSMIP 12025	Landers	0.178	0.218	0.141
		0.178	0.218	0.141
Yermo - Fire Station CSMIP 22074	Landers	0.437	0.283	0.193
		0.445	0.487	0.322
Agnews State Hospital CSMIP 57066	Loma Prieta	0.331	0.219	0.156
		0.448	0.241	0.117
Fremont Mission San Jose CSMIP 57064	Loma Prieta	0.294	0.164	0.058
		0.272	0.212	0.083
Gilroy #2 CSMIP 47380	Loma Prieta	0.837	0.476	0.390
		0.870	0.604	0.206
Gilroy #3 CSMIP 47381	Loma Prieta	0.821	0.478	0.325
		1.340	0.583	0.127
Gilroy #4 CSMIP 57382	Loma Prieta	0.527	0.563	0.263
		0.898	0.447	0.218
Giroy #7 CSMIP 57425	Loma Prieta	0.789	0.279	0.049
		0.613	0.361	0.057
Salinas CSMIP 47179	Loma Prieta	0.270	0.183	0.092
		0.184	0.139	0.071
San Francisco Airport CSMIP 58223	Loma Prieta	0.649	0.623	0.168
		0.655	0.510	0.158
Hollister Airport USGS	Loma Prieta	0.688	0.766	0.219
		0.521	0.665	0.300
Sunnyvale Colton Avenue USGS	Loma Prieta	0.544	0.295	0.231
		0.378	0.370	0.213
Agnews State Hospital CSMIP 57066	Morgan Hill	0.069	0.101	0.069
		0.092	0.073	0.052
Fremont Mission San Jose CSMIP 57064	Morgan Hill	0.058	0.043	0.026
		0.051	0.038	0.032
Gilroy #2 CSMIP 47380	Morgan Hill	0.371	0.191	0.065
		0.246	0.092	0.049
Gilroy #3 CSMIP 47381	Morgan Hill	0.366	0.257	0.097
		0.363	0.179	0.090
Gilroy #4 CSMIP 57382	Morgan Hill	0.662	0.359	0.103
		0.566	0.296	0.141
Giroy #7 CSMIP 57425	Morgan Hill	0.331	0.094	0.025
		0.371	0.096	0.027

TABLE 5-VIII (cont'd) Average spectral acceleration values for ground motions recorded on soil sites

SITE NAME AND NUMBER	EARTHQUAKE	Average S_a ($0.1 < T \leq 0.5$) (g)	Average S_a ($0.5 < T \leq 0.9$) (g)	Average S_a ($0.9 < T \leq 2.5$) (g)
San Francisco Airport CSMIP 58223	Morgan Hill	0.112	0.061	0.022
		0.122	0.057	0.019
Alhambra CSMIP 24461	Northridge	0.227	0.192	0.085
		0.215	0.120	0.040
Arleta CSMIP 24087	Northridge	0.687	0.662	0.243
		0.638	0.538	0.184
LA-Hollywood Storage Bldg. CSMIP 24303	Northridge	0.517	0.430	0.160
		0.836	0.614	0.164
LA - Obregon Park CSMIP 24400	Northridge	0.716	0.284	0.079
		0.996	0.455	0.118
Newhall CSMIP24279	Northridge	1.589	1.009	0.444
		1.455	1.736	0.676
Arcadia Ave., Arcadia USC 0099	Northridge	0.254	0.155	0.081
		0.251	0.152	0.052
Badillo, Covina USC 0070	Northridge	0.236	0.081	0.036
		0.251	0.128	0.069
Birchdale, Downey USC 0079	Northridge	0.367	0.177	0.067
		0.373	0.203	0.062
Briarcliff Dr., La Habra USC 0074	Northridge	0.420	0.185	0.053
		0.275	0.208	0.042
Campus Dr., Arcadia USC 0093	Northridge	0.230	0.120	0.040
		0.275	0.152	0.064
Catskill Ave., Carson USC 0040	Northridge	0.210	0.075	0.036
		0.193	0.119	0.045
Coldwater Can., Hollywood USC 0009	Northridge	0.624	0.386	0.211
		0.692	0.353	0.218
Colima Rd., Hacienda Hghts USC 0073	Northridge	0.142	0.088	0.039
		0.176	0.099	0.044
Del Amo Blvd., Lakewood USC 0084	Northridge	0.333	0.172	0.088
		0.359	0.222	0.069
Flower Ave., Brea USC 0087	Northridge	0.245	0.154	0.032
		0.277	0.172	0.051
Grand Avenue, LA USC 0022	Northridge	0.608	0.429	0.067
		0.702	0.385	0.108
Holly Ave., Baldwin Park USC 0069	Northridge	0.279	0.108	0.048
		0.214	0.071	0.034
Jaboneria, Bell Gardens USC 0094	Northridge	0.186	0.161	0.074
		0.225	0.16	0.053
Joslin St., Santa Fe Springs USC 0077	Northridge	0.342	0.161	0.045
		0.388	0.169	0.041

TABLE 5-VIII (cont'd) Average spectral acceleration values for ground motions recorded on soil sites

SITE NAME AND NUMBER	EARTHQUAKE	Average S_a ($0.1 \leq T \leq 0.5$) (g)	Average S_a ($0.5 < T \leq 0.9$) (g)	Average S_a ($0.9 < T \leq 2.5$) (g)
La Palma Ave., Buena Park USC 0086	Northridge	0.283	0.192	0.068
		0.340	0.195	0.062
New York Ave., La Crescenta USC 0060	Northridge	0.318	0.201	0.049
		0.456	0.258	0.050
Oakbank, Glendora USC 0065	Northridge	0.183	0.084	0.039
		0.109	0.074	0.024
Orange Ave., West Covina USC 0071	Northridge	0.167	0.112	0.047
		0.155	0.127	0.050
Osage Ave., Lawndale USC 0045	Northridge	0.261	0.156	0.084
		0.200	0.166	0.087
RimGrove Ave., La Puente USC 0072	Northridge	0.313	0.186	0.030
		0.326	0.177	0.026
Saturn St., LA USC 0091	Northridge	1.125	0.758	0.195
		0.872	0.595	0.149
Top. Can. Blvd., Canoga Park USC 0053	Northridge	0.895	0.854	0.402
		0.844	0.664	0.241
Vernon Ave., LA USC 0025	Northridge	0.310	0.166	0.072
		0.334	0.157	0.083
Water St., Carson USC 0081	Northridge	0.231	0.173	0.072
		0.206	0.174	0.057
Willoughby Ave., Hollywood USC 0018	Northridge	0.476	0.643	0.237
		0.428	0.296	0.103
Alhambra - Fremont School CSMIP 24461	Whittier Narrows	0.664	0.301	0.094
		0.734	0.404	0.130
Altadena-Eaton Canyon Park CSMIP 24402	Whittier Narrows	0.301	0.109	0.023
		0.507	0.263	0.053
Downey CSMIP 14368	Whittier Narrows	0.272	0.327	0.063
		0.451	0.579	0.136
LA-Hollywood Storage Bldg. CSMIP 24303	Whittier Narrows	0.204	0.180	0.050
		0.310	0.182	0.056
LA - Obregon Park CSMIP 24400	Whittier Narrows	0.789	0.338	0.103
		0.712	0.315	0.099
Long Beach - Los Cerritos CSMIP 14242	Whittier Narrows	0.479	0.384	0.079
		0.354	0.350	0.088
San Marino - South. Acad. CSMIP 24401	Whittier Narrows	0.349	0.332	0.096
		0.226	0.075	0.027

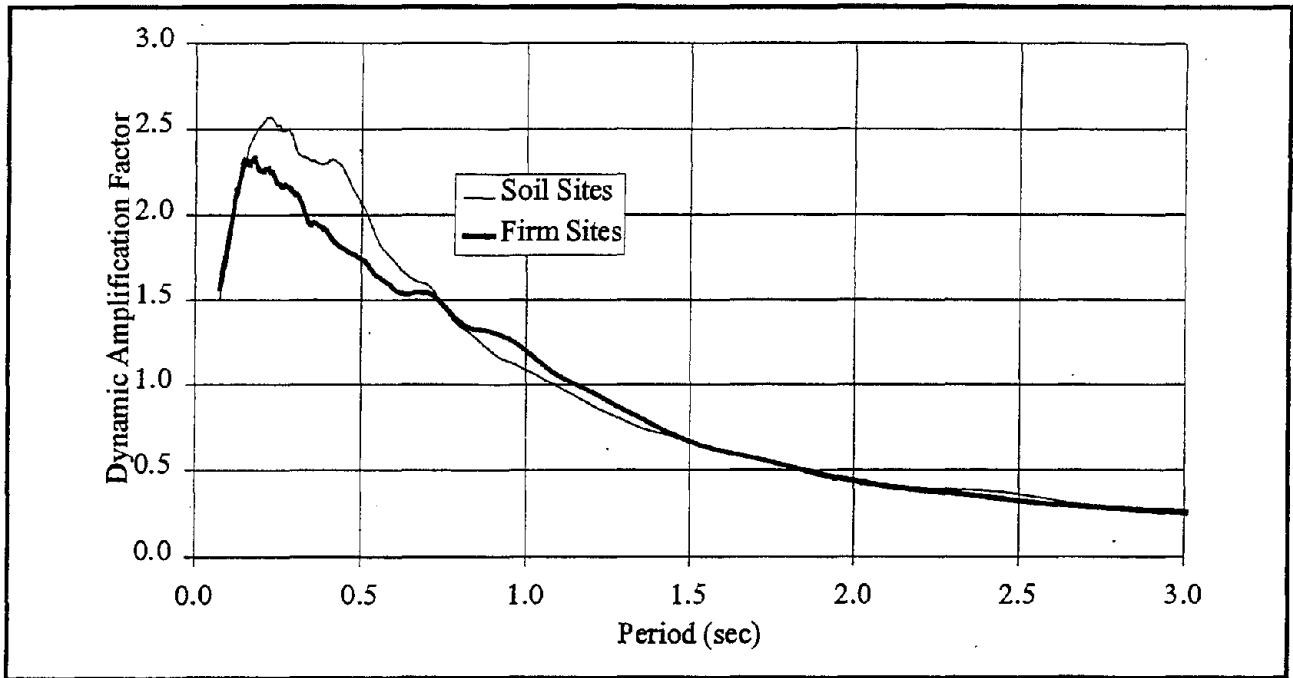


FIGURE 5-25 Comparison of the mean dynamic amplification factors for firm and soil sites

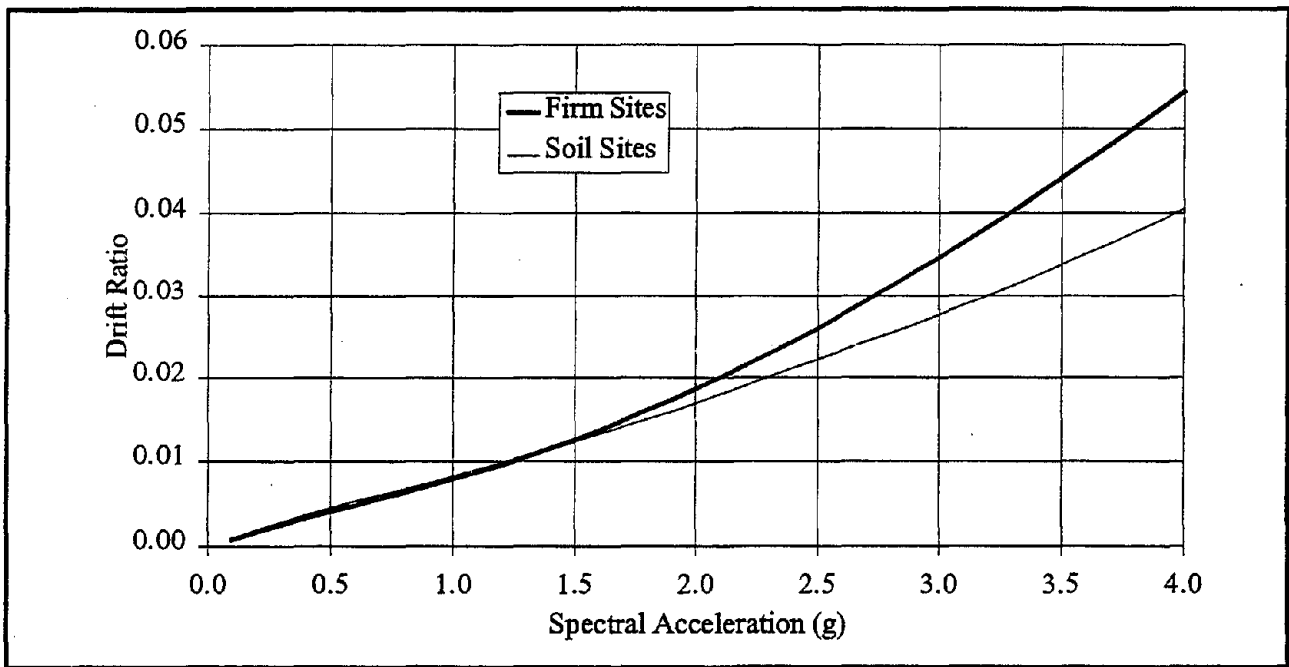


FIGURE 5-26 Comparison of the overall drift ratio for the one bay, two story frame subjected to ground motions recorded on firm and soil sites

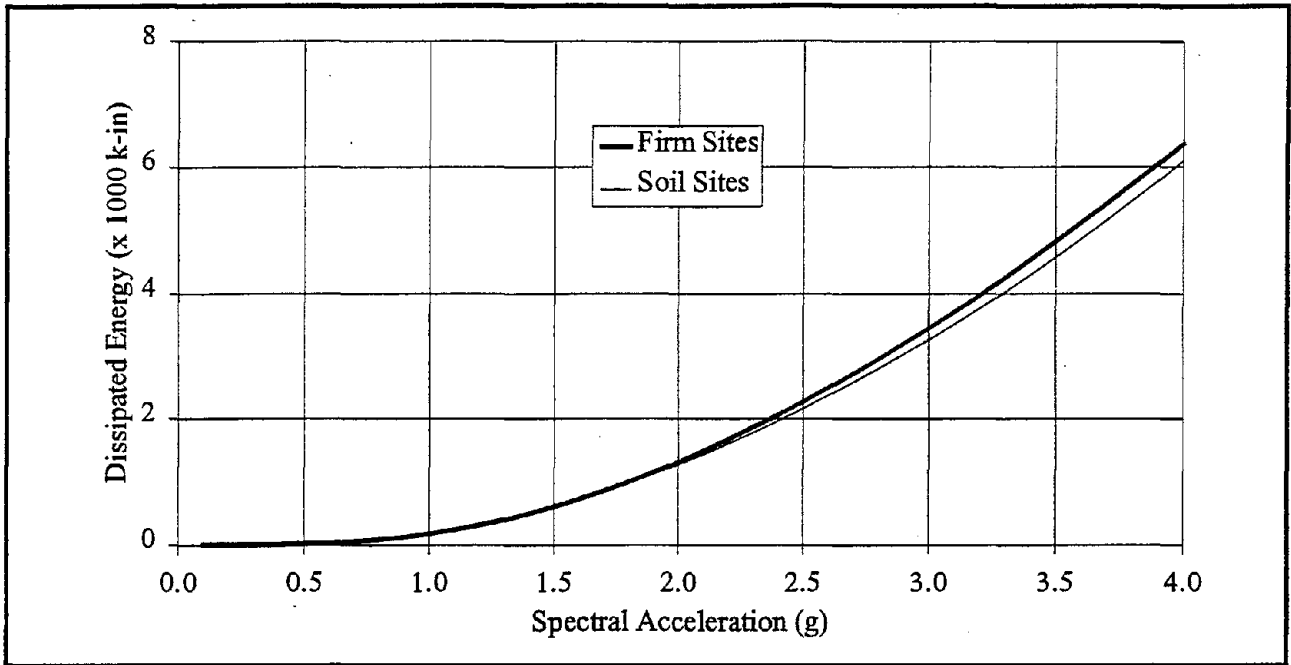


FIGURE 5-27 Comparison of the total dissipated hysteretic energies for the one bay, two story frame subjected to ground motions recorded on firm and soil sites

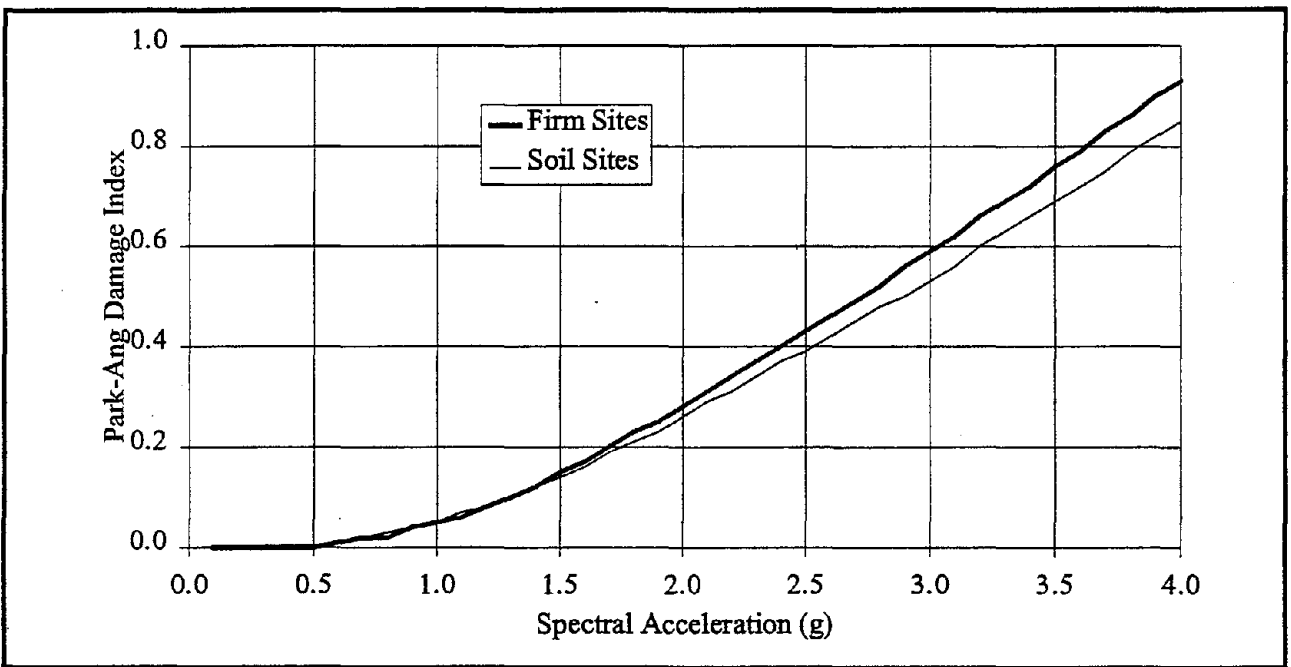


FIGURE 5-28 Comparison of the Park-Ang damage index for the one bay, two story frame subjected to ground motions recorded on firm and soil sites

The site conditions in this study so far have been determined based on the shear wave velocity at that site. However, this relationship results in very similar dynamic amplification factors for firm and soil sites as shown in figure 5-25. Using ground motions recorded on rock and alluvium sites during the Loma Prieta earthquake, Mohraz and Tiv (1991) arrive at the conclusion that the amplification factors for these two sites are very similar. Seed et al. (1976) and Mohraz (1976) arrive at very different amplification factors for rock and alluvial sites, those for alluvial sites being quite similar to those shown in figure 5-25 and to those obtained by Mohraz (1991). It is worthwhile to investigate the effect of the spectral shape on nonlinear dynamic response. To obtain spectral shapes similar to those obtained by Seed et al. (1976) and Mohraz (1976), about forty time histories were selected from the six earthquakes mentioned before. The sites on which these forty time histories were recorded are termed as rock sites for the purpose of this study. The statistics on the dynamic amplification factors for rock sites are presented in figure 5-29, and the comparison of these factors with those for firm sites in figure 5-30. The mean dynamic amplification factors for rock sites shown in figure 5-30 are very similar to the amplification factors for rock sites provided by Seed et al. (1976) and Mohraz (1976).

Figures 5-31 through 5-33 respectively present the comparisons of the overall drift ratios, total dissipated energy, and the Park-Ang damage index for the low rise frame when subjected to ground motions recorded on rock and firm sites. These figures show that there are considerable differences in the responses when the frame is subjected to motions recorded on firm and rock sites. These differences are due to the reduction in seismic demand for the frame subjected to ground motions recorded on rock as the members of the frame progressively yield resulting in the lengthening of the period of the structure. Figure 5-30 depicts the reduction of seismic demand at larger periods. Figures 5-34 through 5-36 respectively present the comparisons of the overall drift ratios, total dissipated energy, and the Park-Ang damage index for the mid rise frame when subjected to ground motions recorded on rock and firm sites. Figures 5-37 through 5-39 respectively present the comparisons of the overall drift ratios, total dissipated energy, and the Park-Ang damage index for the high rise frame when subjected to ground motions recorded on rock and firm sites. Figures 5-34 through 5-39 show that the responses are very similar at lower levels of ground motion, some differences being observed at larger levels of ground motion. The

differences in the responses of the frames when subjected to ground motions recorded on firm and rock sites are due to higher mode effects. Compared to ground motions recorded on firm sites, those recorded on rock sites have more demands at smaller periods for the same level of demands in the period ranges for the mid rise and the high rise frames.

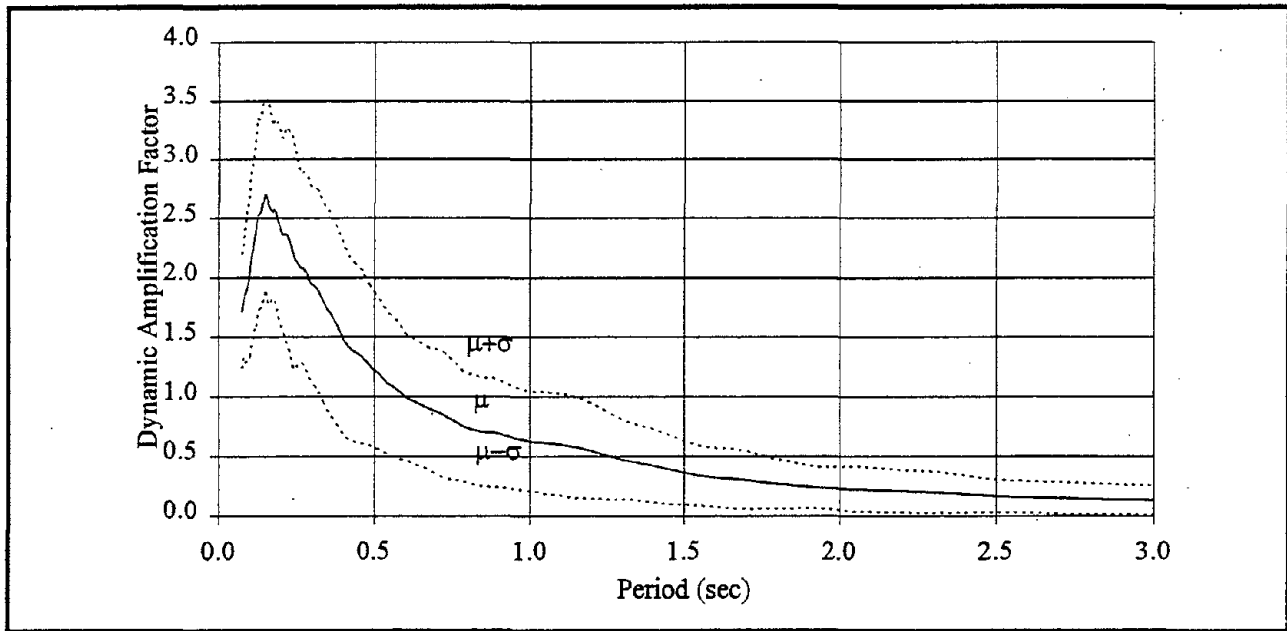


FIGURE 5-29 Dynamic amplification factors for rock sites

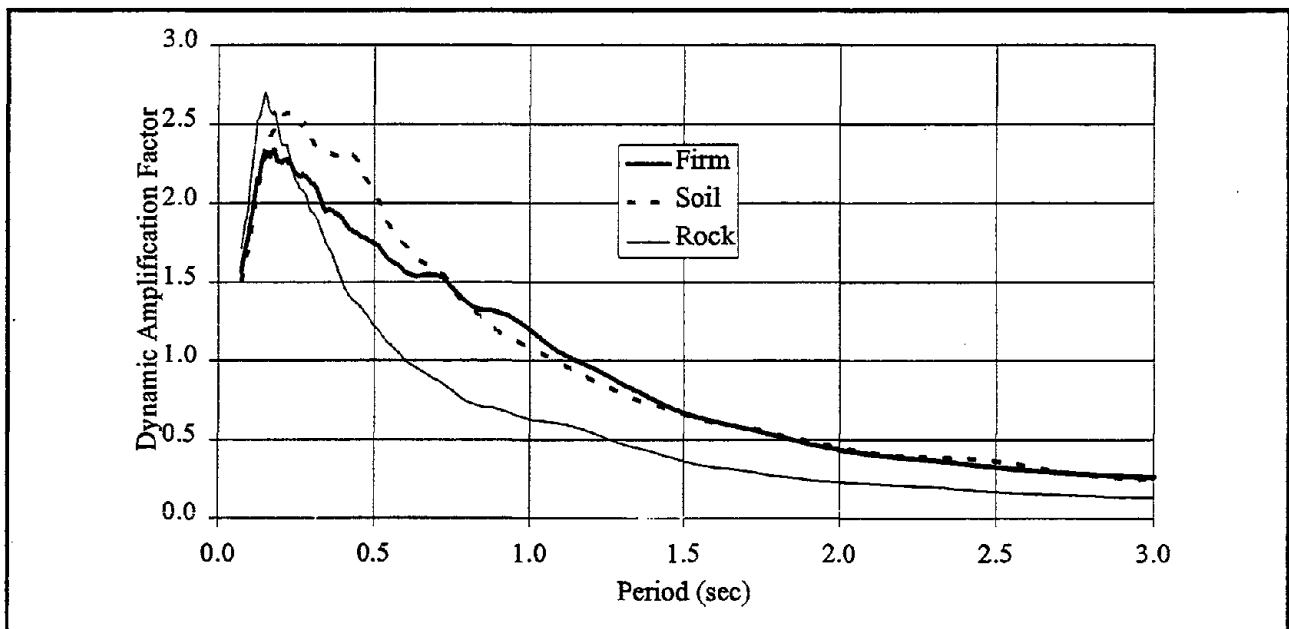


FIGURE 5-30 Comparison of the mean dynamic amplification factors for different sites

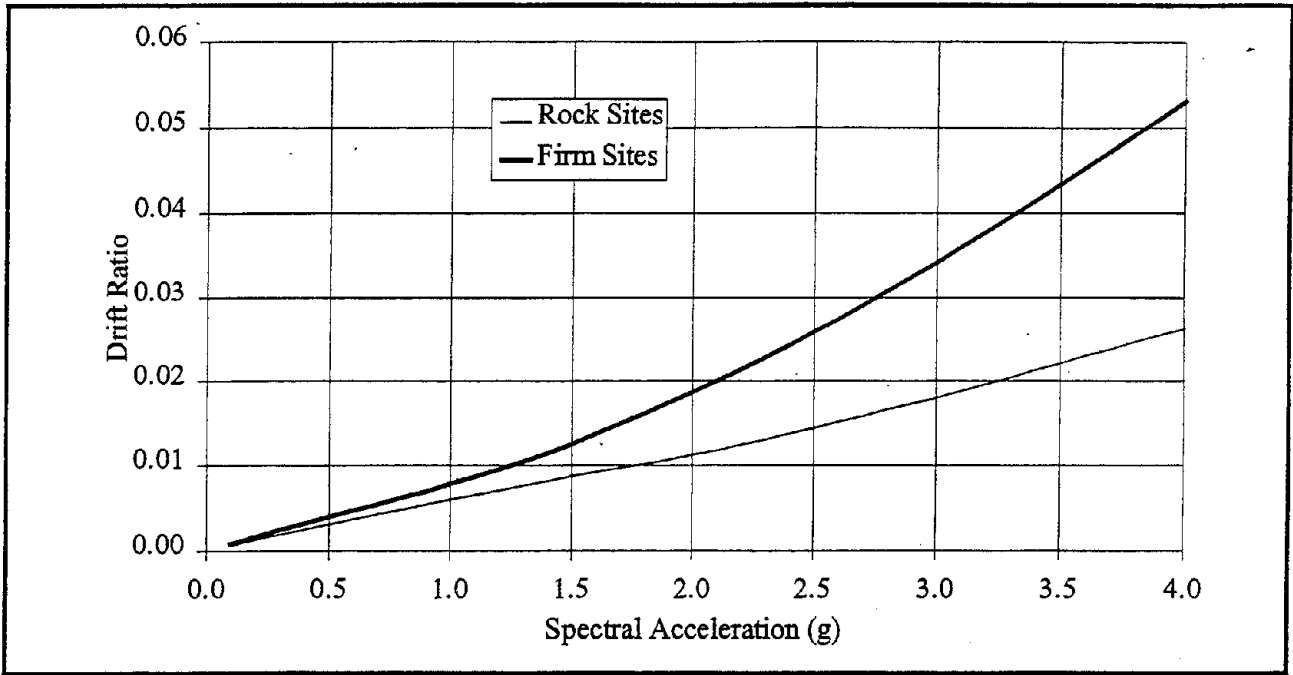


FIGURE 5-31 Comparison of the overall drift ratio for the one bay, two story frame subjected to ground motions recorded on firm and rock sites

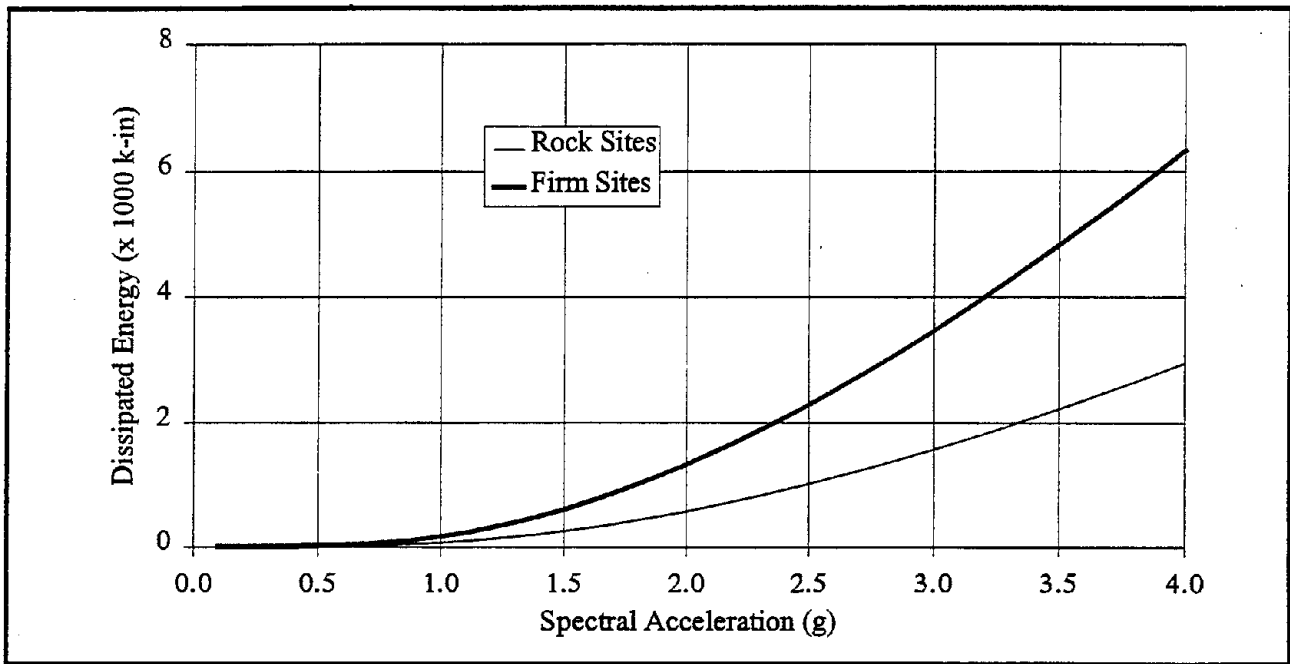


FIGURE 5-32 Comparison of the total dissipated energy for the one bay, two story frame subjected to ground motions recorded on firm and rock sites

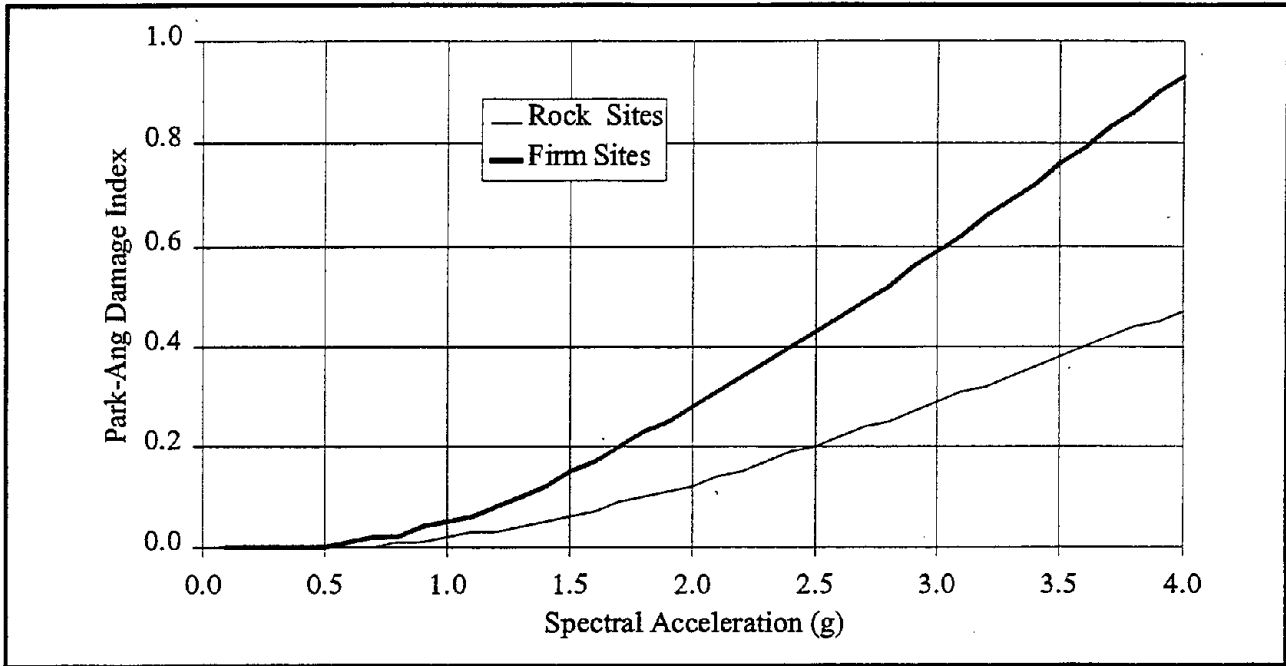


FIGURE 5-33 Comparison of the overall Park-Ang damage index for the one bay, two story frame subjected to ground motions recorded on firm and rock sites

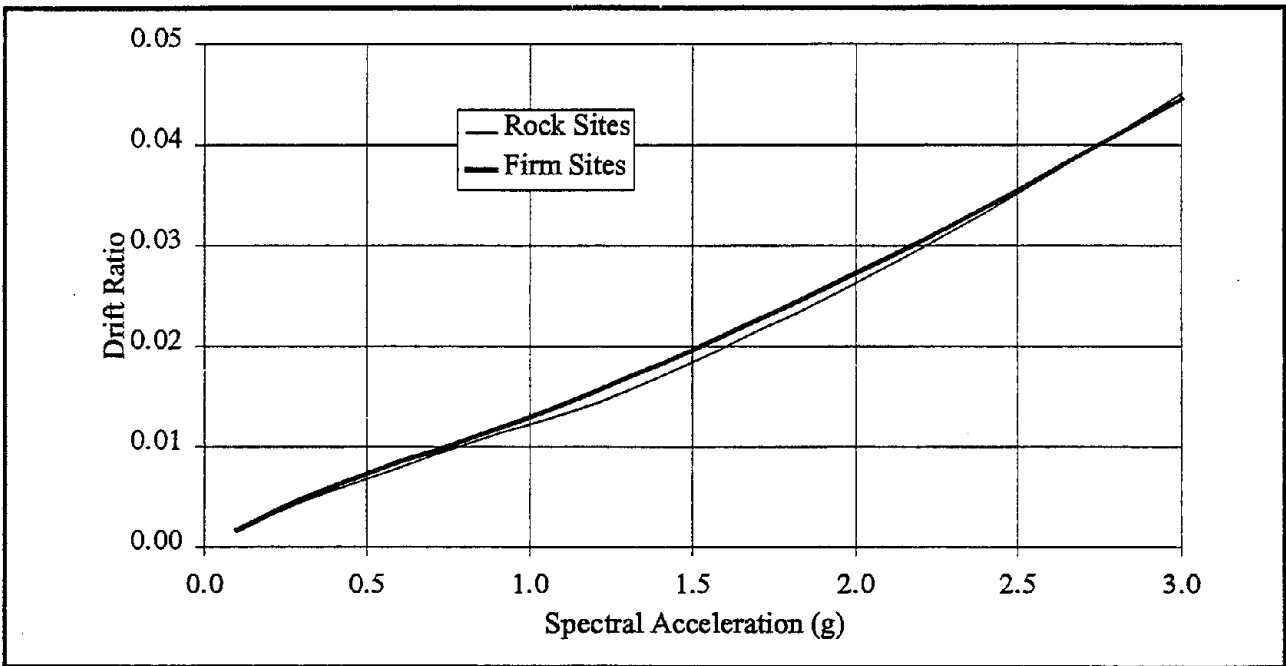


FIGURE 5-34 Comparison of the overall drift ratio for the one bay, five story frame subjected to ground motions recorded on firm and rock sites

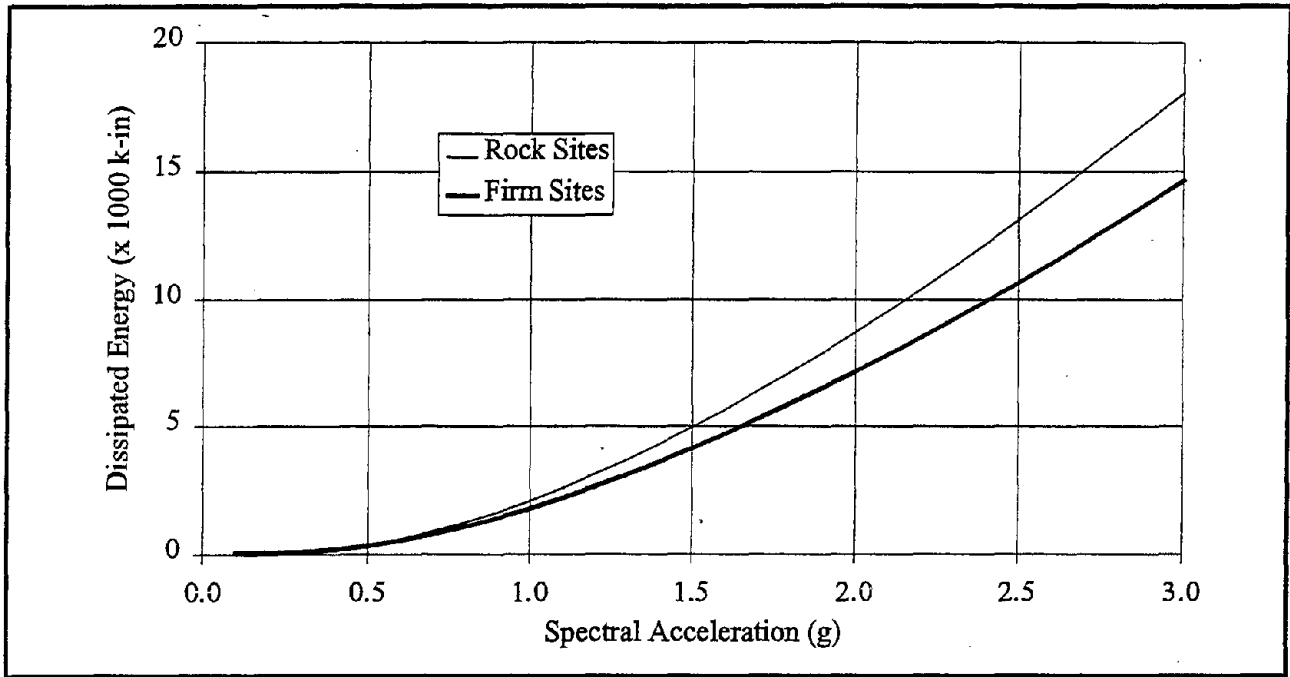


FIGURE 5-35 Comparison of the total dissipated energy for the one bay, five story frame subjected to ground motions recorded on firm and rock sites

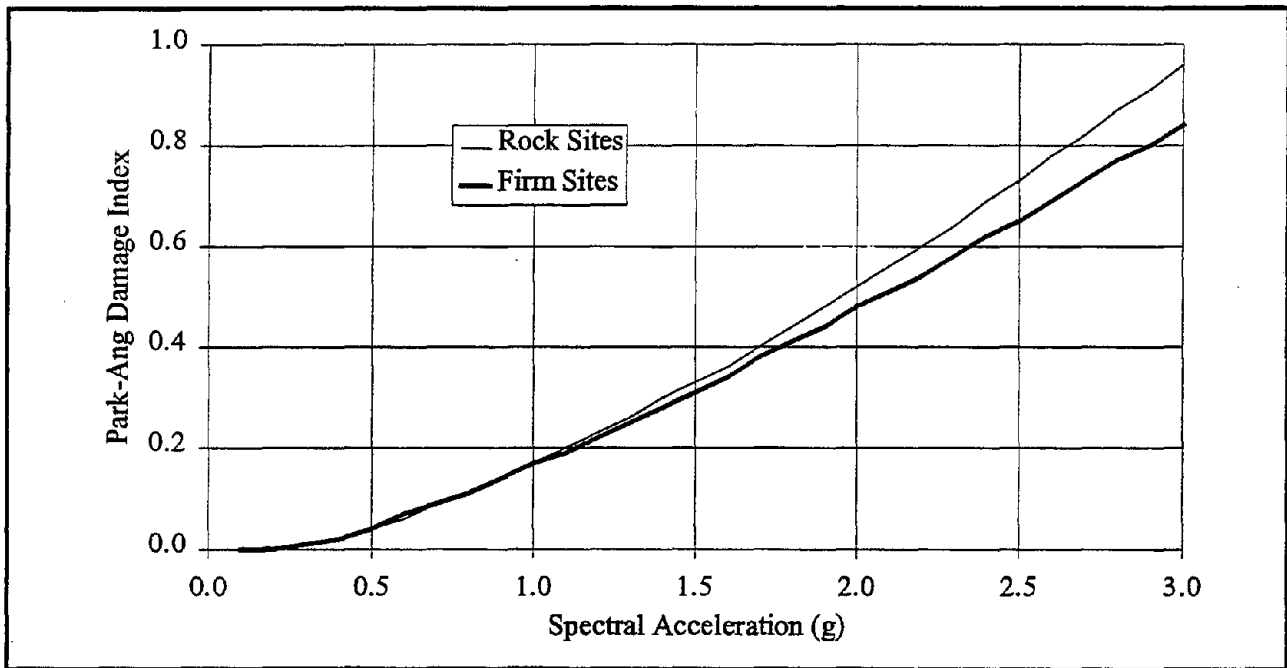


FIGURE 5-36 Comparison of the overall Park-Ang damage index for the one bay, five story frame subjected to ground motions recorded on firm and rock sites

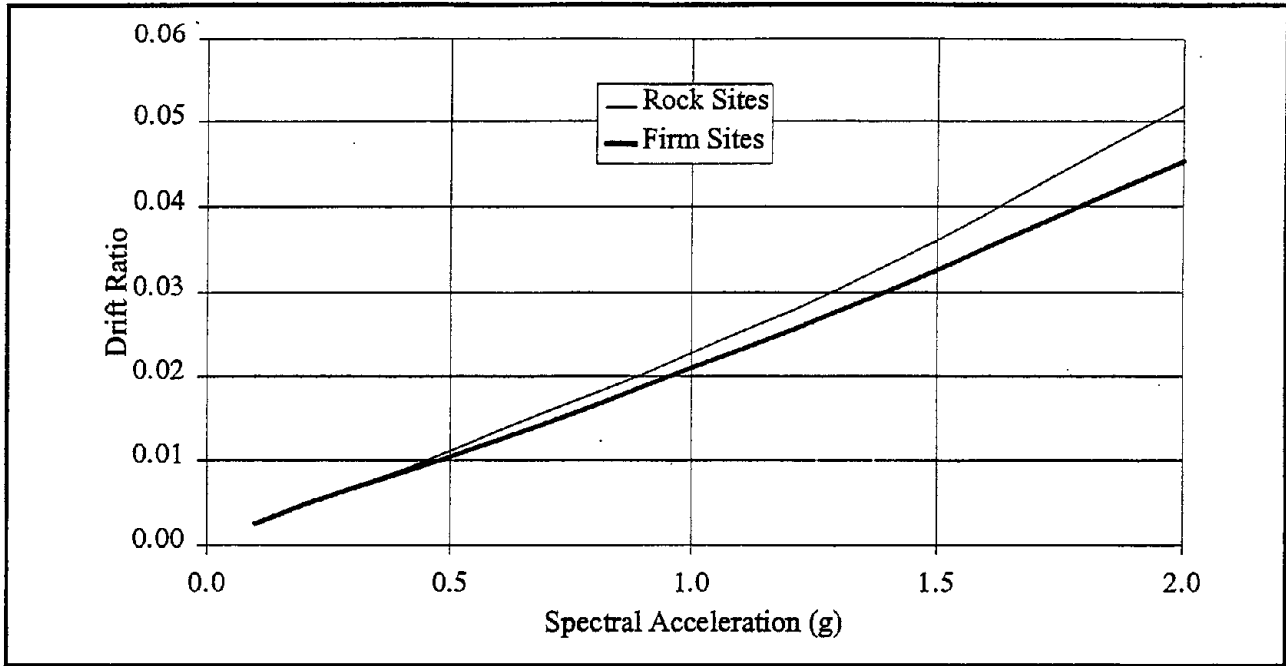


FIGURE 5-37 Comparison of the overall drift ratio for the one bay, twelve story frame subjected to ground motions recorded on firm and rock sites

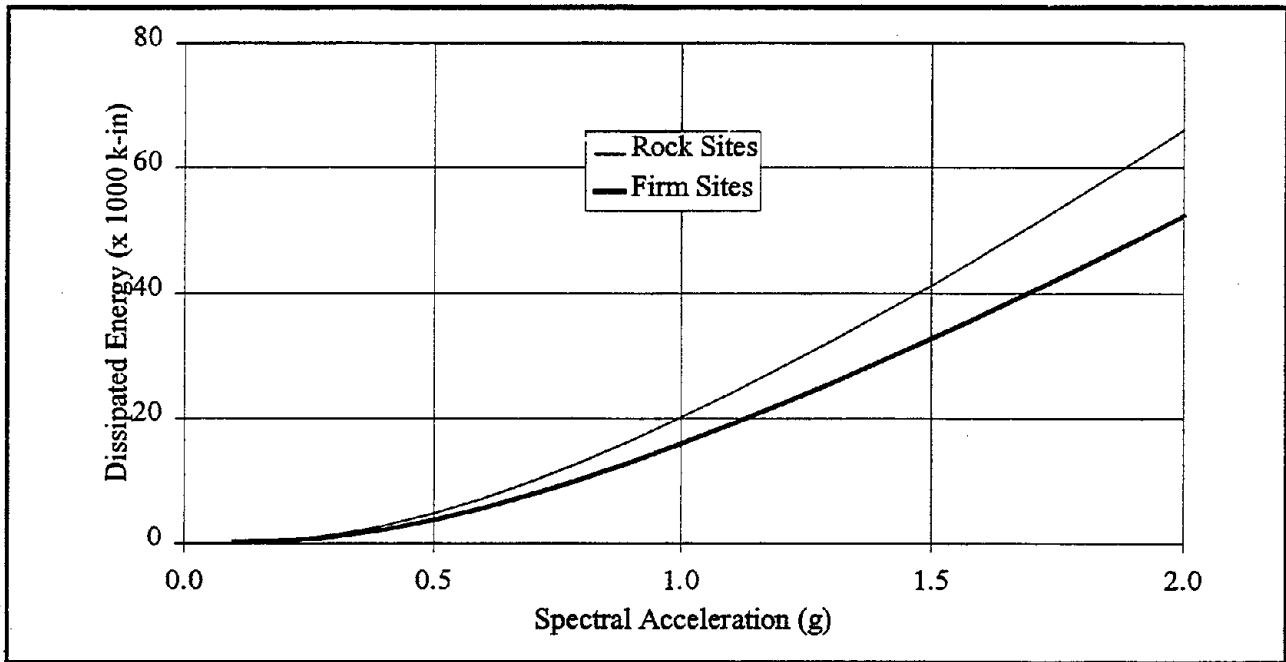


FIGURE 5-38 Comparison of the total dissipated energy for the one bay, twelve story frame subjected to ground motions recorded on firm and rock sites

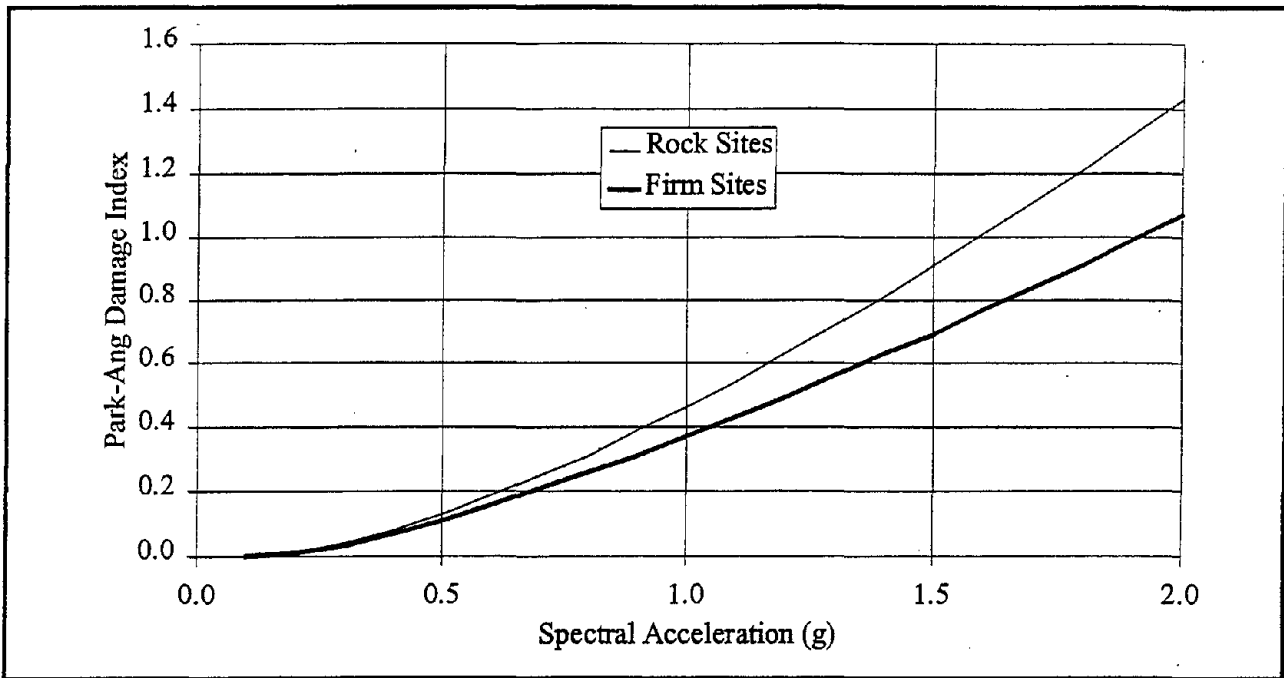


FIGURE 5-39 Comparison of the overall Park-Ang damage index for the one bay, twelve story frame subjected to ground motions recorded on firm and rock sites

5.4 Relationship Between Damage Caused by Deformation and Dissipated Hysteretic Energy

Structural damage is primarily caused by excessive deformation and by the dissipation of hysteretic energy. The Park-Ang damage index is estimated as a linear combination of damage due to deformation and dissipated energy. This section examines the relative values of the two terms of the Park-Ang damage index for the three sample frames when subjected to different levels of ground motion. The comparison is carried out for the typical frames in each structural class: low rise, mid rise, and high rise. Figures 5-40 through 5-42 show the relative contributions of the deformation and the dissipated energy terms to the Park-Ang damage index for the structure. The results presented in these figures are obtained by using the ground motions recorded on firm sites during the six earthquakes discussed earlier. The results from simulated time histories show the same trends except that they have more fluctuations about the values plotted in figures 5-40 through 5-42. Thus, these figures are the mean contributions of the two terms of the damage index. These figures show that the two terms of the damage index contribute almost equally to the damage index.

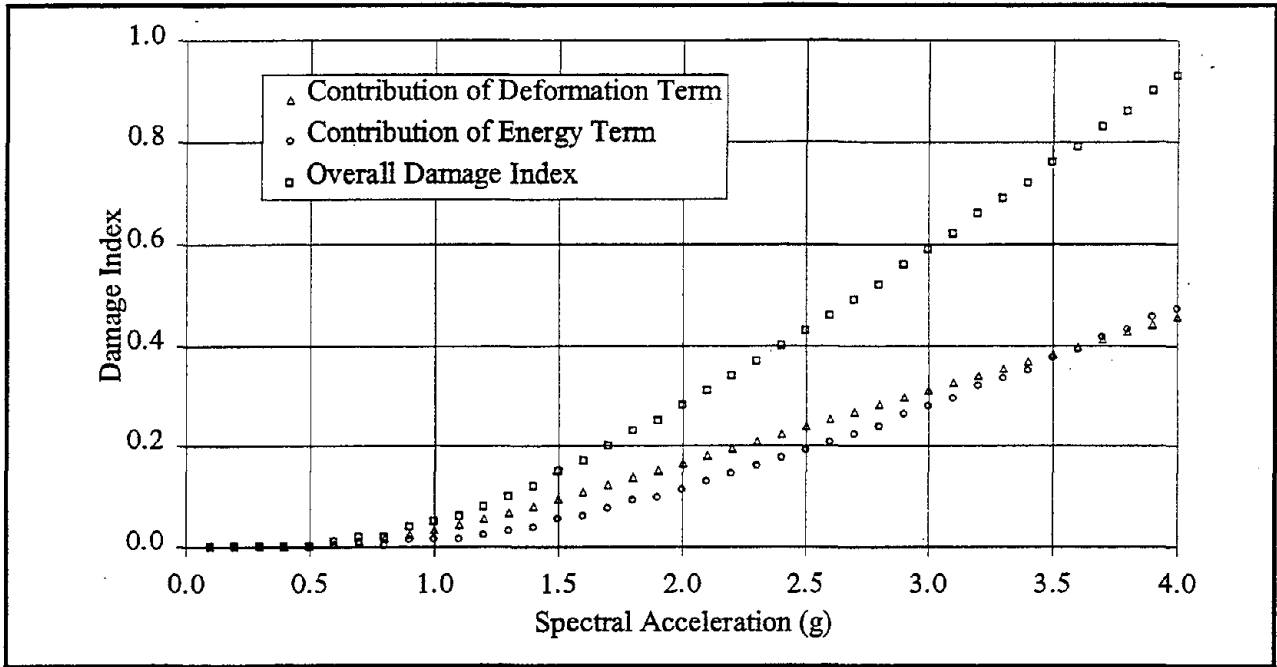


FIGURE 5-40 Relative contributions of the two terms in the Park-Ang damage index for the low rise frame

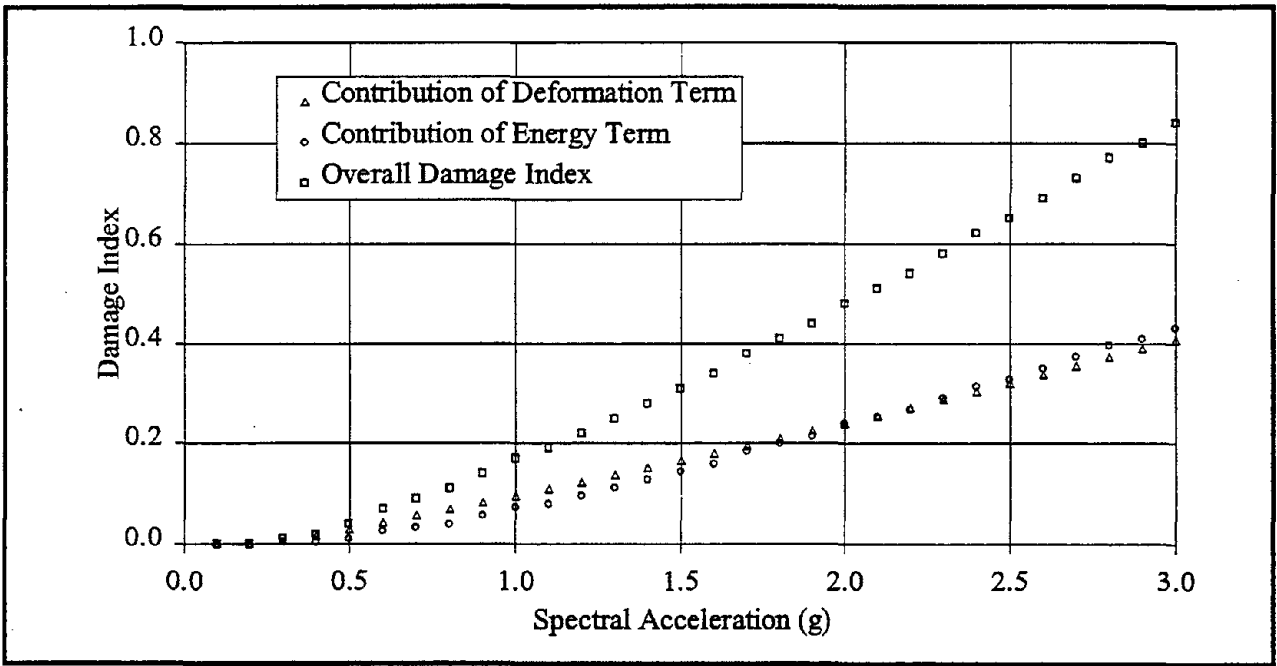


FIGURE 5-41 Relative contributions of the two terms in the Park-Ang damage index for the mid rise frame

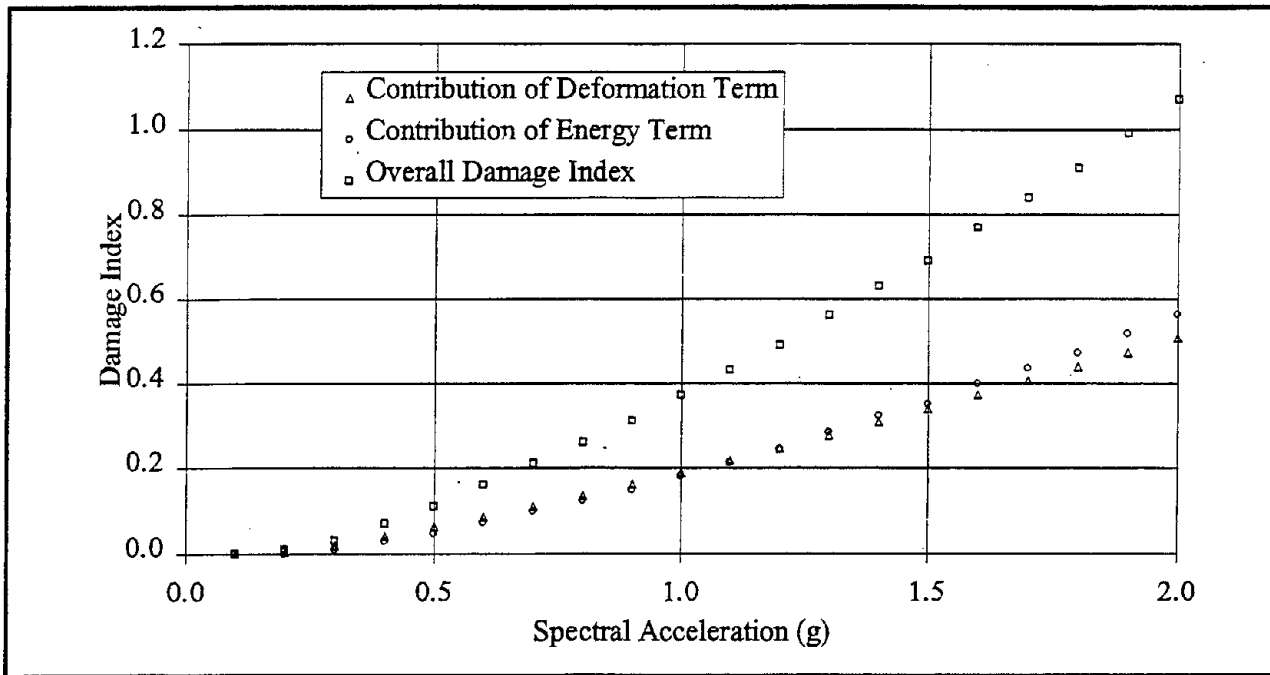


FIGURE 5-42 Relative contributions of the two terms in the Park-Ang damage index for the high rise frame

5.5 Relationship Between Drift Ratios and Park-Ang Damage Index

The drift ratios are often utilized as measures of damage, (e.g., NIBS 1995). Thus, it is worthwhile to examine the correlation between story-drift and the damage index. For the purpose of estimating this correlation, the simulated results are used for the low rise, the mid rise, and the high rise frames. The results for the overall drift ratios and the overall Park-Ang damage index are presented in figures 5-43 through 5-45. A correlation coefficient greater than 99% is observed in all cases.

Figures 5-43 through 5-45 show that the Park-Ang damage index is zero up to a certain level of drift. This observation can be explained by the fact that for very small values of the drift ratio, there is no yielding in the members and so no plastic deformation or hysteretic energy dissipation in the members. Another interesting observation from these figures is that the drift ratios corresponding to the Park-Ang damage index of unity are 0.054, 0.050, and about 0.042 for the low rise, the mid rise, and the high rise frames, respectively. This decrease in the drift ratios is partly explained by the fact that higher modes become significant in the response of the

structure as the structure height is increased. Due to the participation of the higher modes, the overall drift ratio decreases.

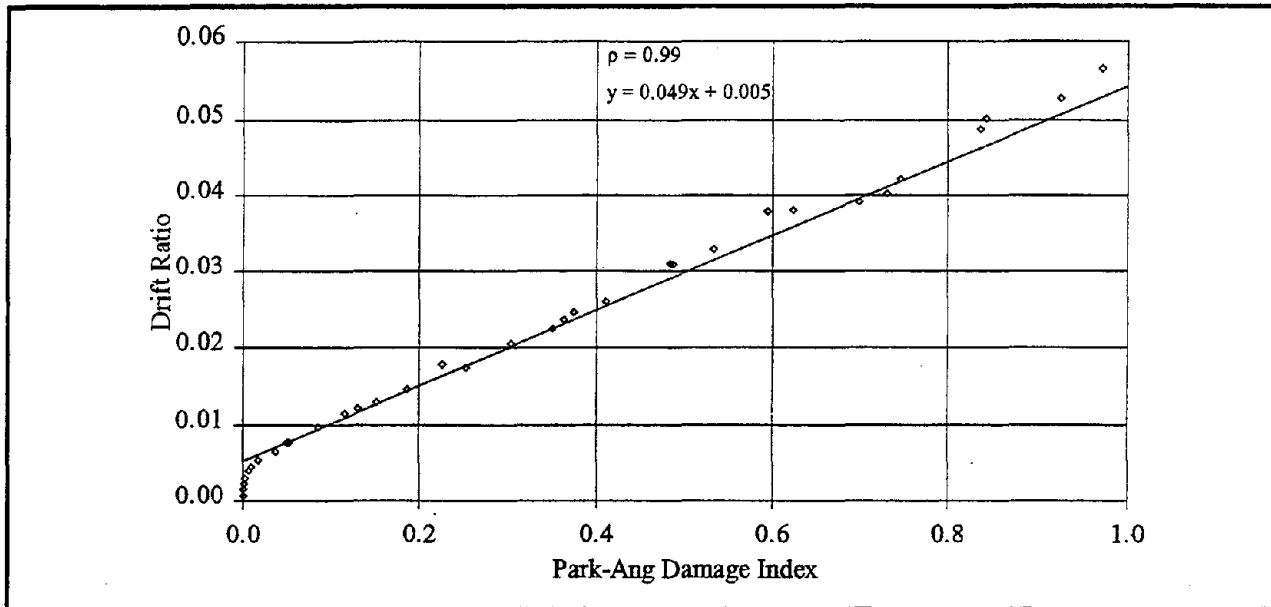


FIGURE 5-43 Relationship between the overall drift ratio and the overall Park-Ang damage index for the low rise frame

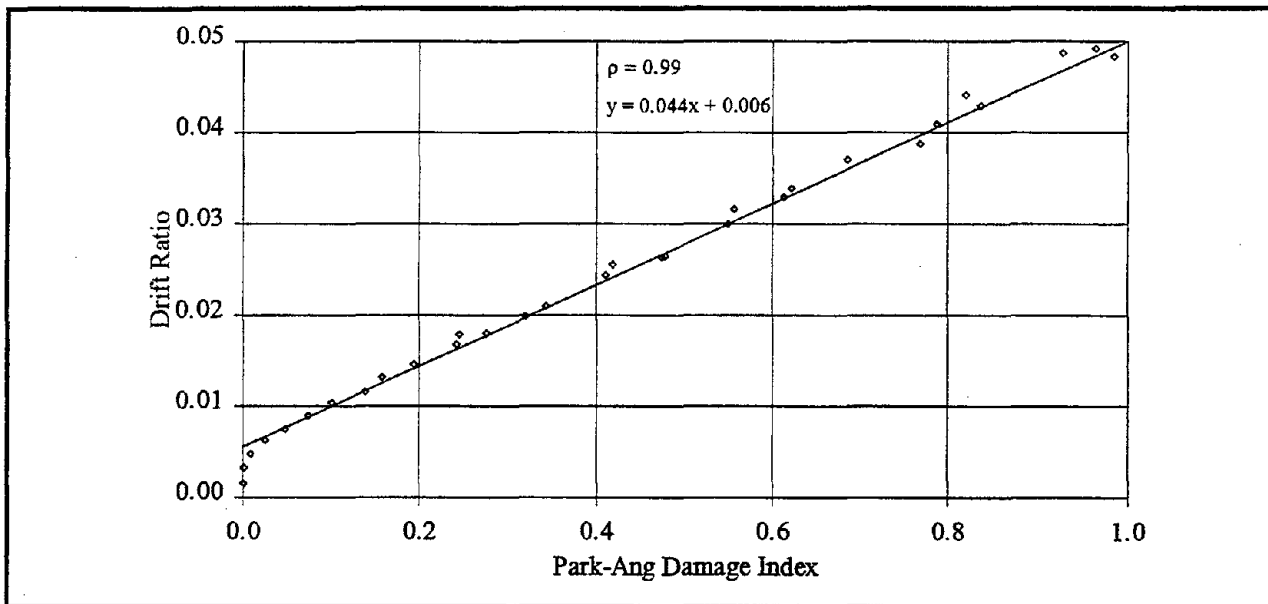


FIGURE 5-44 Relationship between the overall drift ratio and the overall Park-Ang damage index for the mid rise frame

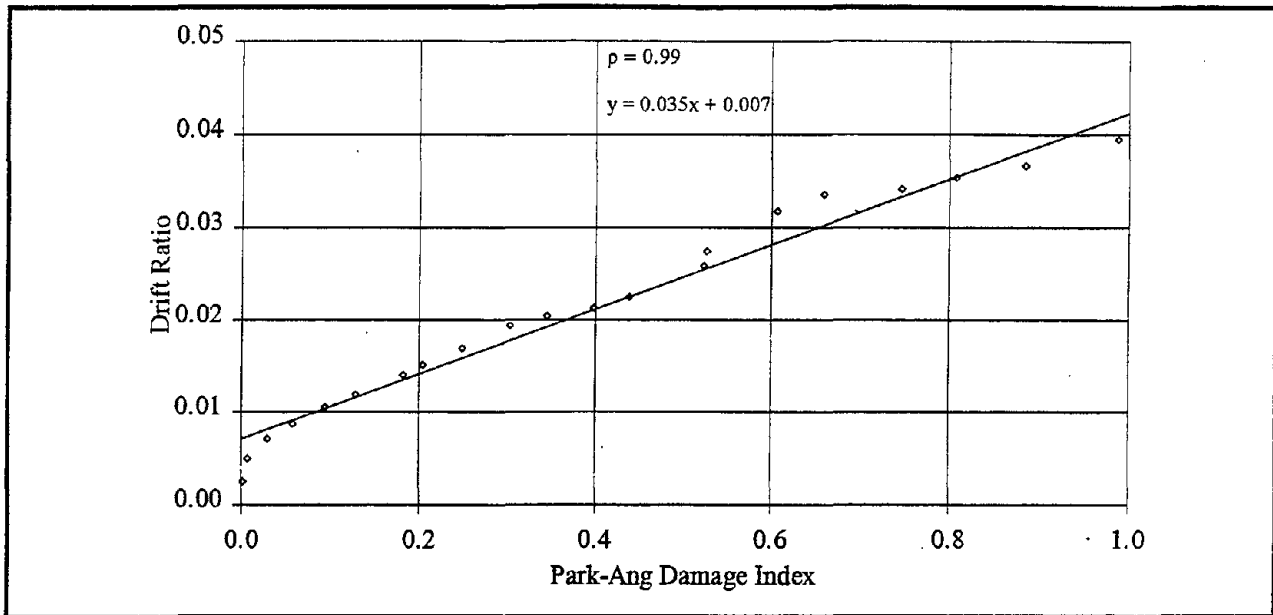


FIGURE 5-45 Relationship between the overall drift ratio and the overall Park-Ang damage index for the high rise frame

5.6 Summary

This section presented fragility curves and DPMs for special moment resisting reinforced concrete frames. In contrast to previous approaches for developing fragility curves and DPMs, the method used does not rely on heuristics or on empirical data. Details on the application of the methodology to reinforced concrete frames were presented in Section 4.

Sensitivity analyses were carried out to study the influence of the different structural attributes on the nonlinear dynamic analysis of structures. These sensitivity analyses were carried out to study how structural damage is affected by the different structural attributes because a sample building is taken to represent a building class in the development of fragility curves. The structural attributes included in the sensitivity studies were the number of bays in a structure, the second-order effects, and the site conditions. The influence of the number of bays is not found to be very significant on structural response. However, the second-order effects has a significant influence on structural response at larger ground motion levels. The second-order effects are found to lead to instability of the structure at higher ground motion levels. Rock ground motions

were also found to influence the response of the structures compared to the firm site ground motions, the most significant influence being observed for the low rise frame.

This section developed sample fragility curves for the three classes of reinforced concrete frames using a sample frame in each class. The uncertainty due to representation of a structural class by a sample frame is discussed in Section 6. The uncertainty associated with representation of a structural class by a single frame can be reduced by taking more sample buildings in each structural class. A better way to reduce this uncertainty is to incorporate observed damage data in the development of fragility curves. The procedure to update the fragility curves on the basis of observed damage data is demonstrated in Section 6 by using damage data from the Northridge earthquake.

SECTION 6

BAYESIAN UPDATING OF MOTION-DAMAGE RELATIONSHIPS

This section presents the concepts of randomness and uncertainty associated with the motion-damage relationships. Bayesian analysis is used to update the fragility curves which were presented in Section 5 based on the data about buildings damaged during the Northridge earthquake. The uncertainty in these relationships is incorporated in terms of the confidence bounds on the fragility curves for each damage state.

6.1 Randomness and Uncertainty

Randomness is associated with the inherent variability in the characteristics of a structure and the environmental demands that are imposed on that structure. The randomness in these structural characteristics includes the variability associated with the material properties of the structure. The randomness in demands includes the variability in the loads to which a structure is subjected. Whereas randomness is intrinsic in nature and beyond our control, uncertainty is extrinsic and to some extent reducible. Geyskens et al. (1993) suggest the following three sources of uncertainty:

- errors of ignorance and simplifications,
- measurement errors, and
- statistical errors.

Errors of ignorance and simplifications arise due to incomplete knowledge and understanding of the physical phenomena governing the behavior of the system. Often, the behavior of the system is idealized and represented by means of simplified functional forms. Measurement errors arise due to the use of uncertain measured values to determine the model parameters. Statistical errors are introduced in the estimation of the model parameters due to the use of a finite data-set to determine the model parameters. Since the model is uncertain, an infinite data-set is required to determine the model parameters exactly. Further information on randomness and uncertainty is provided by Der Kiureghian (1989).

6.2 Randomness and Uncertainty in the Response of RC Frames

The randomness and uncertainty in the response of reinforced concrete (RC) structures has been treated by Park et al. (1984) in terms of their damage index. They examined the variability in the response of RC structures as a result of the randomness and uncertainty associated with the structural parameters and modeling errors. The structural parameters they considered which are relevant to this study include the stiffness and strength, damping, and mass. The variabilities associated with these parameters are summarized in the following sub-sections.

6.2.1 Stiffness and Strength

The variability associated with the stiffness and strength of the different members of a structure consists of the inherent material randomness and the modeling error. The randomness associated with the material properties has already been considered in Section 4.3.2. However, modeling error needs to be incorporated here. Based on test data from 260 RC components, Park et al. (1984) suggest the modeling error, expressed as a coefficient of variation, is equal to 0.29 for stiffness and 0.12 for the yield strength.

The variability in the stiffness and strength of RC members depends on the uncertainty in the member dimensions and the placement of reinforcing steel. Mirza and MacGregor (1979) recommend normal distributions for modeling the geometric properties of in-situ RC beams. For concrete cover to main reinforcement in beams, they recommend a normal distribution with the lower tail truncated at one stirrup or tie diameter. The overall depth of members is important in determining the stiffnesses of the members. The effective depth of the main reinforcement is very important from the point of view of strength. The position of the bottom bars in beams is affected by the height of chairs used to support the bars, and the overall depth of the beams. The factors that lead to the variability in the position of the top bars include the variations in the height of the bottom bars, uncertainty in the vertical dimensions of the stirrups, and conflict with other top bars at beam intersections. The location of vertical bars in columns is influenced by the variabilities in the dimensions of ties and forms, alignment of the columns from floor to

floor, and accuracy in the alignment of the reinforcement cage within the forms. The parameters for the normal distributions for the geometrical properties of beams and columns are shown in tables 6-I and 6-II, respectively.

TABLE 6-I Estimated distributions for geometrical properties of beams (from Mirza and Macgregor, 1979)

Dimension	Nominal range (in.)	Mean deviation from nominal (in.)	Standard deviation (in.)
Width	11-12	+3/32	3/16
Overall depth	18-27	-1/8	1/4
Cover to top reinforcement	1-1/2	+1/8	5/8
Cover to bottom reinforcement	3/4-1	+1/16	7/16

TABLE 6-II Estimated distributions for column dimensions (from Mirza and Macgregor, 1979)

Dimension	Nominal range (in.)	Mean deviation from nominal (in.)	Standard deviation (in.)
Lateral dimension of rectangular columns	11-30	+1/16	1/4
Diameter of circular columns	11-13	0	3/16

6.2.2 Damping

Park et al. (1984) suggest that the viscous damping in structures arises due to the energy dissipation of the soil and the friction between the foundation and the soil. They suggest a coefficient of variation of 0.52 in the damping coefficient of the fundamental mode of RC structures. They also suggest that the large scatter in the damping coefficient is due to the variability of the soil properties.

6.2.3 Mass

Park et al. (1984) suggest a coefficient of variation of 0.12 in the mass of buildings.

6.2.4 Uncertainty in the Park-Ang Damage Index

Park et al. (1984) conclude that the total variability associated with the mean of their damage index has a coefficient of variation equal to 0.6, whereas the inherent randomness in their damage index has a coefficient of variation of 0.5. Thus for this study, the coefficient of variation due to uncertainty in structural response is equal to $\sqrt{0.6^2 - 0.5^2} = 0.33$. Kennedy et al. (1980) provide the uncertainties associated with the capacity of and the demand on reactor buildings. They suggest that the logarithmic standard deviation due to uncertainty associated with the overall response of a reactor building may be taken as 0.38. This value of uncertainty is close to the value adopted in this study. Furthermore, the uncertainty due to representation of a structural class by a sample frame is assumed to be included in the value of uncertainty used in this study. Such uncertainty can be reduced by taking more sample buildings in each structural class. In addition, this uncertainty can be reduced by incorporating observed damage data in the development of the fragility curves.

6.3 Bayesian Updating

The overview of Bayesian analysis was presented in Section 3.5. The Bayesian updating of the Park-Ang damage index, at specified levels of ground motion in terms of spectral acceleration, is presented in this section. The simulations performed in Section 5 provide the prior distributions of the Park-Ang damage index. The observed damage data from the Northridge earthquake provide the likelihood functions required in equation 3.49.

It was shown in Section 5 that a lognormal distribution can be used to represent the probability distribution of the Park-Ang damage index at a specified level of ground motion. The variation of the coefficient of variation of the Park-Ang damage index are plotted in figures 6-1 through 6.3 for the three sample frames of Section 5 subjected to simulated ground motion. The coefficient of variation is larger for the low rise frame in figure 6-1 compared to the case when the frame is subjected to recorded ground motions scaled to different levels of spectral accelerations. These figures show that the coefficient of variation for the three frames converges to constant values at larger levels of ground motion. Therefore, in this study, only the median of the underlying lognormal process is treated as a random variable.

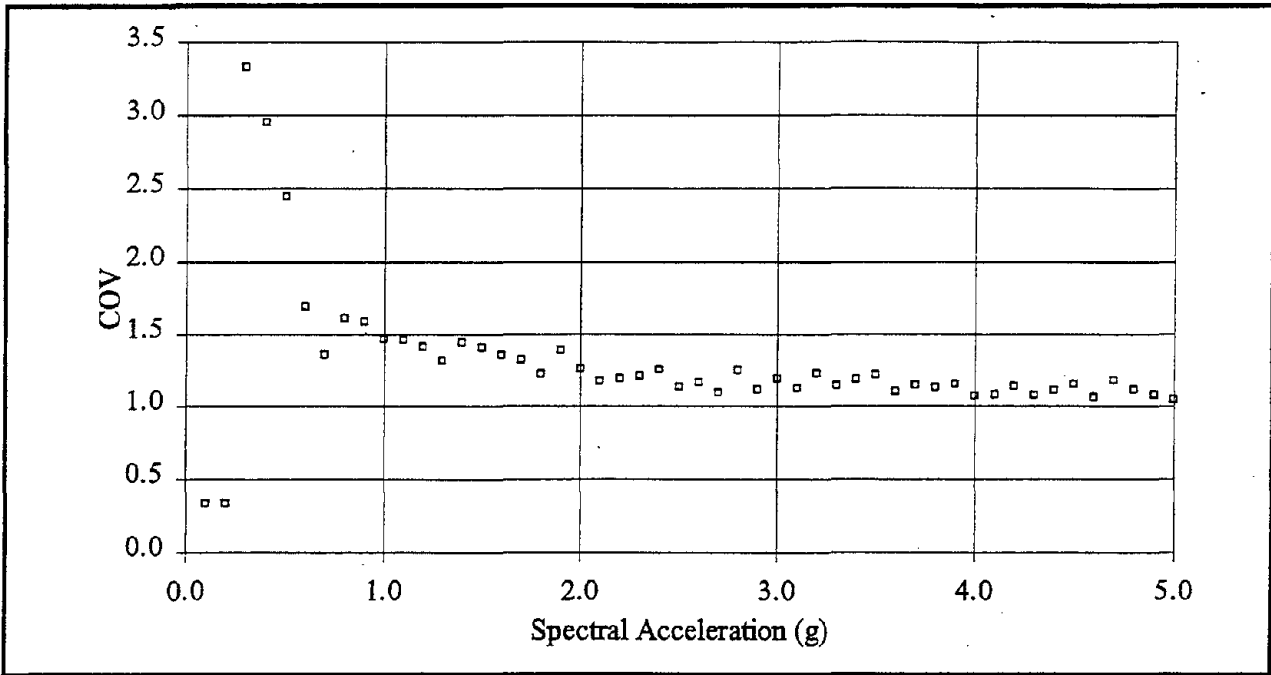


FIGURE 6-1 Variability of the coefficient of variation of the Park-Ang damage index for the low rise frame at different levels of ground motion

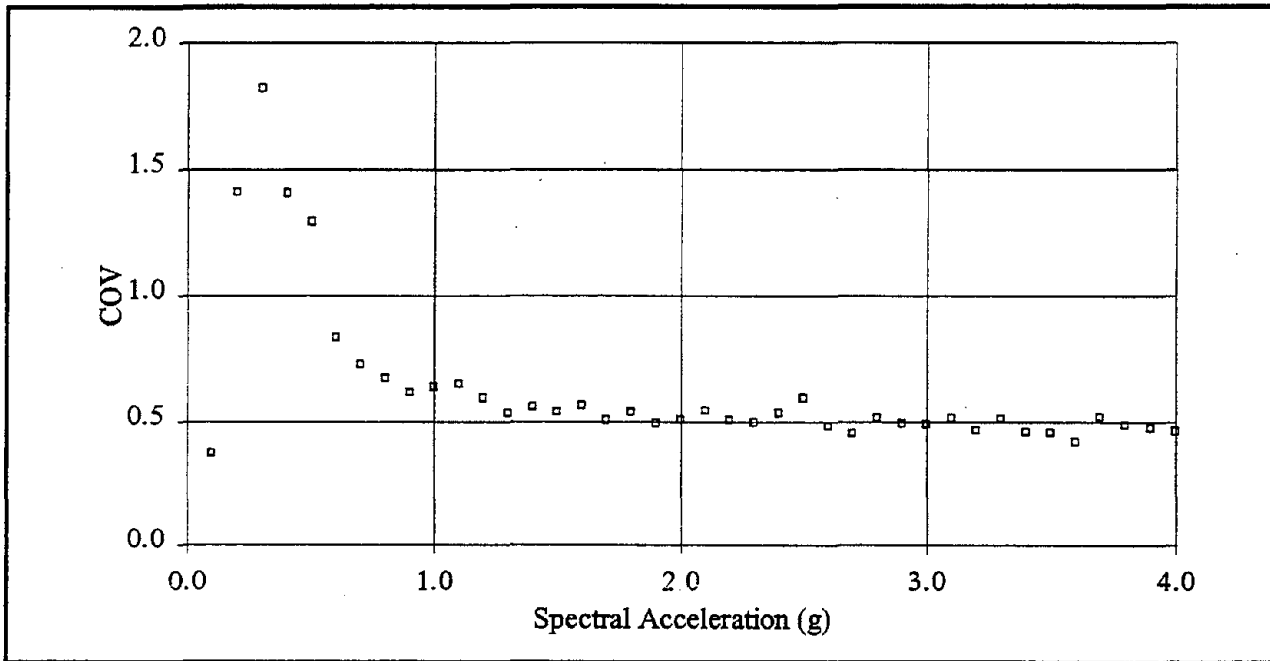


FIGURE 6-2 Variability of the coefficient of variation of the Park-Ang damage index for the mid rise frame at different levels of ground motion

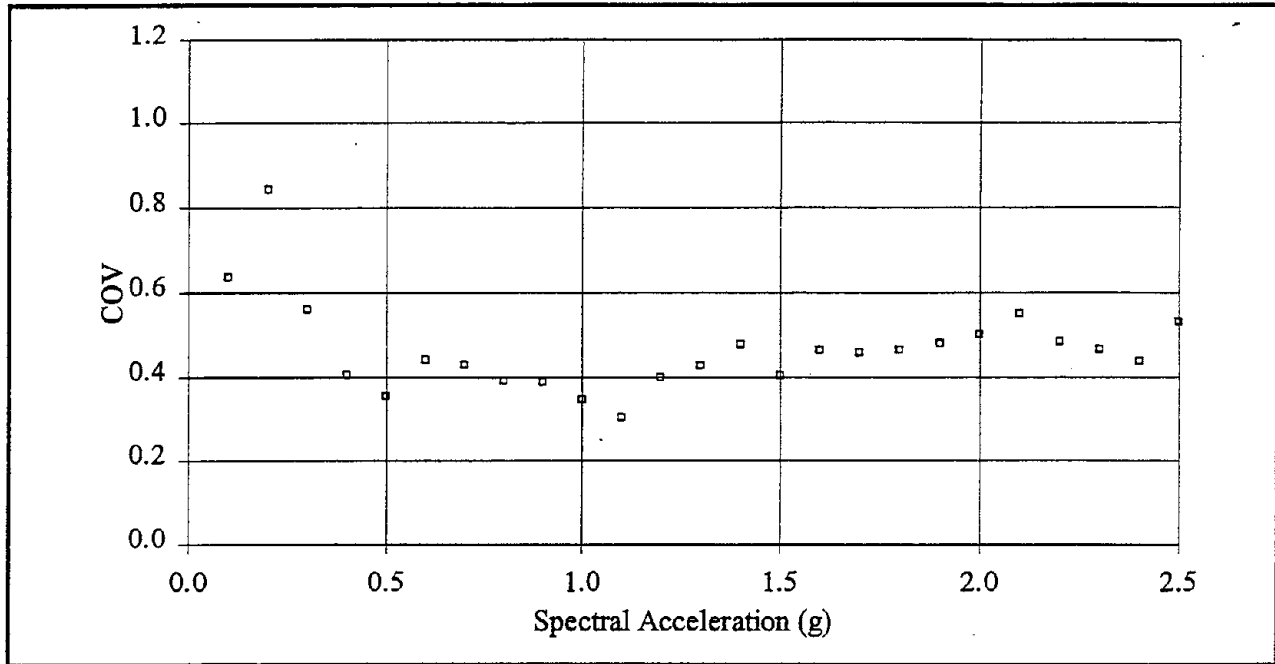


FIGURE 6-3 Variability of the coefficient of variation of the Park-Ang damage index for the high rise frame at different levels of ground motion

6.3.1 Estimation of the Likelihood Functions

A lognormal random variable can be treated as a normal variable by using the natural logarithm of the lognormal variable. Therefore, the estimation of the likelihood functions is presented for the case where the sampling is from a normal process. The likelihood of obtaining observations, $x_1, \dots, x_i, \dots, x_n$, is given as:

$$L(X|\mu, \sigma) = \frac{1}{(2\pi\sigma^2)^{\frac{n}{2}}} e^{-\left[\frac{1}{2\sigma^2} \sum (x_i - \mu)^2\right]} \quad (6.1)$$

where:

X = vector of observations, $x_1, \dots, x_i, \dots, x_n$,

μ = mean of the underlying normal process, and

σ = standard deviation of the underlying normal process.

As mentioned earlier, the variance of the underlying process is assumed to be known. Then, the likelihood function is proportional to:

$$L(X|\mu, \sigma) \propto e^{-\left[\frac{1}{2\sigma^2}n(m-\mu)^2\right]} \quad (6.2)$$

where:

$$m = \frac{1}{n} \sum x_i = \text{mean of the observations.}$$

6.3.2 Posterior Distribution of the Mean

As mentioned in Section 3.5, considerable mathematical simplification can be achieved if conjugate distributions are used. When the likelihood function is given by equation 6.2, a normal distribution is the conjugate distribution for the underlying random variable, the mean, μ , in this study (Raiffa and Schlaifer, 1964). Therefore, if the prior distribution of μ is a normal distribution, the posterior distribution will also be a normal distribution. The prior distribution of μ is given by the following equation:

$$f'_M(\mu) = \frac{1}{\sqrt{2\pi\sigma'^2}} e^{-\left[\frac{(\mu-m')^2}{2\sigma'^2}\right]} \quad (6.3)$$

where:

$f'_M(\mu)$ = prior distribution of μ ,

m' = prior mean of μ , and

σ'^2 = prior variance of μ .

Multiplying the prior distribution by the likelihood function of equation 6.2 and normalizing the product, the posterior distribution of μ is a normal density function given by:

$$f''_{M|X}(\mu|x) = \frac{1}{\sqrt{2\pi\sigma''^2}} e^{-\left[\frac{(\mu-m'')^2}{2\sigma''^2}\right]} \quad (6.4)$$

where the posterior mean and variance are expressed by the following two equations, respectively,

$$m'' = \frac{(1/\sigma'^2)m' + (n/\sigma^2)m}{(1/\sigma'^2) + (n/\sigma^2)} \quad (6.5)$$

and

$$\frac{1}{\sigma''^2} = \frac{1}{\sigma'^2} + \frac{n}{\sigma^2} \quad (6.6)$$

where:

$$\frac{\sigma^2}{n} = \text{variance of the sample mean.}$$

Equation 6.6 shows that as the variance of the prior distribution decreases, the prior information is given more weight in the determination of the posterior distribution.

6.4 Bayesian Analysis With Damage Data from Northridge

The Northridge earthquake is currently the best documented disaster in the history of the United States (OES, 1995). This earthquake caused about 20 billion dollars of direct losses in terms of damage to buildings, utilities, and lifelines. The focus of this study is the structural damage to buildings, specifically to RC frame buildings.

6.4.1 Building Inventory

In order to estimate the likelihood functions in the Bayesian analysis, a description of the inventory of RC frames is required. The *Governor's Office of Emergency Services for the State of California* (OES, 1995) provided information about the inventory for RC frame buildings in the city of Los Angeles in an electronic format. From the tax assessor database for the city of Los Angeles, OES inferred that there are a total of about 1240 RC frame buildings, including both residential and non-residential buildings. Figure 6-4 shows the geographical locations of these RC frame buildings in the city of Los Angeles. In addition, the *Governor's Office of Emergency Services for the State of California* also provided data on damage in terms of "tagging" and estimated dollar loss data. Immediately after the earthquake, building inspections were carried out. The building inspectors affixed a color tag on an inspected structure according to the following guidelines (OES, 1995):

- Green Tag: No apparent hazard found, although repairs may be required. Original lateral load capacity not significantly decreased. No restriction on use or occupancy.
- Yellow Tag: Dangerous condition believed to be present. Entry by owner permitted only for emergency purposes and only at own risk. No usage on continuous basis. Entry by public not permitted. Possible major aftershock hazard.
- Red Tag: Extreme hazard, may collapse. Imminent danger of collapse from an aftershock. Unsafe for occupancy or entry, except by authorities.

The distribution of the red- and yellow-tagged RC frame buildings within the city of Los Angeles is shown in figures 6-5 and 6-6, respectively. These figures show 22 red-tagged and 35 yellow-tagged buildings. Although these figures give an idea of the location and extent of damage to RC frame buildings, the extent of damage is only very approximate as the process of judging the safety of a building is subjective. In this study, the extent of damage is inferred from the dollar loss data for the buildings.

The data provided by the *Governor's Office of Emergency Services for the State of California* (OES, 1995) also contained information on the age of construction, and the number of stories in the buildings. As the number of mid rise and high rise RC frame buildings is very small, Bayesian analysis is only presented for low rise frames. Furthermore, as defined by Anagnos et al. (1995), low rise frames constructed after 1976 may be treated as ductile moment resisting frames. Thus, low rise RC frames built after 1976 are used to update the fragility curves presented in Section 5.

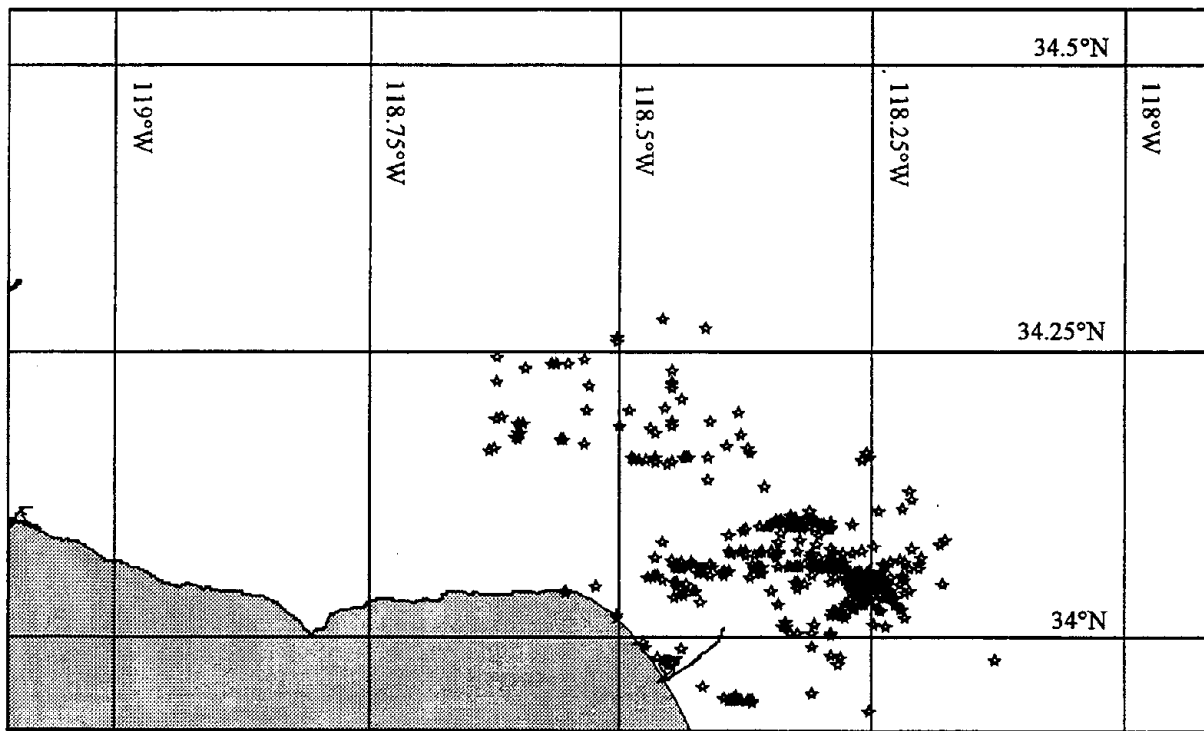


FIGURE 6-4 Geographical location of about 1240 RC frame buildings in the city of Los Angeles

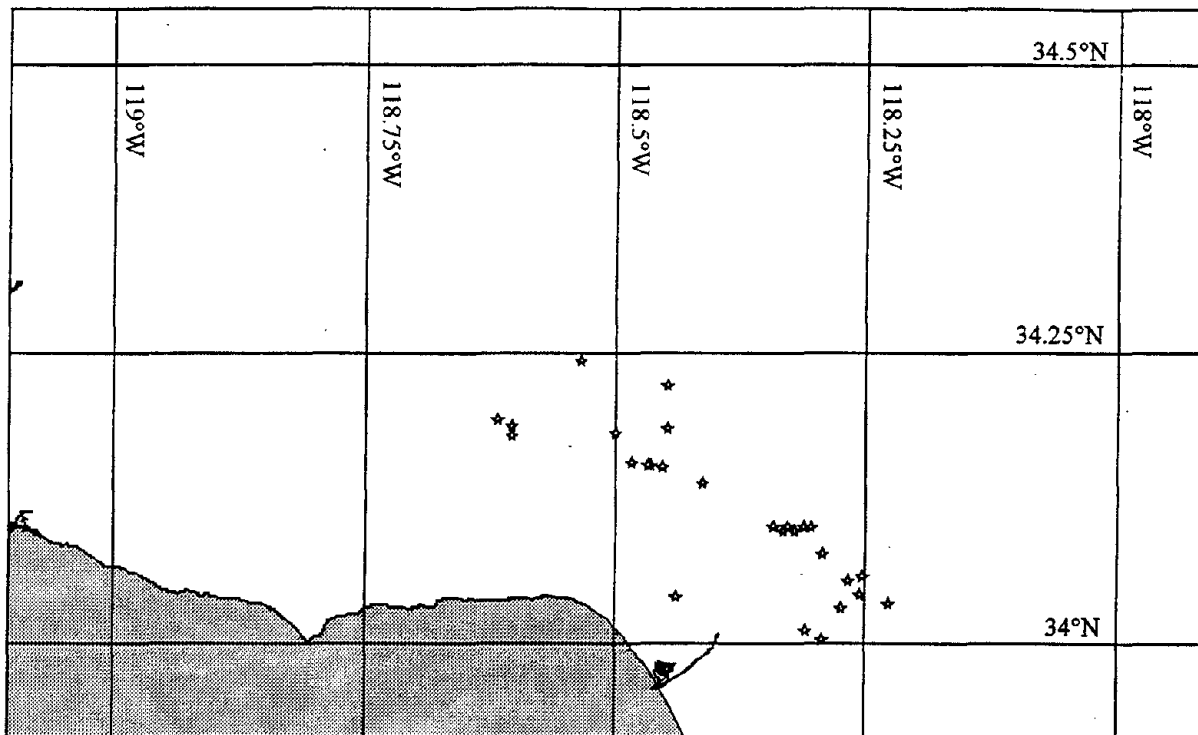


FIGURE 6-5 Geographical location of all 35 yellow-tagged RC frame buildings in the city of Los Angeles

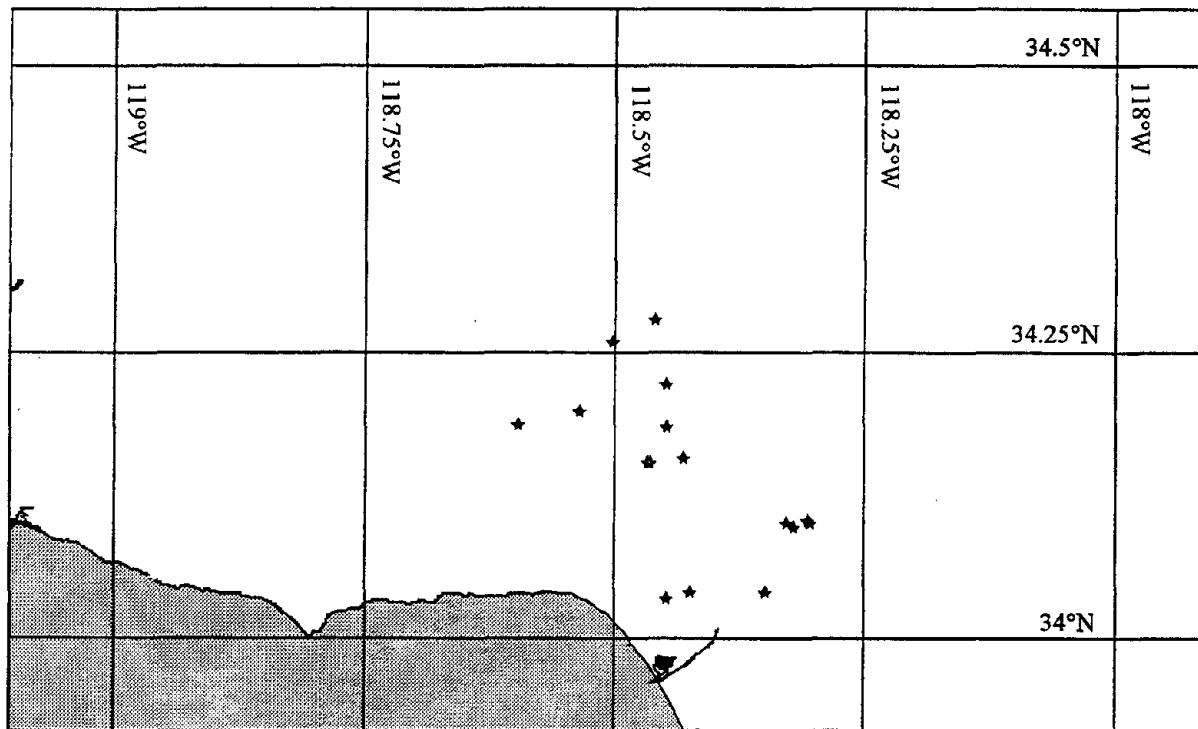


FIGURE 6-6 Geographical location of all 22 red-tagged RC frame buildings in the city of Los Angeles

6.4.2 Posterior Distribution of the Park-Ang Damage Index

In order to evaluate the posterior distribution of the Park-Ang damage index at a specified level of ground motion, one must estimate the level of seismic excitation as well as the corresponding Park-Ang damage index of all the RC frame buildings. The level of seismic excitation is measured in terms of spectral acceleration in the relevant period band. In this study, the site conditions at the building locations is not taken into account in the Bayesian analysis. For the Northridge earthquake, Somerville et al. (1995) developed spectral acceleration contours at five different periods: 0.3, 0.5, 1.0, 2.0 and 3.0 seconds. The spectral acceleration contours for the east-west and the north-south components of ground motion at a period of 0.3 seconds are shown in figures 6-7 and 6-8, respectively. The ground motion levels at the building sites are obtained by overlaying the buildings on the spectral acceleration contours. Figures 3-4 and 4-1 show that for low rise frames, the spectral acceleration at 0.3 seconds may be taken to represent the average value. In fact, the ratio of the dynamic amplification factor at 0.3 seconds to the average value of the dynamic amplification factor in the range of 0.1 - 0.5 seconds is about 0.97. Thus, it is reasonable to assume the average value to be equal to the value of the dynamic amplification factor at 0.3 seconds. For the mid rise frames, the ground motion level may be obtained from the values of spectral acceleration at periods of 0.5 and 1.0 seconds, by assuming a suitable variation of spectral acceleration between these two periods. Similarly, the ground motion level for the high rise frames may be obtained by using the spectral acceleration values at periods of 1.0, 2.0, and 3.0 seconds. Alternatively, as suggested in Section 4.1, spectral velocity contours may be used to arrive at the ground motion level in terms of spectral acceleration for these two classes of frames. However, the ground motion levels for the mid rise and the high rise frames is not explored as the number of buildings belonging to the mid rise and high rise frames is very limited in order to perform the Bayesian analysis. Figures 6-9 and 6-10 respectively present all the low rise, ductile moment resisting RC frames, and the low rise ductile RC frames for which the damage was observed. These figures also present the average spectral acceleration contours used to determine the ground motion level for the frames.

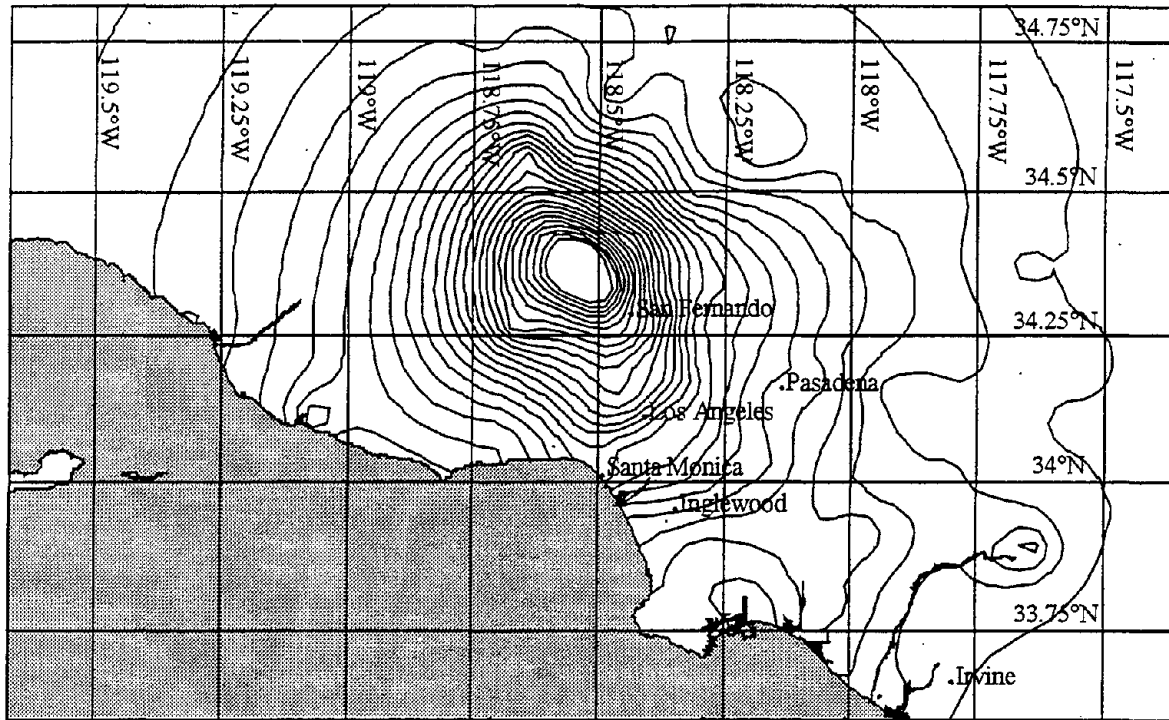


FIGURE 6-7 Spectral acceleration contours from the Northridge earthquake for the east-west component at $T = 0.3$ seconds; the contours are spaced at an interval of $0.05g$ and the value of the innermost contour is $1.4g$

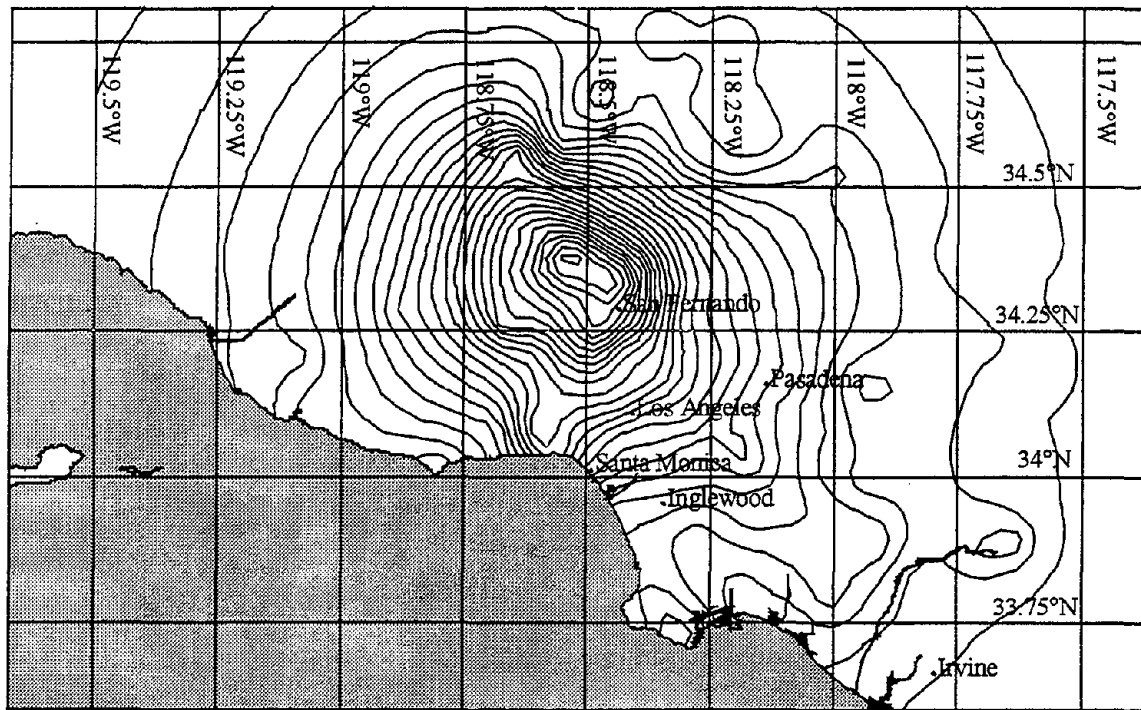


FIGURE 6-8 Spectral acceleration contours from the Northridge earthquake for the north-south component at $T = 0.3$ seconds; the contours are spaced at an interval of $0.05g$ and the value of the innermost contour is $1.4g$

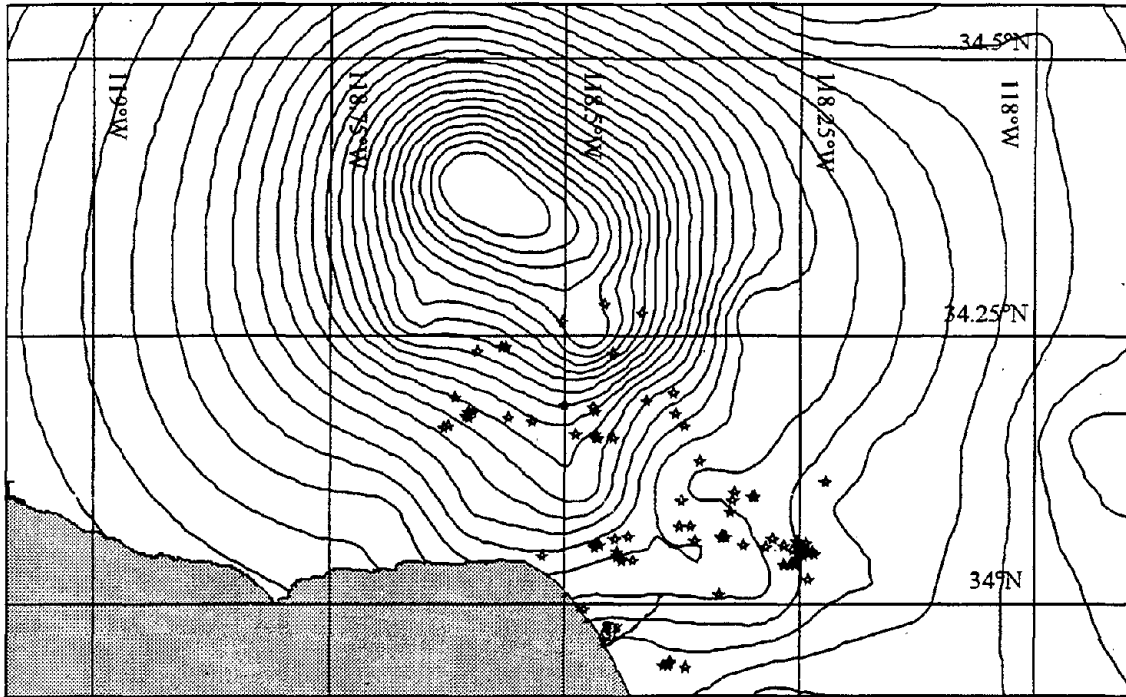


FIGURE 6-9 184 low rise, ductile RC frame buildings and the average spectral acceleration contours from the Northridge earthquake at $T = 0.3$ seconds; the contours are spaced at an interval of 0.05g and the value of the innermost contour is 1.4g

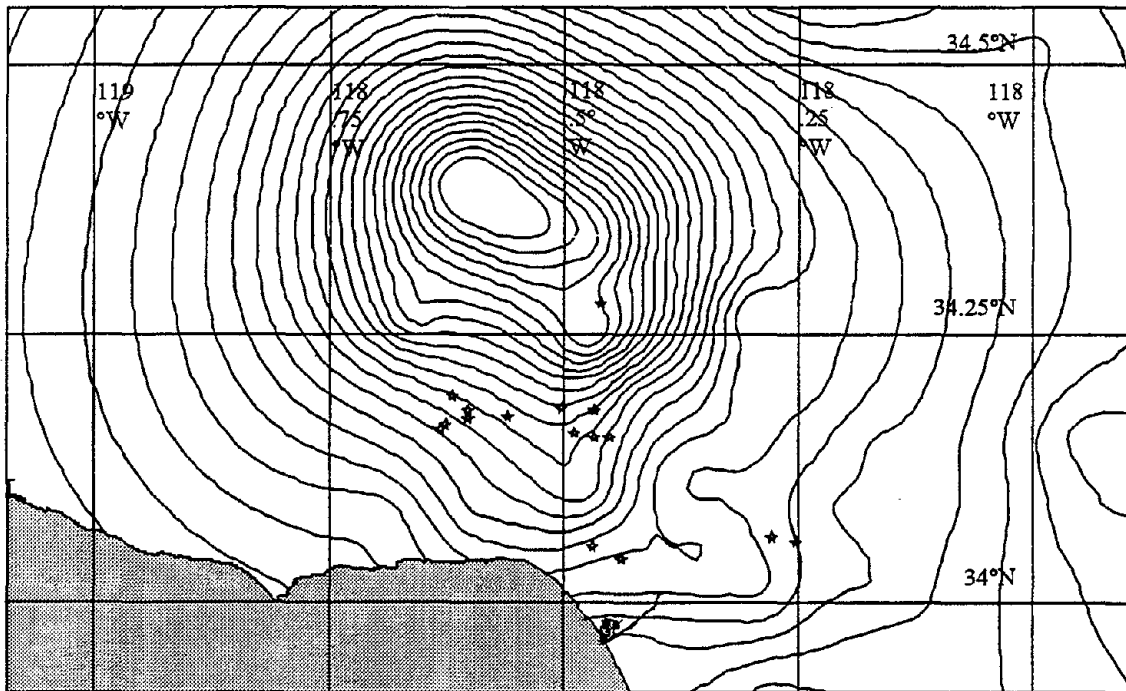


FIGURE 6-10 Seventeen low rise, ductile RC frame buildings for which damage was observed and the average spectral acceleration contours from the Northridge earthquake at $T = 0.3$ seconds; the contours are spaced at an interval of 0.05g and the value of the innermost contour is 1.4g

The extent of damage sustained by the buildings, in terms of the Park-Ang damage index, is determined from the damage factors for these buildings. There are two studies which relate damage factors to damage states. The relationship provided in ATC-13 (1985) is given in table 5-IV. Whitman et al. (1974) proposed another relationship which provides a finer discretization at the lower damage levels when compared to the ATC-13 relationship. Table 6-III provides Whitman et al.'s relationship for the structural damage states:

TABLE 6-III Whitman et al.'s relationship between damage factors and damage states

Damage State	Damage Range (%)
Minor	3.5 - 7.5
Substantial	7.5 - 20
Major	20 - 65
Building Condemned	65 - 100

In this study, the lower bound of the Minor damage state is assumed to have a damage factor of 3.5% as shown in table 6-III. The other damage states are assumed to have the damage factors given in table 5-IV. De Leon and Ang (1993) arrived at a linear relationship between the damage factor and the Park-Ang global damage index for buildings damaged during the Mexico City earthquake. Therefore, in this study, a piecewise linear relationship is assumed between the damage factor and the Park-Ang damage, the relationship being linear for each damage state. Thus, tables 3-I, 5-IV, and 6-III are used to estimate the damage index for each building. The Park-Ang damage index can be expressed by means of the following expression:

$$EDI_i = LDI_i + \left(\frac{DF - LDF_i}{UDF_i - LDF_i} \right) \cdot (UDI_i - LDI_i) \quad (6.7)$$

where:

- i = damage state from the vector {*none, minor, moderate, severe, and collapse*},
- EDI = estimate of the Park-Ang damage index,
- LDI_i = minimum value of the Park-Ang damage index for damage state i as given in table 3-I,
- UDI_i = maximum value of the Park-Ang damage index for damage state i as given in table 3-I,
- DF = damage factor, defined as the ratio of repair to replacement cost, obtained from the OES database,
- LDF_i = minimum value of the damage factor for damage state i , obtained from tables 5-IV or 6-III, and
- UDF_i = maximum value of the damage factor for damage state i , obtained from table 5-IV.

The relationships between the damage factor and the Park-Ang damage index inferred from the relationships between the damage states and the damage factor, proposed by Whitman et al. and ATC-13 are shown in figure 6-11. Figure 6-11 also shows the relationship between the damage factor and the damage index used in this study.

Table 6-IV shows the total number of ductile, low rise RC frame buildings subjected to different levels of ground motion. Although the contours shown in figures 6-7 through 6-10 are at an interval of 0.05g, the ground motion levels for the buildings have been rounded to the nearest 0.1g level in order to account for some uncertainties associated with the geographical location of the buildings as well as the uncertainty in the contours themselves. Furthermore, the fragility curves in Section 5 are obtained from simulations performed for spectral acceleration values at intervals of 0.1g. Thus, the results from Section 5 can be directly used in the Bayesian analysis. Table 6-V lists the buildings for which damage was observed. The spectral acceleration values and the estimated Park-Ang damage indices for these buildings are also listed in table 6-V.

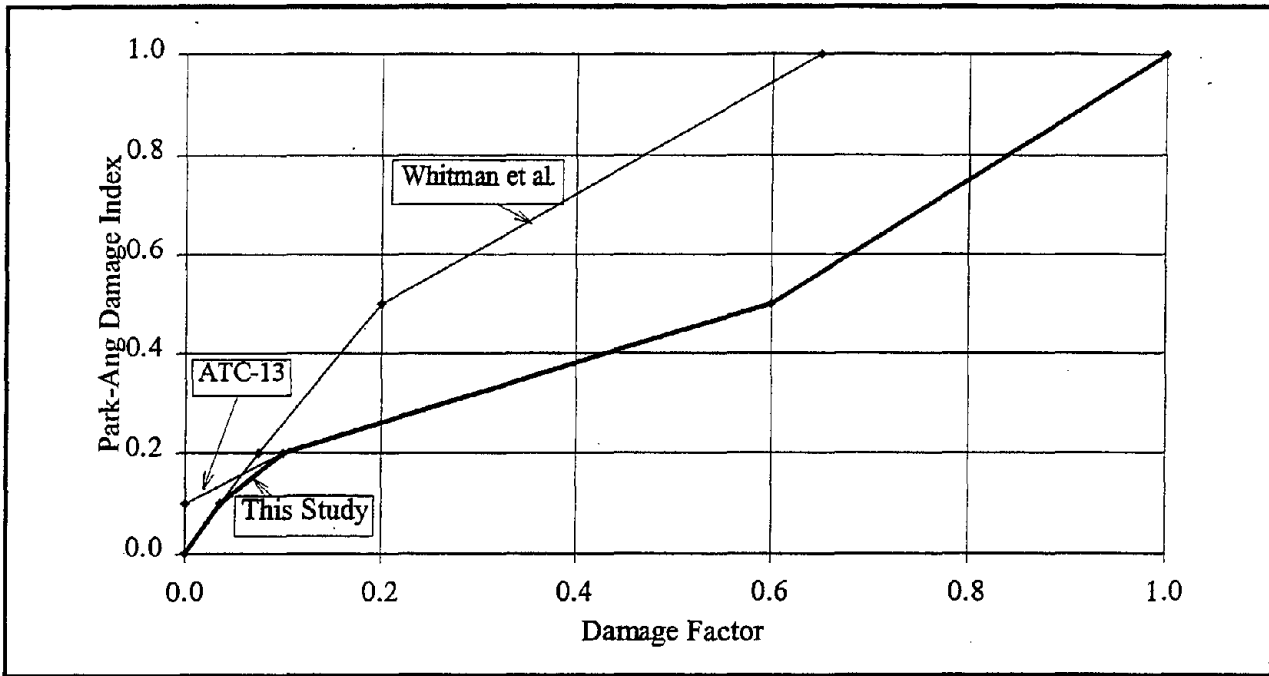


FIGURE 6-11 Mapping of damage factor to the Park-Ang damage index

Table 6-VI provides the logarithmic standard deviation of the Park-Ang damage index at different levels of ground motion. In this study, this logarithmic standard deviation is considered to be a constant. Table 6-VII provides the parameters of the conjugate prior distribution on the logarithmic mean of the Park-Ang damage index. Table 6-VIII lists the sample logarithmic mean of the Park-Ang damage index at different levels of ground motion. This mean was calculated based on the information provided in tables 6-IV and 6-V. The buildings listed in table 6-IV for which damage was not observed were assumed to have a Park-Ang damage index of zero. The mean and standard deviation of the Park-Ang damage index were computed at the different levels of ground motion, and the logarithmic mean of the Park and damage index was calculated by means of the following equation:

$$m_{\ln(DI)} = \ln(m_{DI}) - \frac{1}{2} \sigma_{\ln(DI)}^2 \quad (6.8)$$

where:

$m_{\ln(DI)}$ = logarithmic mean of the observed damage indices,

m_{DI} = sample mean of the observed damage indices,

$$\sigma_{\ln(DI)}^2 = \ln\left(1 + \frac{\sigma_{DI}^2}{m_{DI}^2}\right), \text{ and}$$

σ_{DI}^2 = sample variance of the observed damage indices.

On inspection of the two databases containing the inventory of all the RC frames in Los Angeles City and the damaged frames, respectively, it was found that the second database contains information on several structures at a location, whereas the first database, in most instances, lists only a single structure for the same location. Thus, the second database contains more precise information on the different RC frames at each location. However, this database is inconsistent with the first database. To overcome this inconsistency between the two databases, a single damage factor was estimated for those sites where the second database listed more buildings than the first.

TABLE 6-IV Total number of low rise RC frame buildings at different levels of ground motion

Spectral Acceleration (g)	Number of Buildings
0.4	35
0.5	65
0.6	56
0.7	5
0.8	12
0.9	3
1.0	3
1.1	2
1.2	3

TABLE 6-V Geographical locations, spectral accelerations, and the estimated Park-Ang damage indices for the low rise frames for which damage was observed

Latitude	Longitude	Spectral Acceleration (g)	Park-Ang Damage Index
34.061°N	118.278°W	0.5	0.03
34.057°N	118.252°W	0.5	0.03
34.040°N	118.438°W	0.5	0.03
34.053°N	118.468°W	0.6	0.09
34.163°N	118.631°W	0.7	0.20
34.155°N	118.449°W	0.7	0.13
34.165°N	118.626°W	0.7	0.24
34.154°N	118.465°W	0.8	0.18
34.179°N	118.604°W	0.8	0.07
34.172°N	118.603°W	0.8	0.20
34.157°N	118.488°W	0.8	0.06
34.173°N	118.561°W	0.8	0.20
34.194°N	118.619°W	0.8	0.12
34.179°N	118.466°W	0.8	0.06
34.154°N	118.466°W	0.8	0.25
34.182°N	118.501°W	0.9	0.11
34.280°N	118.459°W	1.2	0.26

TABLE 6-VI Logarithmic standard deviation of the Park-Ang damage index for low rise frames when subjected to different levels of ground motion

Spectral Acceleration	Logarithmic Standard Deviation
0.5	1.394
0.6	1.161
0.7	1.022
0.8	1.131
0.9	1.120
1.0	1.070
1.1	1.069
1.2	1.045

TABLE 6-VII Parameters of the prior distribution of the mean of the logarithm of the Park-Ang damage index for low rise frames when subjected to different levels of ground motion

Spectral Acceleration (g)	Mean	Standard Deviation
0.1	-7.474	0.322
0.2	-7.474	0.322
0.3	-12.281	0.322
0.4	-10.484	0.322
0.5	-8.039	0.322
0.6	-6.115	0.322
0.7	-4.955	0.322
0.8	-4.596	0.322
0.9	-4.249	0.322
1.0	-4.023	0.322
1.1	-3.528	0.322
1.2	-3.153	0.322

Table 6-VIII also provides the parameters of the posterior distribution on the logarithmic mean of the Park-Ang damage index. The posterior parameters are calculated by using equations 6.5 and 6.6. The posterior parameters are only presented for six levels of ground motion for which observed damage data were available. These posterior parameters are used to obtain the probabilities of the different damage states. Figure 6-12 presents the probabilities of the damage states at these six levels of ground motion, along with the probabilities of the damage states at other levels of ground motion presented in Section 5. The fitted curves in figure 6-12 are the same as those shown in figure 5-4. Thus, figure 6-12 shows that the probabilities based on the posterior distributions of the damage index are consistent with those presented in Section 5.

Since the posterior probabilities agree quite well with the fragility curves of figure 5-4, the fragility curves are not revised in figure 6-12. For cases where large differences may be observed, posterior fragility curves should be obtained by fitting curves through the posterior probabilities of the different damage states.

TABLE 6-VIII Parameters of the posterior distribution of the mean of the logarithm of the Park-Ang damage index for low rise frames at different levels of ground motion

Spectral Acceleration (g)	Sample Mean	Posterior Mean	Posterior Standard Deviation
0.5	-8.176	-8.153	0.133
0.6	-8.504	-8.150	0.124
0.7	-2.502	-3.976	0.249
0.8	-2.688	-3.358	0.191
0.9	-4.020	-4.172	0.262
1.2	-3.072	-3.118	0.242

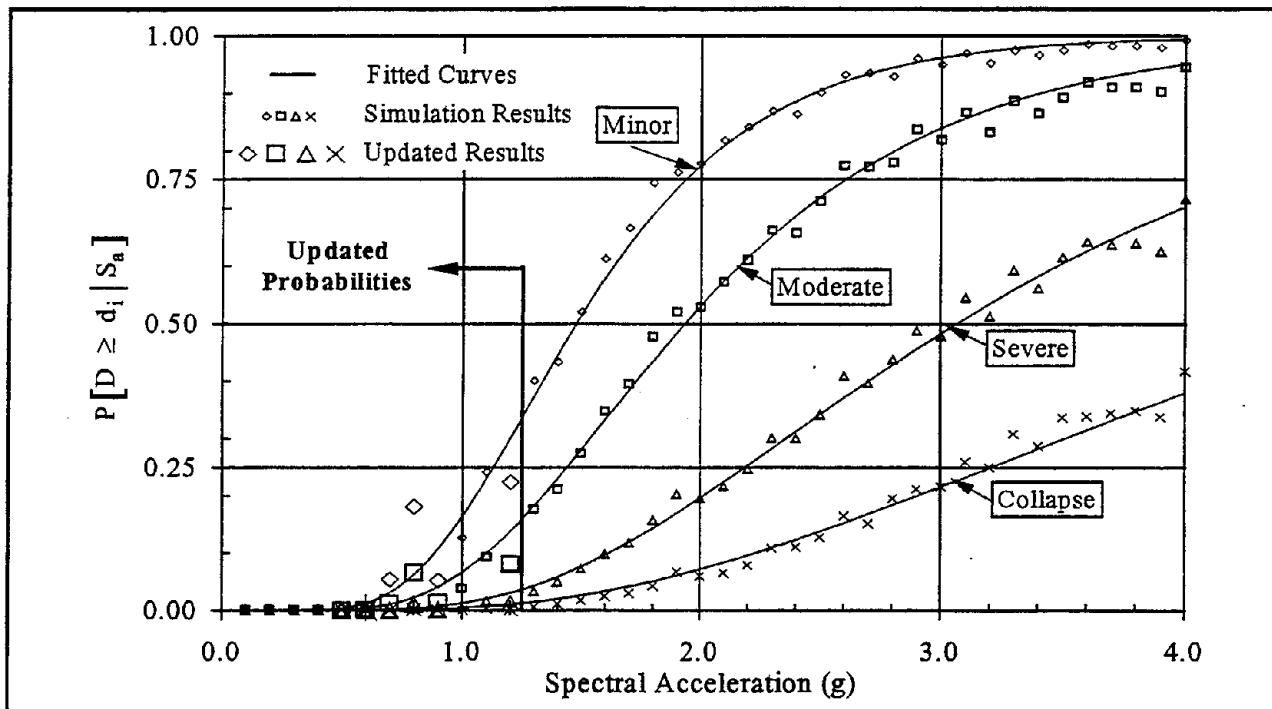


FIGURE 6-12 Updated fragility curves for low rise frames

6.5 Confidence Bounds on the Fragility Curves

The fragility curves for the three classes of frames presented in Section 5 were based on the maximum likelihood value of the median of the Park-Ang damage index at different levels of ground motion. However, there is an uncertainty associated with the median damage index as presented in Section 6.2.4. This uncertainty is taken into account by establishing confidence bounds on the fragility curves. The Bayesian analysis is used to update the median as well as the uncertainty on the median at different levels of ground motion. The Bayesian technique was applied to low rise frames at six levels of ground motion, the results of which are presented in table 6-VIII.

The uncertainty on the median of the Park-Ang damage index is used to establish the 90% confidence bounds on the fragility curves for the different damage states. The median is assumed to have a coefficient of variation of 0.33. A lognormal distribution on the median is used to establish the 5% and the 95% fractiles. These fractiles are then used to form the 90% bounds. Figures 6-1 through 6-3 show that the coefficient of variation of the damage index is almost constant. Therefore, the same logarithmic standard deviation of the Park-Ang damage index as obtained from the simulations is used to establish the bounding fragility curves. For low rise frames, the updated logarithmic standard deviation is used to establish the bounds. Figures 6-13 through 6-18 show the maximum likelihood and the bounding fragility curves for the three classes of frames. The 90% confidence bounds on the fragility curves are obtained by arbitrarily fitting lognormal distribution functions to the discrete results, similar to the way fragility curves were obtained in Section 5. The median and the logarithmic standard deviation, β , of these lognormal curves are presented in tables 6-IX through 6-XI. The maximum likelihood fragility curves are referred to as the median fragility curves in figures 6-13 through 6-18 and in tables 6-IX through 6-XI.

TABLE 6-IX Median and logarithmic standard deviations of the median and the bounding fragility curves for low rise frames

Damage State	5% Bounds		Median Curves		95% Bounds	
	Median	β	Median	β	Median	β
Minor	1.17g	0.40	1.48g	0.40	1.82g	0.45
Moderate	1.55g	0.40	1.93g	0.44	2.48g	0.50
Severe	2.34g	0.50	3.07g	0.50	4.22g	0.55
Collapse	3.35g	0.52	4.81g	0.60	6.69g	0.60

TABLE 6-X Median and logarithmic standard deviations of the median and the bounding fragility curves for mid rise frames

Damage State	5% Bounds		Median Curves		95% Bounds	
	Median	β	Median	β	Median	β
Minor	0.61g	0.32	0.78g	0.30	1.06g	0.35
Moderate	0.86g	0.32	1.11g	0.32	1.58g	0.35
Severe	1.45g	0.37	2.08g	0.35	3.00g	0.37
Collapse	2.34g	0.36	3.46g	0.37	6.05g	0.45

TABLE 6-XI Median and logarithmic standard deviations of the median and the bounding fragility curves for high rise frames

Damage State	5% Bounds		Median Curves		95% Bounds	
	Median	β	Median	β	Median	β
Minor	0.43g	0.20	0.54g	0.25	0.73g	0.25
Moderate	0.62g	0.21	0.79g	0.26	1.15g	0.28
Severe	1.07g	0.25	1.50g	0.30	2.14g	0.32
Collapse	1.67g	0.32	2.39g	0.30	3.49g	0.35

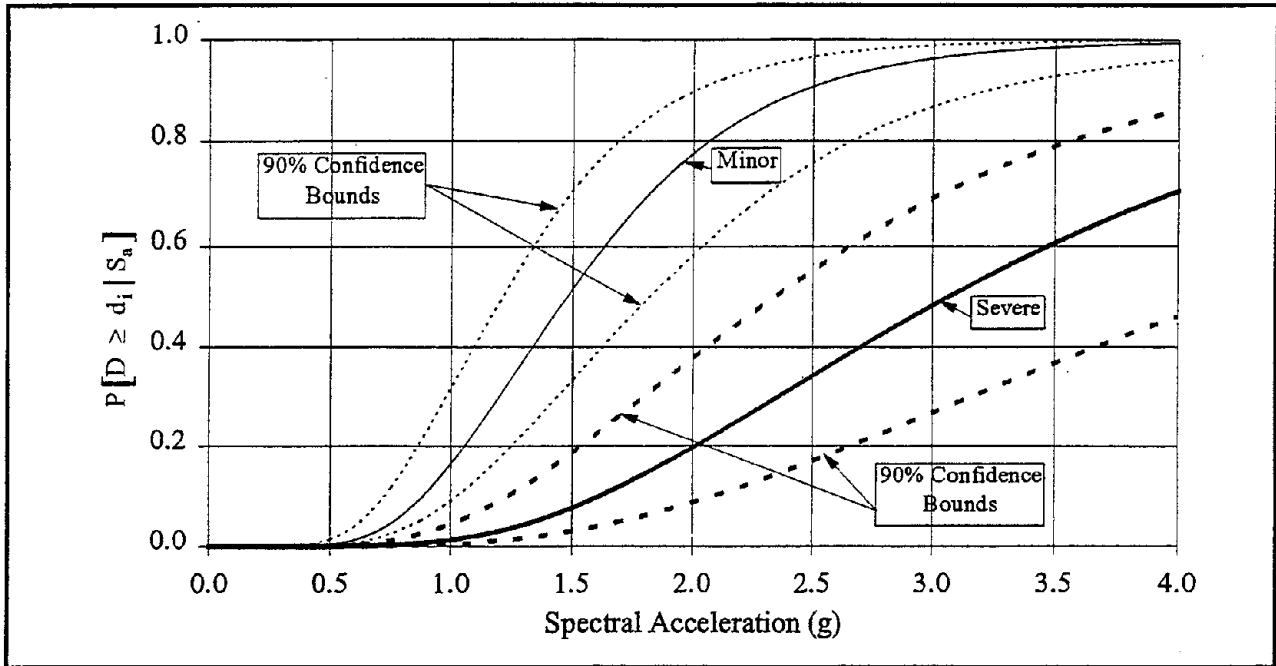


FIGURE 6-13 90% confidence bounds and the median fragility curves for *Minor* and *Severe* damage states for low rise frames

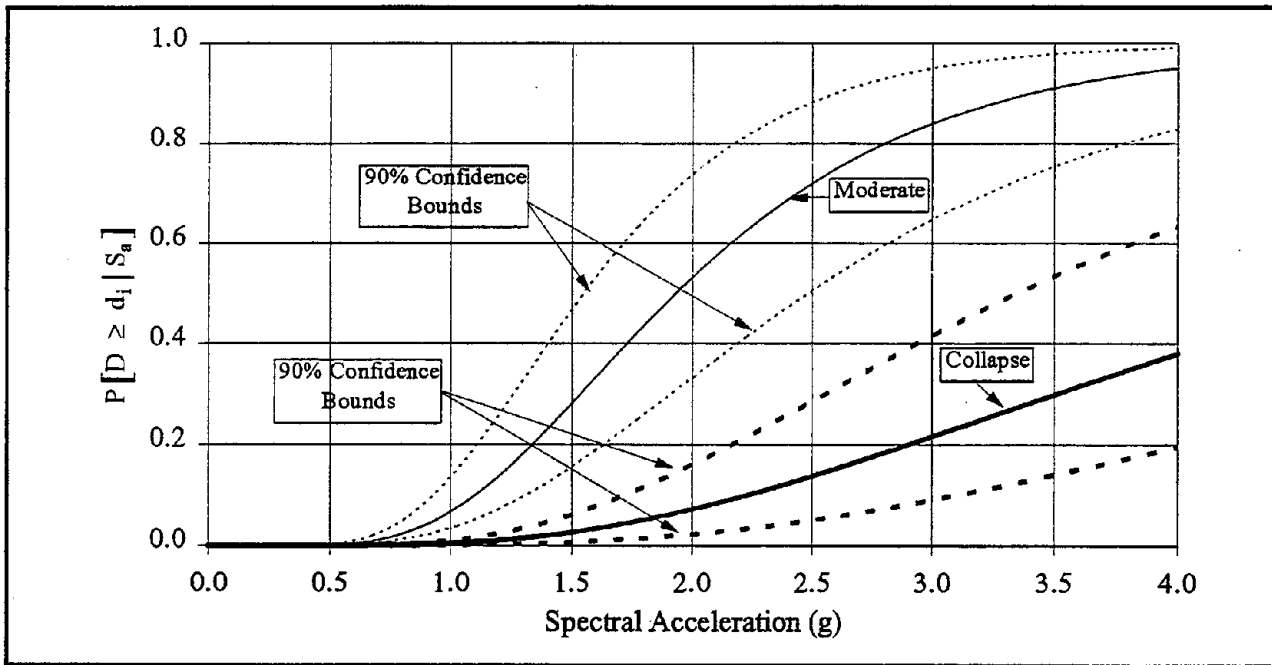


FIGURE 6-14 90% confidence bounds and the median fragility curves for *Moderate* and *Collapse* damage states for low rise frames

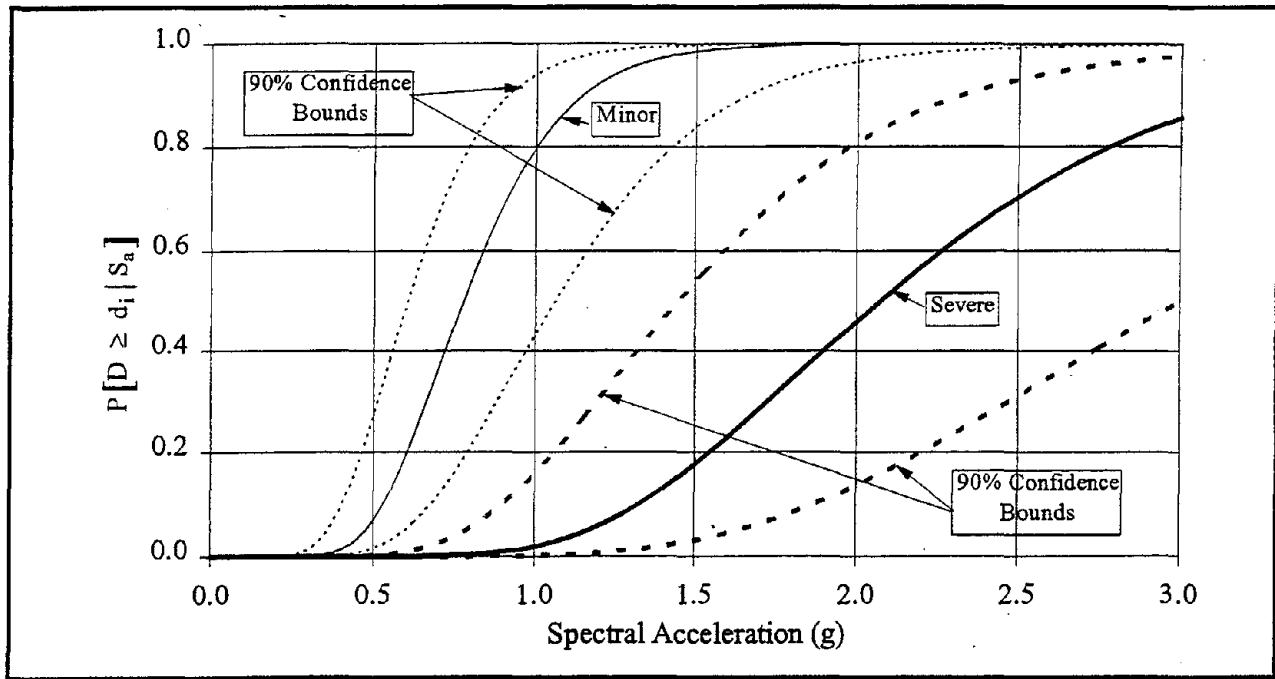


FIGURE 6-15 90% confidence bounds and the median fragility curves for *Minor* and *Severe* damage states for mid rise frames

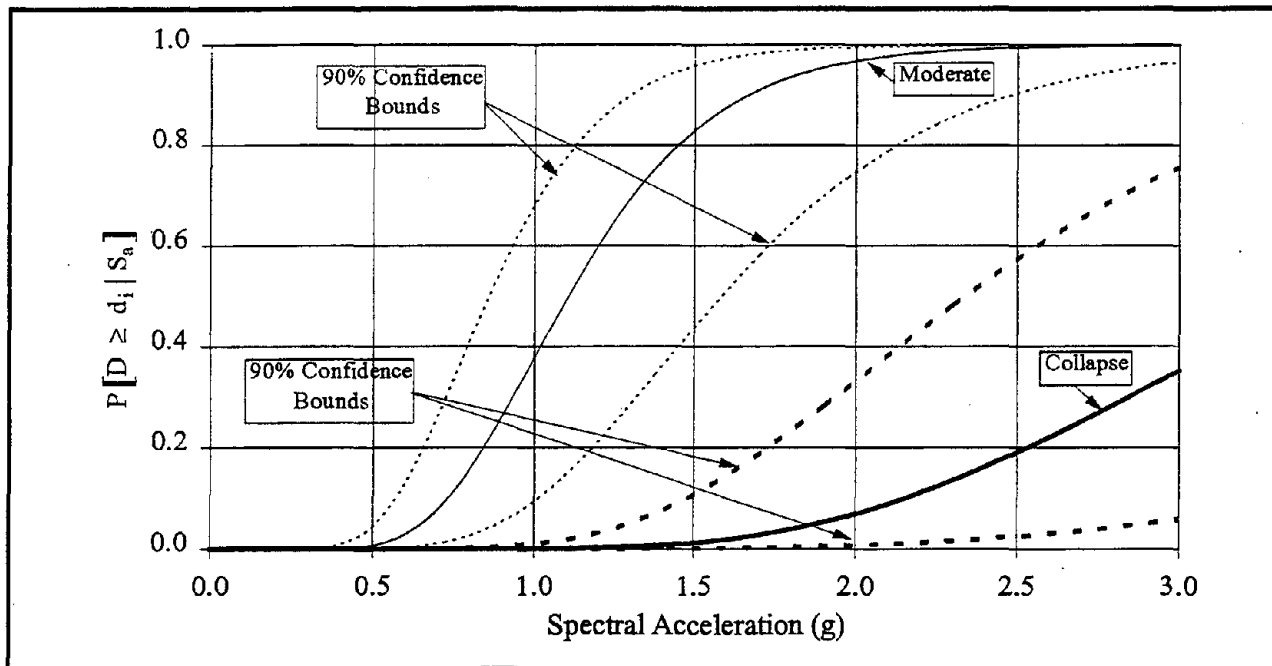


FIGURE 6-16 90% confidence bounds and the median fragility curves for *Moderate* and *Collapse* damage states for mid rise frames

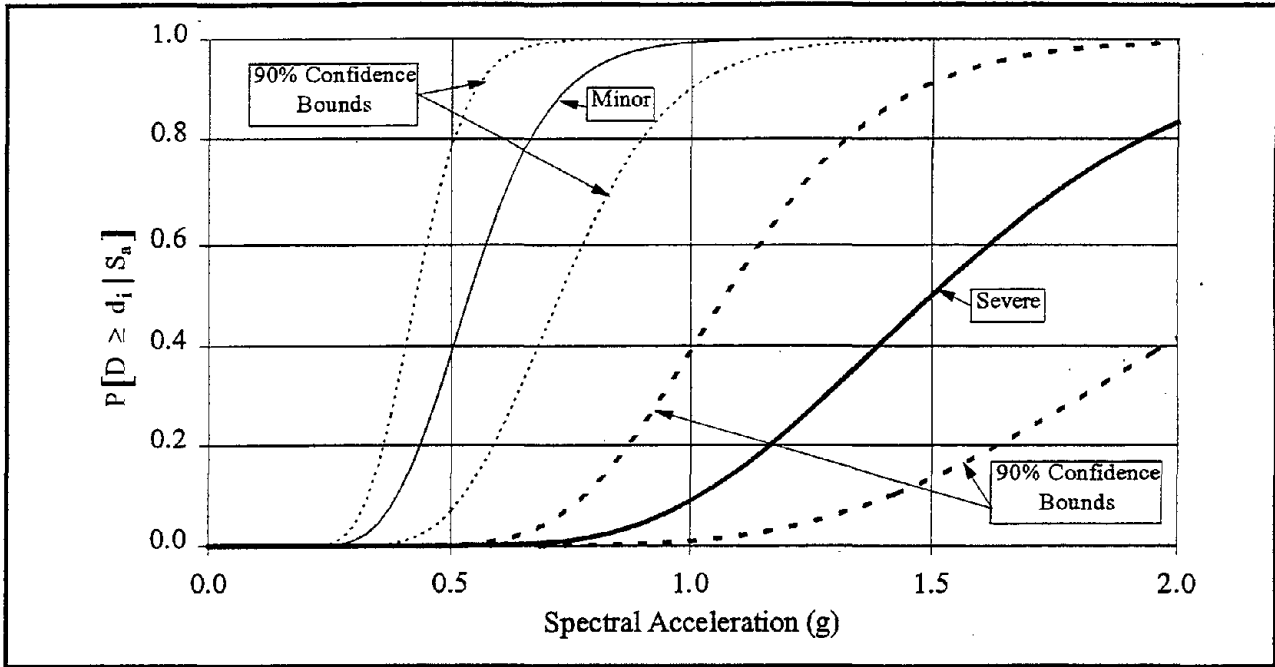


FIGURE 6-17 90% confidence bounds and the median fragility curves for *Minor* and *Severe* damage states for high rise frames

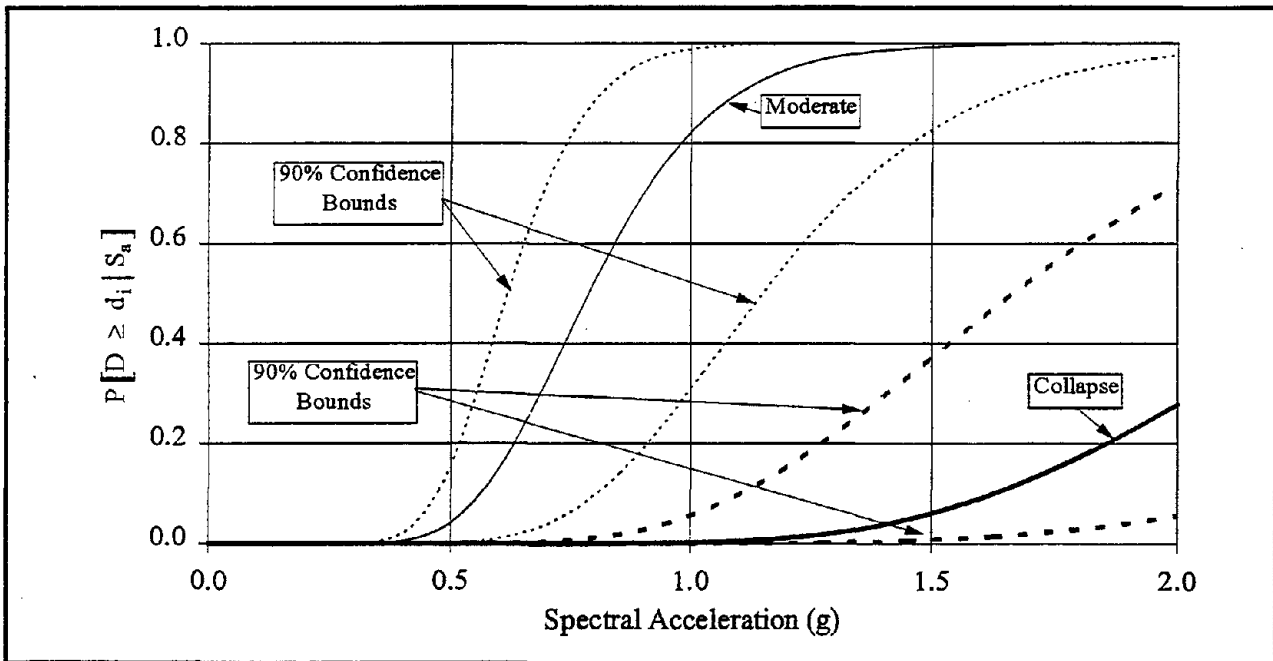


FIGURE 6-18 90% confidence bounds and the median fragility curves for *Moderate* and *Collapse* damage states for high rise frames

6.6 Summary

The first part of this section presented the concepts of randomness and uncertainty as applied to the response of RC frames. The randomness and uncertainty associated with the parameters of RC frames were discussed. In contrast to Section 5 which only considered randomness in ground motion and structural parameters in arriving at the fragility curves, this section incorporated uncertainty in the fragility curves.

The application of the Bayesian analysis to motion-damage relationships was also presented in this section. In this study, only the median of the Park-Ang damage index was considered as a random variable, the logarithmic standard deviation being assumed to be a constant. It is possible to extend the technique presented in this section to include the case where both the median and the logarithmic standard deviation are assumed as random variables. The basic approach will remain the same.

The Bayesian technique was then illustrated for low rise RC frames in Los Angeles City subjected to ground shaking during the Northridge earthquake. Due to insufficient amount of data for the mid rise and the high rise frames, the application of the technique was not attempted for these two classes of frames. For low rise frames, the analytical fragility curves presented in Section 5 provide the best estimates of the updated probabilities.

The uncertainty in the median Park-Ang damage index is used to establish the confidence bounds on the fragility curves. For low rise frames, the uncertainty obtained after Bayesian analysis is used to establish the confidence bounds at those levels of ground motion at which Bayesian analysis is performed.

SECTION 7

CONCLUSIONS AND FUTURE WORK

This research presented a general method for developing relationships between earthquake ground motion and damage. The motion-damage relationships were presented as fragility curves and damage probability matrices (DPMs). Only structural damage was considered in this study.

7.1 Conclusions

This study proposed a general method for developing fragility curves and DPMs. The following are the main characteristics of this methodology.

- Unlike previous approaches, this methodology uses a systematic approach for developing motion-damage relationships and does not rely either on heuristics or on empirical damage data.
- The method utilizes several critical ground motion characteristics and reflects the nonlinear behavior of the structure when subjected to earthquake ground motions.
- Structural damage at different ground motion levels is evaluated using the Monte Carlo simulation approach.
- The Latin hypercube technique is used to increase the efficiency of the Monte Carlo simulation.
- The methodology is applicable to a wide range of structural classes. In this study, the methodology is demonstrated for reinforced concrete (RC) frames.
- The Bayesian technique is presented that will enable periodic updating of fragilities as damage data become available from future earthquake events.

The major components of the proposed methodology consist of (a) characterization of the potential ground motions, (b) characterization of the nonlinear response of the structure when subjected to extreme dynamic loads, (c) application of the methodology to RC frames, (d) sensitivity study for different structural attributes, and (e) Bayesian technique to update the

motion-damage relationships. The conclusions for each of these components are presented below.

Ground Motion Characterization

The methodology developed in this research can be used with any ground motion parameter. However, root mean square (RMS) acceleration and spectral acceleration, S_a , for a specified structural period range are used to develop the methodology. The following conclusions are drawn regarding the ground motion characterization for fragility formulation.

- A correlation coefficient of about 0.7 was observed between the Trifunac and Brady strong motion duration and RMS acceleration.
- Appropriate period bands were defined for the computation of average spectral acceleration to characterize ground motion for RC frames. These period bands are 0.1-0.5 seconds for low rise frames, 0.5-0.9 seconds for mid rise frames, and 0.9-2.5 seconds for high rise frames. These period bands are consistent with the behavior of frames within the three structural classes.
- A poor correlation was observed between the Trifunac and Brady strong motion duration and the average spectral acceleration in the three period bands corresponding to the three classes of RC frames. Therefore, a lognormal distribution of strong motion duration, independent of spectral acceleration, with a median of 10.92 seconds and a logarithmic standard deviation of 0.33 was obtained.
- Conditional distributions for the average spectral acceleration in the three period bands for a given MMI were developed for the first time. The parameters of these conditional lognormal distributions were obtained from regression analyses.
- Lognormal distributions of the dynamic amplification factors (DAFs) were verified by the Kolmogorov-Smirnov analysis at the 5% significance level. These distributions can be used in other applications.

- In order to achieve nonstationarity in both amplitude and frequency content in the simulated ground motion, the nonstationary ARMA(2,1) model was utilized. These two nonstationarities are important for evaluating nonlinear response of structures.
- Parameters of the nonstationary ARMA(2,1) model were estimated for an ensemble of time histories. These parameters can be used in general for simulation in other applications.
- The mean spectral shape of the time histories simulated using the nonstationary ARMA(2,1) model is slightly different from the mean spectral shape of the recorded ground motions. Due to this difference, the damage estimates for the mid rise frames are larger when the frames are subjected to the simulated time histories than when the frames are subjected to recorded ground motions. On the contrary, the damage estimates for the high rise frames are smaller when the frames are subjected to simulated ground motions than when the frames are subjected to recorded ground motions. However, the differences in the response of the frames are small compared to the uncertainties in the ground motion and structural parameters like stiffness and strength of the members.

Nonlinear Dynamic Analysis

The methodology involves the nonlinear dynamic analysis of structures subjected to an ensemble of ground motion time histories. The following conclusions are drawn regarding the nonlinear behavior of structures.

- Several models for performing nonlinear dynamic analyses were compared in order to establish the bounds within which the response of the structures may lie. Nonlinear response from DRAIN-2DX using three elements for each member is similar to that produced from IDARC2D and CU-DYNAMIX. The differences in the response predicted by the programs are likely due to the modeling of strain-hardening and the formulation of the basic inelastic model in the programs.
- The advantages and disadvantages of these three analysis programs are as follows:
 - DRAIN-2DX is computationally a very stable program and is widely used for nonlinear analyses of structures. It is computationally very efficient as it uses an event-to-event

strategy. However, it uses only a bilinear hysteretic model with no deterioration in the hysteretic behavior.

- IDARC2D can incorporate stiffness degradation, strength deterioration, and pinching in the hysteretic model. It is capable of modeling distributed plasticity. However, it is numerically unstable in some analyses.
- CU-DYNAMIX is capable of performing two- and three-dimensional analyses. It models distributed plasticity as well as stiffness degradation. It can analyze only bisymmetric sections and can be used only in an interactive mode.
- Modeling each member using three elements in DRAIN-2DX results in a decrease of the drift ratio and the Park-Ang damage index compared to the case when each member is modeled by a single element.

Motion-Damage Relationships for RC Frames

The methodology was demonstrated by application to RC frames. The following conclusions are drawn from the motion-damage relationships for RC frames.

- New fragility curves for RC frames were developed that can be used for damage assessment and retrofit decision making. These curves are consistent with ground motion and structural parameter uncertainties and do not depend on heuristics.
- At a given ground motion level, the lognormal distributions are excellent representation of the empirical distributions of the Park-Ang damage index based on the Kolmogorv-Smirnov test validated at the 5% significance level.
- A formulation was developed for estimating the DPMs from the fragility curves. This formulation was applied to obtain DPMs for RC frames.
- ATC-13 DPMs show significant probabilities only for the *Minor* and *Moderate* damage states for MMI in the VI to X range. Furthermore, the negligible probability of collapse of the frames at MMI values of XI and XII for the ATC-13 DPMs appear rather unrealistic, particularly in view of the performance of concrete frame structures in recent large

earthquakes. The DPMs developed in this study show significant non-zero probabilities for more damage states at a given level of MMI.

Sensitivity Analyses

Sensitivity analyses were carried to study the influence of different structural attributes on the nonlinear dynamic response of structures. The structural attributes included the number of bays in a structure, the second-order effects, and the site conditions. The following conclusions are drawn from the sensitivity analyses.

- The number of bays did not have a significant influence on the nonlinear response of structures in terms of drift ratios, dissipated hysteretic energies, and the Park-Ang damage index.
- The second-order effects were negligible for lower levels of ground motion. However, second-order effects become increasingly important at higher levels of ground motion as the building height increases.
- Significant differences in the nonlinear response of structures were observed for different site condition. Due to the reduction in seismic demand as the period of the low rise frame elongates, the rock ground motions lead to a considerable reduction in the Park-Ang damage index compared to the firm site ground motions. However, due to higher mode effects for the mid rise and the high rise frames, rock ground motions lead to an increase in the Park-Ang damage index compared to the firm site ground motions.
- For the three sample frames, the deformation and the energy terms of the Park-Ang damage index contribute almost equally to the damage index at different levels of ground motion.
- The overall drift ratios and the Park-Ang damage index at different levels of ground motion are almost perfectly correlated for the three sample frames. A correlation coefficient greater than 0.99 was observed for the three frames.

Bayesian Analysis

The following are the summaries and conclusions of the Bayesian analysis presented in this study.

- The technique presented in this research is the first systematic approach to incorporate damage data with synthetic or heuristic motion-damage relationships.
- The uncertainty due to the use of a limited number of representative structures in the development of synthetic fragility curves is reduced by incorporating observed damage data into the fragility curves.
- In the Bayesian analysis, only the median damage index was assumed as a random variable as the coefficient of variation of the Park-Ang damage index at higher levels of ground motion converges to a value of about 1.1 for the low rise frame, 0.5 for the mid rise and the high rise frame. The reduction in the coefficient of variation for the mid rise and the high rise frames is due to the use of a high-pass, bi-lateral Butterworth filter to remove the low frequency components.
- The methodology is demonstrated with sample data on buildings damaged during the Northridge earthquake. A total of 144 ductile, low rise reinforced concrete frame buildings subjected to different levels of ground motion were used in the Bayesian analysis. Out of these, seventeen buildings sustained different degrees of damage.
- The synthetic fragility curves were found to provide the best estimates of the updated probabilities of the different damage states. The updated probabilities lie both above and below the synthetic fragility curves.
- Confidence bounds on the fragility curves were established. The confidence bounds are wide because they account for the uncertainty in the stiffness and strength of the different members and the uncertainty in damping and mass. The confidence bounds also represent the variation in the behavior of the structures belonging to a class of RC frames.
- The parameters of the updated fragility curves can be used as the prior estimates in the Bayesian analysis as more data become available.

7.2 Future Work

This study examined the vulnerability of reinforced concrete frames to earthquake ground shaking. In general, these buildings may be subjected to other earthquake hazards such as liquefaction and landslides. An approach needs to be developed which can estimate the vulnerability of buildings under all hazards due to earthquakes. Furthermore, this research was limited to the evaluation of structural damage. It is known that nonstructural and contents damage can be a significant portion of the total loss. Therefore, a rational approach for evaluating damage to nonstructural components and building contents is needed.

The method for obtaining analytical fragility curves, developed in this study, requires an ensemble of earthquake time histories for the nonlinear dynamic analysis. Since a large sample of recorded time histories that cover all the different parameter ranges is not currently available, ensembles of time histories need to be simulated at each specified ground motion parameter level. Therefore, further research is needed in the simulation of ground motion. A better simulation model which captures the nonstationarity in amplitude and frequency content, along with the characteristics of travel path, distance, and local soil parameters needs to be investigated.

This research relied on previous relationships between economic loss and damage states. These relationships were used to estimate the damage index of buildings subjected to ground motion during the Northridge earthquake. An estimate of the damage index was needed to perform the Bayesian analysis. A more rational relationship between economic loss and damage states is needed. Such an approach was attempted in Section 3 where the damage states were defined in terms of crack width. Crack width is a parameter which may be easily related to economic loss. However, crack width can only be used for the *Minor* and *Moderate* damage states. Furthermore, the expression for crack width needs to be calibrated or a better expression should be obtained.

In general, a region will consist of buildings belonging to different structural classes, for example, wood, unreinforced masonry, and steel frames. Thus for regional damage evaluation, it is desirable to obtain a consistent set of fragility curves for all structural classes. Such a set is not currently available. This study arrives only at a consistent set of fragility curves for reinforced concrete frames.

Furthermore, the effect of structural characteristics not included in this study also need to be investigated. For example, three-dimensional, non-linear dynamic analyses need to be performed in order to study the effect of plan irregularity on the damage to the structure. For example, the six story Barrington Building is L-shaped and suffered damage during the Northridge earthquake. This building consists of a perimeter frame and irregularly placed shear walls. Mitchell et al. (1995) suggested that torsional effects increased the shear taken by the exterior frames. Furthermore, the column at the southwest corner, farthest from the shear walls, suffered the most damage. Further details on this example as well as the other examples in the remainder of this section can be found in Mitchell et al. (1995) and Holmes and Somers (1996).

The effect of elevation irregularities should also be investigated. Furthermore, in this study, it is assumed that flexural behavior alone causes damage in reinforced concrete members. In reality, different conditions may prevail. For example, in the seven story Saint John's Hospital located in Santa Monica, the second story experienced considerable damage. This story had larger openings compared to other stories, creating an irregularity in stiffness over the height of the building. Thus, the second story experienced damage due to being a weak story. Interestingly, the cracked columns in this story were shorter than the uncracked columns. The shear deformations became important in the short columns leading to shear cracking.

Shear effects were also found to cause damage in Champaign Tower, a 15 story reinforced concrete building located in Santa Monica. This building consists of nonductile moment frames in the longitudinal direction. In this direction, the presence of balcony parapets led to a shortening of the column spans which resulted in their developing diagonal shear cracks in the lower stories.

Another important issue often ignored in analysis is the connection between different members of a reinforced concrete frame. It is assumed that the frame's joints are rigid and do not undergo deformations. However, they may be inadequate in some cases and lead to failure of the structure. For example, the Kaiser Permanente building suffered severe damage due to inadequate connections. The beam-column joints had insufficient amount of confinement steel which led to the complete shattering of these joints.

The influence of soil-structure effects is not fully explored in this study. To determine the sensitivity of response to site conditions, the effect of soil-structure interaction is ignored in this research. Soil-structure effects may be important in some cases, especially if the building is located on softer soil.

A considerable amount of computational effort is required to perform non-linear dynamic analyses for estimating damage. Procedures for obtaining fragility curves with reduced computational effort also need to be investigated.

SECTION 8 REFERENCES

1. Akiyama, H., (1985), "Earthquake resistant limit-state design for buildings", University of Tokyo Press.
2. Anagnos, T., Rojahn, C., and Kiremidjian, A.S., (1995), "NCEER-ATC joint study on fragility of buildings", *NCEER-95-0003*, National Center for Earthquake Engineering Research, State University of New York at Buffalo.
3. Araya, R., and Saragoni, G.R., (1984), "Earthquake acceierogram destructiveness potential", *Proceedings 8th World Conference on Earthquake Engineering*, San Francisco, California, Vol. 2, pp. 835-842.
4. Arias, A., (1970), "A measure of earthquake intensity", *Seismic Design of Nuclear Power Plants*, R. Hansen, Editor, M.I.T. Press, pp. 438-483.
5. ATC 3-06, (Tentative 1978), "Tentative provisions for the development of seismic regulations for buildings", *Applied Technology Council*, NBS Special Publication 510, NSF Publication 78-08.
6. ATC-13, (1985), "Earthquake damage evaluation data for California", *Applied Technology Council*, Redwood City, California.
7. Ayyub, B.M., and Lai, K-L., (1989), "Structural reliability assessment using Latin Hypercube sampling", *Proceedings of the 5th International conference on Structural Safety and Reliability*, pp. 1177-1184.
8. Banon, H., Biggs, J.M, and Irvine, H.M., (1981), "Seismic damage in reinforced concrete frames", *Journal of Structural Engineering*, ASCE, Vol. 107, No. ST9, pp. 1713-1729.
9. Bazant, Z.P., and Oh, B.H., (1983a), "Spacing of cracks in reinforced concrete", *Journal of Structural Engineering*, ASCE, Vol. 109, No. ST9, pp. 2066-2085.
10. Bazant, Z.P., and Oh, B.H., (1983b), "Crack spacing in reinforced concrete: approximate solution", *Journal of Structural Engineering*, ASCE, Vol. 109, No. ST1, pp. 93-108.

11. Bertero, R.D., and Bertero, V.V., (1992), "Tall reinforced concrete buildings: Conceptual earthquake-resistant design methodology", *UCB/EERC-92/16*, Earthquake Engineering Research Center, University of California at Berkeley.
12. Beshara, F.B.A., (1993), "Smearred crack analysis for reinforced concrete structures under blast-type loading", *Engineering Fracture Mechanics*, Vol. 45, No. 1, pp. 119-140.
13. Bolt, B.A., (1973), "Duration of strong ground motions", *Proceedings 5th World Conference on Earthquake Engineering*, Rome, Italy, Vol. 1, pp. 1304-1313.
14. Borchardt, R.D., (1994), "Estimates of site-dependent response spectra for design (methodology and justification)", *Earthquake Spectra*, Vol. 10, No. 4, pp. 617-653.
15. Bracci, J.M., Reinhorn, A.M., Mander, J.B., and Kunnath, S.K., (1989), "Deterministic model for seismic damage evaluation of reinforced concrete structures", *NCEER-89-0033*, National Center for Earthquake Engineering Research, State University of New York at Buffalo.
16. Chung, Y.S., Meyer, C., and Shinozuka, M., (1987), "Seismic assessment of reinforced concrete members", *NCEER-87-0022* National Center for Earthquake Engineering Research, State University of New York at Buffalo.
17. Chung, Y.S., Meyer, C., and Shinozuka, M., (1989), "Modeling of concrete damage", *ACI Structural Journal*, Vol. 86, No. 3, pp. 259-271.
18. Chung, Y.S., Meyer, C., and Shinozuka, M., (1990), "Automatic seismic design of reinforced concrete building frames", *ACI Structural Journal*, Vol. 87, No. 3, pp. 326-340.
19. Conte, J.P., Pister, K.S., and Mahin, S.A., (1992), "Nonstationary ARMA modeling of seismic motions", *Soil Dynamics and Earthquake Engineering*, November, pp. 411-426.
20. Cosenza, E., Manfredi, G., and Ramasco, K., (1990), "An evaluation of the use of damage functionals in earthquake-resistant design", *Proceedings of the 9th European Conference on Earthquake Engineering*, Moscow, Vol. 9, pp. 303-312.

21. Deodatis, G., and Shinozuka, M., (1989), "Simulation of seismic ground motion using stochastic waves", *Journal of Engineering Mechanics*, ASCE, Vol. 115, No. EM12, pp. 2723-2737.
22. De Leon, D., and Ang, A.H-S. (1993), "A damage model for reinforced concrete buildings: Further study with the 1985 Mexico City earthquake", *Proceedings 6th International Conference on Structural Safety and Reliability*, Innsbruck, Austria, Vol. 3, pp. 2081-2087.
23. Der Kiureghian, A., (1989), "Measures of structural safety under imperfect states of knowledge", *Journal of the Structural Division*, ASCE, Vol. 115, No. ST5, pp. 1119-1140.
24. DiPasquale, E., and Cakmak, A.S., (1990), "Seismic damage assessment using linear models", *Soil Dynamics and Earthquake Engineering*, Vol. 9, No. 4, pp. 194-215.
25. El-Tawil, S., (1996), "Inelastic dynamic analysis of mixed steel-concrete systems", *Ph. D. Thesis*, School of Civil and Environmental Engineering, Cornell University, Ithaca, New York.
26. FEMA 223, (1992), "NEHRP recommended provisions for the development of seismic regulations for new buildings: Part 2 - Commentary", *Earthquake Hazards Reduction Series 65*, Federal Emergency Management Agency, Washington, D.C.
27. Galambos, T.V., Ellingwood, B., MacGregor, J.G., and Cornell, C.A., (1982), "Probability based load criteria : Assessment of current design practice", *Journal of the Structural Division*, ASCE, Vol. 108, No. ST5, pp. 959-977.
28. Gere, J., and Shah, H.C., (1984), "Terra Non Ferma - understanding and preparing for earthquakes", W.H. Freeman and Co., San Francisco, California.
29. Gergely, P., and Lutz, L.A., (1968), "Maximum crack width in reinforced concrete flexural members", *Causes, Mechanism, and Control of Cracking in Concrete*, SP-20, American Concrete Institute, Detroit, pp. 87-117.
30. Geyskens, P., Der Kiureghian, A., and Monteiro, P., (1993), "BUMP: Bayesian updating of model parameters", *Report No. UCB/SEMM-93/06*, Structural Engineering, Mechanics

and Materials Program, Department of Civil Engineering, University of California at Berkeley.

31. Gunturi, S.K. (1992). "Building specific earthquake damage estimation", *Ph.D. Thesis* submitted to Stanford University.
32. Hamming, R.W., (1989), "Digital filters", Prentice Hall, Englewood Cliffs, New Jersey.
33. Hatamoto, H., Chung, Y.S., and Shinozuka, M., (1990), "Seismic capacity enhancement of R/C frames by means of damage control design", *Proceedings of Fourth U.S. National Conference on Earthquake Engineering*, Palm Springs, California, Vol. 2, pp. 279-288.
34. Holmes, W.T., and Somers, P. (Technical Editors), (1996), "Chapter 3: Reinforced concrete buildings", *Northridge Earthquake Reconnaissance Report Vol. 2*, Supplement C to Vol. 11, *Earthquake Spectra*, EERI, April.
35. Housner, G.W., (1952), "Intensity of ground motion during strong earthquake", *Earthquake Research Laboratory*, California Institute of Technology, Pasadena, California.
36. Housner, G.W., (1956), "Limit design of structures to resist earthquake", *Proceedings 1st World Conference on Earthquake Engineering*, Berkeley, California, pp. 1-13.
37. Housner, G.W., and Jennings, P.C., (1964), "Generation of artificial earthquakes", *Journal of the Engineering Mechanics Division*, ASCE, Vol. 90, No. EM1, pp. 113-150.
38. Housner, G.W., (1990), "Competing against time", *Report to Governor George Deukmejian* from the Governor's Board of Inquiry on the 1989 Loma Prieta Earthquake, May.
39. Huang, H.H.M., and Jaw, J-W., (1989), "Seismic fragility analysis of shear wall structures", *Proceedings of the 5th International Conference on Structural Safety and Reliability*, San Francisco, California, pp. 399-406.
40. Iman, R.L., and Conover, W.J., (1980), "Small sample sensitivity analysis techniques for computer models, with an application to risk assessment", *Communications in Statistics - Theoretical Methods*, Vol. 17, No. A9, pp. 1749-1842.

41. IMSL, (1991), The International Mathematical and Statistical Library, User's Manual, IMSL, Inc., Houston, TX.
42. Jennings, P.C., (1971), "Engineering features of the San Fernando earthquake of February 9, 1971", *EERL 71-02*, Earthquake Engineering Research Laboratory, Pasadena, California.
43. Jennings, P.C., and Bielak, J., (1973), "Dynamics of building-soil interaction", *Bulletin of the Seismological Society of America*, Vol. 63, No. 1, pp. 9-48.
44. Jeong, G.D., and Iwan, W.D., (1988), "The effect of earthquake duration on the damage of structures", *Earthquake Engineering and Structural Dynamics*, Vol. 16, pp. 1201-1211.
45. Kennedy, R.P., Cornell, C.A., Campbell, R.D., Kaplan, S., and Perla, H.F., (1980), "Probabilistic seismic safety study of an existing nuclear power plant", *Nuclear Engineering and Design*, pp. 315-338.
46. Kennedy, R.P., and Ravindra, M.K., (1984), "Seismic fragilities for nuclear power plant risk studies", *Nuclear Engineering and Design*, pp. 47-68.
47. Kent, D.C., and Park, R., (1971), "Flexural members with confined concrete", *Journal of Structural Engineering*, ASCE, Vol. 97, No. ST7, pp. 1969-1990.
48. Kiremidjian, A.S., and Shah, H.C., (1980), "Probabilistic site-dependent response spectra", *Journal of Structural Engineering*, ASCE, Vol. 106, No. ST1, pp. 69-86.
49. Kiremidjian, A.S., (1985), "Subjective probabilities for earthquake damage and loss", *Structural Safety*, Vol. 2, pp. 309-317.
50. Krawinkler, H., and Zohrei, M., (1983), "Cumulative damage in steel structures subjected to earthquake ground motions", *Computers and Structures*, Vol. 16, pp. 531-541.
51. Krawinkler, H., (1987), "Performance Assessment of Steel Components", *Earthquake Spectra*, Vol. 3, No. 1, pp. 27-41.

52. Kunnath, S.K., Reinhorn, A.M., and Lobo, R.F., (1992), "IDARC Version 3.0: A program for the inelastic damage analysis of reinforced concrete structures", *NCEER-92-0022*, National Center for Earthquake Engineering Research, State University of New York at Buffalo.
53. Kunnath, S.K., and Reinhorn, A.M.,(1994), "IDARC2D Version 3.1: Inelastic damage analysis of RC building structures, Users Manual", Department of Civil Engineering, State University of New York at Buffalo, September.
54. Lai, S.S.P., (1982), "Statistical characterization of strong ground motions using power spectral density function", *Bulletin of the Seismological Society of America*, Vol. 72, No. 1, pp. 259-274.
55. Liu, S.C., and Jhaveri, D.P., (1969), "Spectral simulation and earthquake site properties", *Journal of the Engineering Mechanics Division*, ASCE, Vol. 95, No. EM5, pp. 1145-1168.
56. Liu, S.C., (1970), "Evolutionary power spectral density of strong motion earthquake", *Bulletin of the Seismological Society of America*, Vol. 60, No. 3, pp. 891-900.
57. Luco, J.E., and Mita, A., (1987), "Response of a circular foundation to spatially random ground motion", *Journal of the Engineering Mechanics Division*, ASCE, Vol. 113, No. EM1, pp. 1-15.
58. Maley, R., Acosta, A., Ellis, F., Etheredge, E., Foote, L., Johnson, D., Porcella, R., Salsman, M., and Switzer, J., (1989), "U.S. Geological Survey strong-motion records from the northern California (Loma Prieta) earthquake of October 17, 1989", *Geological Survey Open-File Report No. 89-568*.
59. Manual for Repair Methods of Civil Engineering Structures Damaged by Earthquakes, (1987), Published by the Public Works Research Institute, Ministry of Construction, December.
60. MATLAB, (1994), System Identification Toolbox User's Guide, The Mathworks, Inc., Natick, MA.

61. McCann, M.W., and Shah, H.C., (1979), "Determining Strong-Motion Duration of Earthquakes", *Bulletin of the Seismological Society of America*, Vol. 69, No. 4, pp. 1253-1265.
62. Mirza, S.A., and MacGregor, J.C., (1979), "Variations in dimensions of reinforced concrete members", *Journal of Structural Engineering*, ASCE, Vol. 105, No. ST4, pp. 751-766.
63. Mitchell, D., DeVall, R.H., Saatcioglu, M., Simpson, R., Tinawi, R., and Tremblay, R., (1995), "Damage to concrete structures due to the 1994 Northridge earthquake", *Canadian Journal of Civil Engineering*, Vol. 22, No. 2, pp. 361-377.
64. Mohraz, B., (1976), "A study of earthquake response spectra for different geological conditions", *Bulletin of the Seismological Society of America*, Vol. 66, No. 3, pp. 915-935.
65. Mohraz, B., and Tiv, M., (1991), "Spectral shapes and amplifications for the Loma Prieta earthquake of October 17, 1989", *Proceedings of Third U.S. Conference on Lifeline Earthquake Engineering*, Los Angeles, California, August, pp. 562-571.
66. Mork, K.J., (1992), "Stochastic analysis of reinforced concrete frames under seismic excitation", *Soil Dynamics and Earthquake Engineering*, Vol. 11, No. 3, pp. 145-161.
67. Nassar, A.A., and Krawinkler, H., (1991), "Seismic demands for SDOF and MDOF systems", *John A. Blume Earthquake Engineering Center Report No. 95*, Department of Civil Engineering, Stanford University.
68. Nau, R.F., Oliver, R.M., and Pister, K.S., (1982), "Simulating and analyzing artificial nonstationary ground motions", *Bulletin of the Seismological Society of America*, Vol. 72, No. 2, pp. 615-636.
69. NIBS, (1995), "Development of a standardized earthquake loss-estimation methodology", Draft Technical Manual 100% Submittal, Prepared by Risk Management Solutions, Inc., for National Institute of Building Sciences.

70. Nielsen, S.R.K., Koyluoglu, H.U., and Cakmak, A.S., (1992), "One and two-dimensional maximum softening damage indicators for reinforced concrete structures under seismic excitation", *Soil Dynamics and Earthquake Engineering*, Vol. 11, No. 4, pp. 435-443.
71. Nigam, N.C., (1983), "Introduction to random vibrations", MIT Press, Cambridge, Massachusetts.
72. OES, (1995), "The Northridge earthquake of January 17, 1994: Report of data collection and analysis, Part A: Damage and inventory data", Prepared by EQE International, Inc., and the Geographic Information Systems Group of the Governor's Office of Emergency Services for the Governor's Office of Emergency Services of the State of California.
73. Ogawa, S., Elms, D.G., and Paulay, T., (1988), "A simplified procedure for assessing failure probabilities of reinforced concrete frame buildings under earthquake loading", 88-11, Department of Civil Engineering, University of Canterbury, Christchurch, New Zealand.
74. Oh, B.H., and Kang, Y-J, (1987), "New formulas for maximum crack width and crack spacing in reinforced concrete flexural members", *ACI Structural Journal*, March-April, pp. 103-112.
75. Park, R., and Paulay, T., (1975), "Reinforced concrete structures", John Wiley & Sons, New York.
76. Park, Y-J., Ang, A.H-S., and Wen, Y.K., (1984), "Seismic damage analysis and damage-limiting design of RC buildings", *Structural Research Series, Report No. UILU-ENG-84-2007*, University of Illinois at Urbana-Champaign, Urbana, Illinois, Oct.
77. Park, Y-J., and Ang, A.H-S., (1985a), "Mechanistic seismic damage model for reinforced concrete", *Journal of Structural Engineering*, ASCE, Vol. 111, No. ST4, pp. 722-739.
78. Park, Y-J., and Ang, A.H-S., (1985b), "Seismic damage analysis of reinforced concrete buildings", *Journal of Structural Engineering*, ASCE, Vol. 111, No. ST4, pp. 740-757.
79. Park, Y.J., Ang, A.H-S., and Wen, Y.K., (1987), "Damage-limiting aseismic design of buildings", *Earthquake Spectra*, Vol. 3, No. 1, pp. 1-26.

80. Park, Y.J., Reinhorn, A.M., and Kunnath, S.K., (1987), "IDARC : Inelastic damage analysis of reinforced concrete Frame - Shear-Wall structures", *NCEER-87-0008*, National Center for Earthquake Engineering Research, State University of New York at Buffalo.
81. Paulay, T., and Priestley, M.J.N., (1992), "Seismic design of reinforced concrete and masonry buildings", John Wiley & Sons, New York.
82. Polhemus, N.W., and Cakmak, A.S., (1981), "Simulation of earthquake ground motions using autoregressive moving average (ARMA) models", *Earthquake Engineering and Structural Dynamics*, Vol. 9, pp. 343-354.
83. Powell, G.H., and Allahabadi, R., (1988), "Seismic damage prediction by deterministic methods : concepts and procedures", *Earthquake Engineering and Structural Dynamics*, Vol. 16, pp. 719-734.
84. Prakash, V., and Powell, G.H., (1992), "DRAIN-2DX: user's guide", *Department of Civil Engineering*, University of California at Berkeley.
85. Raiffa, H., and Schlaifer, R., (1961), "Applied statistical decision theory", Division of Research, Graduate School of Business and Administration, Harvard University.
86. Richter, C.F., (1958), "Elementary Seismology", W.H. Freeman, San Francisco.
87. Roufaiel, M.S.L., and Meyer, C., (1987), "Reliability of concrete frames damaged by earthquakes", *Journal of Structural Engineering*, ASCE, Vol. 113, No. ST3, pp. 445-457.
88. Rubinstein, R.Y., (1981), "Simulation and the Monte Carlo method", John Wiley & Sons, New York.
89. Seed, H.B., Ugas, C., and Lysmer, J., (1976), "Site-dependent spectra for earthquake resistance design", *Bulletin of the Seismological Society of America*, Vol. 66, No. 1, pp. 221-243.
90. SEAOC, (1990), "Recommended lateral force requirements and commentary", *Structural Engineers Association of California*.

91. Shakal, A.F., Huang, M.J., Reichle, M., Ventura, C.E., Cao, T.Q., Sherburne, R.W., Savage, M., Darragh, R., and Petersen, C., (1989), "CSMIP strong-motion records from the Santa Cruz Mountains (Loma Prieta), California earthquake of 17 October 1989", *Report No. OSMS 89-06*, California Strong Motion Instrumentation Program, Division of Mines and Geology, California Department of Conservation, November 17.
92. Shakal, A.F., Huang, M.J., Ventura, C.E., Parke, D.L., Cao, T.Q., Sherburne, R.W., and Blazquez, R., (1987), "CSMIP strong-motion records from the Whittier, California earthquake of 1 October 1987", *Report No. OSMS 87-05*, California Strong Motion Instrumentation Program, Division of Mines and Geology, California Department of Conservation, October 31.
93. Shakal, A.F., Huang, M.J., Parke, D.L., and Sherburne, R.W., (1985), "Processed data from the strong-motion records of the Morgan Hill earthquake of 24 April 1984", *Report No. OSMS 85-04*, California Strong Motion Instrumentation Program, Division of Mines and Geology, California Department of Conservation, May.
94. Shahrooz, B.M., and Moehle, J.P., (1990), "Evaluation of seismic performance of reinforced concrete frames", *Journal of Structural Engineering*, ASCE, Vol. 116, No. ST5, pp. 1403-1422.
95. Shinozuka, M., and Sato, Y., (1967), "Simulation of nonstationary random process", *Journal of the Engineering Mechanics Division*, ASCE, Vol. 93, No. EM1, pp. 11-40.
96. Shinozuka, M. and Deodatis G., (1991), "Simulation of stochastic processes by spectral representation", *Applied Mechanics Reviews*, ASME, Vol. 44, No. 4, pp. 191-204.
97. SIMQKE, (1976), User's Manual and Documentation, Department of Civil Engineering, Massachusetts Institute of Technology, November.
98. Somerville, P.G., Graves, R.W., and Saikia, C.K., (1995), "Characterization of ground motions at the sites of subject buildings", Report on Task 4 of the SAC Joint Venture Program for the Reduction of Earthquake Hazards in Steel Moment Frame Buildings.

99. Stone, W.C., and Taylor, A.W., (1994), "ISDP: Integrated approach to seismic design of reinforced concrete structures", *Journal of Structural Engineering*, ASCE, Vol. 120, No. ST12, pp. 3548-3566.
100. Suzuki, S., and Kiremidjian, A.S., (1989), "Risk-consistent ground motions from a geophysical source and source to site model", *Proceedings of the 7th Japan Society of Civil Engineers Conference*, Tokyo, Japan.
101. Tajimi, H., (1960), "A standard method of determining the maximum response of a building structure during an earthquake", *Proceedings 2nd World Conference on Earthquake Engineering*, Vol. 2, pp. 781-798.
102. The Morgan Hill Earthquake of April 24, 1984, (1985), *Earthquake Spectra*, EERI, Vol. 1, Number 3, May.
103. The Whittier Narrows Earthquake of October 1, 1987, (1988), *Earthquake Spectra*, EERI, Vol. 4, Number 1.
104. Trifunac, M.D., and Brady, A.G., (1975), "A study on the duration of strong earthquake ground motion", *Bulletin of the Seismological Society of America*, Vol. 65, No. 3, pp. 581-626.
105. Uang, C.M., and Bertero, V.V., (1990), "Evaluation of seismic energy in structures", *Earthquake Engineering and Structural Dynamics*, Vol. 19, pp. 77-90.
106. Vanmarcke, E.H., (1976), "Structural response to earthquakes", *Seismic Risk and Engineering Decisions*, C. Lomnitz and E. Rosenblueth, eds, Elsevier Publishing Company, pp. 287-337.
107. Vanmarcke, E.H., and Lai, S-S.P., (1980), "Strong-motion duration and RMS amplitude of earthquake records", *Bulletin of the Seismological Society of America*, Vol. 70, No. 4, pp. 1293-1307.
108. Veletsos, A.S., and Meek, J.W., (1974), "Dynamic behaviour of building-foundation systems", *Earthquake Engineering and Structural Dynamics*, Vol. 3, pp. 121-138.

109. Veletsos, A.S., and Prasad, A.M., (1989), "Seismic interaction of structures and soil: Stochastic approach", *Journal of Structural Engineering*, ASCE, Vol. 115, No. ST4, pp. 935-956.
110. Whitman, R.V., Biggs, J.M., Brennan III, J., Cornell, C.A., De Neufville, R., and Vanmarcke, E.H., (1974), "Methodology and pilot application - Seismic design decision analysis", *Report R74-15*, Department of Civil Engineering, Massachusetts Institute of Technology.
111. Williams, M.S., and Sexsmith, R.G., (1995), "Seismic damage indices for concrete structures: a state-of-the-art review", *Earthquake Spectra*, Vol. 11, No. 2, pp. 319-349.
112. Wilson, E.L., and Habibullah, (1987), "Static and dynamic analysis of multi-story buildings, including p-delta effects", *Earthquake Spectra*, Vol. 3, No. 2, pp. 289-298.
113. Yao, J.T.P., Kozin, F., Wen, Y.K., Yang, J.N., Schueller, G.I., Ditlevsen, O., (1986), "Stochastic fatigue, fracture and damage analysis", *Structural Safety*, Vol. 3, pp. 231-267.
114. Yeh, C.H., and Wen, Y.K., (1990), "Modeling of nonstationary ground motion and analysis of inelastic structural response", *Structural Safety*, Vol. 8, pp. 281-298.
115. Zhu, T.J., Tso, W.K., Heidebrecht, A.C., (1988), "Effect of peak ground a/v ratio on structural damage", *Journal of Structural Engineering*, Vol. 114, No. 5, pp. 1019-1037.

APPENDIX A
COMPUTATION OF MOMENT AND CURVATURE FOR AN EXAMPLE RC
SECTION

The example section is assumed to have overall dimensions of 14" x 18". It has four No. 9 longitudinal bars at the bottom and two No. 9 longitudinal bars at the top. The beam has No. 3 closed stirrups at 4" centers. The cover to the hoops is 1.5". The details of the section are shown in figure A-1. The reinforcing steel has a trilinear stress-strain relationship shown in figure A-2. The steel is assumed to have a yield strength, f_y , of 60 ksi, a modulus of elasticity, E , of 29,000 ksi, and a strain hardening modulus, E_s , of $E/60$. The strain at the commencement of strain hardening, ϵ_{sh} , is assumed to be 0.03. The concrete is assumed to have a cylinder strength of 4 ksi. The Kent and Park stress-strain relationship discussed in Section 4 is used for concrete.

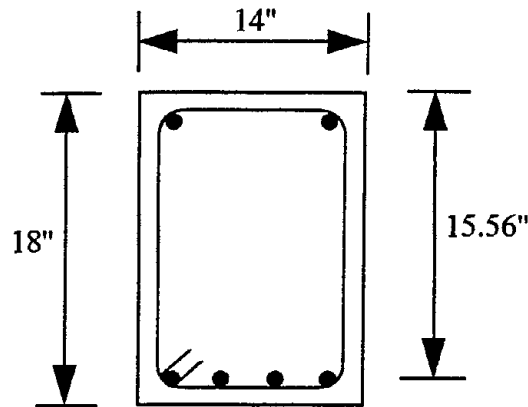


FIGURE A-1 Details of the example section

Based on the spacing of stirrups and the section dimensions, the ratio of the volume of transverse reinforcement to volume of concrete core, ρ_s , is calculated as:

$$\rho_s = \frac{0.11 \times 2(10.63 + 14.63)}{11 \times 15 \times 4} = 0.0084 \quad (\text{A.1})$$

The slope of the descending portion of the Kent and Park stress-strain relationship, Z , is calculated by the following expression as defined in Section 4:

$$Z = \frac{0.5}{\frac{3 + 0.002f'_c}{f'_c - 1000} + \frac{3}{4}\rho_s\sqrt{\frac{b''}{s_h}} - 0.002} \quad (\text{A.2})$$

where:

- f'_c = compressive strength of concrete,
- b'' = width of confined core measured to outside of hoops, and
- s_h = spacing of hoops.

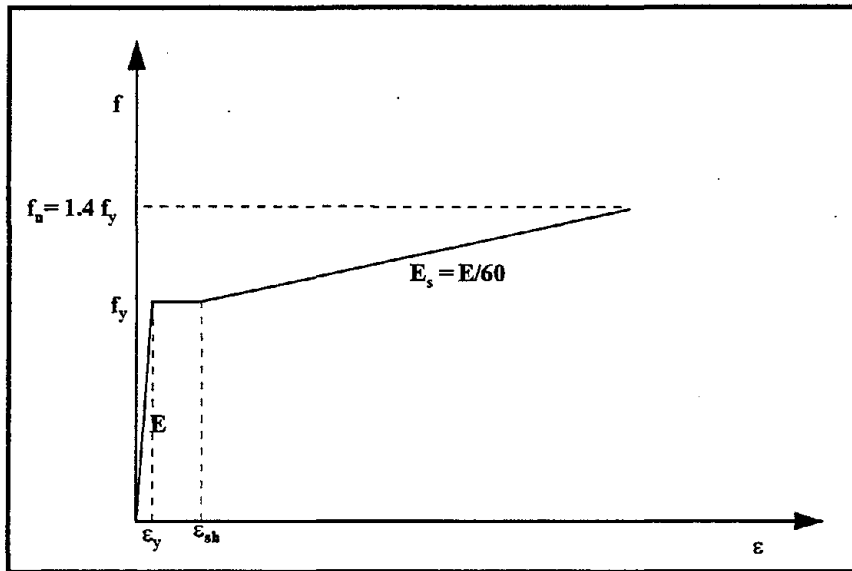


FIGURE A-2 Stress-strain relationship for reinforcing steel

Thus,

$$Z = \frac{0.5}{\frac{(3+8)}{3000} + \frac{3}{4} \times 0.0084 \sqrt{11/4} - 0.002} = 41 \quad (\text{A.3})$$

The calculations of the moments and curvatures corresponding to the yield and ultimate conditions are presented below.

Yield Condition

The yield moment and curvature are the respective values when the tensile (bottom) steel first reaches its yield strain. The following values are computed when the tensile steel yields:

Depth of neutral axis:	5.98 in
Compressive strain in extreme concrete fiber:	0.0013
Yield Moment:	3186 k-in
Yield Curvature:	0.0002 per in

Ultimate Condition

The ultimate moment and curvature are the respective values when either the compressive strain in concrete reaches its ultimate value or when the tensile steel reaches its ultimate strength. For this example section, the ultimate condition is governed by the concrete reaching its ultimate compressive strain. As implemented in IDARC2D (Kunnath and Reinhorn, 1994), the ultimate strain in concrete is defined as the strain corresponding to a stress of 20% of the compressive strength of concrete on the falling branch of the Kent and Park stress-strain relationship. This value is close to the value obtained by using expression 4.7 suggested by Paulay and Priestley (1992). It is assumed that the concrete outside the hoops does not spall off. The following values are computed when the ultimate condition is reached:

Depth of neutral axis:	4.67 in
Compressive strain in extreme concrete fiber:	0.0215
Ultimate Moment:	3603 k-in
Ultimate Curvature:	0.0046 per in



**NATIONAL CENTER FOR EARTHQUAKE ENGINEERING RESEARCH
LIST OF TECHNICAL REPORTS**

The National Center for Earthquake Engineering Research (NCEER) publishes technical reports on a variety of subjects related to earthquake engineering written by authors funded through NCEER. These reports are available from both NCEER Publications and the National Technical Information Service (NTIS). Requests for reports should be directed to NCEER Publications, National Center for Earthquake Engineering Research, State University of New York at Buffalo, Red Jacket Quadrangle, Buffalo, New York 14261. Reports can also be requested through NTIS, 5285 Port Royal Road, Springfield, Virginia 22161. NTIS accession numbers are shown in parenthesis, if available.

- NCEER-87-0001 "First-Year Program in Research, Education and Technology Transfer," 3/5/87, (PB88-134275, A04, MF-A01).
- NCEER-87-0002 "Experimental Evaluation of Instantaneous Optimal Algorithms for Structural Control," by R.C. Lin, T.T. Soong and A.M. Reinhorn, 4/20/87, (PB88-134341, A04, MF-A01).
- NCEER-87-0003 "Experimentation Using the Earthquake Simulation Facilities at University at Buffalo," by A.M. Reinhorn and R.L. Ketter, to be published.
- NCEER-87-0004 "The System Characteristics and Performance of a Shaking Table," by J.S. Hwang, K.C. Chang and G.C. Lee, 6/1/87, (PB88-134259, A03, MF-A01). This report is available only through NTIS (see address given above).
- NCEER-87-0005 "A Finite Element Formulation for Nonlinear Viscoplastic Material Using a Q Model," by O. Gyebe and G. Dasgupta, 11/2/87, (PB88-213764, A08, MF-A01).
- NCEER-87-0006 "Symbolic Manipulation Program (SMP) - Algebraic Codes for Two and Three Dimensional Finite Element Formulations," by X. Lee and G. Dasgupta, 11/9/87, (PB88-218522, A05, MF-A01).
- NCEER-87-0007 "Instantaneous Optimal Control Laws for Tall Buildings Under Seismic Excitations," by J.N. Yang, A. Akbarpour and P. Ghaemmaghami, 6/10/87, (PB88-134333, A06, MF-A01). This report is only available through NTIS (see address given above).
- NCEER-87-0008 "IDARC: Inelastic Damage Analysis of Reinforced Concrete Frame - Shear-Wall Structures," by Y.J. Park, A.M. Reinhorn and S.K. Kunnath, 7/20/87, (PB88-134325, A09, MF-A01). This report is only available through NTIS (see address given above).
- NCEER-87-0009 "Liquefaction Potential for New York State: A Preliminary Report on Sites in Manhattan and Buffalo," by M. Budhu, V. Vijayakumar, R.F. Giese and L. Baumgras, 8/31/87, (PB88-163704, A03, MF-A01). This report is available only through NTIS (see address given above).
- NCEER-87-0010 "Vertical and Torsional Vibration of Foundations in Inhomogeneous Media," by A.S. Veletsos and K.W. Dotson, 6/1/87, (PB88-134291, A03, MF-A01). This report is only available through NTIS (see address given above).
- NCEER-87-0011 "Seismic Probabilistic Risk Assessment and Seismic Margins Studies for Nuclear Power Plants," by Howard H.M. Hwang, 6/15/87, (PB88-134267, A03, MF-A01). This report is only available through NTIS (see address given above).
- NCEER-87-0012 "Parametric Studies of Frequency Response of Secondary Systems Under Ground-Acceleration Excitations," by Y. Yong and Y.K. Lin, 6/10/87, (PB88-134309, A03, MF-A01). This report is only available through NTIS (see address given above).
- NCEER-87-0013 "Frequency Response of Secondary Systems Under Seismic Excitation," by J.A. HoLung, J. Cai and Y.K. Lin, 7/31/87, (PB88-134317, A05, MF-A01). This report is only available through NTIS (see address given above).

- NCEER-87-0014 "Modelling Earthquake Ground Motions in Seismically Active Regions Using Parametric Time Series Methods," by G.W. Ellis and A.S. Cakmak, 8/25/87, (PB88-134283, A08, MF-A01). This report is only available through NTIS (see address given above).
- NCEER-87-0015 "Detection and Assessment of Seismic Structural Damage," by E. DiPasquale and A.S. Cakmak, 8/25/87, (PB88-163712, A05, MF-A01). This report is only available through NTIS (see address given above).
- NCEER-87-0016 "Pipeline Experiment at Parkfield, California," by J. Isenberg and E. Richardson, 9/15/87, (PB88-163720, A03, MF-A01). This report is available only through NTIS (see address given above).
- NCEER-87-0017 "Digital Simulation of Seismic Ground Motion," by M. Shinozuka, G. Deodatis and T. Harada, 8/31/87, (PB88-155197, A04, MF-A01). This report is available only through NTIS (see address given above).
- NCEER-87-0018 "Practical Considerations for Structural Control: System Uncertainty, System Time Delay and Truncation of Small Control Forces," J.N. Yang and A. Akbarpour, 8/10/87, (PB88-163738, A08, MF-A01). This report is only available through NTIS (see address given above).
- NCEER-87-0019 "Modal Analysis of Nonclassically Damped Structural Systems Using Canonical Transformation," by J.N. Yang, S. Sarkani and F.X. Long, 9/27/87, (PB88-187851, A04, MF-A01).
- NCEER-87-0020 "A Nonstationary Solution in Random Vibration Theory," by J.R. Red-Horse and P.D. Spanos, 11/3/87, (PB88-163746, A03, MF-A01).
- NCEER-87-0021 "Horizontal Impedances for Radially Inhomogeneous Viscoelastic Soil Layers," by A.S. Veletsos and K.W. Dotson, 10/15/87, (PB88-150859, A04, MF-A01).
- NCEER-87-0022 "Seismic Damage Assessment of Reinforced Concrete Members," by Y.S. Chung, C. Meyer and M. Shinozuka, 10/9/87, (PB88-150867, A05, MF-A01). This report is available only through NTIS (see address given above).
- NCEER-87-0023 "Active Structural Control in Civil Engineering," by T.T. Soong, 11/11/87, (PB88-187778, A03, MF-A01).
- NCEER-87-0024 "Vertical and Torsional Impedances for Radially Inhomogeneous Viscoelastic Soil Layers," by K.W. Dotson and A.S. Veletsos, 12/87, (PB88-187786, A03, MF-A01).
- NCEER-87-0025 "Proceedings from the Symposium on Seismic Hazards, Ground Motions, Soil-Liquefaction and Engineering Practice in Eastern North America," October 20-22, 1987, edited by K.H. Jacob, 12/87, (PB88-188115, A23, MF-A01).
- NCEER-87-0026 "Report on the Whittier-Narrows, California, Earthquake of October 1, 1987," by J. Pantelic and A. Reinhorn, 11/87, (PB88-187752, A03, MF-A01). This report is available only through NTIS (see address given above).
- NCEER-87-0027 "Design of a Modular Program for Transient Nonlinear Analysis of Large 3-D Building Structures," by S. Srivastav and J.F. Abel, 12/30/87, (PB88-187950, A05, MF-A01). This report is only available through NTIS (see address given above).
- NCEER-87-0028 "Second-Year Program in Research, Education and Technology Transfer," 3/8/88, (PB88-219480, A04, MF-A01).
- NCEER-88-0001 "Workshop on Seismic Computer Analysis and Design of Buildings With Interactive Graphics," by W. McGuire, J.F. Abel and C.H. Conley, 1/18/88, (PB88-187760, A03, MF-A01). This report is only available through NTIS (see address given above).
- NCEER-88-0002 "Optimal Control of Nonlinear Flexible Structures," by J.N. Yang, F.X. Long and D. Wong, 1/22/88, (PB88-213772, A06, MF-A01).

- NCEER-88-0003 "Substructuring Techniques in the Time Domain for Primary-Secondary Structural Systems," by G.D. Manolis and G. Juhn, 2/10/88, (PB88-213780, A04, MF-A01).
- NCEER-88-0004 "Iterative Seismic Analysis of Primary-Secondary Systems," by A. Singhal, L.D. Lutes and P.D. Spanos, 2/23/88, (PB88-213798, A04, MF-A01).
- NCEER-88-0005 "Stochastic Finite Element Expansion for Random Media," by P.D. Spanos and R. Ghanem, 3/14/88, (PB88-213806, A03, MF-A01).
- NCEER-88-0006 "Combining Structural Optimization and Structural Control," by F.Y. Cheng and C.P. Pantelides, 1/10/88, (PB88-213814, A05, MF-A01).
- NCEER-88-0007 "Seismic Performance Assessment of Code-Designed Structures," by H.H-M. Hwang, J-W. Jaw and H-J. Shau, 3/20/88, (PB88-219423, A04, MF-A01). This report is only available through NTIS (see address given above).
- NCEER-88-0008 "Reliability Analysis of Code-Designed Structures Under Natural Hazards," by H.H-M. Hwang, H. Ushiba and M. Shinozuka, 2/29/88, (PB88-229471, A07, MF-A01). This report is only available through NTIS (see address given above).
- NCEER-88-0009 "Seismic Fragility Analysis of Shear Wall Structures," by J-W Jaw and H.H-M. Hwang, 4/30/88, (PB89-102867, A04, MF-A01).
- NCEER-88-0010 "Base Isolation of a Multi-Story Building Under a Harmonic Ground Motion - A Comparison of Performances of Various Systems," by F-G Fan, G. Ahmadi and I.G. Tadjbakhsh, 5/18/88, (PB89-122238, A06, MF-A01). This report is only available through NTIS (see address given above).
- NCEER-88-0011 "Seismic Floor Response Spectra for a Combined System by Green's Functions," by F.M. Lavelle, L.A. Bergman and P.D. Spanos, 5/1/88, (PB89-102875, A03, MF-A01).
- NCEER-88-0012 "A New Solution Technique for Randomly Excited Hysteretic Structures," by G.Q. Cai and Y.K. Lin, 5/16/88, (PB89-102883, A03, MF-A01).
- NCEER-88-0013 "A Study of Radiation Damping and Soil-Structure Interaction Effects in the Centrifuge," by K. Weissman, supervised by J.H. Prevost, 5/24/88, (PB89-144703, A06, MF-A01).
- NCEER-88-0014 "Parameter Identification and Implementation of a Kinematic Plasticity Model for Frictional Soils," by J.H. Prevost and D.V. Griffiths, to be published.
- NCEER-88-0015 "Two- and Three- Dimensional Dynamic Finite Element Analyses of the Long Valley Dam," by D.V. Griffiths and J.H. Prevost, 6/17/88, (PB89-144711, A04, MF-A01).
- NCEER-88-0016 "Damage Assessment of Reinforced Concrete Structures in Eastern United States," by A.M. Reinhorn, M.J. Seidel, S.K. Kunnath and Y.J. Park, 6/15/88, (PB89-122220, A04, MF-A01). This report is only available through NTIS (see address given above).
- NCEER-88-0017 "Dynamic Compliance of Vertically Loaded Strip Foundations in Multilayered Viscoelastic Soils," by S. Ahmad and A.S.M. Israil, 6/17/88, (PB89-102891, A04, MF-A01).
- NCEER-88-0018 "An Experimental Study of Seismic Structural Response With Added Viscoelastic Dampers," by R.C. Lin, Z. Liang, T.T. Soong and R.H. Zhang, 6/30/88, (PB89-122212, A05, MF-A01). This report is available only through NTIS (see address given above).
- NCEER-88-0019 "Experimental Investigation of Primary - Secondary System Interaction," by G.D. Manolis, G. Juhn and A.M. Reinhorn, 5/27/88, (PB89-122204, A04, MF-A01).

- NCEER-88-0020 "A Response Spectrum Approach For Analysis of Nonclassically Damped Structures," by J.N. Yang, S. Sarkani and F.X. Long, 4/22/88, (PB89-102909, A04, MF-A01).
- NCEER-88-0021 "Seismic Interaction of Structures and Soils: Stochastic Approach," by A.S. Veletsos and A.M. Prasad, 7/21/88, (PB89-122196, A04, MF-A01). This report is only available through NTIS (see address given above).
- NCEER-88-0022 "Identification of the Serviceability Limit State and Detection of Seismic Structural Damage," by E. DiPasquale and A.S. Cakmak, 6/15/88, (PB89-122188, A05, MF-A01). This report is available only through NTIS (see address given above).
- NCEER-88-0023 "Multi-Hazard Risk Analysis: Case of a Simple Offshore Structure," by B.K. Bhartia and E.H. Vanmarcke, 7/21/88, (PB89-145213, A05, MF-A01).
- NCEER-88-0024 "Automated Seismic Design of Reinforced Concrete Buildings," by Y.S. Chung, C. Meyer and M. Shinozuka, 7/5/88, (PB89-122170, A06, MF-A01). This report is available only through NTIS (see address given above).
- NCEER-88-0025 "Experimental Study of Active Control of MDOF Structures Under Seismic Excitations," by L.L. Chung, R.C. Lin, T.T. Soong and A.M. Reinhorn, 7/10/88, (PB89-122600, A04, MF-A01).
- NCEER-88-0026 "Earthquake Simulation Tests of a Low-Rise Metal Structure," by J.S. Hwang, K.C. Chang, G.C. Lee and R.L. Ketter, 8/1/88, (PB89-102917, A04, MF-A01).
- NCEER-88-0027 "Systems Study of Urban Response and Reconstruction Due to Catastrophic Earthquakes," by F. Kozin and H.K. Zhou, 9/22/88, (PB90-162348, A04, MF-A01).
- NCEER-88-0028 "Seismic Fragility Analysis of Plane Frame Structures," by H.H-M. Hwang and Y.K. Low, 7/31/88, (PB89-131445, A06, MF-A01).
- NCEER-88-0029 "Response Analysis of Stochastic Structures," by A. Kardara, C. Bucher and M. Shinozuka, 9/22/88, (PB89-174429, A04, MF-A01).
- NCEER-88-0030 "Nonnormal Accelerations Due to Yielding in a Primary Structure," by D.C.K. Chen and L.D. Lutes, 9/19/88, (PB89-131437, A04, MF-A01).
- NCEER-88-0031 "Design Approaches for Soil-Structure Interaction," by A.S. Veletsos, A.M. Prasad and Y. Tang, 12/30/88, (PB89-174437, A03, MF-A01). This report is available only through NTIS (see address given above).
- NCEER-88-0032 "A Re-evaluation of Design Spectra for Seismic Damage Control," by C.J. Turkstra and A.G. Tallin, 11/7/88, (PB89-145221, A05, MF-A01).
- NCEER-88-0033 "The Behavior and Design of Noncontact Lap Splices Subjected to Repeated Inelastic Tensile Loading," by V.E. Sagan, P. Gergely and R.N. White, 12/8/88, (PB89-163737, A08, MF-A01).
- NCEER-88-0034 "Seismic Response of Pile Foundations," by S.M. Mamoon, P.K. Banerjee and S. Ahmad, 11/1/88, (PB89-145239, A04, MF-A01).
- NCEER-88-0035 "Modeling of R/C Building Structures With Flexible Floor Diaphragms (IDARC2)," by A.M. Reinhorn, S.K. Kunnath and N. Panahshahi, 9/7/88, (PB89-207153, A07, MF-A01).
- NCEER-88-0036 "Solution of the Dam-Reservoir Interaction Problem Using a Combination of FEM, BEM with Particular Integrals, Modal Analysis, and Substructuring," by C-S. Tsai, G.C. Lee and R.L. Ketter, 12/31/88, (PB89-207146, A04, MF-A01).
- NCEER-88-0037 "Optimal Placement of Actuators for Structural Control," by F.Y. Cheng and C.P. Pantelides, 8/15/88, (PB89-162846, A05, MF-A01).

- NCEER-88-0038 "Teflon Bearings in Aseismic Base Isolation: Experimental Studies and Mathematical Modeling," by A. Mokha, M.C. Constantinou and A.M. Reinhorn, 12/5/88, (PB89-218457, A10, MF-A01). This report is available only through NTIS (see address given above).
- NCEER-88-0039 "Seismic Behavior of Flat Slab High-Rise Buildings in the New York City Area," by P. Weidlinger and M. Ettouney, 10/15/88, (PB90-145681, A04, MF-A01).
- NCEER-88-0040 "Evaluation of the Earthquake Resistance of Existing Buildings in New York City," by P. Weidlinger and M. Ettouney, 10/15/88, to be published.
- NCEER-88-0041 "Small-Scale Modeling Techniques for Reinforced Concrete Structures Subjected to Seismic Loads," by W. Kim, A. El-Attar and R.N. White, 11/22/88, (PB89-189625, A05, MF-A01).
- NCEER-88-0042 "Modeling Strong Ground Motion from Multiple Event Earthquakes," by G.W. Ellis and A.S. Cakmak, 10/15/88, (PB89-174445, A03, MF-A01).
- NCEER-88-0043 "Nonstationary Models of Seismic Ground Acceleration," by M. Grigoriu, S.E. Ruiz and E. Rosenblueth, 7/15/88, (PB89-189617, A04, MF-A01).
- NCEER-88-0044 "SARCF User's Guide: Seismic Analysis of Reinforced Concrete Frames," by Y.S. Chung, C. Meyer and M. Shinozuka, 11/9/88, (PB89-174452, A08, MF-A01).
- NCEER-88-0045 "First Expert Panel Meeting on Disaster Research and Planning," edited by J. Pantelic and J. Stoyke, 9/15/88, (PB89-174460, A05, MF-A01). This report is only available through NTIS (see address given above).
- NCEER-88-0046 "Preliminary Studies of the Effect of Degrading Infill Walls on the Nonlinear Seismic Response of Steel Frames," by C.Z. Chrysostomou, P. Gergely and J.F. Abel, 12/19/88, (PB89-208383, A05, MF-A01).
- NCEER-88-0047 "Reinforced Concrete Frame Component Testing Facility - Design, Construction, Instrumentation and Operation," by S.P. Pessiki, C. Conley, T. Bond, P. Gergely and R.N. White, 12/16/88, (PB89-174478, A04, MF-A01).
- NCEER-89-0001 "Effects of Protective Cushion and Soil Compliancy on the Response of Equipment Within a Seismically Excited Building," by J.A. HoLung, 2/16/89, (PB89-207179, A04, MF-A01).
- NCEER-89-0002 "Statistical Evaluation of Response Modification Factors for Reinforced Concrete Structures," by H.H-M. Hwang and J-W. Jaw, 2/17/89, (PB89-207187, A05, MF-A01).
- NCEER-89-0003 "Hysteretic Columns Under Random Excitation," by G-Q. Cai and Y.K. Lin, 1/9/89, (PB89-196513, A03, MF-A01).
- NCEER-89-0004 "Experimental Study of 'Elephant Foot Bulge' Instability of Thin-Walled Metal Tanks," by Z-H. Jia and R.L. Ketter, 2/22/89, (PB89-207195, A03, MF-A01).
- NCEER-89-0005 "Experiment on Performance of Buried Pipelines Across San Andreas Fault," by J. Isenberg, E. Richardson and T.D. O'Rourke, 3/10/89, (PB89-218440, A04, MF-A01). This report is available only through NTIS (see address given above).
- NCEER-89-0006 "A Knowledge-Based Approach to Structural Design of Earthquake-Resistant Buildings," by M. Subramani, P. Gergely, C.H. Conley, J.F. Abel and A.H. Zaghaw, 1/15/89, (PB89-218465, A06, MF-A01).
- NCEER-89-0007 "Liquefaction Hazards and Their Effects on Buried Pipelines," by T.D. O'Rourke and P.A. Lane, 2/1/89, (PB89-218481, A09, MF-A01).

- NCEER-89-0008 "Fundamentals of System Identification in Structural Dynamics," by H. Imai, C-B. Yun, O. Maruyama and M. Shinozuka, 1/26/89, (PB89-207211, A04, MF-A01).
- NCEER-89-0009 "Effects of the 1985 Michoacan Earthquake on Water Systems and Other Buried Lifelines in Mexico," by A.G. Ayala and M.J. O'Rourke, 3/8/89, (PB89-207229, A06, MF-A01).
- NCEER-89-R010 "NCEER Bibliography of Earthquake Education Materials," by K.E.K. Ross, Second Revision, 9/1/89, (PB90-125352, A05, MF-A01). This report is replaced by NCEER-92-0018.
- NCEER-89-0011 "Inelastic Three-Dimensional Response Analysis of Reinforced Concrete Building Structures (IDARC-3D), Part I - Modeling," by S.K. Kunnath and A.M. Reinhorn, 4/17/89, (PB90-114612, A07, MF-A01).
- NCEER-89-0012 "Recommended Modifications to ATC-14," by C.D. Poland and J.O. Malley, 4/12/89, (PB90-108648, A15, MF-A01).
- NCEER-89-0013 "Repair and Strengthening of Beam-to-Column Connections Subjected to Earthquake Loading," by M. Corazao and A.J. Durrani, 2/28/89, (PB90-109885, A06, MF-A01).
- NCEER-89-0014 "Program EXKAL2 for Identification of Structural Dynamic Systems," by O. Maruyama, C-B. Yun, M. Hoshiya and M. Shinozuka, 5/19/89, (PB90-109877, A09, MF-A01).
- NCEER-89-0015 "Response of Frames With Bolted Semi-Rigid Connections, Part I - Experimental Study and Analytical Predictions," by P.J. DiCorso, A.M. Reinhorn, J.R. Dickerson, J.B. Radziminski and W.L. Harper, 6/1/89, to be published.
- NCEER-89-0016 "ARMA Monte Carlo Simulation in Probabilistic Structural Analysis," by P.D. Spanos and M.P. Mignolet, 7/10/89, (PB90-109893, A03, MF-A01).
- NCEER-89-P017 "Preliminary Proceedings from the Conference on Disaster Preparedness - The Place of Earthquake Education in Our Schools," Edited by K.E.K. Ross, 6/23/89, (PB90-108606, A03, MF-A01).
- NCEER-89-0017 "Proceedings from the Conference on Disaster Preparedness - The Place of Earthquake Education in Our Schools," Edited by K.E.K. Ross, 12/31/89, (PB90-207895, A012, MF-A02). This report is available only through NTIS (see address given above).
- NCEER-89-0018 "Multidimensional Models of Hysteretic Material Behavior for Vibration Analysis of Shape Memory Energy Absorbing Devices, by E.J. Graesser and F.A. Cozzarelli, 6/7/89, (PB90-164146, A04, MF-A01).
- NCEER-89-0019 "Nonlinear Dynamic Analysis of Three-Dimensional Base Isolated Structures (3D-BASIS)," by S. Nagarajaiah, A.M. Reinhorn and M.C. Constantinou, 8/3/89, (PB90-161936, A06, MF-A01). This report has been replaced by NCEER-93-0011.
- NCEER-89-0020 "Structural Control Considering Time-Rate of Control Forces and Control Rate Constraints," by F.Y. Cheng and C.P. Pantelides, 8/3/89, (PB90-120445, A04, MF-A01).
- NCEER-89-0021 "Subsurface Conditions of Memphis and Shelby County," by K.W. Ng, T-S. Chang and H-H.M. Hwang, 7/26/89, (PB90-120437, A03, MF-A01).
- NCEER-89-0022 "Seismic Wave Propagation Effects on Straight Jointed Buried Pipelines," by K. Elhmadi and M.J. O'Rourke, 8/24/89, (PB90-162322, A10, MF-A02).
- NCEER-89-0023 "Workshop on Serviceability Analysis of Water Delivery Systems," edited by M. Grigoriu, 3/6/89, (PB90-127424, A03, MF-A01).
- NCEER-89-0024 "Shaking Table Study of a 1/5 Scale Steel Frame Composed of Tapered Members," by K.C. Chang, J.S. Hwang and G.C. Lee, 9/18/89, (PB90-160169, A04, MF-A01).

- NCEER-89-0025 "DYNA1D: A Computer Program for Nonlinear Seismic Site Response Analysis - Technical Documentation," by Jean H. Prevost, 9/14/89, (PB90-161944, A07, MF-A01). This report is available only through NTIS (see address given above).
- NCEER-89-0026 "1:4 Scale Model Studies of Active Tendon Systems and Active Mass Dampers for Aseismic Protection," by A.M. Reinhorn, T.T. Soong, R.C. Lin, Y.P. Yang, Y. Fukao, H. Abe and M. Nakai, 9/15/89, (PB90-173246, A10, MF-A02).
- NCEER-89-0027 "Scattering of Waves by Inclusions in a Nonhomogeneous Elastic Half Space Solved by Boundary Element Methods," by P.K. Hadley, A. Askar and A.S. Cakmak, 6/15/89, (PB90-145699, A07, MF-A01).
- NCEER-89-0028 "Statistical Evaluation of Deflection Amplification Factors for Reinforced Concrete Structures," by H.H.M. Hwang, J-W. Jaw and A.L. Ch'ng, 8/31/89, (PB90-164633, A05, MF-A01).
- NCEER-89-0029 "Bedrock Accelerations in Memphis Area Due to Large New Madrid Earthquakes," by H.H.M. Hwang, C.H.S. Chen and G. Yu, 11/7/89, (PB90-162330, A04, MF-A01).
- NCEER-89-0030 "Seismic Behavior and Response Sensitivity of Secondary Structural Systems," by Y.Q. Chen and T.T. Soong, 10/23/89, (PB90-164658, A08, MF-A01).
- NCEER-89-0031 "Random Vibration and Reliability Analysis of Primary-Secondary Structural Systems," by Y. Ibrahim, M. Grigoriu and T.T. Soong, 11/10/89, (PB90-161951, A04, MF-A01).
- NCEER-89-0032 "Proceedings from the Second U.S. - Japan Workshop on Liquefaction, Large Ground Deformation and Their Effects on Lifelines, September 26-29, 1989," Edited by T.D. O'Rourke and M. Hamada, 12/1/89, (PB90-209388, A22, MF-A03).
- NCEER-89-0033 "Deterministic Model for Seismic Damage Evaluation of Reinforced Concrete Structures," by J.M. Bracci, A.M. Reinhorn, J.B. Mander and S.K. Kunnath, 9/27/89, (PB91-108803, A06, MF-A01).
- NCEER-89-0034 "On the Relation Between Local and Global Damage Indices," by E. DiPasquale and A.S. Cakmak, 8/15/89, (PB90-173865, A05, MF-A01).
- NCEER-89-0035 "Cyclic Undrained Behavior of Nonplastic and Low Plasticity Silts," by A.J. Walker and H.E. Stewart, 7/26/89, (PB90-183518, A10, MF-A01).
- NCEER-89-0036 "Liquefaction Potential of Surficial Deposits in the City of Buffalo, New York," by M. Budhu, R. Giese and L. Baumgrass, 1/17/89, (PB90-208455, A04, MF-A01).
- NCEER-89-0037 "A Deterministic Assessment of Effects of Ground Motion Incoherence," by A.S. Veletsos and Y. Tang, 7/15/89, (PB90-164294, A03, MF-A01).
- NCEER-89-0038 "Workshop on Ground Motion Parameters for Seismic Hazard Mapping," July 17-18, 1989, edited by R.V. Whitman, 12/1/89, (PB90-173923, A04, MF-A01).
- NCEER-89-0039 "Seismic Effects on Elevated Transit Lines of the New York City Transit Authority," by C.J. Costantino, C.A. Miller and E. Heymsfield, 12/26/89, (PB90-207887, A06, MF-A01).
- NCEER-89-0040 "Centrifugal Modeling of Dynamic Soil-Structure Interaction," by K. Weissman, Supervised by J.H. Prevost, 5/10/89, (PB90-207879, A07, MF-A01).
- NCEER-89-0041 "Linearized Identification of Buildings With Cores for Seismic Vulnerability Assessment," by I-K. Ho and A.E. Aktan, 11/1/89, (PB90-251943, A07, MF-A01).
- NCEER-90-0001 "Geotechnical and Lifeline Aspects of the October 17, 1989 Loma Prieta Earthquake in San Francisco," by T.D. O'Rourke, H.E. Stewart, F.T. Blackburn and T.S. Dickerman, 1/90, (PB90-208596, A05, MF-A01).

- NCEER-90-0002 "Nonnormal Secondary Response Due to Yielding in a Primary Structure," by D.C.K. Chen and L.D. Lutes, 2/28/90, (PB90-251976, A07, MF-A01).
- NCEER-90-0003 "Earthquake Education Materials for Grades K-12," by K.E.K. Ross, 4/16/90, (PB91-251984, A05, MF-A05). This report has been replaced by NCEER-92-0018.
- NCEER-90-0004 "Catalog of Strong Motion Stations in Eastern North America," by R.W. Busby, 4/3/90, (PB90-251984, A05, MF-A01).
- NCEER-90-0005 "NCEER Strong-Motion Data Base: A User Manual for the GeoBase Release (Version 1.0 for the Sun3)," by P. Friberg and K. Jacob, 3/31/90 (PB90-258062, A04, MF-A01).
- NCEER-90-0006 "Seismic Hazard Along a Crude Oil Pipeline in the Event of an 1811-1812 Type New Madrid Earthquake," by H.H.M. Hwang and C-H.S. Chen, 4/16/90, (PB90-258054, A04, MF-A01).
- NCEER-90-0007 "Site-Specific Response Spectra for Memphis Sheahan Pumping Station," by H.H.M. Hwang and C.S. Lee, 5/15/90, (PB91-108811, A05, MF-A01).
- NCEER-90-0008 "Pilot Study on Seismic Vulnerability of Crude Oil Transmission Systems," by T. Ariman, R. Dobry, M. Grigoriu, F. Kozin, M. O'Rourke, T. O'Rourke and M. Shinozuka, 5/25/90, (PB91-108837, A06, MF-A01).
- NCEER-90-0009 "A Program to Generate Site Dependent Time Histories: EQGEN," by G.W. Ellis, M. Srinivasan and A.S. Cakmak, 1/30/90, (PB91-108829, A04, MF-A01).
- NCEER-90-0010 "Active Isolation for Seismic Protection of Operating Rooms," by M.E. Talbott, Supervised by M. Shinozuka, 6/8/9, (PB91-110205, A05, MF-A01).
- NCEER-90-0011 "Program LINEARID for Identification of Linear Structural Dynamic Systems," by C-B. Yun and M. Shinozuka, 6/25/90, (PB91-110312, A08, MF-A01).
- NCEER-90-0012 "Two-Dimensional Two-Phase Elasto-Plastic Seismic Response of Earth Dams," by A.N. Yiagos, Supervised by J.H. Prevost, 6/20/90, (PB91-110197, A13, MF-A02).
- NCEER-90-0013 "Secondary Systems in Base-Isolated Structures: Experimental Investigation, Stochastic Response and Stochastic Sensitivity," by G.D. Manolis, G. Juhn, M.C. Constantinou and A.M. Reinhorn, 7/1/90, (PB91-110320, A08, MF-A01).
- NCEER-90-0014 "Seismic Behavior of Lightly-Reinforced Concrete Column and Beam-Column Joint Details," by S.P. Pessiki, C.H. Conley, P. Gergely and R.N. White, 8/22/90, (PB91-108795, A11, MF-A02).
- NCEER-90-0015 "Two Hybrid Control Systems for Building Structures Under Strong Earthquakes," by J.N. Yang and A. Danielians, 6/29/90, (PB91-125393, A04, MF-A01).
- NCEER-90-0016 "Instantaneous Optimal Control with Acceleration and Velocity Feedback," by J.N. Yang and Z. Li, 6/29/90, (PB91-125401, A03, MF-A01).
- NCEER-90-0017 "Reconnaissance Report on the Northern Iran Earthquake of June 21, 1990," by M. Mehrain, 10/4/90, (PB91-125377, A03, MF-A01).
- NCEER-90-0018 "Evaluation of Liquefaction Potential in Memphis and Shelby County," by T.S. Chang, P.S. Tang, C.S. Lee and H. Hwang, 8/10/90, (PB91-125427, A09, MF-A01).
- NCEER-90-0019 "Experimental and Analytical Study of a Combined Sliding Disc Bearing and Helical Steel Spring Isolation System," by M.C. Constantinou, A.S. Mokha and A.M. Reinhorn, 10/4/90, (PB91-125385, A06, MF-A01). This report is available only through NTIS (see address given above).

- NCEER-90-0020 "Experimental Study and Analytical Prediction of Earthquake Response of a Sliding Isolation System with a Spherical Surface," by A.S. Mokha, M.C. Constantinou and A.M. Reinhorn, 10/11/90, (PB91-125419, A05, MF-A01).
- NCEER-90-0021 "Dynamic Interaction Factors for Floating Pile Groups," by G. Gazetas, K. Fan, A. Kaynia and E. Kausel, 9/10/90, (PB91-170381, A05, MF-A01).
- NCEER-90-0022 "Evaluation of Seismic Damage Indices for Reinforced Concrete Structures," by S. Rodriguez-Gomez and A.S. Cakmak, 9/30/90, PB91-171322, A06, MF-A01).
- NCEER-90-0023 "Study of Site Response at a Selected Memphis Site," by H. Desai, S. Ahmad, E.S. Gazetas and M.R. Oh, 10/11/90, (PB91-196857, A03, MF-A01).
- NCEER-90-0024 "A User's Guide to Strongmo: Version 1.0 of NCEER's Strong-Motion Data Access Tool for PCs and Terminals," by P.A. Friberg and C.A.T. Susch, 11/15/90, (PB91-171272, A03, MF-A01).
- NCEER-90-0025 "A Three-Dimensional Analytical Study of Spatial Variability of Seismic Ground Motions," by L-L. Hong and A.H.-S. Ang, 10/30/90, (PB91-170399, A09, MF-A01).
- NCEER-90-0026 "MUMOID User's Guide - A Program for the Identification of Modal Parameters," by S. Rodriguez-Gomez and E. DiPasquale, 9/30/90, (PB91-171298, A04, MF-A01).
- NCEER-90-0027 "SARCF-II User's Guide - Seismic Analysis of Reinforced Concrete Frames," by S. Rodriguez-Gomez, Y.S. Chung and C. Meyer, 9/30/90, (PB91-171280, A05, MF-A01).
- NCEER-90-0028 "Viscous Dampers: Testing, Modeling and Application in Vibration and Seismic Isolation," by N. Makris and M.C. Constantinou, 12/20/90 (PB91-190561, A06, MF-A01).
- NCEER-90-0029 "Soil Effects on Earthquake Ground Motions in the Memphis Area," by H. Hwang, C.S. Lee, K.W. Ng and T.S. Chang, 8/2/90, (PB91-190751, A05, MF-A01).
- NCEER-91-0001 "Proceedings from the Third Japan-U.S. Workshop on Earthquake Resistant Design of Lifeline Facilities and Countermeasures for Soil Liquefaction, December 17-19, 1990," edited by T.D. O'Rourke and M. Hamada, 2/1/91, (PB91-179259, A99, MF-A04).
- NCEER-91-0002 "Physical Space Solutions of Non-Proportionally Damped Systems," by M. Tong, Z. Liang and G.C. Lee, 1/15/91, (PB91-179242, A04, MF-A01).
- NCEER-91-0003 "Seismic Response of Single Piles and Pile Groups," by K. Fan and G. Gazetas, 1/10/91, (PB92-174994, A04, MF-A01).
- NCEER-91-0004 "Damping of Structures: Part 1 - Theory of Complex Damping," by Z. Liang and G. Lee, 10/10/91, (PB92-197235, A12, MF-A03).
- NCEER-91-0005 "3D-BASIS - Nonlinear Dynamic Analysis of Three Dimensional Base Isolated Structures: Part II," by S. Nagarajaiah, A.M. Reinhorn and M.C. Constantinou, 2/28/91, (PB91-190553, A07, MF-A01). This report has been replaced by NCEER-93-0011.
- NCEER-91-0006 "A Multidimensional Hysteretic Model for Plasticity Deforming Metals in Energy Absorbing Devices," by E.J. Graesser and F.A. Cozzarelli, 4/9/91, (PB92-108364, A04, MF-A01).
- NCEER-91-0007 "A Framework for Customizable Knowledge-Based Expert Systems with an Application to a KBES for Evaluating the Seismic Resistance of Existing Buildings," by E.G. Ibarra-Anaya and S.J. Fenves, 4/9/91, (PB91-210930, A08, MF-A01).

- NCEER-91-0008 "Nonlinear Analysis of Steel Frames with Semi-Rigid Connections Using the Capacity Spectrum Method," by G.G. Deierlein, S-H. Hsieh, Y-J. Shen and J.F. Abel, 7/2/91, (PB92-113828, A05, MF-A01).
- NCEER-91-0009 "Earthquake Education Materials for Grades K-12," by K.E.K. Ross, 4/30/91, (PB91-212142, A06, MF-A01). This report has been replaced by NCEER-92-0018.
- NCEER-91-0010 "Phase Wave Velocities and Displacement Phase Differences in a Harmonically Oscillating Pile," by N. Makris and G. Gazetas, 7/8/91, (PB92-108356, A04, MF-A01).
- NCEER-91-0011 "Dynamic Characteristics of a Full-Size Five-Story Steel Structure and a 2/5 Scale Model," by K.C. Chang, G.C. Yao, G.C. Lee, D.S. Hao and Y.C. Yeh," 7/2/91, (PB93-116648, A06, MF-A02).
- NCEER-91-0012 "Seismic Response of a 2/5 Scale Steel Structure with Added Viscoelastic Dampers," by K.C. Chang, T.T. Soong, S-T. Oh and M.L. Lai, 5/17/91, (PB92-110816, A05, MF-A01).
- NCEER-91-0013 "Earthquake Response of Retaining Walls; Full-Scale Testing and Computational Modeling," by S. Alampalli and A-W.M. Elgarnal, 6/20/91, to be published.
- NCEER-91-0014 "3D-BASIS-M: Nonlinear Dynamic Analysis of Multiple Building Base Isolated Structures," by P.C. Tsopelas, S. Nagarajaiah, M.C. Constantinou and A.M. Reinhorn, 5/28/91, (PB92-113885, A09, MF-A02).
- NCEER-91-0015 "Evaluation of SEAOC Design Requirements for Sliding Isolated Structures," by D. Theodossiou and M.C. Constantinou, 6/10/91, (PB92-114602, A11, MF-A03).
- NCEER-91-0016 "Closed-Loop Modal Testing of a 27-Story Reinforced Concrete Flat Plate-Core Building," by H.R. Somaprasad, T. Toksoy, H. Yoshiyuki and A.E. Aktan, 7/15/91, (PB92-129980, A07, MF-A02).
- NCEER-91-0017 "Shake Table Test of a 1/6 Scale Two-Story Lightly Reinforced Concrete Building," by A.G. El-Attar, R.N. White and P. Gergely, 2/28/91, (PB92-222447, A06, MF-A02).
- NCEER-91-0018 "Shake Table Test of a 1/8 Scale Three-Story Lightly Reinforced Concrete Building," by A.G. El-Attar, R.N. White and P. Gergely, 2/28/91, (PB93-116630, A08, MF-A02).
- NCEER-91-0019 "Transfer Functions for Rigid Rectangular Foundations," by A.S. Veletsos, A.M. Prasad and W.H. Wu, 7/31/91, to be published.
- NCEER-91-0020 "Hybrid Control of Seismic-Excited Nonlinear and Inelastic Structural Systems," by J.N. Yang, Z. Li and A. Danielians, 8/1/91, (PB92-143171, A06, MF-A02).
- NCEER-91-0021 "The NCEER-91 Earthquake Catalog: Improved Intensity-Based Magnitudes and Recurrence Relations for U.S. Earthquakes East of New Madrid," by L. Seeber and J.G. Armbruster, 8/28/91, (PB92-176742, A06, MF-A02).
- NCEER-91-0022 "Proceedings from the Implementation of Earthquake Planning and Education in Schools: The Need for Change - The Roles of the Changemakers," by K.E.K. Ross and F. Winslow, 7/23/91, (PB92-129998, A12, MF-A03).
- NCEER-91-0023 "A Study of Reliability-Based Criteria for Seismic Design of Reinforced Concrete Frame Buildings," by H.H.M. Hwang and H-M. Hsu, 8/10/91, (PB92-140235, A09, MF-A02).
- NCEER-91-0024 "Experimental Verification of a Number of Structural System Identification Algorithms," by R.G. Ghanem, H. Gavin and M. Shinozuka, 9/18/91, (PB92-176577, A18, MF-A04).
- NCEER-91-0025 "Probabilistic Evaluation of Liquefaction Potential," by H.H.M. Hwang and C.S. Lee," 11/25/91, (PB92-143429, A05, MF-A01).
- NCEER-91-0026 "Instantaneous Optimal Control for Linear, Nonlinear and Hysteretic Structures - Stable Controllers," by J.N. Yang and Z. Li, 11/15/91, (PB92-163807, A04, MF-A01).

- NCEER-91-0027 "Experimental and Theoretical Study of a Sliding Isolation System for Bridges," by M.C. Constantinou, A. Kartoum, A.M. Reinhorn and P. Bradford, 11/15/91, (PB92-176973, A10, MF-A03).
- NCEER-92-0001 "Case Studies of Liquefaction and Lifeline Performance During Past Earthquakes, Volume 1: Japanese Case Studies," Edited by M. Hamada and T. O'Rourke, 2/17/92, (PB92-197243, A18, MF-A04).
- NCEER-92-0002 "Case Studies of Liquefaction and Lifeline Performance During Past Earthquakes, Volume 2: United States Case Studies," Edited by T. O'Rourke and M. Hamada, 2/17/92, (PB92-197250, A20, MF-A04).
- NCEER-92-0003 "Issues in Earthquake Education," Edited by K. Ross, 2/3/92, (PB92-222389, A07, MF-A02).
- NCEER-92-0004 "Proceedings from the First U.S. - Japan Workshop on Earthquake Protective Systems for Bridges," Edited by I.G. Buckle, 2/4/92, (PB94-142239, A99, MF-A06).
- NCEER-92-0005 "Seismic Ground Motion from a Haskell-Type Source in a Multiple-Layered Half-Space," A.P. Theoharis, G. Deodatis and M. Shinozuka, 1/2/92, to be published.
- NCEER-92-0006 "Proceedings from the Site Effects Workshop," Edited by R. Whitman, 2/29/92, (PB92-197201, A04, MF-A01).
- NCEER-92-0007 "Engineering Evaluation of Permanent Ground Deformations Due to Seismically-Induced Liquefaction," by M.H. Baziar, R. Dobry and A-W.M. Elgamal, 3/24/92, (PB92-222421, A13, MF-A03).
- NCEER-92-0008 "A Procedure for the Seismic Evaluation of Buildings in the Central and Eastern United States," by C.D. Poland and J.O. Malley, 4/2/92, (PB92-222439, A20, MF-A04).
- NCEER-92-0009 "Experimental and Analytical Study of a Hybrid Isolation System Using Friction Controllable Sliding Bearings," by M.Q. Feng, S. Fujii and M. Shinozuka, 5/15/92, (PB93-150282, A06, MF-A02).
- NCEER-92-0010 "Seismic Resistance of Slab-Column Connections in Existing Non-Ductile Flat-Plate Buildings," by A.J. Durrani and Y. Du, 5/18/92, (PB93-116812, A06, MF-A02).
- NCEER-92-0011 "The Hysteretic and Dynamic Behavior of Brick Masonry Walls Upgraded by Ferrocement Coatings Under Cyclic Loading and Strong Simulated Ground Motion," by H. Lee and S.P. Prawl, 5/11/92, to be published.
- NCEER-92-0012 "Study of Wire Rope Systems for Seismic Protection of Equipment in Buildings," by G.F. Demetriades, M.C. Constantinou and A.M. Reinhorn, 5/20/92, (PB93-116655, A08, MF-A02).
- NCEER-92-0013 "Shape Memory Structural Dampers: Material Properties, Design and Seismic Testing," by P.R. Witting and F.A. Cozzarelli, 5/26/92, (PB93-116663, A05, MF-A01).
- NCEER-92-0014 "Longitudinal Permanent Ground Deformation Effects on Buried Continuous Pipelines," by M.J. O'Rourke, and C. Nordberg, 6/15/92, (PB93-116671, A08, MF-A02).
- NCEER-92-0015 "A Simulation Method for Stationary Gaussian Random Functions Based on the Sampling Theorem," by M. Grigoriu and S. Balopoulou, 6/11/92, (PB93-127496, A05, MF-A01).
- NCEER-92-0016 "Gravity-Load-Designed Reinforced Concrete Buildings: Seismic Evaluation of Existing Construction and Detailing Strategies for Improved Seismic Resistance," by G.W. Hoffmann, S.K. Kunnath, A.M. Reinhorn and J.B. Mander, 7/15/92, (PB94-142007, A08, MF-A02).
- NCEER-92-0017 "Observations on Water System and Pipeline Performance in the Limón Area of Costa Rica Due to the April 22, 1991 Earthquake," by M. O'Rourke and D. Ballantyne, 6/30/92, (PB93-126811, A06, MF-A02).
- NCEER-92-0018 "Fourth Edition of Earthquake Education Materials for Grades K-12," Edited by K.E.K. Ross, 8/10/92, (PB93-114023, A07, MF-A02).

- NCEER-92-0019 "Proceedings from the Fourth Japan-U.S. Workshop on Earthquake Resistant Design of Lifeline Facilities and Countermeasures for Soil Liquefaction," Edited by M. Hamada and T.D. O'Rourke, 8/12/92, (PB93-163939, A99, MF-E11).
- NCEER-92-0020 "Active Bracing System: A Full Scale Implementation of Active Control," by A.M. Reinhorn, T.T. Soong, R.C. Lin, M.A. Riley, Y.P. Wang, S. Aizawa and M. Higashino, 8/14/92, (PB93-127512, A06, MF-A02).
- NCEER-92-0021 "Empirical Analysis of Horizontal Ground Displacement Generated by Liquefaction-Induced Lateral Spreads," by S.F. Bartlett and T.L. Youd, 8/17/92, (PB93-188241, A06, MF-A02).
- NCEER-92-0022 "IDARC Version 3.0: Inelastic Damage Analysis of Reinforced Concrete Structures," by S.K. Kunnath, A.M. Reinhorn and R.F. Lobo, 8/31/92, (PB93-227502, A07, MF-A02).
- NCEER-92-0023 "A Semi-Empirical Analysis of Strong-Motion Peaks in Terms of Seismic Source, Propagation Path and Local Site Conditions, by M. Kamiyama, M.J. O'Rourke and R. Flores-Berrones, 9/9/92, (PB93-150266, A08, MF-A02).
- NCEER-92-0024 "Seismic Behavior of Reinforced Concrete Frame Structures with Nonductile Details, Part I: Summary of Experimental Findings of Full Scale Beam-Column Joint Tests," by A. Beres, R.N. White and P. Gergely, 9/30/92, (PB93-227783, A05, MF-A01).
- NCEER-92-0025 "Experimental Results of Repaired and Retrofitted Beam-Column Joint Tests in Lightly Reinforced Concrete Frame Buildings," by A. Beres, S. El-Borgi, R.N. White and P. Gergely, 10/29/92, (PB93-227791, A05, MF-A01).
- NCEER-92-0026 "A Generalization of Optimal Control Theory: Linear and Nonlinear Structures," by J.N. Yang, Z. Li and S. Vongchavalitkul, 11/2/92, (PB93-188621, A05, MF-A01).
- NCEER-92-0027 "Seismic Resistance of Reinforced Concrete Frame Structures Designed Only for Gravity Loads: Part I - Design and Properties of a One-Third Scale Model Structure," by J.M. Bracci, A.M. Reinhorn and J.B. Mander, 12/1/92, (PB94-104502, A08, MF-A02).
- NCEER-92-0028 "Seismic Resistance of Reinforced Concrete Frame Structures Designed Only for Gravity Loads: Part II - Experimental Performance of Subassemblages," by L.E. Aycardi, J.B. Mander and A.M. Reinhorn, 12/1/92, (PB94-104510, A08, MF-A02).
- NCEER-92-0029 "Seismic Resistance of Reinforced Concrete Frame Structures Designed Only for Gravity Loads: Part III - Experimental Performance and Analytical Study of a Structural Model," by J.M. Bracci, A.M. Reinhorn and J.B. Mander, 12/1/92, (PB93-227528, A09, MF-A01).
- NCEER-92-0030 "Evaluation of Seismic Retrofit of Reinforced Concrete Frame Structures: Part I - Experimental Performance of Retrofitted Subassemblages," by D. Choudhuri, J.B. Mander and A.M. Reinhorn, 12/8/92, (PB93-198307, A07, MF-A02).
- NCEER-92-0031 "Evaluation of Seismic Retrofit of Reinforced Concrete Frame Structures: Part II - Experimental Performance and Analytical Study of a Retrofitted Structural Model," by J.M. Bracci, A.M. Reinhorn and J.B. Mander, 12/8/92, (PB93-198315, A09, MF-A03).
- NCEER-92-0032 "Experimental and Analytical Investigation of Seismic Response of Structures with Supplemental Fluid Viscous Dampers," by M.C. Constantinou and M.D. Symans, 12/21/92, (PB93-191435, A10, MF-A03).
- NCEER-92-0033 "Reconnaissance Report on the Cairo, Egypt Earthquake of October 12, 1992," by M. Khater, 12/23/92, (PB93-188621, A03, MF-A01).
- NCEER-92-0034 "Low-Level Dynamic Characteristics of Four Tall Flat-Plate Buildings in New York City," by H. Gavin, S. Yuan, J. Grossman, E. Pekelis and K. Jacob, 12/28/92, (PB93-188217, A07, MF-A02).

- NCEER-93-0001 "An Experimental Study on the Seismic Performance of Brick-Infilled Steel Frames With and Without Retrofit," by J.B. Mander, B. Nair, K. Wojtkowski and J. Ma, 1/29/93, (PB93-227510, A07, MF-A02).
- NCEER-93-0002 "Social Accounting for Disaster Preparedness and Recovery Planning," by S. Cole, E. Pantoja and V. Razak, 2/22/93, (PB94-142114, A12, MF-A03).
- NCEER-93-0003 "Assessment of 1991 NEHRP Provisions for Nonstructural Components and Recommended Revisions," by T.T. Soong, G. Chen, Z. Wu, R-H. Zhang and M. Grigoriu, 3/1/93, (PB93-188639, A06, MF-A02).
- NCEER-93-0004 "Evaluation of Static and Response Spectrum Analysis Procedures of SEAOC/UBC for Seismic Isolated Structures," by C.W. Winters and M.C. Constantinou, 3/23/93, (PB93-198299, A10, MF-A03).
- NCEER-93-0005 "Earthquakes in the Northeast - Are We Ignoring the Hazard? A Workshop on Earthquake Science and Safety for Educators," edited by K.E.K. Ross, 4/2/93, (PB94-103066, A09, MF-A02).
- NCEER-93-0006 "Inelastic Response of Reinforced Concrete Structures with Viscoelastic Braces," by R.F. Lobo, J.M. Bracci, K.L. Shen, A.M. Reinhorn and T.T. Soong, 4/5/93, (PB93-227486, A05, MF-A02).
- NCEER-93-0007 "Seismic Testing of Installation Methods for Computers and Data Processing Equipment," by K. Kosar, T.T. Soong, K.L. Shen, J.A. HoLung and Y.K. Lin, 4/12/93, (PB93-198299, A07, MF-A02).
- NCEER-93-0008 "Retrofit of Reinforced Concrete Frames Using Added Dampers," by A. Reinhorn, M. Constantinou and C. Li, to be published.
- NCEER-93-0009 "Seismic Behavior and Design Guidelines for Steel Frame Structures with Added Viscoelastic Dampers," by K.C. Chang, M.L. Lai, T.T. Soong, D.S. Hao and Y.C. Yeh, 5/1/93, (PB94-141959, A07, MF-A02).
- NCEER-93-0010 "Seismic Performance of Shear-Critical Reinforced Concrete Bridge Piers," by J.B. Mander, S.M. Waheed, M.T.A. Chaudhary and S.S. Chen, 5/12/93, (PB93-227494, A08, MF-A02).
- NCEER-93-0011 "3D-BASIS-TABS: Computer Program for Nonlinear Dynamic Analysis of Three Dimensional Base Isolated Structures," by S. Nagarajaiah, C. Li, A.M. Reinhorn and M.C. Constantinou, 8/2/93, (PB94-141819, A09, MF-A02).
- NCEER-93-0012 "Effects of Hydrocarbon Spills from an Oil Pipeline Break on Ground Water," by O.J. Helweg and H.H.M. Hwang, 8/3/93, (PB94-141942, A06, MF-A02).
- NCEER-93-0013 "Simplified Procedures for Seismic Design of Nonstructural Components and Assessment of Current Code Provisions," by M.P. Singh, L.E. Suarez, E.E. Matheu and G.O. Maldonado, 8/4/93, (PB94-141827, A09, MF-A02).
- NCEER-93-0014 "An Energy Approach to Seismic Analysis and Design of Secondary Systems," by G. Chen and T.T. Soong, 8/6/93, (PB94-142767, A11, MF-A03).
- NCEER-93-0015 "Proceedings from School Sites: Becoming Prepared for Earthquakes - Commemorating the Third Anniversary of the Loma Prieta Earthquake," Edited by F.E. Winslow and K.E.K. Ross, 8/16/93, (PB94-154275, A16, MF-A02).
- NCEER-93-0016 "Reconnaissance Report of Damage to Historic Monuments in Cairo, Egypt Following the October 12, 1992 Dahshur Earthquake," by D. Sykora, D. Look, G. Croci, E. Karaesmen and E. Karaesmen, 8/19/93, (PB94-142221, A08, MF-A02).
- NCEER-93-0017 "The Island of Guam Earthquake of August 8, 1993," by S.W. Swan and S.K. Harris, 9/30/93, (PB94-141843, A04, MF-A01).

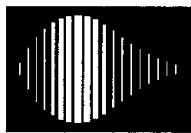
- NCEER-93-0018 "Engineering Aspects of the October 12, 1992 Egyptian Earthquake," by A.W. Elgamal, M. Amer, K. Adalier and A. Abul-Fadl, 10/7/93, (PB94-141983, A05, MF-A01).
- NCEER-93-0019 "Development of an Earthquake Motion Simulator and its Application in Dynamic Centrifuge Testing," by I. Krstelj, Supervised by J.H. Prevost, 10/23/93, (PB94-181773, A-10, MF-A03).
- NCEER-93-0020 "NCEER-Taisei Corporation Research Program on Sliding Seismic Isolation Systems for Bridges: Experimental and Analytical Study of a Friction Pendulum System (FPS)," by M.C. Constantinou, P. Tsopelas, Y-S. Kim and S. Okamoto, 11/1/93, (PB94-142775, A08, MF-A02).
- NCEER-93-0021 "Finite Element Modeling of Elastomeric Seismic Isolation Bearings," by L.J. Billings, Supervised by R. Shepherd, 11/8/93, to be published.
- NCEER-93-0022 "Seismic Vulnerability of Equipment in Critical Facilities: Life-Safety and Operational Consequences," by K. Porter, G.S. Johnson, M.M. Zadeh, C. Scawthorn and S. Eder, 11/24/93, (PB94-181765, A16, MF-A03).
- NCEER-93-0023 "Hokkaido Nansei-oki, Japan Earthquake of July 12, 1993, by P.I. Yanev and C.R. Scawthorn, 12/23/93, (PB94-181500, A07, MF-A01).
- NCEER-94-0001 "An Evaluation of Seismic Serviceability of Water Supply Networks with Application to the San Francisco Auxiliary Water Supply System," by I. Markov, Supervised by M. Grigoriu and T. O'Rourke, 1/21/94, (PB94-204013, A07, MF-A02).
- NCEER-94-0002 "NCEER-Taisei Corporation Research Program on Sliding Seismic Isolation Systems for Bridges: Experimental and Analytical Study of Systems Consisting of Sliding Bearings, Rubber Restoring Force Devices and Fluid Dampers," Volumes I and II, by P. Tsopelas, S. Okamoto, M.C. Constantinou, D. Ozaki and S. Fujii, 2/4/94, (PB94-181740, A09, MF-A02 and PB94-181757, A12, MF-A03).
- NCEER-94-0003 "A Markov Model for Local and Global Damage Indices in Seismic Analysis," by S. Rahman and M. Grigoriu, 2/18/94, (PB94-206000, A12, MF-A03).
- NCEER-94-0004 "Proceedings from the NCEER Workshop on Seismic Response of Masonry Infills," edited by D.P. Abrams, 3/1/94, (PB94-180783, A07, MF-A02).
- NCEER-94-0005 "The Northridge, California Earthquake of January 17, 1994: General Reconnaissance Report," edited by J.D. Goltz, 3/11/94, (PB193943, A10, MF-A03).
- NCEER-94-0006 "Seismic Energy Based Fatigue Damage Analysis of Bridge Columns: Part I - Evaluation of Seismic Capacity," by G.A. Chang and J.B. Mander, 3/14/94, (PB94-219185, A11, MF-A03).
- NCEER-94-0007 "Seismic Isolation of Multi-Story Frame Structures Using Spherical Sliding Isolation Systems," by T.M. Al-Hussaini, V.A. Zayas and M.C. Constantinou, 3/17/94, (PB193745, A09, MF-A02).
- NCEER-94-0008 "The Northridge, California Earthquake of January 17, 1994: Performance of Highway Bridges," edited by I.G. Buckle, 3/24/94, (PB94-193851, A06, MF-A02).
- NCEER-94-0009 "Proceedings of the Third U.S.-Japan Workshop on Earthquake Protective Systems for Bridges," edited by I.G. Buckle and I. Friedland, 3/31/94, (PB94-195815, A99, MF-A06).
- NCEER-94-0010 "3D-BASIS-ME: Computer Program for Nonlinear Dynamic Analysis of Seismically Isolated Single and Multiple Structures and Liquid Storage Tanks," by P.C. Tsopelas, M.C. Constantinou and A.M. Reinhorn, 4/12/94, (PB94-204922, A09, MF-A02).
- NCEER-94-0011 "The Northridge, California Earthquake of January 17, 1994: Performance of Gas Transmission Pipelines," by T.D. O'Rourke and M.C. Palmer, 5/16/94, (PB94-204989, A05, MF-A01).

- NCEER-94-0012 "Feasibility Study of Replacement Procedures and Earthquake Performance Related to Gas Transmission Pipelines," by T.D. O'Rourke and M.C. Palmer, 5/25/94, (PB94-206638, A09, MF-A02).
- NCEER-94-0013 "Seismic Energy Based Fatigue Damage Analysis of Bridge Columns: Part II - Evaluation of Seismic Demand," by G.A. Chang and J.B. Mander, 6/1/94, (PB95-18106, A08, MF-A02).
- NCEER-94-0014 "NCEER-Taisei Corporation Research Program on Sliding Seismic Isolation Systems for Bridges: Experimental and Analytical Study of a System Consisting of Sliding Bearings and Fluid Restoring Force/Damping Devices," by P. Tsopelas and M.C. Constantinou, 6/13/94, (PB94-219144, A10, MF-A03).
- NCEER-94-0015 "Generation of Hazard-Consistent Fragility Curves for Seismic Loss Estimation Studies," by H. Hwang and J-R. Huo, 6/14/94, (PB95-181996, A09, MF-A02).
- NCEER-94-0016 "Seismic Study of Building Frames with Added Energy-Absorbing Devices," by W.S. Pong, C.S. Tsai and G.C. Lee, 6/20/94, (PB94-219136, A10, A03).
- NCEER-94-0017 "Sliding Mode Control for Seismic-Excited Linear and Nonlinear Civil Engineering Structures," by J. Yang, J. Wu, A. Agrawal and Z. Li, 6/21/94, (PB95-138483, A06, MF-A02).
- NCEER-94-0018 "3D-BASIS-TABS Version 2.0: Computer Program for Nonlinear Dynamic Analysis of Three Dimensional Base Isolated Structures," by A.M. Reinhorn, S. Nagarajaiah, M.C. Constantinou, P. Tsopelas and R. Li, 6/22/94, (PB95-182176, A08, MF-A02).
- NCEER-94-0019 "Proceedings of the International Workshop on Civil Infrastructure Systems: Application of Intelligent Systems and Advanced Materials on Bridge Systems," Edited by G.C. Lee and K.C. Chang, 7/18/94, (PB95-252474, A20, MF-A04).
- NCEER-94-0020 "Study of Seismic Isolation Systems for Computer Floors," by V. Lambrou and M.C. Constantinou, 7/19/94, (PB95-138533, A10, MF-A03).
- NCEER-94-0021 "Proceedings of the U.S.-Italian Workshop on Guidelines for Seismic Evaluation and Rehabilitation of Unreinforced Masonry Buildings," Edited by D.P. Abrams and G.M. Calvi, 7/20/94, (PB95-138749, A13, MF-A03).
- NCEER-94-0022 "NCEER-Taisei Corporation Research Program on Sliding Seismic Isolation Systems for Bridges: Experimental and Analytical Study of a System Consisting of Lubricated PTFE Sliding Bearings and Mild Steel Dampers," by P. Tsopelas and M.C. Constantinou, 7/22/94, (PB95-182184, A08, MF-A02).
- NCEER-94-0023 "Development of Reliability-Based Design Criteria for Buildings Under Seismic Load," by Y.K. Wen, H. Hwang and M. Shinozuka, 8/1/94, (PB95-211934, A08, MF-A02).
- NCEER-94-0024 "Experimental Verification of Acceleration Feedback Control Strategies for an Active Tendon System," by S.J. Dyke, B.F. Spencer, Jr., P. Quast, M.K. Sain, D.C. Kaspari, Jr. and T.T. Soong, 8/29/94, (PB95-212320, A05, MF-A01).
- NCEER-94-0025 "Seismic Retrofitting Manual for Highway Bridges," Edited by I.G. Buckle and I.F. Friedland, published by the Federal Highway Administration (PB95-212676, A15, MF-A03).
- NCEER-94-0026 "Proceedings from the Fifth U.S.-Japan Workshop on Earthquake Resistant Design of Lifeline Facilities and Countermeasures Against Soil Liquefaction," Edited by T.D. O'Rourke and M. Hamada, 11/7/94, (PB95-220802, A99, MF-E08).
- NCEER-95-0001 "Experimental and Analytical Investigation of Seismic Retrofit of Structures with Supplemental Damping: Part 1 - Fluid Viscous Damping Devices," by A.M. Reinhorn, C. Li and M.C. Constantinou, 1/3/95, (PB95-266599, A09, MF-A02).

- NCEER-95-0002 "Experimental and Analytical Study of Low-Cycle Fatigue Behavior of Semi-Rigid Top-And-Seat Angle Connections," by G. Pekcan, J.B. Mander and S.S. Chen, 1/5/95, (PB95-220042, A07, MF-A02).
- NCEER-95-0003 "NCEER-ATC Joint Study on Fragility of Buildings," by T. Anagnos, C. Rojahn and A.S. Kiremidjian, 1/20/95, (PB95-220026, A06, MF-A02).
- NCEER-95-0004 "Nonlinear Control Algorithms for Peak Response Reduction," by Z. Wu, T.T. Soong, V. Gattulli and R.C. Lin, 2/16/95, (PB95-220349, A05, MF-A01).
- NCEER-95-0005 "Pipeline Replacement Feasibility Study: A Methodology for Minimizing Seismic and Corrosion Risks to Underground Natural Gas Pipelines," by R.T. Eguchi, H.A. Seligson and D.G. Honegger, 3/2/95, (PB95-252326, A06, MF-A02).
- NCEER-95-0006 "Evaluation of Seismic Performance of an 11-Story Frame Building During the 1994 Northridge Earthquake," by F. Naeim, R. DiSulio, K. Benuska, A. Reinhorn and C. Li, to be published.
- NCEER-95-0007 "Prioritization of Bridges for Seismic Retrofitting," by N. Basöz and A.S. Kiremidjian, 4/24/95, (PB95-252300, A08, MF-A02).
- NCEER-95-0008 "Method for Developing Motion Damage Relationships for Reinforced Concrete Frames," by A. Singhal and A.S. Kiremidjian, 5/11/95, (PB95-266607, A06, MF-A02).
- NCEER-95-0009 "Experimental and Analytical Investigation of Seismic Retrofit of Structures with Supplemental Damping: Part II - Friction Devices," by C. Li and A.M. Reinhorn, 7/6/95, (PB96-128087, A11, MF-A03).
- NCEER-95-0010 "Experimental Performance and Analytical Study of a Non-Ductile Reinforced Concrete Frame Structure Retrofitted with Elastomeric Spring Dampers," by G. Pekcan, J.B. Mander and S.S. Chen, 7/14/95, (PB96-137161, A08, MF-A02).
- NCEER-95-0011 "Development and Experimental Study of Semi-Active Fluid Damping Devices for Seismic Protection of Structures," by M.D. Symans and M.C. Constantinou, 8/3/95, (PB96-136940, A23, MF-A04).
- NCEER-95-0012 "Real-Time Structural Parameter Modification (RSPM): Development of Innervated Structures," by Z. Liang, M. Tong and G.C. Lee, 4/11/95, (PB96-137153, A06, MF-A01).
- NCEER-95-0013 "Experimental and Analytical Investigation of Seismic Retrofit of Structures with Supplemental Damping: Part III - Viscous Damping Walls," by A.M. Reinhorn and C. Li, 10/1/95, (PB96-176409, A11, MF-A03).
- NCEER-95-0014 "Seismic Fragility Analysis of Equipment and Structures in a Memphis Electric Substation," by J-R. Huo and H.H.M. Hwang, (PB96-128087, A09, MF-A02), 8/10/95.
- NCEER-95-0015 "The Hanshin-Awaji Earthquake of January 17, 1995: Performance of Lifelines," Edited by M. Shinozuka, 11/3/95, (PB96-176383, A15, MF-A03).
- NCEER-95-0016 "Highway Culvert Performance During Earthquakes," by T.L. Youd and C.J. Beckman, available as NCEER-96-0015.
- NCEER-95-0017 "The Hanshin-Awaji Earthquake of January 17, 1995: Performance of Highway Bridges," Edited by I.G. Buckle, 12/1/95, to be published.
- NCEER-95-0018 "Modeling of Masonry Infill Panels for Structural Analysis," by A.M. Reinhorn, A. Madan, R.E. Valles, Y. Reichmann and J.B. Mander, 12/8/95.
- NCEER-95-0019 "Optimal Polynomial Control for Linear and Nonlinear Structures," by A.K. Agrawal and J.N. Yang, 12/11/95, (PB96-168737, A07, MF-A02).

- NCEER-95-0020 "Retrofit of Non-Ductile Reinforced Concrete Frames Using Friction Dampers," by R.S. Rao, P. Gergely and R.N. White, 12/22/95, (PB97-133508, A10, MF-A02).
- NCEER-95-0021 "Parametric Results for Seismic Response of Pile-Supported Bridge Bents," by G. Mylonakis, A. Nikolaou and G. Gazetas, 12/22/95, (PB97-100242, A12, MF-A03).
- NCEER-95-0022 "Kinematic Bending Moments in Seismically Stressed Piles," by A. Nikolaou, G. Mylonakis and G. Gazetas, 12/23/95.
- NCEER-96-0001 "Dynamic Response of Unreinforced Masonry Buildings with Flexible Diaphragms," by A.C. Costley and D.P. Abrams, 10/10/96.
- NCEER-96-0002 "State of the Art Review: Foundations and Retaining Structures," by I. Po Lam, to be published.
- NCEER-96-0003 "Ductility of Rectangular Reinforced Concrete Bridge Columns with Moderate Confinement," by N. Wehbe, M. Saiidi, D. Sanders and B. Douglas, 11/7/96, (PB97-133557, A06, MF-A02).
- NCEER-96-0004 "Proceedings of the Long-Span Bridge Seismic Research Workshop," edited by I.G. Buckle and I.M. Friedland, to be published.
- NCEER-96-0005 "Establish Representative Pier Types for Comprehensive Study: Eastern United States," by J. Kulicki and Z. Prucz, 5/28/96.
- NCEER-96-0006 "Establish Representative Pier Types for Comprehensive Study: Western United States," by R. Imbsen, R.A. Schamber and T.A. Osterkamp, 5/28/96.
- NCEER-96-0007 "Nonlinear Control Techniques for Dynamical Systems with Uncertain Parameters," by R.G. Ghanem and M.I. Bujakov, 5/27/96, (PB97-100259, A17, MF-A03).
- NCEER-96-0008 "Seismic Evaluation of a 30-Year Old Non-Ductile Highway Bridge Pier and Its Retrofit," by J.B. Mander, B. Mahmoodzadegan, S. Bhadra and S.S. Chen, 5/31/96.
- NCEER-96-0009 "Seismic Performance of a Model Reinforced Concrete Bridge Pier Before and After Retrofit," by J.B. Mander, J.H. Kim and C.A. Ligozio, 5/31/96.
- NCEER-96-0010 "IDARC2D Version 4.0: A Computer Program for the Inelastic Damage Analysis of Buildings," by R.E. Valles, A.M. Reinhorn, S.K. Kunnath, C. Li and A. Madan, 6/3/96, (PB97-100234, A17, MF-A03).
- NCEER-96-0011 "Estimation of the Economic Impact of Multiple Lifeline Disruption: Memphis Light, Gas and Water Division Case Study," by S.E. Chang, H.A. Seligson and R.T. Eguchi, 8/16/96, (PB97-133490, A11, MF-A03).
- NCEER-96-0012 "Proceedings from the Sixth Japan-U.S. Workshop on Earthquake Resistant Design of Lifeline Facilities and Countermeasures Against Soil Liquefaction, Edited by M. Hamada and T. O'Rourke, 9/11/96, (PB97-133581, A99, MF-A06).
- NCEER-96-0013 "Chemical Hazards, Mitigation and Preparedness in Areas of High Seismic Risk: A Methodology for Estimating the Risk of Post-Earthquake Hazardous Materials Release," by H.A. Seligson, R.T. Eguchi, K.J. Tierney and K. Richmond, 11/7/96.
- NCEER-96-0014 "Response of Steel Bridge Bearings to Reversed Cyclic Loading," by J.B. Mander, D-K. Kim, S.S. Chen and G.J. Premus, 11/13/96, (PB97-140735, A12, MF-A03).
- NCEER-96-0015 "Highway Culvert Performance During Past Earthquakes," by T.L. Youd and C.J. Beckman, 11/25/96, (PB97-133532, A06, MF-A01).

- NCEER-97-0001 "Evaluation, Prevention and Mitigation of Pounding Effects in Building Structures," by R.E. Valles and A.M. Reinhorn, 2/20/97, (PB97-159552, A14, MF-A03).
- NCEER-97-0002 "Seismic Design Criteria for Bridges and Other Highway Structures," by C. Rojahn, R. Mayes, D.G. Anderson, J. Clark, J.H. Hom, R.V. Nutt and M.J. O'Rourke, 4/30/97, (PB97-194658, A06, MF-A03).
- NCEER-97-0003 "Proceedings of the U.S.-Italian Workshop on Seismic Evaluation and Retrofit," Edited by D.P. Abrams and G.M. Calvi, 3/19/97, (PB97-194666, A13, MF-A03).
- NCEER-97-0004 "Investigation of Seismic Response of Buildings with Linear and Nonlinear Fluid Viscous Dampers," by A.A. Seleemah and M.C. Constantinou, 5/21/97.
- NCEER-97-0005 "Proceedings of the First Workshop on Earthquake Engineering Frontiers in Transportation Facilities," Edited by G.C. Lee and I.M. Friedland, 8/29/97.
- NCEER-97-0006 "Cumulative Seismic Damage of Reinforced Concrete Bridge Piers," by S.K. Kunnath, A. El-Bahy, A. Taylor and W. Stone, 9/2/97.
- NCEER-97-0007 "Structural Details to Accommodate Seismic Movements of Highway Bridges and Retaining Walls," by R.A. Imbsen, R.A. Schamber, E. Thorkildsen, A. Kartoum, B.T. Martin, T.N. Rosser and J.M. Kulicki, 9/3/97.
- NCEER-97-0008 "A Method for Earthquake Motion-Damage Relationships with Application to Reinforced Concrete Frames," by A. Singhal and A.S. Kiremidjian, 9/10/97.



NATIONAL
CENTER FOR
EARTHQUAKE
ENGINEERING
RESEARCH

Headquartered at the State University of New York at Buffalo

State University of New York at Buffalo
Red Jacket Quadrangle
Buffalo, New York 14261
Telephone: 716/645-3391
FAX: 716/645-3399

ISSN 1088-3800

NTIS does not permit return of items for credit or refund. A replacement will be provided if an error is made in filling your order, if the item was received in damaged condition, or if the item is defective.

Reproduced by NTIS

National Technical Information Service
Springfield, VA 22161

*This report was printed specifically for your order
from nearly 3 million titles available in our collection.*

For economy and efficiency, NTIS does not maintain stock of its vast collection of technical reports. Rather, most documents are printed for each order. Documents that are not in electronic format are reproduced from master archival copies and are the best possible reproductions available. If you have any questions concerning this document or any order you have placed with NTIS, please call our Customer Service Department at (703) 487-4660.

About NTIS

NTIS collects scientific, technical, engineering, and business related information — then organizes, maintains, and disseminates that information in a variety of formats — from microfiche to online services. The NTIS collection of nearly 3 million titles includes reports describing research conducted or sponsored by federal agencies and their contractors; statistical and business information; U.S. military publications; audiovisual products; computer software and electronic databases developed by federal agencies; training tools; and technical reports prepared by research organizations worldwide. Approximately 100,000 *new* titles are added and indexed into the NTIS collection annually.

For more information about NTIS products and services, call NTIS at (703) 487-4650 and request the free *NTIS Catalog of Products and Services*, PR-827LPG, or visit the NTIS Web site <http://www.ntis.gov>.

NTIS

*Your indispensable resource for government-sponsored
information—U.S. and worldwide*



U.S. DEPARTMENT OF COMMERCE
Technology Administration
National Technical Information Service
Springfield, VA 22161 (703) 487-4650
